Cranfield University

Alexander John

Application of Microbubbles to Ozonation for Drinking Water Treatment

Cranfield Water Science Institute

EngD

Academic Year: 2021 – 2022

Supervisors: Prof. Peter Jarvis, Dr. Irene Carra & Prof. Bruce Jefferson

Cranfield University

Cranfield Water Science Institute

EngD

Academic Year: 2021 – 2022

Alexander John

Application of Microbubbles to Ozonation for Drinking Water Treatment

Supervisors: Prof. Peter Jarvis, Dr. Irene Carra & Prof. Bruce Jefferson

This thesis is submitted in partial fulfilment of the requirements for the degree of EngD.

Abstract

Ozonation is a widely used water treatment process that is used to oxidise contaminants as well as disinfect water. Conventional ozone contactors have a large energy requirement and deep tanks to ensure adequate mass transfer. As a result, the delivery of ozone into water is an energy intensive and expensive process.

The use of microbubbles in water treatment is a new technology that has been shown to significantly improve gas-liquid contacting processes. Microbubbles have diameters ranging from 1 – 100 µm, whereas conventional bubbles used in typical ozone contactors have diameters ranging from 2 – 6 mm. Due to their small size, microbubbles have a larger interfacial area and a lower rise velocity than conventional bubbles. Therefore, ozone in the gas phase may be transported more efficiently into the liquid phase. Despite the favourable properties of microbubbles, the mechanism by which microbubbles outperform conventional bubbles is not fully understood, with various conflicting interpretations having been presented in the literature.

This work is comprised of several direct-comparison studies of microbubble and conventional bubble ozonation systems under identical conditions. Experiments were normalised for both input and effective ozone dose in order to determine a number of critical performance parameters including: hydroxyl radical production, volumetric mass transfer coefficient, ozone self-decomposition, rate and extent of compound removal and bromate formation. Overall, the observed performance enhancement was attributed to an increase in the volumetric mass transfer coefficient through the combination of an increase in bubble specific interfacial area and a decrease in the mass transfer coefficient. When normalised to effective ozone dose, no enhancement in hydroxyl radical production or increase in bromate formation was observed. In addition, the generation of microbubbles results in a distribution of bubbles containing both micro- and nanobubbles. It was concluded that in order to optimise the overall ozonation process, emphasis should be placed on understanding how to manage the size distribution of the microbubble fraction as the risk of residual ozone from nanobubble survival was deemed insignificant.

These findings were then applied to the design of microbubble contactors to determine the economic viability of microbubble generation when applied to ozonation at full scale compared with a conventional bubble ozone contactor.

Acknowledgements

I would like to extend my thanks to all of those who have helped me throughout this project. Thank you to EPSRC, Anglian Water and Aeration & Mixing for supporting my work. Thank you to those involved with STREAM. Paul, Pablo and especially Tania.

A very special thank you to Pete, Irene and Bruce for your positivity, kindness, wisdom, patience and endless support throughout the trials and tribulations of the past five years. This would not have been possible without you.

I am very grateful for all of the technical support I have received over the years with a particular thanks to Paul and Monika. Thank you for sharing your expertise and thank you for your friendship.

To my Cranfield friends, I bet you thought this day would never come. You really are reading my thesis. I am just as shocked as you are. Thank you Gareth, Laura, Michele, Niall, Ben, Miles, Priya and Sophie for your friendship over the years. I know lunch will not be the same without me and, quite frankly, I do not know how you will cope. Just kidding. You will not get rid of me that easily. Also, stop reading this and do your own writing.

To my parents, sister and partner Laura, thank you for always believing in me.

In Loving Memory

Dinah & Daisy

Table of Contents

List of Figures

List of Tables

List of Equations and Reactions

Chapter 1. Introduction

1.1. Background

Gas-liquid contacting processes are some of the most energy intensive and expensive processes in water and wastewater treatment (Pasini et al., 2021). In the treatment of drinking water, ozonation is widely used due to its oxidation and disinfection capabilities (Wang et al., 2022). Ozonation is highly effective in the removal of a broad spectrum of contaminants such as colour and odour-causing compounds (Dong et al., 2022; Hu and Xia et al., 2018; Zhang et al., 2018; Khuntia et al., 2016), pharmaceuticals (Azuma et al., 2019; Lee et al., 2019), aromatic organic compounds (Nam et al., 2021; Yang et al., 2021; Cheng et al., 2019; Wu et al., 2019) and a variety of other micropollutants (Derco et al., 2021). Molecular ozone is a powerful, selective oxidant that, when transferred into the aqueous phase, undergoes a series of complex self-decomposition reactions resulting in the formation of a number of products including the desirable hydroxyl radical, a powerful non-selective oxidant. Ozone is a highly reactive, unstable gas that must be generated on-site and cannot be stored. Due to the energy required to generate ozone, there is high associated operating cost with an energy demand of ~ 0.8–16 kWh kg^{-1} O_3 (Jodzis and Zięba, 2018; Santana et al., 2014; Alonso et al., 2005; Magara et al., 1995), which represents approximately 15 % of the non-pumping process cost of drinking water treatment (Santana et al., 2014). In addition, the delivery of ozone into the aqueous phase is an inefficient process due to the relative inefficiency of ozone generation (Li et al., 2019; Vezzù et al., 2019; Kotlarz et al., 2018), its comparatively low solubility and high resistance to mass transfer (Wei et al., 2017). Ozone transfer is typically achieved through the use of fine-pore diffusers which produce conventional bubbles with a diameter of 2 – 6 mm (Baquero-Rodríguez et al., 2018; Behnisch et al., 2018; Garrido-Baserba et al., 2018; Terashima et al., 2016). A significant water depth is required as bubbles of this size rise quickly through the liquid and burst at the surface; leading to losses through off-gas. As a result, most ozone contactors have a depth of around 7 m (Niazi et al., 2017; Zhang et al., 2014).

One potential route to optimise the ozonation process is through the use of microbubbles. Microbubbles are defined as bubbles with a diameter of 1 – 100 μm (ISO 20480-1:2017). Microbubble technology has recently emerged as a way of enhancing the performance of

the ozonation process (Singh et al., 2021). Microbubble performance enhancement is often associated with the large size difference between microbubbles and conventional bubbles (Temesgen et al., 2017) which results in a significantly enhanced interfacial area (Parmar and Majumder, 2013), a decrease in rise velocity and an extended contact time for microbubble systems compared with conventional systems (Shangguan et al., 2018). These properties result in a higher gas utilisation efficiency (Zhang et al., 2018), higher rate of mass transfer (Wu et al., 2019) and a greater speed and extent of contaminant removal (Azuma et al., 2019). As such, they are now being considered to replace conventional bubble systems. The challenges associated with the implementation of microbubbles are evidenced through a lack of supply chain, uncertainty of capital and operational costs and an unclear understanding of the performance enhancement that microbubbles can offer. As a result, industrial partners have sponsored this EngD project to gain further insights into the benefits of microbubbles with the intention of moving towards application in industry.

1.2. Aim and Objectives

The aim of this project was to understand the mechanism by which microbubbles enhance the performance of ozonation and to assess the viability of the application of microbubbles to ozonation for drinking water treatment. In order to meet this aim, the following objectives were developed:

Objective 1. To produce a state-of-the-art critical literature review assessing the current state of microbubble technology for application in ozonation.

Objective 2. To understand the controlling mechanisms by which microbubbles enhance the performance of ozonation.

Objective 3. To identify and quantify the risks associated with the application of microbubbles to ozonation for drinking water treatment.

Objective 4. To quantify residual nanobubbles formed during microbubble generation and determine their significance for treatment during ozonation.

Objective 5. To determine the economic viability of the application of microbubbles to ozonation for drinking water treatment.

1.3. Thesis Structure and Format

This thesis is composed of a series of chapters that have been prepared in paper format. All papers were written by Alexander John and edited by Prof. Peter Jarvis, Dr. Irene Carra and Prof. Bruce Jefferson. All experiments were carried out by Alexander John at Cranfield University (UK) with additional contributions as follows:

Chapter 3. Monika Jodkowska (Cranfield University, UK)

Method development for the detection and quantification of 4-chlorobenzoic acid.

Chapter 4. Stuart Knott (Anglian Water Services, UK)

Co-ordination of the collection and transport of part-treated, pre-ozone water from a drinking water treatment works to Cranfield University

Co-ordination of the external analysis of bromate for the part-treated, pre-ozone natural water.

Initially, a critical literature review was completed to determine the current evidence base for the enhancement of ozonation by using microbubbles. The review provided evidence of the enhancement afforded by microbubbles and identified important remaining questions on the mechanisms that drive the enhancement, the appropriate contactor depths and the optimum bubble size. In addition, questions were raised on the potential for microbubbles to generate increased concentrations of hydroxyl radicals (Chapter 2, paper 1 – John, A., Brookes, A., Carra, I., Jefferson, B. and Jarvis, P., 2022. Microbubbles and their application to ozonation in water treatment: A critical review exploring their benefit and future application. *Critical Reviews in Environmental Science and Technology*, 52(9), pp.1561-1603).

Chapter 4 examined the potential mechanisms that drive the enhancements observed with microbubble systems through a series of controlled experiments that aimed to differentiate between the different potential mechanism (Chapter 4, paper 3 - John, A., Brookes, A., Carra, I., Jefferson, B. and Jarvis, P., in preparation. Intensification of

ozonation using microbubbles: micropollutant removal, mass transfer and bromate formation. *Chemical Engineering Journal.).* This work also determined how background constituents within the water may influence the observed enhancements and whether they would lead to additional challenges associated with bromate formation. In addition, the hypothesis that microbubbles generate an enhanced production of hydroxyl radical was directly assessed (Chapter 3, paper 2 - John, A., Carra, I., Jefferson, B., Jodkowska, M., Brookes, A. and Jarvis, P., 2022. Are microbubbles magic or just small? a direct comparison of hydroxyl radical generation between microbubble and conventional bubble ozonation under typical operational conditions. *Chemical Engineering Journal*, 435, p.134854).

A key observation from the literature review was that there was a paucity of available data on bubble sizes for experiments that compared microbubble and conventional bubble systems. The work presented in Chapter 5 helped to resolve this through comprehensive bubble size characterisation. This included determination of the concentration, size and role of any nanobubbles that may be formed by the microbubble generator (Chapter 5, paper 4 – John, A., Brookes, A., Carra, I., Jefferson, B. and Jarvis, P., submitted. Size distributions of micro-nano bubbles (MNBs) generated by a regenerative turbine microbubble generator using ozone: Significance and potential importance of the nanobubble fractions. *Journal of Water Process Engineering*).

Chapter 6 then discusses the implications of the key findings through an economic analysis that aimed to establish an evidence base for a business case for incorporation of microbubble technology into operational practice.

Finally, Chapter 7 presents the key conclusions along with recommendations for future work. Table 1 – 1 summarises this thesis plan and the status of the associated papers.

Table 1 – 1. Summary of thesis structure.

Chapter	Objective	Title	Journal	Status
2	1	Microbubbles and Their Application to Ozonation in Water Treatment: A Critical Review Exploring Their Benefit and Future Application	*Critical Reviews in Environmental Science and Technology*	Published
3	2	Are Microbubbles Magic or Just Small? A Direct Comparison of Hydroxyl Radical Generation Between Microbubble and Conventional Bubble Ozonation	*Chemical Engineering Journal*	Published
4	2, 3	Intensification of Ozonation Using Microbubbles – Micropollutant Removal, Mass Transfer and Bromate Formation	-	In preparation
5	3, 4	Size Distributions of Micro-nano Bubbles (MNBs) Generated by a Regenerative Turbine Microbubble Generator using Ozone: Significance and Potential Importance of the Nanobubble Fractions	-	In preparation
6	5	Economic Viability of the Implementation of Microbubble Technology at Full Scale	*n/a*	n/a
7	1, 2, 3, 4, 5	Conclusion	*n/a*	n/a

1.4. Publications

Two chapters of this thesis have been published in international peer-reviewed journals:

Chapter 2. John, A., Brookes, A., Carra, I., Jefferson, B. and Jarvis, P., 2022. Microbubbles and their application to ozonation in water treatment: A critical review exploring their benefit and future application. *Critical Reviews in Environmental Science and Technology*, 52(9), pp.1561-1603.

Chapter 3. John, A., Carra, I., Jefferson, B., Jodkowska, M., Brookes, A. and Jarvis, P., 2022. Are microbubbles magic or just small? a direct comparison of hydroxyl

radical generation between microbubble and conventional bubble ozonation under typical operational conditions. *Chemical Engineering Journal*, 435, p.134854.

The findings from this research have also been disseminated through a number of presentation and posters at a variety of academic and industrial conferences and seminars:

Platform Presentations

2017 Anglian Water Student Symposium (Peterborough, UK).

Cranfield University: Science for a Circular Economy: How to Tackle the Water, Energy and Food Nexus (Cranfield, UK).

2019 Anglian Water Student Symposium (Peterborough, UK).

International Water Association Leading Edge Technology Conference on Water and Wastewater Technologies (Edinburgh, UK).

American Water Works Association Water Quality Technology Conference (Texas, USA).

2020 Anglian Water Student Symposium (Online).

STREAM Annual Conference (Online).

Conference of the UK Network on Potable Water Treatment and Supply (Online).

Posters

2017 Anglian Water Student Symposium (Peterborough, UK).

STREAM Annual Conference (Leeuwarden, NL).

2018 International Water Association Young Water Professionals Conference (Cranfield, UK).

2019 Anglian Water Student Symposium (Peterborough, UK).

Conference of the UK Network on Potable Water Treatment and Supply (Cranfield, UK).

Disrupt19 (Belfast, UK).

International Water Association Leading Edge Technology Conference on Water and Wastewater Technologies (Edinburgh, UK).

STREAM Annual Conference (Kenilworth, UK).

1.5. References

Alonso, J., Garcia, J., Calleja, A., Ribas, J. and Cardesin, J., 2005. Analysis, design, and experimentation of a high-voltage power supply for ozone generation based on current-fed parallel-resonant push–pull inverter. *IEEE Transactions on Industry Applications*, 41(5), pp.1364-1372.

Azuma, T., Otomo, K., Kunitou, M., Shimizu, M., Hosomaru, K., Mikata, S., Mino, Y. and Hayashi, T., 2019. Removal of pharmaceuticals in water by introduction of ozonated microbubbles. *Separation and Purification Technology*, 212, pp.483-489.

Baquero-Rodríguez, G., Lara-Borrero, J., Nolasco, D. and Rosso, D., 2018. A Critical Review of the Factors Affecting Modeling Oxygen Transfer by Fine-Pore Diffusers in Activated Sludge. *Water Environment Research*, 90(5), pp.431-441.

Behnisch, J., Ganzauge, A., Sander, S., Herrling, M. and Wagner, M., 2018. Improving aeration systems in saline water: measurement of local bubble size and volumetric mass transfer coefficient of conventional membrane diffusers. *Water Science and Technology*, 78(4), pp.860-867.

Chen, X., Yao, J., Jiang, S., Liu, C., Guo, M., Gao, N. and Zhang, Z., 2020. An improved CFD modeling approach applied for the simulation of gas–liquid interaction in the ozone contactor along with structure optimization. *Chemical Engineering Journal*, 384, p.123322.

Cheng, W., Jiang, L., Quan, X., Cheng, C., Huang, X., Cheng, Z. and Yang, L., 2019. Ozonation process intensification of p-nitrophenol by in situ separation of hydroxyl radical scavengers and microbubbles. *Water Science and Technology*, 80(1), pp.25-36.

Derco, J., Gotvajn, A., Čižmárová, O., Dudáš, J., Sumegová, L. and Šimovičová, K., 2021. Removal of micropollutants by ozone-based processes. *Processes*, 9(6), p.1013.

Dong, J., Yao, J., Tao, J., Shi, X. and Wei, F., 2022. Degradation of Methyl Orange by ozone microbubble process with packing in the bubble column reactor. *Environmental Technology*, pp.1-28.

Gardoni, D., Vailati, A. and Canziani, R., 2012. Decay of ozone in water: a review. *Ozone: Science & Engineering*, 34(4), pp.233-242.

Garrido-Baserba, M., Asvapathanagul, P., Park, H., Kim, T., Baquero-Rodriguez, G., Olson, B. and Rosso, D., 2018. Impact of fouling on the decline of aeration efficiency under different operational conditions at WRRFs. *Science of The Total Environment*, 639, pp.248-257.

Hu, L. and Xia, Z., 2018. Application of ozone micro-nano-bubbles to groundwater remediation. *Journal of Hazardous Materials*, 342, pp.446-453.

International Organization for Standardization. (2017). *ISO/TC 281: Fine bubble technology*. ISO. Retrieved June 1, 2020, from https://www.iso.org/committee/4856666.html

Jodzis, S. and Zięba, M., 2018. Energy efficiency of an ozone generation process in oxygen. Analysis of a pulsed DBD system. *Vacuum*, 155, pp.29-37.

Khuntia, S., Majumder, S. and Ghosh, P., 2016. Catalytic ozonation of dye in a microbubble system: Hydroxyl radical contribution and effect of salt. *Journal of Environmental Chemical Engineering*, 4(2), pp.2250-2258.

Kotlarz, N., Rockey, N., Olson, T., Haig, S., Sanford, L., LiPuma, J. and Raskin, L., 2018. Biofilms in full-scale drinking water ozone contactors contribute viable bacteria to ozonated water. *Environmental Science & Technology*, 52(5), pp.2618-2628.

Lee, Y., Park, Y., Lee, G., Kim, Y. and Chon, K., 2019. Enhanced degradation of pharmaceutical compounds by a microbubble ozonation process: effects of temperature, pH, and humic acids. *Energies*, 12(22), p.4373.

Li, K., Xu, L., Zhang, Y., Cao, A., Wang, Y., Huang, H. and Wang, J., 2019. A novel electro-catalytic membrane contactor for improving the efficiency of ozone on wastewater treatment. *Applied Catalysis B: Environmental*, 249, pp.316-321.

Loganathan, P., Kandasamy, J., Jamil, S., Ratnaweera, H. and Vigneswaran, S., 2022. Ozonation/adsorption hybrid treatment system for improved removal of natural organic matter and organic micropollutants from water – A mini review and future perspectives. *Chemosphere*, 296, p.133961.

Magara, Y., Itoh, M. and Morioka, T., 1995. Application of ozone to water treatment and power consumption of ozone generating systems. *Progress in Nuclear Energy*, 29, pp.175-182.

Mao, Y., Qi, S., Guo, X., Yang, H. and Xie, Y., 2021. Optimization of ozone dosage in an ozone contact tank using a numerical model. *Environmental Science and Pollution Research*, 28(33), pp.44987-44997.

Nam, G., Mohamed, M. and Jung, J., 2019. Enhanced degradation of benzo[a]pyrene and toxicity reduction by microbubble ozonation. *Environmental Technology*, 42(12), pp.1853-1860.

Niazi, S., Kalbasi, M. and Bahramian, A., 2017. Hydraulic and disinfection efficiency of an ozonation contactor for a municipal water treatment plant using computational fluid dynamics. *The Canadian Journal of Chemical Engineering*, 95(11), pp.2063-2072.

Pasini, F., Garrido-Baserba, M., Ahmed, A., Nakhla, G., Santoro, D. and Rosso, D., 2021. Oxygen transfer and plant-wide energy assessment of primary screening in WRRFs. *Water Environment Research*, 93(5), pp.677-692.

Peng, S., Deng, B., Wu, J. and Xu, L., 2021. The impact of turbulence models on the simulation of residence time distribution in a multichamber ozone contactor. *Water Supply*, 21(7), pp.3976-3986.

Santana, M., Zhang, Q. and Mihelcic, J., 2014. Influence of water quality on the embodied energy of drinking water treatment. *Environmental Science & Technology*, 48(5), pp.3084-3091.

Singh, B., Shukla, N., Cho, C., Kim, B., Park, M. and Kim, K., 2021. Effect and application of micro- and nanobubbles in water purification. *Toxicology and Environmental Health Sciences*, 13(1), pp.9-16.

Temesgen, T., Bui, T., Han, M., Kim, T. and Park, H., 2017. Micro and nanobubble technologies as a new horizon for water-treatment techniques: A review. *Advances in Colloid and Interface Science*, 246, pp.40-51.

Terasaka, K., Hirabayashi, A., Nishino, T., Fujioka, S. and Kobayashi, D., 2011. Development of microbubble aerator for waste water treatment using aerobic activated sludge. *Chemical Engineering Science*, 66(14), pp.3172-3179.

Terashima, M., So, M., Goel, R. and Yasui, H., 2016. Determination of diffuser bubble size in computational fluid dynamics models to predict oxygen transfer in spiral roll aeration tanks. *Journal of Water Process Engineering*, 12, pp.120-126.

Vezzù, G., Lopez, J., Freilich, A. and Becker, K., 2009. Optimization of large-scale ozone generators. *IEEE Transactions on Plasma Science*, 37(6), pp.890-896.

Wang, Y., Wang, S., Li, J., Yan, X., Li, C., Zhang, M., Yu, J. and Ren, L., 2022. The formation and control of ozonation by-products during drinking water advanced treatment in a pilot-scale study. *Science of The Total Environment*, 808, p.151921.

Wei, C., Zhang, F., Hu, Y., Feng, C. and Wu, H., 2017. Ozonation in water treatment: the generation, basic properties of ozone and its practical application. *Reviews in Chemical Engineering*, 33(1), pp49-89.

Wu, C., Li, P., Xia, S., Wang, S., Wang, Y., Hu, J., Liu, Z. and Yu, S., 2019. The role of interface in microbubble ozonation of aromatic compounds. *Chemosphere*, 220, pp.1067-1074.

Yang, X., Liu, Z., Manhaeghe, D., Yang, Y., Hogie, J., Demeestere, K. and Van Hulle, S., 2021. Intensified ozonation in packed bubble columns for water treatment: Focus on mass transfer and humic acids removal. *Chemosphere*, 283, p.131217.

Zhang, H., Li, P., Zhang, A., Sun, Z., Liu, J., Héroux, P. and Liu, Y., 2021. Enhancing interface reactions by introducing microbubbles into a plasma treatment process for efficient decomposition of PFOA. *Environmental Science & Technology*, 55(23), pp.16067-16077.

Zhang, J., Huang, G., Liu, C., Zhang, R., Chen, X. and Zhang, L., 2018. Synergistic effect of microbubbles and activated carbon on the ozonation treatment of synthetic dyeing wastewater. *Separation and Purification Technology*, 201, pp.10-18.

Zhang, J., Tejada-Martínez, A., Zhang, Q. and Lei, H., 2014. Evaluating hydraulic and disinfection efficiencies of a full-scale ozone contactor using a RANS-based modeling framework. *Water Research*, 52, pp.155-167.

Chapter 2. Microbubbles and Their Application to Ozonation in Water Treatment: A Critical Review Exploring Their Benefit and Future Application

Alexander John[a], Adam Brookes[b], Irene Carra[a], Bruce Jefferson[a] and Peter Jarvis[a]

[a]School of Water, Energy and Environment, Cranfield Water Science Institute, Cranfield, UK.

[b]Anglian Water, Thorpe Wood House, Peterborough, UK.

Abstract

Ozonation is a widely applied water treatment process, used for oxidation of contaminants, as well as for the disinfection of water. However, the conventional ozonation process demands a high energy requirement and deep tanks to ensure effective mass transfer and oxidation. Microbubble technologies have emerged which have the potential to improve gas-liquid contacting. Microbubbles have diameters of 1 – 100 µm, while conventional bubbles used in ozonation are between 2 and 6 mm. Microbubbles have many favourable characteristics that make them suitable for ozonation. In this review, the attributes of microbubbles for ozonation have been compared with those of conventional bubbles. The higher interfacial area and lower rise velocity of microbubbles compared with conventional bubbles means that ozone in the gas phase can be more efficiently transferred into the aqueous phase. This is due to a higher contact time and increased contact area of the bubble with the bulk liquid. The analysis reveals that the volumetric mass transfer coefficient can be significantly enhanced through the use of microbubbles. In addition, the steady state dissolved ozone concentration was positively impacted by the use of microbubbles. Microbubbles were shown to be able to oxidise a broader range of organic compounds more quickly than for conventional bubbles. However, the review highlighted that comparison of microbubbles with conventional bubbles is not always carried out in a fair and consistent way with respect to reactor configuration. Requirements for future research, more consistent experimental comparisons and the steps needed to enable implementation of microbubbles have been discussed.

2.1. Introduction

Ozonation is one of the most widely used gas-liquid contacting processes in water treatment for oxidation and disinfection applications (Merle et al., 2017; Lim et al., 2019; Wolf et al., 2019; Tekle-Röttering et al., 2020). Molecular ozone is an unstable and strong oxidant that has a standard oxidation potential of 2.07 V (Muruganandham et al., 2014). When dissolved into the aqueous phase, ozone rapidly undergoes self-decomposition. The self-decomposition of ozone results in the formation of a number of products and intermediates including short lived radicals such as $HO^{\bullet}$, $O_2^{\bullet-}$, $O_3^{\bullet-}$, $HO_3^{\bullet-}$, and $HO_2^{\bullet}$ (Gardoni et al., 2012). One of the most desirable decomposition products is the hydroxyl radical, $HO^{\bullet}$, which is a non-selective, powerful oxidant with a standard oxidation potential of 2.8 V (Wang et al., 2018). Due to the strong oxidizing ability of molecular ozone and the hydroxyl radical, ozonation is particularly effective in the removal of aromatic organic compounds (Chedeville et al., 2009; Wu et al., 2019), pharmaceuticals (Azuma et al., 2019; Paucar et al., 2019), micropollutants (Wang et al., 2019), algal by-products (Wu et al., 2012) and contaminants that cause water colouration (Khuntia et al., 2016). In a water treatment works (WTWs), a typical ozone contactor consists of a baffled reactor split into 1 – 2 dosing chambers and > 2 reaction zones (von Gunten et al., 1999). Ozone gas is supplied through diffuser plates at the base of the dosing chamber(s), producing bubbles with a size between 2 and 6 mm (Terashima et al., 2016; Baquero-Rodríguez et al., 2018; Behnisch et al., 2018; Garrido-Baserba et al., 2018) (Figure 2 – 1). In addition to this design, some water and wastewater treatment works use a side-stream design in which a portion of the aqueous flow is injected with ozone, typically with a venturi system, and returned to the bulk aqueous flow (Wert et al., 2017). Ozone contactors typically have a large footprint and deep tank depth, and therefore require significant resources, which varies depending upon the treatment objectives and water quality (Rakness et al., 2018). While reactor volume changes depending on flow treated, all ozonation contactors have deep tanks, typically around 7 m (Tang et al., 2005; Zhang et al., 2014). This depth is required in order to ensure effective mass transfer of ozone from bubbles formed using conventional diffusers. In addition to capital investment, ozonation has significant operating costs as ozone gas must be generated in-situ and cannot be stored on site due to its instability. The generation of ozone is an energy and opex intensive process with an energy demand of ~ 3.3 – 16 kWh / kg O_3 (Magara et al.,

1995; Jodzis and Zięba, 2018). The cost of the power required to generate ozone is between 50 % and 75 % of the ozonation process cost (Evans et al., 2003) and around 15 % of the total non-pumping energy requirement for a WTWs using ozone (Santana et al., 2014). Whilst ozone is usually delivered in the form of conventional millimetre sized bubbles, recent developments have allowed for the use of smaller bubbles known as microbubbles and nanobubbles. There has been some debate in the literature with respect to the size boundaries used to describe these small bubbles, with a range of definitions having been used (see supplementary information [SI] Table 2 – S1). However, since 2017 there has been a standardised definition of microbubbles and nanobubbles from the International Organization for Standardization (ISO), as being bubbles with a diameter of 1 – 100 μm and 1 – 1000 nm, respectively (ISO 20480-1:2017). Over the past few decades, interest in the application of microbubbles to water treatment has increased greatly due to their high surface area to volume ratio (Temesgen et al., 2017), low rising velocity (Terasaka et al., 2011), increased gas utilisation efficiency (Zhang et al., 2018), increased rate of mass transfer (Wu et al., 2019) and increased rate of contaminant removal (Azuma et al., 2019). Microbubbles have the potential to decrease operational cost from a reduction in the required ozone input dose and a decreased requirement for off-gas destruction (Chu et al., 2008). In addition, increased treatment rates may afford opportunities for reductions in contact tank dimensions and plant footprint. Microbubble generation has historically been considered an energy intensive process in which the cost was deemed too high to be economically viable. This was due to the high power required to produce microbubbles, using generation methods involving compression or ultrasonic cavitation (Zimmerman et al., 2008). Recently, however, lower powered microbubble generators have been developed. Modern developments include microbubble generators such as those produced by spherical bodies (Sadatomi et al., 2005), orifice plates (Sadatomi et al., 2012), venturis (Deendarlianto et al., 2017), membranes (Kukuzaki et al., 2010; Liu et al., 2012, 2013) and fluidic oscillators (Zimmerman et al., 2011a; Al-Mashhadani et al., 2015; Hanotu et al., 2016, 2017; Kamaroddin et al., 2016, 2020). These types of microbubble generator utilise a restriction in the fluid flow to cause a pressure drop and an automatic suction of gas (Parmar and Majumder, 2013). Many of these developments have occurred without a specific application in mind, however they now offer a more realistic opportunity for application of microbubbles in water treatment. To

date, there has not been a comprehensive review of microbubbles for ozonation, despite a significant expansion of research into this application. Accordingly, this review aims to critically review the literature to establish the current state of evidence on the potential benefits of microbubbles systems with regards to the use of ozone. The review will explore both the mass transfer and treatment aspects of bubble size on ozone applications. The review will then consider whether full scale microbubble ozonation is a feasible option and then discuss the challenges and future perspectives associated with the use of microbubbles.

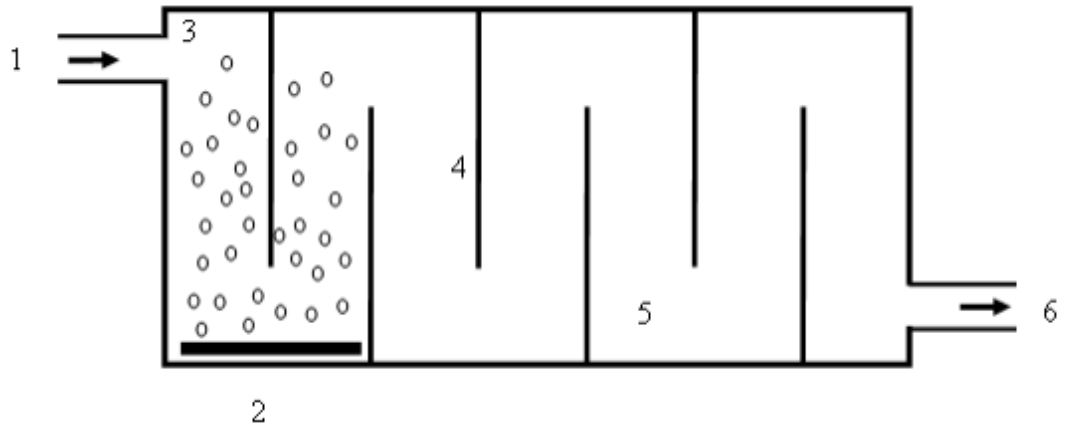

Figure 2 – 1. A typical baffled ozone contactor where (1) liquid inlet (2) diffuser plates (3) dosing chambers (4) baffles (5) reaction chambers (6) liquid outlet.

2.2. Mass Transfer

The transfer of gas into liquid is dependent upon the mixing conditions, the size and number of bubbles and, in the case of reactive gases such as ozone, the kinetics of decomposition (Fuchun and Cunli, 1990; Shin et al., 1999). The rate at which ozone gas is transferred into liquid is described through the liquid phase mass transfer coefficient and can be defined for a bubble that follows Stokes' law (Clift et al., 1978):

$$k_L = \frac{D_L}{d}\left[1 + \left(1 + \frac{dU}{D_L}\right)^{\frac{1}{3}}\right]$$ Equation 2 – 1

Where k_L is the liquid side mass transfer coefficient (m s^{-1}), D_L is the diffusivity of gas in liquid (m^2 s^{-1}), d is the bubble diameter (m) and U is the bubble rising velocity (m s^{-1}). The Stokes' equation (Talaia, 2007) is valid for particles/bubbles at low Reynolds numbers (< ~ 1) (Park et al., 2017):

$$U_{\infty(S)} = \frac{gd^2(\rho_l - \rho_g)}{18\mu_l}$$ Equation 2 – 2

Where $U_{\infty(S)}$ is the Stokes' terminal rising velocity (m s^{-1}), g is gravitational acceleration (m s^{-2}), ρ_l is liquid density (kg m^{-3}), ρ_g is gas density (kg m^{-3}) and μ is dynamic viscosity of the liquid (Pa s). When the bubble size is < ~ 100 µm the internal pressure within the bubble increases its surface rigidity leading to a reduction in frictional resistance such that the terminal rise velocity deviates from that described by Stokes' law and is better described by the Hadamard-Rybczynski equation (Parkinson et al., 2008):

$$U_{\infty(H-R)} = \frac{3}{2}U_{\infty(S)} = \frac{gd^2(\rho_l - \rho_g)}{12\mu_l}$$ Equation 2 – 3

Where $U_{\infty(H-R)}$ is the Hadamard-Rybczynski terminal rising velocity (m s^{-1}). In addition, decreases in bubble size reduces the associated buoyant force leading to a low rise velocity and hence a longer contact time such that a higher proportion of gas is retained in the bulk liquid and is not lost as off-gas (Shangguan et al., 2018). It is therefore expected that this will increase the rate of mass transfer and gas utilisation efficiency (Suwartha et al., 2020). The larger bubble sizes associated with conventional ozonation means that the bubbles will rise quickly through the liquid and burst at the surface (Figure 2 – 2). The large bubble size in conventional contactors has been associated with non-ideal mixing behaviours such as internal recirculation within the reaction chambers and the formation of dead-zones in the centre of the chambers (Kim et al., 2010). In order to

aid mixing, counter-current contactors are often used in favour of co-current contactors and can achieve better contact between the gas and liquid (Jakubiak and Kordylewski, 2011). A number of other factors impact the overall rate of mass transfer including the rate of ozone self-decomposition (Wu et al., 2019), the concentration gradient between the gas phase and the steady state liquid concentration, the gas flow rate (in terms of its impact on bubble size and number density) and accumulation and surface coating of material at the bubble-liquid interface. The following considers how these factors influence the mass transfer of ozone.

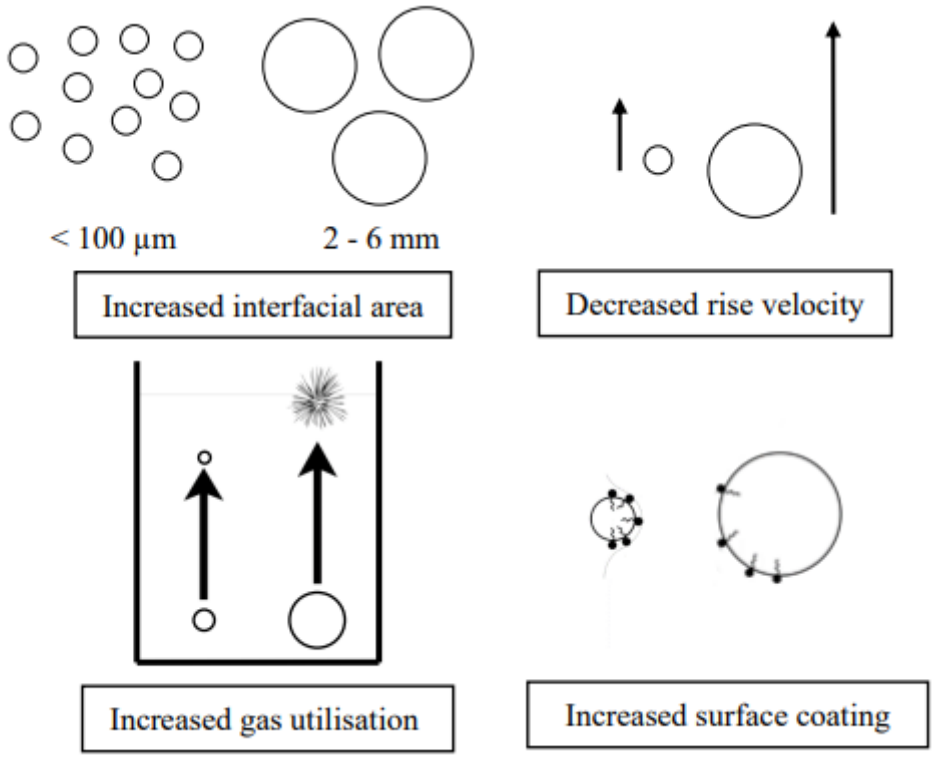

Figure 2 – 2. Notable properties of microbubbles in comparison to conventional bubbles.

2.2.1. Volumetric Mass Transfer Coefficient, $k_L a$

The liquid side mass transfer, k_L, cannot be easily determined experimentally as in most cases the interfacial area is either unknown or cannot be reliably measured (Khuntia et al., 2012). However, the volumetric mass transfer coefficient, $k_L a$, which is defined as a function of k_L and the interfacial area, a (m^{-1}), can be more easily obtained. Thus, the rate

of mass transfer is often expressed in terms of $k_L a$: The measured volumetric mass transfer coefficient is also dependent upon the rate of self-decomposition and the steady-state concentration (Wu et al., 2019):

$$\frac{dC}{dt} = (k_L a - k_D)(C_s - C) \qquad \text{Equation 2 – 4}$$

$$k_L a^M = k_L a - k_D \qquad \text{Equation 2 – 5}$$

Where $k_L a^M$ is the measured volumetric mass transfer coefficient (min^{-1}), $k_L a$ is the actual volumetric mass transfer coefficient (min^{-1}), C_s is the steady-state dissolved ozone concentration (mg L^{-1}), C is the dissolved ozone concentration (mg L^{-1}) and k_D is the rate constant for ozone self-decomposition (min^{-1}). The reporting of $k_L a$ in the literature is somewhat inconsistent with some studies reporting a measured $k_L a$ without the inclusion of k_D and other studies reporting an actual $k_L a$ including k_D in the calculation. For this reason, all of the data has been recalculated to include k_D. The actual $k_L a$ has been used if reported. If an apparent $k_L a$ was reported, then an average k_D was applied to ensure a consistent comparison has been made (Section 2.2.6).

The determination of the volumetric mass transfer coefficient for ozone can be problematic due to its relative insolubility and instability in water (Huang et al., 1998), low rate of mass transfer and losses in the off-gas (Mitani et al., 2005). It is also influenced by direct and indirect reactions with pollutants (Chiu et al., 2003). For example, it has been established that the consumption of ozone through the reaction with contaminants can be faster than the rate of mass transfer into the water (Levanov et al., 2017). As such, mass transfer experiments are usually performed in deionised water at a controlled temperature where consumption by contaminants is negligible and self-decomposition is the only reaction route (Wu et al., 2019). There have been several studies that have directly compared the ozone $k_L a$ for microbubbles and conventional bubbles (Shin et al., 1999; Xu et al., 2012; Zheng et al., 2015; Zhang et al., 2018; Gao et al., 2019; Wu et al., 2019; Nam et al., 2021). The range of $k_L a$ values reported for microbubbles at pH 7 ranged between 0.09 and 1.5 min^{-1} and between 0.1 and 1.4 min^{-1} for conventional bubbles (Figure 2 – 3). The maximum observed enhancement was 5.2 times (Zhang et al.,

2018). There were two instances where no improvement was observed. In both of these cases, the apparent $k_L a$ was extremely small and the applied k_D represented a large proportion of the total value. When the above data was aggregated and considered as a whole, the average enhancement in $k_L a$ when comparing microbubble to conventional bubble trials was 2.5 ± 1.3 times. From this analysis it was evident that while there was a large variation in the enhancement factors reported across different studies, microbubbles outperformed conventional systems. The microbubble enhancement factor is commonly attributed to an increase in surface area. The small size of microbubbles promotes a larger interfacial area to maximize contact between the gas and liquid (Akimov et al., 2011). As an example, the surface area to volume ratio of a 25 mm bubble compared to a 2 µm bubble is 80 times higher for a given volume of gas. However, it should be noted that in most cases, the measurement and reporting of bubble diameters (especially for conventional bubbles), is not routinely carried out. In almost all cases, conventional bubble size is approximated, or not stated, so a determination of the relationship between $k_L a$ and bubble diameter is not possible. Further to this, there is considerable variation in the reported $k_L a$ values between authors. This reflects variations in the systems used, both in terms of the bubbles generated with respect to their size, distribution and the experimental apparatus used to conduct the measurements. This includes differences in: the method of generating bubbles; bubble diameters and concentration; reactor geometries and liquid depths; and gas flow rates ([SI] Table 2 - S2). Some of the important bubble parameters such as size and concentration are often either not reported or do not consider variable bubble size distributions. For example, we could only find one example where bubble concentration was reported in the paper (micro/nanobubble concentration between 4.35 and 4.63 x 10^7 bubbles per mL (Hu and Xia, 2018)). It is therefore particularly difficult to compare the effects of different parameters on ozone transfer across multiple studies. Accordingly, when comparing data across multiple studies, the underlying trends have been considered more important than consideration of absolute data values. Direct comparison between microbubble and conventional bubble systems from the same study are usually more reasonable as they are typically performed under similar experimental conditions. The following section considers how different variables influence mass transfer for both conventional and microbubble ozonation.

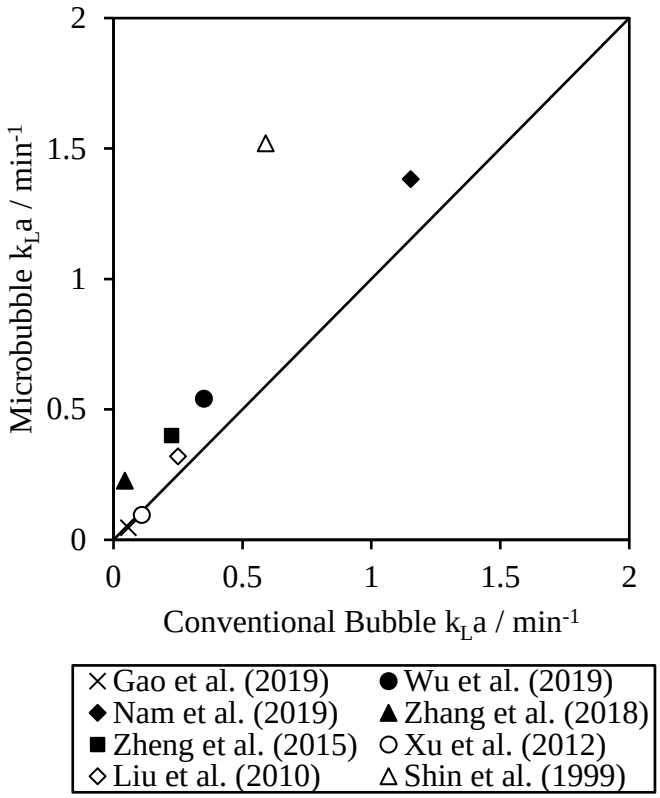

Figure 2 – 3. Volumetric mass transfer coefficient for microbubbles and conventional bubbles in direct-comparison experiments at pH 7.

2.2.2. Effect of pH on $k_L a$

In ozonation, the pH of the water is an important parameter because it influences the self-decomposition of ozone. At higher pH, ozone decomposes more quickly due to the increased amount of hydroxide ions present in the bulk solution which initiate and accelerate the self-decomposition reaction chain. The effect of changing pH is observed through the associated changes in the water chemistry with the impact seen in relation to the rate of self-decomposition (Section 2.2.6) and steady-state concentration (Section 2.2.7). Direct comparison of microbubbles and conventional bubbles at pH's other than 7 is rarely investigated (Figure 2 – 4). One example comes from Wu et al. (2019) who observed that the $k_L a$ increased with increasing pH from 0.34 min^{-1} at pH 3 up to 0.58 min^{-1} at pH 9 for microbubble ozonation. Lower values were seen for conventional bubble ozonation, increasing from 0.27 min^{-1} at pH 3 up to 0.37 min^{-1} at pH 9. Comparison under acidic conditions have reported enhancement factors of 1.8 at pH 2 (Chu et al., 2007) and

2.1 at pH 3 (Sun et al., 2020) when comparing microbubbles with conventional bubbles. There have also been microbubble studies which have looked at the effect of changing pH without comparison with conventional bubble systems that indicate an enhancement in transfer coefficients under more alkaline conditions (Figure 2 – 5). The observed increase in $k_L a$ with increasing pH has been described as a function of k_D (Khuntia et al., 2013). As k_D increases with pH, the steady state dissolved ozone concentration decreases. Therefore, at high pH a steady state ozone concentration is reached faster than for a comparably lower pH system. To illustrate, in a tap water study using microbubbles of < 30 µm diameter, the $k_L a$ increased from 0.30 min^{-1} to 0.41 min^{-1} as the pH increased from 6 to 9 (Jabesa and Ghosh, 2016a). This has also been observed with different ozone input concentrations where the $k_L a$ ranged from 0.10 – 0.14 min^{-1} at pH 6 to 0.16 – 0.24 min^{-1} at pH 9 for input concentrations of 329 – 1000 mg L^{-1} with a microbubble diameter of 25 µm. Increasing $k_L a$ as pH goes up is in line with expectations since $k_L a$ is directly linked to both k_D and the steady-state dissolved ozone concentration.

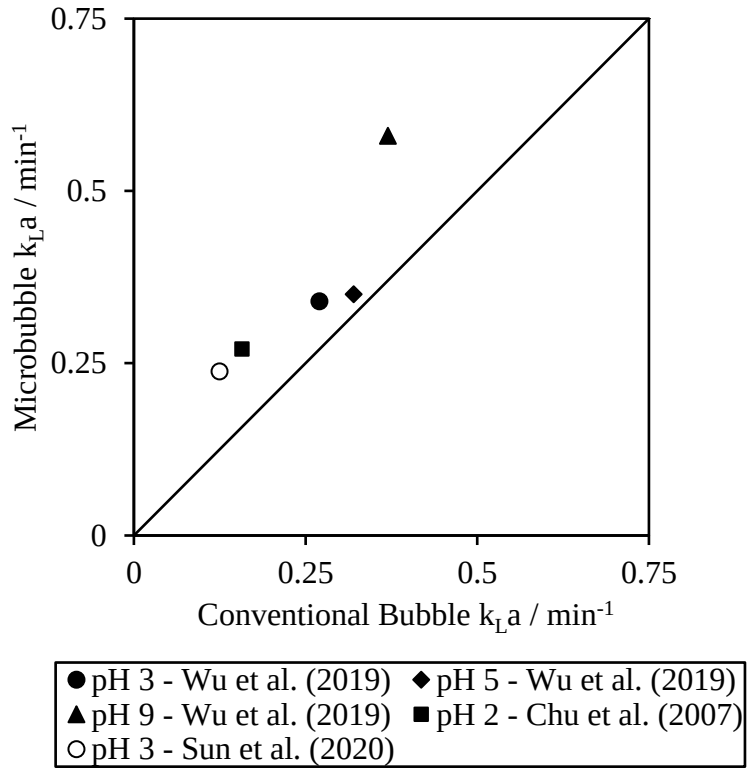

Figure 2 – 4. Volumetric mass transfer coefficient for microbubbles and conventional bubbles at varying pH's in direct-comparison experiments.

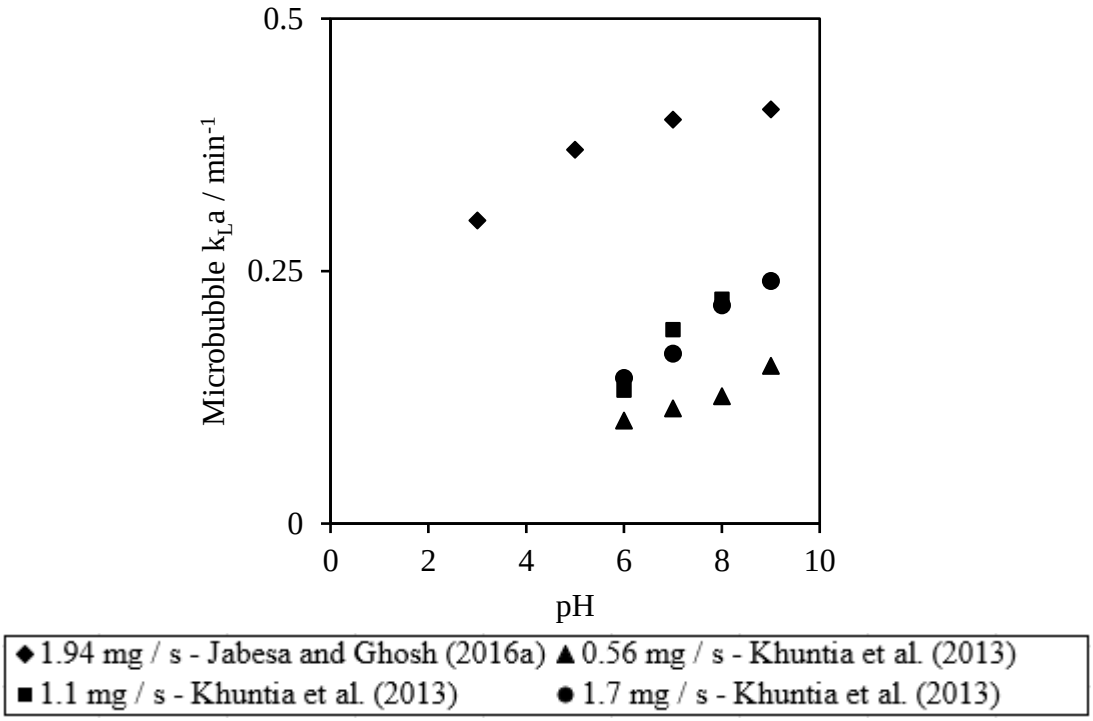

Figure 2 – 5. The change in ozone $k_L a$ for microbubbles with increasing pH at different ozone input doses.

2.2.3. Effect of Ozone Input Concentration on $k_L a$

Increasing the concentration of ozone in the input gas is one method for increasing the quantity ozone delivered per unit of time. For a given ozone gas input concentration, it has been observed that microbubble systems achieve a higher $k_L a$ when directly compared with conventional bubble systems (Table 2 – 1). With an ozone input concentration that ranged from 10 to 233 mg L^{-1}, the range of reported $k_L a$ values was between 0.023 – 1.5 min^{-1} for microbubbles and 0.0055 – 1.11 min^{-1} for conventional bubbles. The maximum observed enhancement was 5.2 times with microbubbles (Zhang et al., 2018). The minimum observed enhancement was 1.2 times (Liu et al., 2010). The average observed enhancement factor was 2.5 ± 1.3 times. While it is apparent that more reliable comparisons are needed, the data shows that for a given ozone concentration, the mass transfer of ozone into water is significantly higher for microbubbles than when compared to conventional bubbles. The main driver for this improvement is linked to the increased surface area available for gas transfer. The effect of ozone input dose on $k_L a$

has also been studied for microbubbles without comparison to conventional bubbles. Zhang et al. (2013) found that increasing the ozone input dose from 40 to 140 mg L^{-1} resulted in an increase in $k_L a$ from 0.18 to 0.32 min^{-1}. Similarly, Khuntia et al. (2013) found that increasing the ozone input dose from 329 to 1000 mg L^{-1} resulted in an increase in $k_L a$ from 0.11 to 0.17 min^{-1}. In contrast, when the ozone input concentration was increased from 30 to 75 mg L^{-1}, Huang et al. (2020) observed no increase in $k_L a$ which remained at 0.73 min^{-1}. Where an increase has been seen, the authors have explained this as a function of increasing ozone input concentration. Since there is a higher concentration of ozone in the input gas, both the concentration and rate of ozonation increased (Khuntia et al., 2013). An alternative view is that the steady-state concentration should increase linearly with increasing ozone input concentration but $k_L a$ should remain almost constant irrespective of input dose since (Al-Abduly et al., 2014). Further data is needed to confirm whether these mechanisms hold true for all circumstances where microbubbles are used.

Table 2 – 1. Enhancement factor of microbubble $k_L a$ against conventional bubble $k_L a$ for a fixed input concentration.

Input Concentration / mg L^{-1}	Microbubble $k_L a$ / min^{-1}	Conventional $k_L a$ / min^{-1}	Enhancement Factor	Reference
90	0.23	0.11	2.09	Sun et al. (2020)
20	0.54	0.35	1.54	Wu et al. (2019)
25	1.36	1.11	1.23	Nam et al. (2019)
233	0.023	0.0055	4.18	Gao et al. (2019)
47.5	0.23	0.044	5.23	Zhang et al. (2018)
12	0.38	0.17	2.24	Zheng et al. (2015)
36	0.3	0.2	1.50	Liu et al. (2010)
132	0.26	0.14	1.86	Chu et al. (2007)
10	1.5	0.54	2.78	Shin et al. (1999)

2.2.4. Effect of Superficial Gas Velocity on $k_L a$

The gas flow rate determines the total amount of ozone that is delivered per unit time and can impact bubble size and number concentration. It is conventional to express the flow

rate as a superficial gas velocity to account for variations in reactor sizes. The superficial gas velocity is the apparent speed that a gas moves through the liquid as a function of gas flow rate (Muroyama et al., 2013):

$$u_g = \frac{Q_g}{A} \qquad \text{Equation 2 – 6}$$

Where u_g is superficial gas velocity (m s^{-1}), Q_g is gas flow rate (m^3 s^{-1}) and A is cross sectional area (m^2). Typical superficial gas velocities in full scale plants are 0.26 – 0.87 m min^{-1} (Secula et al., 2013) and this compares to experimental systems which vary between 0.0038 and 0.26 m min^{-1}. For a given superficial gas velocity, several comparisons of microbubbles and conventional bubbles are available (Figure 2 – 6). It has been found that the average $k_L a$ enhancement factor is 2.3 ± 1.3 where the minimum enhancement was 1.2 times (Nam et al., 2021) and the maximum was 5.2 times (Zhang et al., 2018). Studies that have looked at the effect of superficial gas velocity for microbubble $k_L a$ have been undertaken but have not been directly compared with results from conventional bubbles. Li and Tsuge (2006) observed a linear increase in $k_L a$ from 0.12 to 0.44 min^{-1} when the superficial gas velocity was increased from 8 x 10^{-3} to 4.8 x 10^{-2} m min^{-1}. Huang et al. (2020) extended the range to higher superficial gas velocities of 6.5 x 10^{-2} to 0.26 m min^{-1} and saw an increase of $k_L a$ from 0.64 to 0.79 min^{-1} for a microbubble system using 20 – 30 µm bubbles in deionized water.

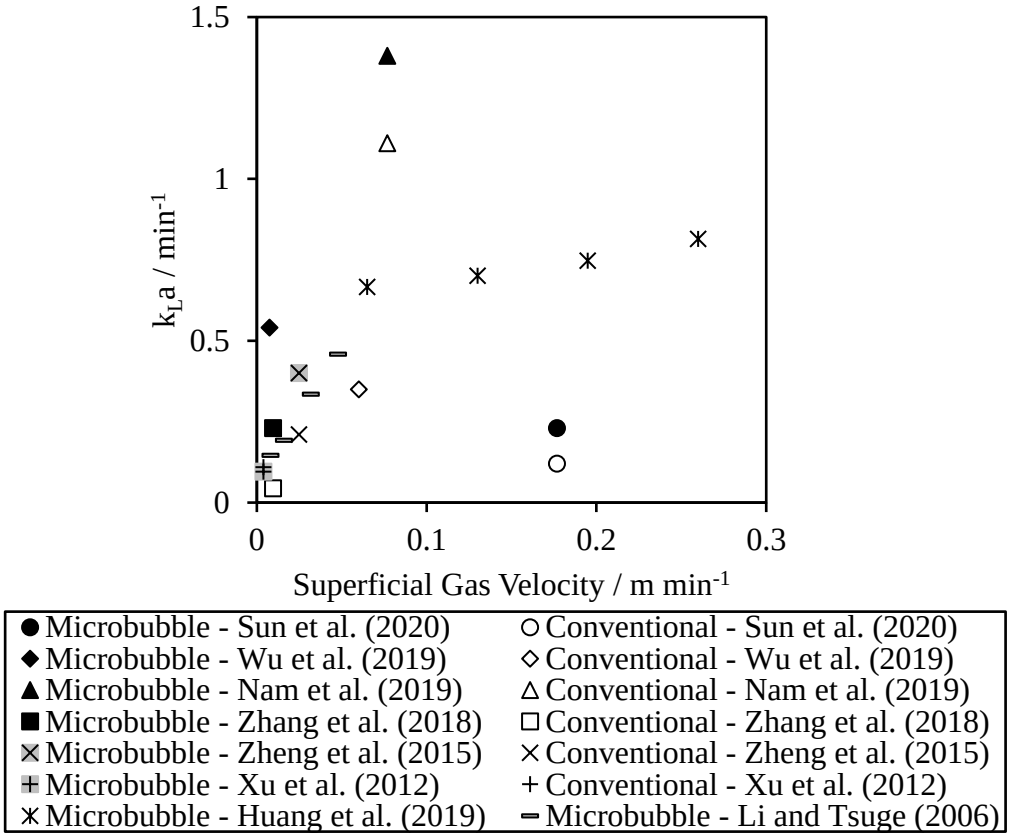

Figure 2 – 6. k_La vs. superficial gas velocity for microbubble and conventional bubble ozonation.

2.2.5. Gas Utilisation Efficiency

Gas utilisation efficiency relates to how much of the supplied gas is transferred into the liquid and is calculated as (Tizaoui and Zhang, 2010; Zhang et al., 2013):

$$UTE = 100\left(\frac{C_{in} - C_{out}}{C_{in}}\right) \qquad \text{Equation 2 – 7}$$

Where UTE is the gas utilisation efficiency (%), C_{in} is the inlet ozone concentration (mg L^{-1}) and C_{out} is the ozone off-gas concentration (mg L^{-1}).

Since the percentage of ozone by weight in the output gas for an air fed ozone generator is typically around 6 % (Achar et al., 2020), optimisation of gas transfer is critical to

minimising energy and associated operating costs. The ability to increase gas utilisation efficiency is one of the most frequently mentioned favourable properties of microbubbles. Despite this, gas utilisation efficiency is one of the least frequently reported measurements and there is a paucity of direct comparisons between microbubbles and conventional bubbles (Table 2 – 2). The studies that have been reported confirm the expected enhancement when using microbubbles. For instance, Zhang et al. (2018) reported a gas utilisation efficiency of 96 % for ~ 51 µm bubbles compared with 60 % for conventional bubbles (size not reported) in a shallow 32 cm deep tank with deionised water. A similar enhancement of 85 % compared with 48 % was also reported by Zheng et al. (2015) who compared < 45 µm bubbles with a conventional system in "clean" water using a 1.2 m deep tank. Similarly, gas utilisation efficiency was observed to improve from 72 – 79 % to 99.0 – 99.5 % in another study that compared conventional bubbles (size not reported) with 50 µm microbubbles (Liu et al., 2010). Tank depth was not reported in this work. The overall view is that microbubbles have great potential for application with respect to gas utilisation efficiency. However, an observation that has consistently arisen from ozonation studies that have compared microbubbles with conventional bubbles has been the use of relatively shallow columns. The maximum column height used was 1.2 m, with some used as low as 0.3 m (Table 2 – 3). However, as has been noted, gas transfer tanks are typically much deeper, typically > 3 m (DeMoyer et al., 2001). This tank depth allows sufficient residence time of conventional bubbles, which rise through the water at much faster rates than small bubbles. As a consequence, the use of shallow column heights biases the results in favour of the microbubble systems due to the differences in residence time as a function of bubble size. To illustrate, the residence time for a 50 µm and 2 mm bubble has been calculated for the different sized column heights used in experiments reported in the literature (Table 2 – 3). Residence time for the larger bubble was between 0.12 and 0.66 s compared to 197 to 1053 s for the microbubble. To date, there has been no work reported that considers equivalent reactor volume normalized for bubble residence time. For instance, the impact of the height required to transfer 50 % of the contents of a bubble has been calculated as a function of bubble size (Figure 2 – 7). In the case of a 50 µm bubble, 50 % of its contents can be transferred in less than 2 m of liquid. For a 7 m deep tank, bubbles must be no larger than approximately 200 µm to ensure 50% utilization (Mueller et al., 2002). If a typical 2 mm

bubble is used, water depths exceeding 9 m would be required. While there is compelling evidence for enhanced gas utilisation when using microbubbles, it is clear that better experimental comparisons are required that take into account bubble residence times in the reactor to determine whether reactor volume as well as tank depth can also be reduced when using microbubbles.

Table 2 – 2. Gas utilisation efficiencies for microbubble (MB) and conventional bubble (CB) ozonation.

Column Height / m	Gas Utilisation Efficiency / %		Gas Utilisation Efficiency / % m^{-1}		Reference
	MB	CB	MB	CB	
Not reported (NR)	92.2 - 99.5	NR	NR	NR	Liu et al. (2018)
0.32	96	60	300	187.5	Zhang et al. (2018)
1.2	85	48	70.8	40	Zheng et al. (2015)
NR	83 - 95	NR	NR	NR	Zhang et al. (2013)
NR	99 - 99.5	72 - 79	NR	NR	Liu et al. (2010)

Table 2 – 3. Reported water heights used in microbubble and conventional bubble comparison experiments.

Column Height / cm	Bubble Residence Time / s			Reference
	50 µm Diameter	2 mm Diameter	Difference	
30 (MB) / 60 (CB)	197	0.25	196.75	Wu et al. (2019)
160	1053	0.66	1052.34	Nam et al. (2019)
30	197	0.12	196.88	Azuma et al. (2019)
80	526	0.33	525.67	Hu and Xia (2018)
31.8	209	0.13	208.87	Zhang et al. (2018)
120	790	0.49	789.51	Zheng et al. (2015)
60	395	0.25	394.75	Xu et al. (2012)
120	789	0.49	788.51	Li and Tsuge (2006)
30	197	0.12	196.88	Shin et al. (1999)

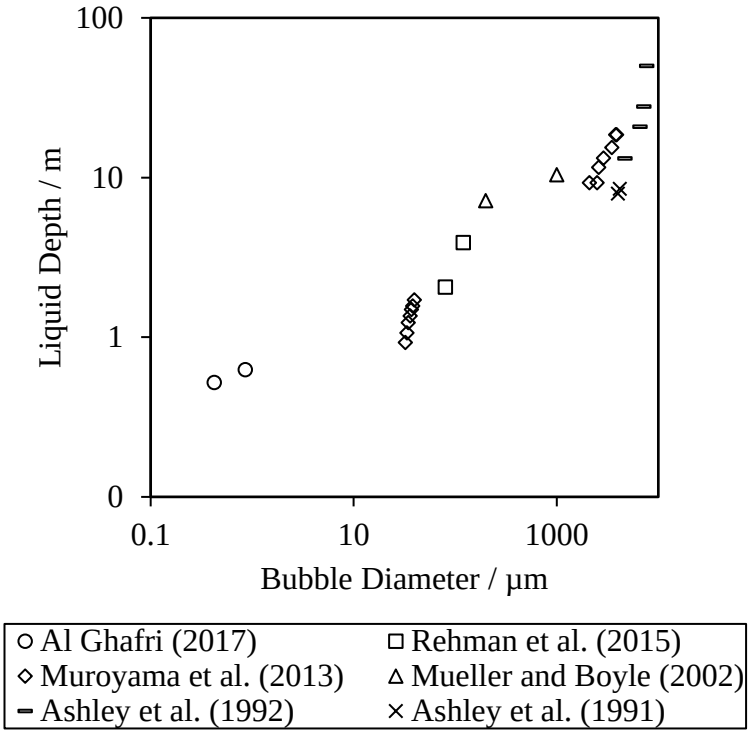

Figure 2 – 7. Liquid depth required for 50 % diffusion to occur for a given bubble diameter.

2.2.6. Rate Constant for Ozone Self-Decomposition, k_D

When ozone is dissolved in water, it undergoes a complex self-decomposition reaction chain. The current generally accepted decomposition model is based around the peroxone process (Reactions 2 – 1 to 2 – 7) (Bezbarua and Reckhow, 2004; Fabian, 2006; Ignatiev et al., 2008). The hydroxide ion is an initiator in the self-decomposition of ozone (Reaction 2 – 1) and the hydroxyl radical, a nonselective, highly oxidizing species, is a desirable decomposition product which can react with compounds that are not readily oxidized by molecular ozone (Reaction 2 – 7). Ozone is not only consumed during decomposition; it is also regenerated. This means that the rate of ozone self-decomposition cannot be inferred from the rate of oxygen and electron transfer but must incorporate the regeneration step (Reaction 2 – 7) (Gardoni et al., 2012).

$O_3 + HO^- \rightarrow O_2 + HO_2^-$	$k_1 = 70$ M^{-1} s^{-1}	Reaction 2 – 1
$O_3 + HO_2^- \rightarrow O_3^{\bullet-} + HO_2^{\bullet}$	$k_2 = 2.8\ x\ 10^6$ M^{-1} s^{-1}	Reaction 2 – 2
$HO_2^{\bullet} \leftrightarrow O_2^{\bullet-} + H^+$	$k_3 = 3.2\ x\ 10^5$ s^{-1} $k_{-3} = 2.0\ x\ 10^{10}$ M^{-1} s^{-1}	Reaction 2 – 3
$O_2^{\bullet-} + O_3 \rightarrow O_3^{\bullet-} + O_2$	$k_4 = 1.6\ x\ 10^9$ M^{-1} s^{-1}	Reaction 2 – 4
$O_3^{\bullet-} + H^+ \leftrightarrow HO_3^{\bullet}$	$k_5 = 5.2\ x\ 10^{10}$ M^{-1} s^{-1} $k_{-5} = 3.3\ x\ 10^2$ s^{-1}	Reaction 2 – 5
$HO_3^{\bullet} \rightarrow HO^{\bullet} + O_2$	$k_6 = 1.1\ x\ 10^5$ s^{-1}	Reaction 2 – 6
$O_3^{\bullet-} + HO^{\bullet} \rightarrow O_3 + HO^-$	$k_7 = 2.5\ x\ 10^9$ M^{-1} s^{-1}	Reaction 2 – 7

A second reaction chain involving HO_4^- and HO_5^- intermediates has since been proposed (Reactions 2 – 8 to 2 – 17) (Sein et al., 2007; von Sonntag, 2008). However, the HO_5^- intermediate has not been observed experimentally (Gardoni et al., 2012).

$O_3 + HO^- \rightarrow HO_4^-$	$k_8 = k_1$	Reaction 2 – 8
$HO_4^- \leftrightarrow HO_2^{\bullet} + O_2^{\bullet-}$	$k_9 \approx 10^7$ s^{-1} $k_{-9} = 5.0\ x\ 10^9$ M^{-1} s^{-1}	Reaction 2 – 9
$HO_2^{\bullet} + O_2^{\bullet-} \rightarrow HO_2^- + O_2$	$k_{10} = 10^8$ M^{-1} s^{-1}	Reaction 2 – 10
$O_3 + HO_2^- \rightarrow HO_5^-$	$k_{11} = k_2$	Reaction 2 – 11
$HO_5^- \leftrightarrow HO_2^{\bullet} + O_3^{\bullet-}$	$k_{12} \approx 10^7$ s^{-1} $k_{-12} = k_{-9}$	Reaction 2 – 12
$HO_2^{\bullet} \leftrightarrow O_2^{\bullet-} + H^+$	$k_{13} = k_3$ $k_{-13} = k_{-3}$	Reaction 2 – 13
$O_2^{\bullet-} + O_3 \rightarrow O_3^{\bullet-} + O_2$	$k_{14} = k_4$	Reaction 2 – 14
$O_3^{\bullet-} \leftrightarrow O^{\bullet-} + O_2$	$k_{15} = 1.94\ x\ 10^3$ s^{-1} $k_{-15} = 3.5\ x\ 10^9$ M^{-1} s^{-1}	Reaction 2 – 15
$O^{\bullet-} + H_2O \leftrightarrow HO^{\bullet} + HO^-$	$k_{16} = 9.6\ x\ 10^7$ s^{-1} $k_{-16} = 1.2\ x\ 10^{10}$ M^{-1} s^{-1}	Reaction 2 – 16
$HO^{\bullet} + O_3 \rightarrow O_2 + HO_2^{\bullet}$	$k_{17} = 1.0\ x\ 10^9$ M^{-1} s^{-1}	Reaction 2 – 17

As such, there is yet no agreed upon model for the self-decomposition of ozone, despite being studied for 100 years (Gardoni et al., 2012). Consensus leans toward the use of first order degradation kinetics (López-López et al., 2007; Vyong Tkhi et al., 2009), although 1.5 order (Kuo et al., 1977; Ku et al., 1996) and second order (Gurol and Singer, 1982; Kong et al., 2003; Ershov and Morozov, 2009) kinetics have also been proposed. Reaction orders that are pH dependent have also been considered (Morooka et al., 1978; Haruta and Takeyama, 1981; Sotelo et al., 1987; Hsu et al., 2002). These differences arise due to the complex reaction chemistry of aqueous ozone and the difficulty of experimental reproducibility (Fábián, 2006). Across the majority of these models, temperature and pressure are considered critical factors because increases in either of these accelerate self-decomposition (Sotelo et al., 1987). Several parameters within the water matrix have also been reported to have significant effects on self-decomposition kinetics including alkalinity, hardness, solids, organic matter and metal ions (Hoigne, 1994). This is because different contaminants, present in trace concentrations (Bińk, 2013), can initiate, promote or terminate the self-decomposition reaction chain depending on how the particular contaminant interacts with molecular ozone and its decomposition products. For instance, if the water matrix contains high concentrations of initiators that promote the decomposition of ozone, then indirect ozonation reactions will predominate. Similarly, appreciable concentrations of compounds that terminate the decomposition reaction chain, for example radical scavengers such as tert-butyl alcohol, will result in the domination of direct molecular ozone reactions (Gardoni et al., 2012). The k_D value in conventional bubble ozonation systems has been experimentally derived or modelled across the full pH range (Figure 2 – 8). In contrast, there have been relatively few attempts to characterize the self-decomposition profile for microbubble systems or compare k_D in microbubble and conventional systems directly. Where the k_D values of microbubble and conventional systems have been compared (Wu et al., 2019) it was found that at pH < 7, the k_D values for both systems were almost identical with values of 0.009 min^{-1} at pH 3 and 0.01 min^{-1} at pH 5. The microbubble system showed a slightly higher k_D at pH 7 with a value of 0.031 min^{-1} compared with 0.023 min^{-1} for the conventional system. The difference between the two systems increased further at pH 9 with values of 0.16 and 0.14 min^{-1} for the microbubble and conventional bubble systems, respectively. The increase in k_D is promoted at higher pH when there are more hydroxide ions present in the water

since the hydroxide ion initiates the self-decomposition reaction chain (Equations 2 – 8 and 2 – 15). This leads to a higher concentration of hydroxyl radicals since it is a product of self-decomposition and more extensive initiation of the reaction chain will result in higher concentrations of decomposition products (Equations 2 – 13 and 2 – 23). This is the reason why pH elevation is considered as one of the most effective methods for enhancing ozonation processes through increased hydroxyl radical formation (Miklos et al., 2018). The explanation for the increase in k_D for microbubbles over conventional bubble systems is frequently explained by an increase in hydroxyl radical formation for the microbubble systems as a result of the spontaneous collapse of these smaller bubbles. It has been reported that, since the internal pressure of a bubble is inversely proportional to its spherical diameter, a localized region of high pressure is formed during the collapsing process and forms a hot-spot due to adiabatic compression (Agarwal et al., 2011). It has been proposed that this phenomena causes the spontaneous generation of hydroxyl radicals due to pyrolytic decomposition of ions at the gas liquid interface. There is some evidence to suggest that strongly acidic conditions could alter the zeta potential such that bubble collapse is accelerated enough due to increased repulsion of the bubble wall to cause the generation of hydroxyl radicals (Takahashi et al., 2007). Another study found that the k_D for microbubble ozonation in deionized water was higher than that seen for conventional bubbles with values of 0.049 min^{-1} and 0.0135 min^{-1} (Zhang et al., 2018). Again, the increase in k_D was attributed to the spontaneous generation of hydroxyl radicals upon the collapse of microbubbles. Increased hydroxyl radical formation from bubble collapse in microbubble ozonation has also been reported to increase the degradation rate of pollutants (Section 2 – 3). However, it has been argued that the collapse of a microbubble is not strong enough to cause the spontaneous generation of hydroxyl radicals under normal conditions with no external stimulus since this would require localised temperatures in the region of 5000 Kelvin. Such conditions can normally only be achieved when using a stimulus such as ultrasound (Takahashi et al., 2007; Agarwal et al., 2011). In most reported cases of reactive oxygen species being formed directly from bubble collapse, these observations relate to small nanobubbles (Liu et al., 2016). The increased production of hydroxyl radicals in microbubble systems is therefore still under debate and is an area that warrants further investigation. This is particularly the case when considered alongside other reported k_D values for microbubbles and

conventional bubbles that have not been compared directly in the same studies (Figure 2 – 8). These values have been aggregated and averaged for both microbubbles and conventional bubbles to provide a comprehensive comparison between the two. The comparison shows that the k_D is, on average, slightly lower for microbubbles than for conventional bubbles, albeit not statistically different. To illustrate, the k_D average value from 6 researchers for microbubbles was 0.026 ± 0.014 min^{-1} at pH 7 (Kukuzaki et al., 2010; Khuntia et al., 2013; Jabesa and Ghosh, 2016b; Zhang et al., 2018; Wu et al., 2019). The average k_D value from 9 researchers for conventional bubbles was 0.047 ± 0.038 min^{-1} at pH 7 (Sotelo et al., 1987; Gao et al., 2005; Ignatiev et al., 2008; Lovato et al., 2009; Uhm et al., 2009; Valdes et al., 2009; Dehouli et al., 2010; Zhang et al., 2018; Wu et al., 2019). The evidence therefore points to the view that the improvements in microbubble performance are more linked to the fact that these small bubbles reside in the bulk liquid and diffuse their contents longer than is seen for conventional bubbles rather than accelerated hydroxyl radical formation from bubble collapse; the latter mechanism only being important for much smaller bubble sizes.

pH	Number of Reports	
	MB	CB
1 - 1.9	-	1
2 - 2.9	-	4
3 - 3.9	1	3
4 - 4.9	-	5
5 - 5.9	3	6
6 - 6.9	-	7
7 - 7.9	5	9
8 - 8.9	-	4
9 - 9.9	3	4
10 - 10.9	-	1
11 - 11.9	-	3
12 - 12.9	-	2
13 - 13.9	-	2
14	-	1

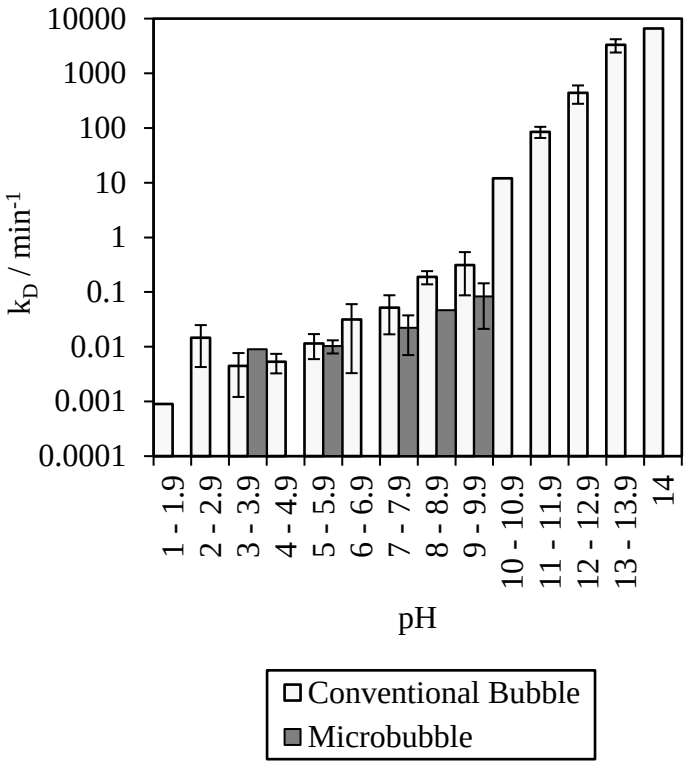

Figure 2 – 8. Aggregated k_D values for microbubble and conventional bubble ozone self-decomposition with respect to pH, where MB is microbubble and CB is conventional bubble.

2.2.7. Steady-State Dissolved Ozone Concentration, C_s

The steady-state ozone concentration is an important process consideration for contactor sizing and design. The aim is to achieve a sufficient ozone residual suitable for treatment, without sending the residual ozone downstream of the contactor. The steady-state ozone concentration is influenced by numerous factors. This includes the gas phase ozone input concentration, gas utilisation efficiency, ozone consumption from reactions with contaminants, temperature, pH and the rate of ozone self-decomposition (Lage Filho, 2010). To determine the steady-state condition for a given system, non-steady-state semi-batch tests are conducted until the mass balance reaches equilibrium (Equation 2 – 8) (Wu et al., 2019):

$$0 = k_L a(C^* - C_s) + k_D C_s \qquad \text{Equation 2 – 8}$$

Where C^* is the steady-state equilibrium ozone concentration (mg L^{-1}) and C_s is the steady-state ozone concentration in the bulk liquid (mg L^{-1}). Due to the self-decomposition of ozone, the steady-state concentration in the bulk liquid is lower than the ozone concentration at equilibrium (Rischbieter et al., 2000). The higher gas utilisation efficiency and higher observed volumetric mass transfer coefficient means that microbubble systems deliver more ozone at a faster rate into the liquid phase than when compared to conventional bubbles. As a result, and based on previous mass transfer observations, a higher steady-state concentration of dissolved ozone is typically achievable when using microbubbles (Figure 2 – 9). Wu et al. (2019) observed a 1.15 – 1.7 times higher steady state ozone concentration for microbubble ozonation across the pH range 3 – 11 when compared to conventional bubble systems. Steady-state concentrations that were 1.1 (Chu et al., 2007), 1.15 (Zheng et al., 2015), 1.23 (Nam et al., 2021) and 2.7 (Takahashi et al., 2012) times higher have also been observed. Zhang et al. (2018) did not observe a significant difference between microbubble and conventional bubble steady-state concentrations, with reported ozone concentrations of 5.5 and 5.7 mg L^{-1}, respectively. However, in this case, the microbubble system reached the steady-state condition considerably faster with $k_L a$ values of 0.227 and 0.044 min^{-1}. Hu and Xia (2018) reported a steady-state ozone concentration of 10.09 and 0.64 mg L^{-1} with microbubbles and conventional bubbles, respectively: an observed increase of 15.8 times. It was not always clear why some studies reported differences in steady state ozone concentration, while others did not. This was most probably linked to the differences in reactor geometry and depth and the variable experimental set-ups used ([SI] Table 2 – S3). In the case of Hu and Xia (2018), the large difference in steady state concentration was thought to driven by the size of the bubbles generated. Hu and Xia (2018) reported the use of "micro-nano" bubbles with a Sauter mean diameter of 247 ± 9 nm, approximately two orders of magnitude smaller than microbubbles used in other studies. The main difference between microbubbles and conventional bubble systems was the rate at which the steady-state was achieved. Where microbubbles and conventional bubbles have been directly compared, the microbubble $k_L a$ has been shown to be higher than for the conventional bubble $k_L a$. The implication of a higher achievable steady-state

concentration for a given ozone input is that the amount of ozone generation required to maintain equivalent treatment is decreased due to the more efficient gas transfer. The following section considers how this translates to degradation of pollutants in water by ozone.

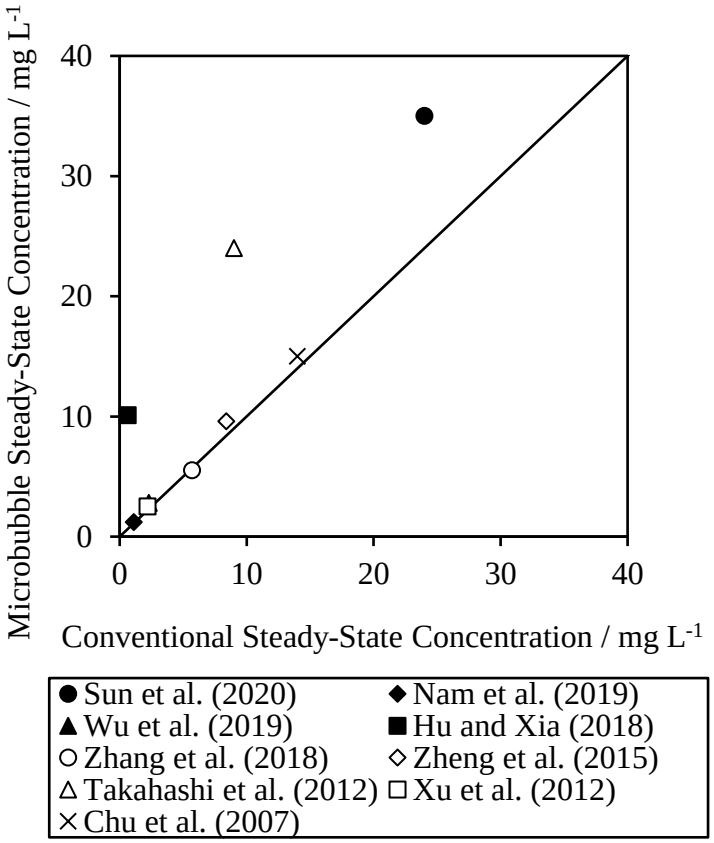

Figure 2 – 9. Observed microbubble steady-state dissolved ozone concentration vs. observed conventional bubble steady-state dissolved concentration in direct comparison experiments.

2.3. Application of Microbubble Ozonation for Compound Degradation

Ozone-based oxidation and disinfection can be broadly categorized into two types of reaction: direct reactions with molecular ozone and indirect radical reactions. Unsaturated organic compounds are typically easily oxidized through direct reactions with molecular ozone (Figure 2 – 10). Indirect ozone reactions are much more complex and stem from the decomposition of ozone into hydroxyl radicals. The hydroxyl radical is associated

with the nonselective removal of recalcitrant compounds due to its powerful oxidizing capability. Degradation of different contaminant groupings by ozone oxidation delivered by microbubbles and conventional microbubbles are considered in the following sections.

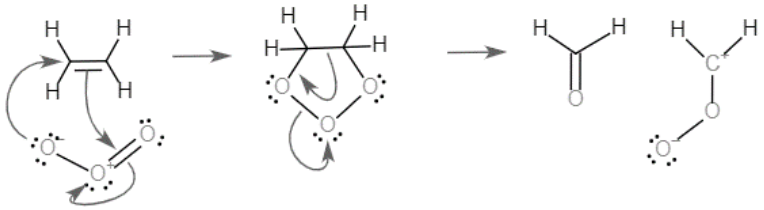

Figure 2 – 10. A typical direct ozone reaction with an unsaturated organic molecule.

2.3.1. Dyestuff

Ozone is commonly used for the degradation of dyes (Takahashi et al., 2012) and the use of microbubble systems has been considered as a way of increasing their rate of removal. Comparison of reported studies supports this view, with enhanced pseudo first-order reaction rate constants between 1.1 and 29 times that seen in the comparative conventional system (Figure 2 – 11). To illustrate, the rate constant for the removal of red 3 R dye was increased from 0.061 min^{-1} in the conventional system compared to 0.11 min^{-1} using ~ 51 µm microbubbles in a 0.32 m deep tank (Zhang et al., 2018). Similar enhancements have been observed for the treatment of Congo red dye from 0.235 min^{-1} with conventional bubble ozonation to 0.385 min^{-1} with microbubble ozonation (Khuntia et al., 2016), reactive black 5 (RB5) dye from 0.092 to 0.16 min^{-1} (Chu et al., 2007) and methyl orange from 8.1 x 10^{-3} to 0.24 min^{-1} (Hu and Xia, 2018). Similarly, Takahashi et al. (2012) tested four different dyes (reactive blue, reactive yellow, direct yellow, orange I) and observed that the rate constant was enhanced by 1.1 – 3.1 times when using a microbubble system with a bubble size of 15 – 40 µm in a water depth of 1.2 m.

Whilst the rate constants for degradation were different, the absolute removal of contaminants over the total duration of the experiments was similar for microbubbles and conventional bubbles. This has been seen over a 60-minute exposure experiment using acid red 3 R dye (Zhang et al., 2018), for reactive blue and orange I dyes over a 120-minute experiment (Takahashi et al., 2012), Congo red dye over 20 minutes (Khuntia et

al., 2012) and for RB5 dye during a 120-minute experiment (Chu et al., 2007). Slight differences were observed when treating reactive yellow and direct yellow dyes in 2 m deep reactor columns. For conventional ozonation, 94 % and 90 % removal was observed for reactive yellow and direct yellow dyes after 90 – 120 minutes. This was in contrast to 95 % and 98 %, respectively for the microbubble ozonation system in a (Takahashi et al., 2012). More significant differences have been reported in an experiment over a shorter duration, treating methyl orange in a 0.8 m tank for 30 minutes (Hu and Xia, 2018). The conventional system achieved only 15 % removal compared to 100 % for the microbubble equivalent. It was posited that this was due to the high concentration of dissolved ozone that could be delivered by the microbubble system which reached a maximum of 10 mg L^{-1} whereas the conventional system achieved only 0.64 mg L^{-1}.

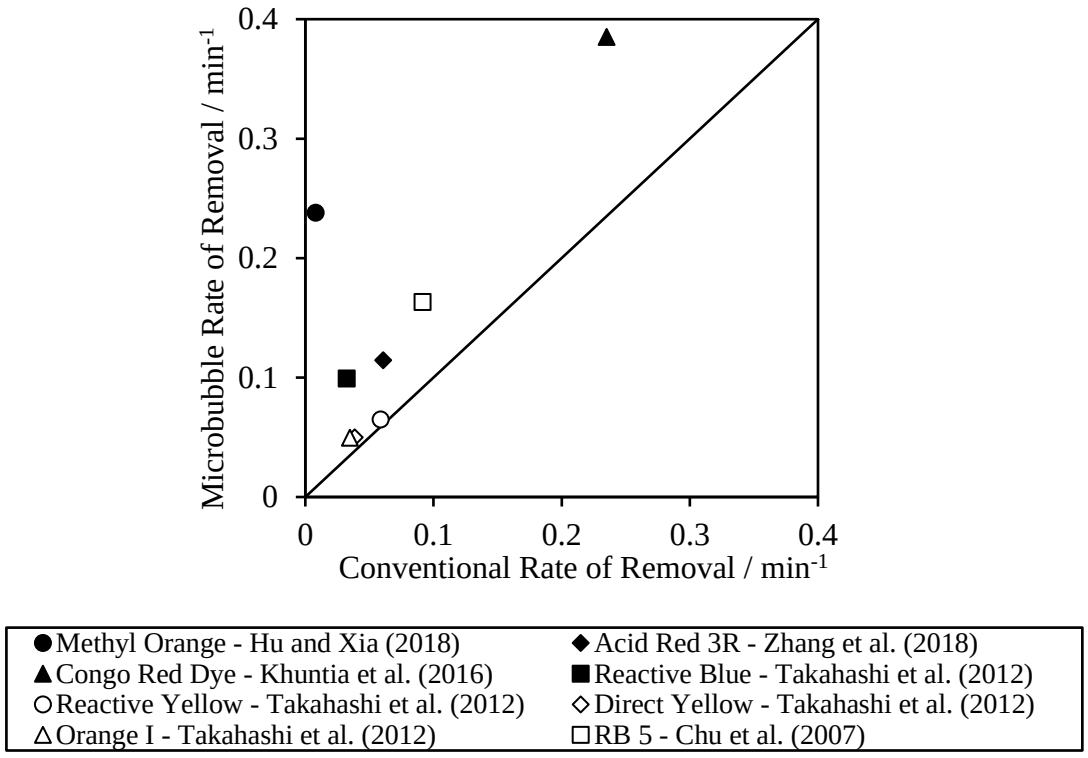

Figure 2 – 11. Microbubble vs. conventional rate of removal of dyestuff in direct comparison experiments.

2.3.2. Pharmaceuticals

The removal of pharmaceuticals with ozone using microbubble and conventional systems reveal a broader range of impacts, but with the majority of cases showing an improvement when using microbubbles (Figure 2 – 12). For instance, Azuma et al. (2019) investigated the removal of 39 pharmaceuticals in a 5-minute test using a 0.3 m deep tank. The majority of the compounds were considered to react relatively well with ozone and resulted in more than 99 % removal irrespective of the bubble size used. In contrast, eleven pharmaceuticals showed significantly enhanced removal with microbubble ozonation. These compounds were not easily removed by ozonation. This offers evidence of the potential to extend the range of treatable compounds with ozone by using microbubble delivery systems. These experiments were normalized for input dose over a fixed time period so it can be inferred that the microbubble systems delivered a higher effective dose of ozone. For these experiments, the ozone input concentration was 6.5 mg L^{-1} with a flow rate of 0.018 m^3 hr^{-1} corresponding to a feed rate of 1.0 mg L^{-1} min^{-1}. The calculation of an effective dose was not possible due to the lack of data on gas utilisation and dissolved ozone concentration. However, based on ozone consumption there was 2.2 times more ozone consumed with the microbubble system after 5 minutes when compared to the conventional system. This reinforces the view that the explanatory reason for the microbubble improvements is primarily related to the increased in the effective ozone dose supplied. Three further pharmaceuticals (atenolol, ethinylestradiol, and ibuprofen) were investigated by Lee et al. (2019) and it was found a 1.3 – 2.5 times improvement in the total removal after 5 minutes of ozonation with microbubble ozonation compared with the conventional system. Whilst the overall removal is important, the rate of degradation should also be considered as it gives a more explicit comparison of the performance differences between microbubbles and conventional bubbles. A faster rate of degradation was observed for 35 of the 39 pharmaceuticals for the microbubble system. The range of removal enhancements was between 1.05 and 104 times, with a median of 2.4, for the microbubble system over the conventional bubbles (Azuma et al., 2019). The explanation for these observations was consistent with an increase in the effective ozone dose applied in the microbubble reactor, which in turn led to higher ozone consumption and oxidation. It should be noted that these experiments were performed in a shallow reactor (0.3 m) that would provide much longer residence times for the microbubbles, giving them a longer

time period over which to discharge their contents when compared to the conventional bubbles.

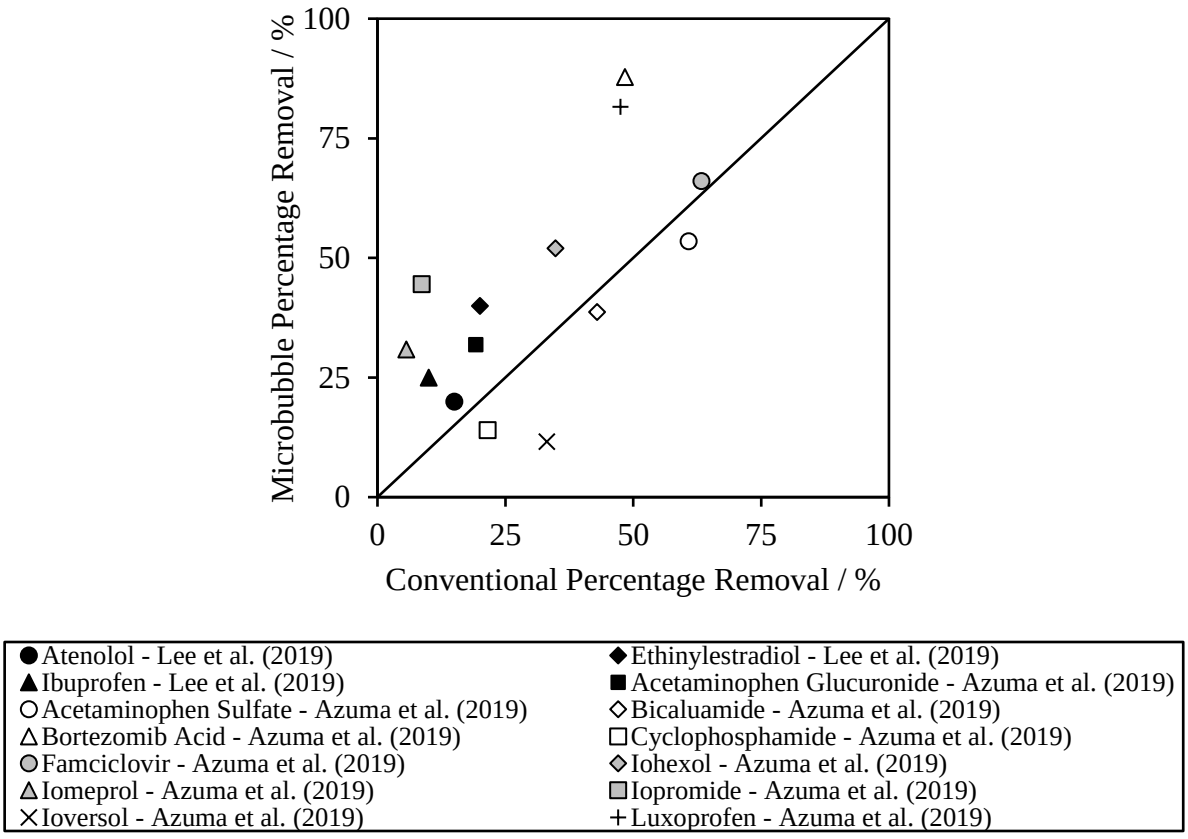

Figure 2 – 12. Microbubble percentage removal vs. conventional percentage removal for pharmaceuticals in direct comparison experiments.

2.3.3. Other Organic Compounds

Microbubble ozonation has been shown to significantly enhance the rate of degradation of a range of other organic compounds (Figure 2 – 13). For example, the switch from conventional bubble to microbubble ozonation significantly improved the rate of degradation of p-nitrophenol, with the rate constant increasing from 0.015 to 0.16 min^{-1} (Cheng et al., 2019), nitrobenzene from 0.032 to 0.10 min^{-1} (Wu et al., 2019) and the heterocyclic compound 1,4-dioxane with an increase from 0.001 to 0.0025 min^{-1} (Xu et al., 2012). For other compounds, a more modest enhancement has been observed, for example for phenol that had an enhancement from 0.072 to 0.30 min^{-1} based on a 20 – 50

μm microbubble system with a water depth of 0.3 m (Wu et al., 2019). The pH of the water has been established to be critical on the rate of compound degradation as the rate of ozone self-decomposition and the generation of hydroxyl radicals are both heavily dependent upon pH. For instance, Wu et al. (2019) tested the effectiveness of microbubble ozonation of phenol and nitrobenzene at different pH values (Figure 2 – 14). Phenol is a compound that is readily degraded in the presence of both molecular ozone and hydroxyl radicals. It is reported to have a reaction rate constant with molecular ozone of 1.8×10^5 L mol^{-1} s^{-1} (Joshi and Shambaugh, 1982) compared with 6.6×10^9 L mol^{-1} s^{-1} for hydroxyl radicals (Buxton et al., 1988). Nitrobenzene is a compound that has a very low reactivity with molecular ozone, with a rate constant of 9×10^{-2} L mol^{-1} s^{-1} (Hoigné and Bader, 1983). This is negligible compared to its reaction rate with the hydroxyl radical, reported to be $3.2 \pm 0.4 \times 10^9$ L mol^{-1} s^{-1} (Neta and Dorfman, 1968; Beltrán, 2004). Thus, the extent of degradation of nitrobenzene gives an indirect indication of hydroxyl radical production. The degradation rate of both compounds increased with increasing pH (Wu et al., 2019). For example, the degradation rate constant for the microbubble ozonation of phenol increased from 0.16 min^{-1} at pH 3 to 0.31 min^{-1} at pH 7 to 0.43 min^{-1} at pH 11 in which the dissociation of phenol at high pH may have also contributed. The rate constants were lower for the conventional bubbles but increased from 0.037 min^{-1} at pH 3 to 0.072 min^{-1} at pH 7 and 0.24 min^{-1} at pH 11. For nitrobenzene, the rate constants were less than those seen for phenol but increased with an increase in pH for both systems. To illustrate, the degradation rate constant increased from 0.014 min^{-1} at pH 3 to 0.032 min^{-1} at pH 7 and to 0.061 min^{-1} at pH 11 for the conventional systems. Higher rate constants were seen for the microbubble system which increased with pH from 0.037 min^{-1} at pH 3 to 0.10 min^{-1} at pH 7 and to 0.16 min^{-1} at pH 11. These results are consistent with the increase in hydroxyl radical formation with increasing pH as a result of the self-decomposition of ozone (Section 2.2.6). In some cases, the reported rates of removal with microbubble ozonation has not followed the expected increase with pH. For example, Khuntia et al. (2016) reported that an increase in pH from 3 to 7 to 9 resulted in a consistent increase in the rate of colour removal of Congo red dye with conventional bubble ozonation from 0.21 to 0.235 to 0.255 min^{-1}. The microbubble system, however, followed a different pattern in which reaction kinetics were similar at pH 3, 7 and 9, resulting in rate constants of 0.40, 0.385 and 0.41 min^{-1}, respectively. In this case, the rate constants for degradation

of this compound were comparatively high, suggesting that the compound was efficiently degraded by ozone. As there was little sensitivity to pH, molecular ozone was likely to be responsible for breaking down the dye molecule and hence the removal of colour from the water. The results show that in most comparisons, microbubble processes have faster reaction kinetics than seen for conventional bubbles for a range of contaminants and micropollutants. The pH of the reaction is important for a range of compounds, with higher pH increasing the reaction rate, a result consistent for both conventional bubble and microbubble ozonation. The degree of improvement is dependent on the sensitivity of the compound to degradation by either ozone or hydroxyl radicals.

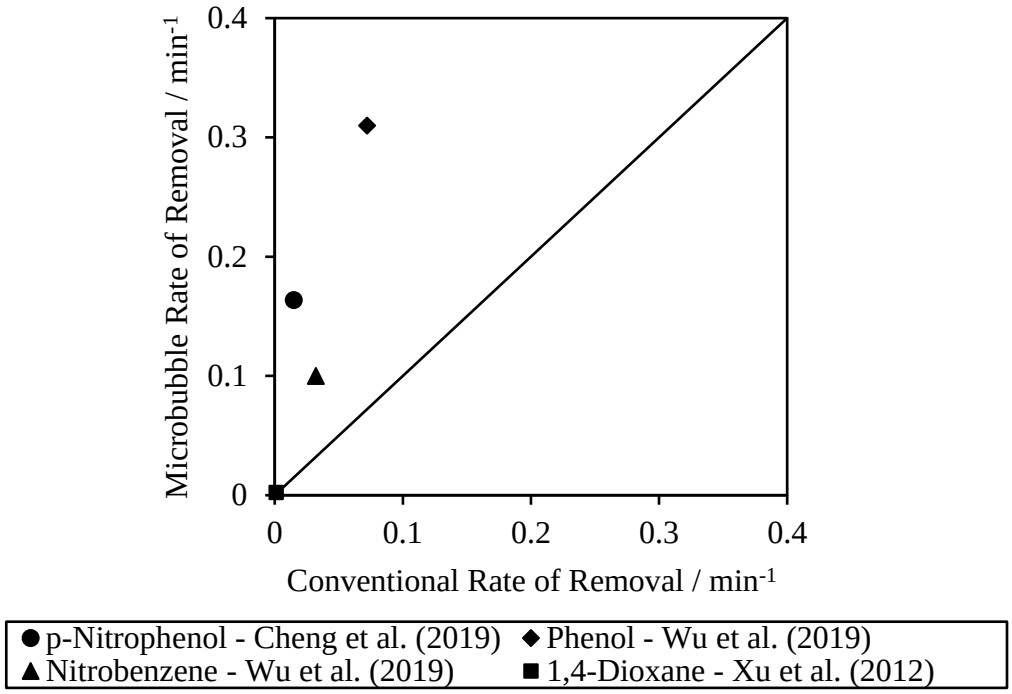

Figure 2 – 13. Microbubble rate of removal vs. conventional rate of removal for organic compounds where they have been directly compared.

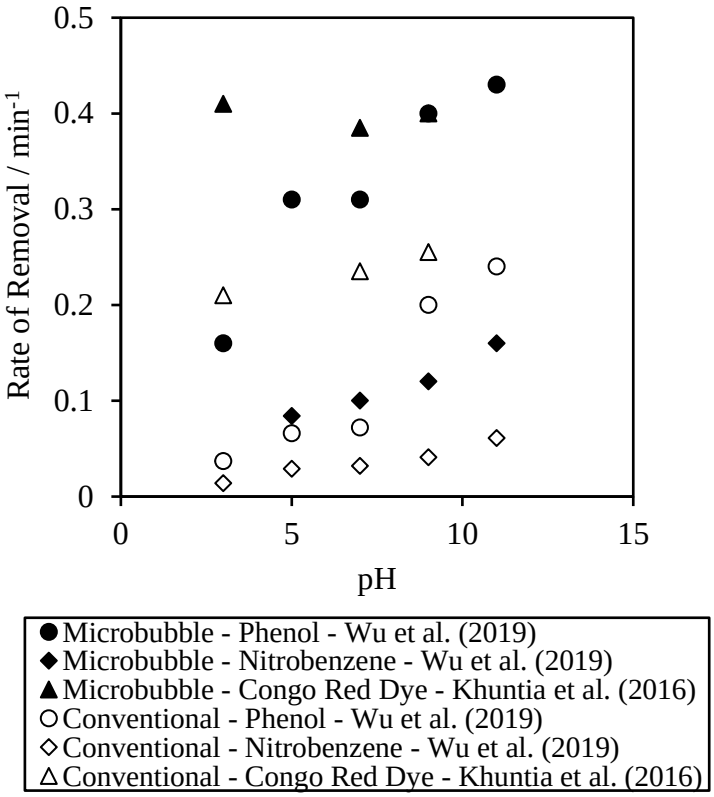

Figure 2 – 14. The impact of increasing pH on the rate of removal of various compounds for microbubbles and conventional bubbles.

2.3.4. Disinfection

Several studies have demonstrated the disinfection capability of microbubbles when used in conjunction with ozonation (Table 2 – 4). For example, the inactivation of *F. oxysporum f. sp. melonis* reached the detection limit in 45 seconds with microbubble ozonation compared with 60 seconds for conventional bubble ozonation with a bacterial concentration of 1 x 10^3 – 1 x 10^4 colony-forming units (CFU) mL^{-1} and an ozone concentration of 1.5 mg L^{-1} (Tamaki et al., 2018). Similarly, Kobayashi et al. (2011) found 2.6 log of surviving cells with microbubble ozonation after 180 seconds compared with 2.9 log for conventional bubble ozonation with the same microorganism at a concentration of 1.0 x 10^3 CFU mL^{-1} and an ozone dose of 0.1 mg L^{-1}. Studies that include a direct comparison with conventional bubble ozonation have rarely been conducted and several studies have assessed the disinfection capability of microbubble ozonation

without comparison. For example, 2.0 and 2.6 log reduction for *Alternaria solani sorauer conidia* and *S. typhimurium* at concentrations of 1 x 10^5 and 1 x 10^6 – 1 x 10^7 CFU mL^{-1} have been observed with microbubble ozonation at ozone doses of 1.6 and 1.0 mg L^{-1} respectively (Phaephiphat et al., 2018; He et al., 2015). In addition, disinfection efficienies of 96.11 and 97.92 % have been reported for *S. agalactiae* and *A. veonii* at initial concentrations of 3.45 x 10^6 and 1.65 x 10^6 CFU mL^{-1} have been reported after 10 minutes of ozonation (Jhunkeaw et al., 2021). 100 % disinfection efficiency has been reported on two occasions for *V. parahaemolyticus* at initial concentrations of 1 x 10^6 and 1.8 x 10^5 CFU mL^{-1} after 5 (Imaizumi et al., 2018) and 6 (Nghia et al., 2021) minutes of ozonation.

Table 2 – 4. Disinfection applications for microbubble ozonation where CFU is colony-forming units.

Target	Concentration (CFU mL^{-1})	Microbubble Performance	Reference
S. agalactiae	3.45×10^6	96.11 % disinfection efficiency	Jhunkeaw et al. (2021)
A. veronii	1.65×10^6	97.92 % disinfection efficiency	
V. parahaemolyticus	10^6	100 % disinfection efficiency	Nghia et al. (2021)
V. parahaemolyticus	1.8×10^5	100 % disinfection efficiency	Imaizumi et al. (2018)
S. typhimurium	$1 \times 10^6 – 1 \times 10^7$	2.6 log reduction	Phaephiphat et al. (2018)
F. oxysporum f. sp. melonis	$1 \times 10^3 – 1 \times 10^4$	Reached detection limit within 45 seconds	Tamaki et al. (2018)
Alternaria solani sorauer conidia	1×10^5	2.0 log reduction	He et al. (2015)
F. oxysporum f. sp. melonis	1×10^3	2.6 log reduction	Kobayashi et al. (2011)

2.4. Challenges and Future Prospects of Microbubble Ozonation

The advantages of enhanced ozone mass transfer for microbubble systems have been shown to be predominantly related to the increase in specific surface area and the increased bubble residence time within the water column. The review of comparative studies has shown that microbubbles afford opportunities for improving existing ozonation systems. The following section discusses how microbubbles could be practically implemented by considering: (1) microbubble generation methods; (2) reactor configurations; and (3) further challenges to address.

2.4.1. Microbubble Generation Methods

The main challenges associated with the application of microbubble generators in water treatment are around scale-up and process design. At present, the vast majority of work, particularly for low-powered microbubble generators, has been carried out at laboratory and pilot scale (Table 2 – 5). Those systems that have been developed for full-scale implementation can treat water flows of around 1 megalitre per day (MLD) with an energy requirement under 1 kWh m^{-3}. As such, commercially available microbubble generators would only be able to treat relatively modest flows. However, advancements in generation systems are making the application more feasible for larger systems. There are several different methods for generating microbubbles and their modes of action has been comprehensively reviewed previously (Khuntia et al., 2012; Parmar and Majumder, 2013; Temesgen et al., 2017). All of these generators produce bubbles based on a reduction in pressure caused by surface tension and a change in energy causing cavitation and bubble formation (Temesgen et al., 2017). Cavitation can be achieved hydrodynamically or through the application of an acoustic field. The hydrodynamic approach is the most widely used method due to a more favourable energy balance and is the focus of the discussion here. The most common types of hydrodynamic microbubble generator are ones that use turbulent flow, mechanical shear, pressurized dissolution and forced bubble detachment (Table 2 – 5). Specifically for ozone applications, mechanical shear and pressurized dissolution types of system have been used, often in combination with one another. Mechanical shear microbubble generators utilise some form of rotating and pumping device, using centrifugal pumps (da Silva Henauth et al., 2017), turbine

pumps (Yao et al., 2016) or external mixing (Li et al., 2016). These systems physically shear the injected gas into microbubbles. In some cases, automatic gas suction is achievable through the introduction of a pressure from a rapidly rotating impeller, but such systems are often used in conjunction with a gas supply (Wu et al., 2019). There is currently little published evidence of large-scale application for ozonation using these types of microbubble generator, with the highest reported liquid flow rate of 4.5 m^3 hr^{-1} (Nam et al., 2021). These types of microbubble generator are often limited by their capacity for gas flow, which is often only a small percentage of the liquid flow capacity. The highest reported gas flow rate for ozonation was 0.25 m^3 hr^{-1} with a liquid flow rate of 2.4 m^3 hr^{-1} (Takahashi et al., 2012). However, these types of microbubble generators have potential at larger scales, as commercial units are available for dissolved air flotation applications for liquid flow capacities of up to 58 m^3 hr^{-1} and a gas flow capacity of 4.6 m^3 hr^{-1} with an energy consumption of 0.52 kWh m^{-3} (www.nikunijapan.com). The limiting factors for scale up of these types of microbubble generators is that they require a constant liquid flow, require some level of contactor redesign and require significant power input. In the case of ozonation, preferable application may be to consider dosing ozone into a smaller side-stream flow prior to mixing the concentrated liquid into a larger main flow. The turbulent flow microbubble generator operates by placing a restriction in a pipe of flowing liquid. As the liquid passes through the restriction, the velocity of the flowing liquid increases and causes a pressure drop to below atmospheric pressure in the region immediately after the restriction. A series of holes allow for the automatic suction of gas. Common types of turbulent flow microbubble generators include the spherical body (Sadatomi et al., 2005, 2007; Kawahara et al., 2009; Budhijanto et al., 2015; Deendarlianto et al., 2015), orifice (Sadatomi et al., 2012), Venturi (Baylar et al., 2007, 2010; Rahman et al., 2014; Majid et al., 2018; Huang et al., 2019) and swirling flow (Terasaka et al., 2011; Li, Hu, Song, et al., 2013; Li, Hu and Xia, 2013; ; Levitsky et al., 2016; Yamashita and Ando, 2017; Hu and Xia, 2018; Xu et al., 2018). The advantage of these types of microbubble generator is that they have no moving parts and require no power. These systems are somewhat similar to a conventional diffuser, although they require a constant liquid flow in order to operate optimally. The turbulent flow-microbubble generators are scalable, with reported liquid flow rates of up to 30 m^3 hr^{-1} (Sun et al., 2017). Commercial Venturi systems are already available for ozonation and

are typically operated by dosing a high ozone concentration into a side stream flow before being mixed back with the main flow, enabling application in large scale municipal treatment plants. One of the most novel types of microbubble generator is the fluidic oscillator. This type of generator has a unique mode of operation in which the gas flow oscillates through a specially designed channel which causes the premature detachment of bubbles at the diffuser pores. The research studies undertaken to date with this type of technology have all been associated with small scale trials using gas flow rates of 0.06 m^3 hr^{-1}. However, commercial processes for aeration of wastewater have been developed treating surface overflow rates of 40 m^3 hr^{-1} and above (http://perlemax.com/downloads/WW_DZFO_info.pdf). The fluidic oscillator has been demonstrated to be superior to a standalone diffuser, primarily in aeration and flotation applications (Hanotu et al., 2012, 2014, 2016, 2017; Al-Mashhadani et al., 2015; Abdulrazzaq et al., 2016). Although no published examples of fluidic oscillation for ozonation were identified, the advantage of this type of microbubble generator being that it would act effectively as an in-line addition to existing diffusers and would not require extensive redesign of ozone contactors (Zimmerman et al., 2011a). The key consideration for the more wide-scale application of microbubble generators is the operational limitation associated with gas and liquid flows. Unlike conventional diffusers, the majority of microbubble generators require a liquid flow. Particularly for the generators that use automatic gas suction or pumping, a constant velocity of liquid passing through the generator is therefore important. In addition, for these types of generator, the gas flow rate is also dependent on water depth (Sadatomi et al., 2012), flow rate (Sadatomi et al., 2005), velocity (Sadatomi et al., 2007), number, size and location of drilled holes (Sadatomi et al., 2005) and the size of the restriction. It has also been shown that the diameter of the resulting microbubbles is heavily influenced by the gas and liquid flow rates. Majid et al. (2018) observed an increase in bubble diameter from 700 to 1250 µm when gas flow rate was increased from 0.012 to 0.066 m^3 hr^{-1}. However, a decrease in diameter from 700 to 400 µm was observed when the liquid flow rate was increased from 1.8 to 4.8 L min^{-1}. It was also noted that increasing gas flow rate decreased the $k_L a$. As such, these factors need to be considered as the capacity of microbubbles systems improves. In WTWs, where the flow is variable, maintaining a constant flow and velocity of water through the generator will becomes an operational challenge. Often the

maximum achievable gas flow rate is linked to the liquid flow rate of the generator and it appears that many types of microbubble generator are limited in their ability to significantly adjust gas flow rate. These features mean that the most likely application of microbubbles may be to dissolve ozone into a side stream prior to mixing with the main flow.

Table 2 – 5. Different types of microbubble generator and their operational gas and liquid flow rates.

Category	Type	Gas	Gas Flow Rate / L min^{-1}	Liquid Flow Rate / L min^{-1}	Reference
Turbulent Flow	Spherical body	Air	0.2	33.3	Majid et al. (2016)
			0.6	33.3	Deendarlianto et al. (2015)
			0.8	2.5	Budhijanto et al. (2015)
			3.4	36	Kawahara et al. (2009)
			8.5	62	Sadatomi et al. (2007)
			15	42	Sadatomi et al. (2005)
	Orifice		1	80	Juwana et al. (2018; 2019)
			0.75	266.67	Majid et al. (2016)
			0.8	61.67	Deendarlianto et al. (2015)
			18	62	Sadatomi et al. (2012)
	Swirling flow	Ozone	4	270	Hu and Xia (2018)
		Air	8.8	11.6	Xu et al. (2018)
		Ozone	0.3	Not reported	Zhang et al. (2018)
		Air	Not reported	1	Levitsky et al. (2016)
		Air / Ozone	1	19.5	Li et al. (2006)
		Ozone	1	19.5	Li and Tsuge (2006)
	Venturi	Air	1	80	Majid et al. (2018)
			1	80	Deendarlianto et al. (2017)
			2	500	Sun et al. (2017)
Mechanical Shear	Gas-liquid mixing pump	Ozone	3	Not reported	Cheng et al. (2019)
	Shear force generator		0.5		Gao et al. (2019)
	Gas-liquid mixing pump		3		Huang et al. (2019)
	Shear force generator		1	75	Nam et al. (2021)
	Centrifugal pump		0.5	10	Wu et al. (2019)
	Gyratory accelerator		0.65	Not reported	Zhang et al. (2013)
	Shear force generator		4	40	Takahashi et al. (2012a)
			0.03	Not reported	Xu et al. (2012)
	Gyratory accelerator		0.5		Chu et al. (2007)
Pressurized Dissolution	Not reported		0.3		Azuma et al. (2019)
			2		Liu et al. (2018)
			Not reported		Jabesa and Ghosh (2016a)
					Khuntia et al. (2016)
			0.5		Zheng et al. (2015)
			Not reported		Khuntia et al. (2013)
					Liu et al. (2010)
Diffuser	0.22 - 0.55 μm device		0.5		Sun et al. (2020)
Forced Bubble Detachment	Fluidic oscillation	Air	0.2 – 9*		Hanotu et al. (2017)
			0.1 - 0.9*		Hanotu et al. (2016)
			1*		Abdulrazzq et al. (2015)

2.4.2. Reactor Configuration

With the incorporation of microbubble generators into ozonation, there is the potential for significant changes to reactor configuration which in turn may reduce capital and operational costs in several areas, including chemical consumption, off-gas destruction, ozone generation and plant footprint. As has been demonstrated, the gas utilisation efficiency of ~100 % for microbubbles (Chu et al., 2007, 2008; Zhang et al., 2018) has the potential to reduce or remove the need for expensive off-gas destruction systems (Zimmerman et al., 2011b). The enhanced gas utilisation efficiency infers that less ozone is required in order to achieve a target ozone residual. Based on the difference in $k_L a$ for direct comparisons of conventional bubbles with microbubbles, it may be possible to reduce reactor volume by between 16 % and 81 % when using microbubbles (based on the minimum and maximum $k_L a$ enhancement seen by Nam et al. (2021) and Zhang et al. (2018), respectively), while still achieving similar or better residual ozone concentration (Figure 2 – 15). As a consequence, a smaller nominal ozone contactor volume when using microbubbles might be feasible when compared to systems developed using conventionally sized bubbles. Given that the capital cost of an ozonation system is typically 65 % of the total cost of an ozonation system, significant reductions may therefore be realised through application of microbubbles (Mundy et al., 2018). These savings need to be considered alongside the capital costs of multiple microbubble generators (costs not available), as well their operation and maintenance costs. Whilst the reviewed data presents a strong evidence base for the enhancement that can be delivered through the use of microbubble systems it must be stressed that these data are based on results from laboratory trials. Two approaches for implementation of microbubbles into ozone systems can be considered: in-line or side-stream ozonation (Figure 2 – 16). Importantly, the experimental methods employed in most research to date have used relatively shallow water depths, which biases the results in favour of microbubbles in a way that might not be realized in practice. For instance, the high gas utilisation efficiencies reported for microbubbles (Table 2 – 2) suggest that microbubbles will diffuse the entirety of their contents in less than 1 m of water depth. While this might encourage design of shallower contactors for new ozone installations, there may be more challenging considerations if retrofitting of microbubble ozone systems was being considered. In such cases, the water would require mixing to avoid stratified zones of

either high or no dissolved ozone in the reactor. This would have to be achieved through external mixing which will impart additional energy costs which are not generally considered. However, this also affords an opportunity where ozone mass transfer could be conducted in a side stream unit. The ozonated water in the side-stream would then be recombined into the main flow, maximizing energy utilisation and enabling constant flow to the contactor to be easily achieved (Figure 2 – 16). This approach would also better align with the limited gas and liquid flow rates achievable with current microbubble generators, enabling treatment of larger flows.

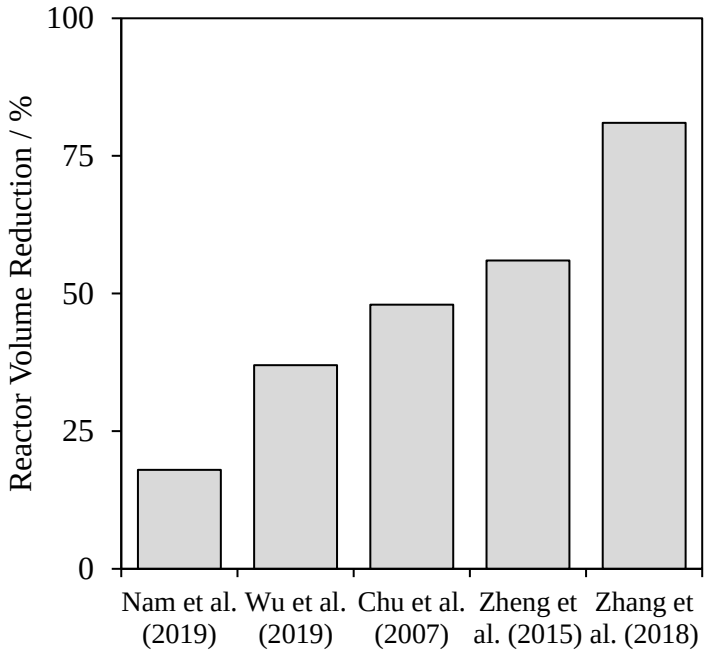

Figure 2 – 15. Reactor volume reductions for microbubbles based on $k_L a$ difference between experiments carried out for conventional and microbubble systems. Assumption based on removal of fast reacting compounds in mass transfer limited systems.

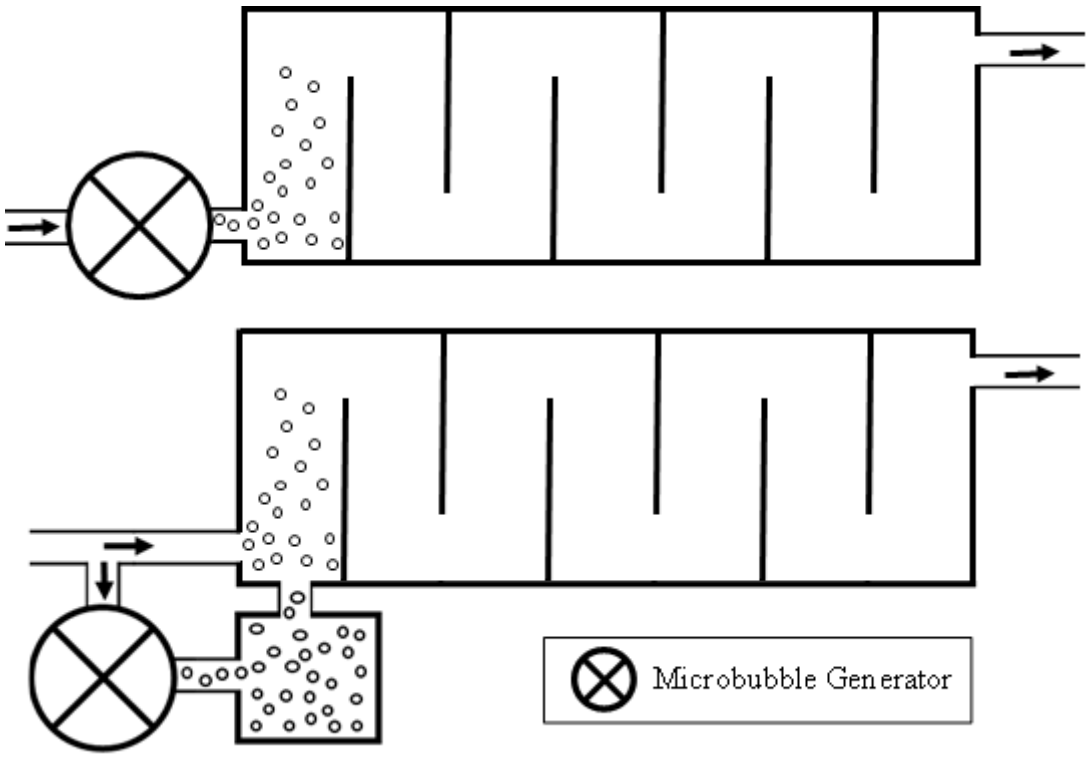

Figure 2 – 16. Possible microbubble generator arrangements at full scale where top is in-line and bottom is the side-stream.

2.4.3. Further Challenges to Address

Given the faster reaction kinetics observed for microbubbles in shallow columns in comparison to conventional bubbles, this might afford opportunities for reduced volumes and contact times in shallower reactors. Accordingly, the impact of water depth on the assessment of the efficacy of microbubble compared to conventional systems requires further investigation. In addition, this would provide clear evidence of the true impact of reducing bubble size on the enhancement of mass transfer and degradation kinetics to enable translation into real systems. This would also provide the framework for a standard approach to testing, enabling comparison between different microbubble technologies. To achieve this, more consistent and accurate bubble sizing is also required that covers both microbubbles and conventional systems to better refine the comparisons and reactor geometries. This also needs to consider variables that are not usually reported in comparative studies, such as bubble delivery in the water column and the density

(concentration) of bubbles. While the high surface area to volume ratio confers significant mass transfer advantages for microbubbles, this feature may also result in disadvantages when bubble coating is considered. Microbubble systems will be potentially more impacted by material accumulation from surface active compounds than when larger bubbles are used (Parkinson et al., 2008). This is an important aspect to consider given that most of the aforementioned microbubble ozonation studies have investigated contaminant degradation in pure water matrices. Accumulated material at the gas-liquid interface increases surface rigidity, decreases the net buoyancy force by adding weight and adds an additional resistance to mass transfer (Rosso and Stenstrom, 2006). For instance, from the limited studies carried out, surface coating has been associated with a 1.4 reduction in dissolution time (Tanaka et al., 2020) and has been shown to retard the efficacy of degradation of pharmaceuticals (Lee et al., 2019). To illustrate, the degradation rate of ethinylestradiol decreased from 0.10 to 0.07 min^{-1} for microbubbles with and without humic acid surface coatings, corresponding to a 30 % retardation of the degradation due to surface coating effects. The equivalent was also seen for conventional bubbles where the coating decreased the degradation rate constant from 0.07 to 0.04 min^{-1}. Similar results were also observed for degradation of ibuprofen and atenolol, with the bigger impact observed for the conventional bubble systems in all cases indicating that the increased surface area reduced the adsorbed layer thickness. However, this is an under explored area as smaller bubbles contain less active reactant material per bubble and so it is suggested that a critical layer thickness to bubble size ratio will exist beyond which all the reactant is utilised in oxidizing the compounds within the surface coating. In such cases, the microbubble systems would exhibit a preferential focus toward hydrophobic compounds and potentially restrict efficacy toward degradation of hydrophilic compounds. The importance of surface coating on microbubble ozonation therefore needs to be established to ensure that the improvements seen in pure water laboratory tests translates across to more complex water matrices containing background organic matter. There has also been an emergence of studies combining ozone microbubbles with other chemicals and catalyst materials to facilitate enhanced degradation of various contaminants. For example, researchers have combined iron nanoparticles or powdered activated carbon with ozone microbubbles for catalytic treatment of various organic contaminants (Zhang et al., 2018; Hou et al., 2020). Much greater understanding of the

role ozone microbubbles play in these processes is required, but there may be potential for the development of systems more comparable with advanced oxidation processes (AOPs) that are currently used for highly recalcitrant pollutants.

2.5. Conclusions

The adoption of microbubble delivery systems for use with ozone is shown to enhance both the mass transfer rate and the steady state concentration that can be achieved. The enhanced mass transfer rates are observed *ceteris paribus* with specific evidence in relation to input ozone concentration and the superficial gas velocity. Further, the ozone self-decomposition rate appears unaffected by changing bubble size such that the enhanced mass transfer corresponds to an improvement of degradation of target compounds. There was no evidence to show that collapse of microbubbles was a mechanism that contributed to the enhanced performance of the smaller bubbles. The results indicate that more effective treatment of compounds that are currently poorly degraded by conventional ozone systems may be achievable when using microbubbles. However, the evidence is based on experiments utilising shallow water depth that will positively bias results toward the microbubble systems, which may not be realizable in all practical situations. As such, it is recommended that future work explores the role of water depth along with surface coating to establish a standardised approach for the comparison and selection of microbubble ozone delivery systems for use in water treatment.

2.6. Acknowledgements

This research is gratefully supported by the Engineering and Physical Sciences Research Council (EPSRC) through their funding of the STREAM Industrial Doctorate Center (EP/G037094/1) and from the project sponsor Anglian Water.

2.7. References

Abdulrazzaq, N., Al-Sabbagh, B., Rees, J. and Zimmerman, W., 2015. Separation of azeotropic mixtures using air microbubbles generated by fluidic oscillation. *AIChE Journal*, 62(4), pp.1192-1199.

Achar, J., Nam, G., Jung, J., Klammler, H., and Mohamed, M., 2020. Microbubble ozonation of the antioxidant butylated hydroxytoluene: Degradation kinetics and toxicity reduction. *Environmental Research*, 186, p.109496.

Agarwal, A., Ng, W., and Liu, Y., 2011. Principle and applications of microbubble and nanobubble technology for water treatment. *Chemosphere*, 84(9), pp.1175-1180.

Akimov, V., Dmitriev, E., and Trushin, A., 2011. Mass transfer in the chemosorption of CO2 in a membrane microbubble apparatus. *Theoretical Foundations of Chemical Engineering*, 45(6), pp.811-817.

Al-Abduly, A., Christensen, P., Harvey, A. and Zahng, K., 2014. Characterization and optimization of an oscillatory baffled reactor (OBR) for ozone-water mass transfer. *Chemical Engineering and Processing: Process Intensification*, 84, pp.82-89.

Al-Mashhadani, M., Wilkinson, S., and Zimmerman, W., 2015. Airlift bioreactor for biological applications with microbubble mediated transport processes. *Chemical Engineering Science*, 137, pp.243-253.

Ashley, K., Hall, K., and Mavinic, D., 1991. Factors influencing oxygen transfer in fine pore diffused aeration. *Water Research*, 25(12), pp.1479-1486.

Ashley, K., Mavinik, D., and Hall, K., 1992. Bench-scale study of oxygen transfer in coarse bubble diffused aeration. *Water Research*, 26(10), pp.1289-1295.

Azuma, T., Otomo, K., Kunitou, M., Shimizu, M., Hosomaru, K., Mikata, S., Mino, Y. and Hayashi, T., 2019. Removal of pharmaceuticals in water by introduction of ozonated microbubbles. *Separation and Purification Technology*, 212, pp.483-489.

Baquero-Rodríguez, G., Lara-Borrero, J., Nolasco, D., and Rosso, D., 2019. Review of the factors affecting modeling oxygen transfer by fine-pore diffusers in activated sludge. *Water Environment Research*, 90(5), pp.431-441.

Baylar, A., Ozkan, F., and Unsal, M., 2007. On the use of venturi tubes in aeration. *CLEAN – Soil, Air, Water*, 35(2), 183-185.

Baylar, A., Ozkan, F., and Unsal, M., 2010. Effect of air inlet hole diameter of venturi tube on air injection rate. *KSCE Journal of Civil Engineering*, 14(4), pp.489-492.

Behnisch, J., Ganzauge, A., Sander, S., Herrling, M., and Wagner, M., 2018. Improving aeration systems in saline water: measurement of local bubble size and volumetric mass transfer coefficient of conventional membrane diffusers. *Water Science and Technology*, 78(4), pp.860-867.

Beltrán, F., 2004. *Ozone reaction kinetics for water and wastewater systems*. Lewis Publishers.

Bezbarua, B., and Reckhow, D., 2004. Modification of the standard neutral ozone decomposition model. *Ozone: Science and Engineering*, 26(4), pp.345-357.

Bińi, A., 2013. Comments on "Decay of ozone in water: a review" by D. Gardoni, A. Vailati, and R. Canziani (Ozone: Science and Engineering, 34(4): 233–242). *Ozone: Science and Engineering*, 35(1), pp.3-5.

Bredwell, M., and Worden, R., 1998. Mass-transfer properties of microbubbles. 1. Experimental studies. *Biotechnology Progress*, 14(1), pp.31-38.

Budhijanto, W., Deendarlianto, D., Kristiyani, H., and Satriawan, D., 2015. Enhancement of aerobic wastewater treatment by the application of attached growth microorganisms and microbubble generator. *International Journal of Technology*, 6(7), p.1101.

Buxton, G., Greenstock, C., Helman, W., and Ross, A., 1988. Critical review of rate constants for reactions of hydrated electrons, hydrogen atoms and hydroxyl radicals (·OH/·O−) in Aqueous Solution. *Journal of Physical and Chemical Reference Data*, 17(2), pp.513-886.

Chedeville, O., Debacq, M., and Porte, C., 2009. Removal of phenolic compounds present in olive mill wastewaters by ozonation. *Desalination*, 249(2), pp.865-869.

Cheng, W., Jiang, L., Quan, X., Cheng, C., Huang, X., Cheng, Z., and Yang, L., 2019. Ozonation process intensification of p-nitrophenol by in situ separation of hydroxyl radical scavengers and microbubbles. *Water Science and Technology*, 80(1), pp.25-36.

Cheng, X., Xie, Y., Zheng, H., Yang, Q., Zhu, D., and Xie, J., 2016. Effect of the different shapes of air diffuser on oxygen mass transfer coefficients in microporous aeration systems. *Procedia Engineering*, 154, pp.1079-1086.

Chiu, C., Chang, C., Chen, Y., Yu, Y., Chiang, P. and Ku, Y., 2003. Ozone mass transfer with combined effects of ozone decomposition and reaction with pollutants in a semibatch stirred vessel. *Journal of the Chinese Institute of Chemical Engineers*, 34(3), pp.281-289.

Chu, L., Xing, X., Yu, A., Zhou, Y., Sun, X., and Jurcik, B., 2007. Enhanced ozonation of simulated dyestuff wastewater by microbubbles. *Chemosphere*, 68(10), pp.1854-1860.

Chu, L., Yan, S., Xing, X., Yu, A., Sun, X., and Jurcik, B., 2008. Enhanced sludge solubilization by microbubble ozonation. *Chemosphere*, 72(2), pp.205-212.

Clift, R., Grace, J., and Weber, M., 1978. *Bubbles, Drops and Particles*. Academic Press.

da Silva Henauth, R., de Souza Vasconcelos, R., de Moura, A., Sarubbo, L., and dos Santos, V., 2016. Microbubble generation with the aid of a centrifugal pump. *Chemical Engineering and Technology*, 40(1), pp.138-144.

Deendarlianto, D., Indarto, I., Juwana, W., Afisna, L., and Nugroho, F., 2017. Performance of porous-venturi microbubble generator for aeration process. *Journal of Energy, Mechanical, Material and Manufacturing Engineering*, 2(2).

Deendarlianto, D., Wiratni, W., Tontowi, A. E., Indarto, I., and Iriawan, A. G. W., 2015. The implementation of a developed microbubble generator on the aerobic wastewater treatment. *International Journal of Technology*,, 6(6), p.924.

Dehouli, H., Chedeville, O., Cagnon, B., Caqueret, V., and Porte, C., 2010. Influences of pH, temperature and activated carbon properties on the interaction ozone/activated carbon for a wastewater treatment process. *Desalination*, 254(1-3), pp.12-16.

DeMoyer, C., Gulliver, J., and Wilhelms, S., 2001. Comparison of submerged aerator effectiveness. *Lake and Reservoir Management*, 17(2), pp.139-152.

Ershov, B., and Morozov, P., 2009. The kinetics of ozone decomposition in water, the influence of pH and temperature. *Russian Journal of Physical Chemistry A*, 83(8), pp.1295-1299.

Evans, H., Bauer, M., Luckman, I., and Page, M., 2003. An assessment of the benefits afforded by the continuous versus intermittent operation of ozone for drinking water treatment. *Ozone: Science and Engineering*, 25(5), pp.417-430.

Fábián, I., 2006. Reactive intermediates in aqueous ozone decomposition: A mechanistic approach. *Pure and Applied Chemistry*, 78(8), pp.1559-1570.

Fuchun, X., and Cunli, L., 1990. Mass balance analysis of ozone in a conventional bubble column. *Ozone: Science and Engineering*, 12(3), pp.269-279.

Gao, M., Hirata, M., Takanashi, H., and Hano, T., 2005. Ozone mass transfer in a new gas–liquid contactor–Karman contactor. *Separation and Purification Technology*, 42(2), pp.145-149.

Gao, Y., Duan, Y., Fan, W., Guo, T., Huo, M., and Yang, W. *et al*., 2019. Intensifying ozonation treatment of municipal secondary effluent using a combination of microbubbles and ultraviolet irradiation. *Environmental Science and Pollution Research*, 26(21), pp.21915-21924.

Gardoni, D., Vailati, A., and Canziani, R., 2012. Decay of ozone in water: a review. *Ozone: Science and Engineering*, 34(4), pp.233-242.

Garrido-Baserba, M., Asvapathanagul, P., Park, H., Kim, T., Baquero-Rodriguez, G., Olson, B., and Rosso, D., 2018. Impact of fouling on the decline of aeration efficiency under different operational conditions at WRRFs. *Science of The Total Environment*, 639, pp.248-257.

Gurol, M., and Singer, P., 1982. Kinetics of ozone decomposition: a dynamic approach. *Environmental Science and Technology*, 16(7), pp.377-383.

Hanotu, J., Bandulasena, H., and Zimmerman, W., 2012. Microflotation performance for algal separation. *Biotechnology and Bioengineering*, 109(7), pp.1663-1673.

Hanotu, J., Karunakaran, E., Bandulasena, H., Biggs, C., and Zimmerman, W., 2014. Harvesting and dewatering yeast by microflotation. *Biochemical Engineering Journal*, 82, pp.174-182.

Hanotu, J., Kong, D., and Zimmerman, W., 2016. Intensification of yeast production with microbubbles. *Food and Bioproducts Processing*, 100, pp.424-431.

Hanotu, J., Bandulasena, H., and Zimmerman, W., 2017. Aerator design for microbubble generation. *Chemical Engineering Research and Design*, 123, pp.367-376.

Haruta, K., and Takeyama, T., 1981. Kinetics of oxidation of aqueous bromide ion by ozone. *The Journal of Physical Chemistry*, 85(16), pp.2383-2388.

He, H., Zheng, L., Li, Y. and Song, W., 2015. Research on the feasibility of spraying micro/nano bubble ozonated water for airborne disease prevention. *Ozone: Science and Engineering*, 37(1), pp.78-84.

Hoigné, J., and Bader, H., 1983. Rate constants of reactions of ozone with organic and inorganic compounds in water—I. *Water Research*, 17(2), pp.173-183.

Hoigné, J., 1994. Characterization of water quality criteria for ozonation processes. part i: minimal set of analytical data. *Ozone: Science and Engineering*, 16(2), pp.113-120.

Hou, S., Jia, S., Jia, J., He, Z., Li, G., Zuo, Q., and Zhuang, H., 2020. Fe3O4 nanoparticles loading on cow dung based activated carbon as an efficient catalyst for catalytic microbubble ozonation of biologically pretreated coal gasification wastewater. *Journal of Environmental Management*, 267, p.110615.

Hu, L., and Xia, Z., 2018. Application of ozone micro-nano-bubbles to groundwater remediation. *Journal of Hazardous Materials*, 342, pp.446-453.

Huang, W., Chang, C., Chiu, C., Lee, S., Yu, Y., Liou, H., Ku, Y. and Chen, J., 1998. A refined model for ozone mass transfer in a bubble column. *Journal of Environmental Science and Health, Part A*, 33(3), pp.441-460.

Huang, X., Cheng, W., Quan, X., Cheng, C., Cheng, Z., and Yang, L., 2018. Catalytic ozonation of biologically treated leachate from municipal solid waste in a microbubble reactor. *Ozone: Science and Engineering*, 41(5), pp.415–426.

Huang, X., Quan, X., Cheng, W., Cheng, C., Cheng, Z., Yang, L., and Jiang, L., 2019. Enhancement of ozone mass transfer by stainless steel wire mesh and its effect on hydroxyl radical generation. *Ozone: Science and Engineering*, 1-10.

Hsu, Y., Chen, T., Chen, J., and Lay, C., 2002. Ozone transfer into water in a gas-inducing reactor. *Industrial and Engineering Chemistry Research*, 41(1), pp.120-127.

Ignatiev, A., Pryakhin, A., and Lunin, V., 2008. Numerical simulation of the kinetics of ozone decomposition in an aqueous solution. *Russian Chemical Bulletin*, 57(6), pp.1172-1178.

Imaizumi, K., Tinwongger, S., Kondo, H. and Hirono, I., 2018. Disinfection of an EMS/AHPND strain of Vibrio parahaemolyticus using ozone nanobubbles. *Journal of Fish Diseases*, 41(4), pp.725-727.

International Organization for Standardization, 2017. *ISO/TC 281 - Fine bubble technology*. ISO. Retrieved from https://www.iso.org/committee/4856666.html.

Jabesa, A., and Ghosh, P., 2016a. Removal of diethyl phthalate from water by ozone microbubbles in a pilot plant. *Journal of Environmental Management*, 180, pp.476-484.

Jabesa, A., and Ghosh, P., 2016b. Removal of dimethyl phthalate from water by ozone microbubbles. *Environmental Technology*, 38(16), pp.2093-2103.

Jakubiak, M. and Kordylewski, W., 2011. The effect of ozone feeding mode on the effectiveness of NO oxidation. *Chemical and Process Engineering*, 32(3).

Jhunkeaw, C., Khongcharoen, N., Rungrueng, N., Sangpo, P., Panphut, W., Thapinta, A., Senapin, S., St-Hilaire, S. and Dong, H., 2021. Ozone nanobubble treatment in freshwater effectively reduced pathogenic fish bacteria and is safe for Nile tilapia (Oreochromis niloticus). *Aquaculture*, 534, p.736286.

Jodzis, S., and Zięba, M., 2018. Energy efficiency of an ozone generation process in oxygen. Analysis of a pulsed DBD system. *Vacuum*, 155, pp.29-37.

Joshi, M., and Shambaugh, R., 1982. The kinetics of ozone-phenol reaction in aqueous solutions. *Water Research*, 16(6), pp.933-938.

Juwana, W. E., Widyatama, A., Wiratni, Indarto, and Deendarlianto., 2018. An evaluation of the horizontal injection microbubble generator. *AIP Conference Proceedings*, 030018, pp.1-7.

Juwana, W. E., Widyatama, A., Dinaryanto, O., Budhijanto, W., Indarto, and Deendarlianto., 2019. Hydrodynamic characteristics of the microbubble dissolution in liquid using orifice type microbubble generator. *Chemical Engineering Research and Design*, 141, pp.436–448.

Kamaroddin, M., Hanotu, J., Gilmour, D., and Zimmerman, W., 2016. In-situ disinfection and a new downstream processing scheme from algal harvesting to lipid extraction using ozone-rich microbubbles for biofuel production. *Algal Research*, 17, pp.217-226.

Kamaroddin, M., Rahaman, A., Gilmour, D., and Zimmerman, W., 2020. Optimization and cost estimation of microalgal lipid extraction using ozone-rich microbubbles for biodiesel production. *Biocatalysis and Agricultural Biotechnology*, 23, pp.101462.

Kawahara, A., Sadatomi, M., Matsuyama, F., Matsuura, H., Tominaga, M., and Noguchi, M., 2009. Prediction of micro-bubble dissolution characteristics in water and seawater. *Experimental Thermal and Fluid Science*, 33(5), pp.883–894.

Khuntia, S., Majumder, S., and Ghosh, P., 2012. Microbubble-aided water and wastewater purification: a review. *Reviews in Chemical Engineering*, 28(4-6).

Khuntia, S., Majumder, S., and Ghosh, P., 2013. Removal of ammonia from water by ozone microbubbles. *Industrial and Engineering Chemistry Research*, 52(1), pp.318-326.

Khuntia, S., Majumder, S., and Ghosh, P., 2016. Catalytic ozonation of dye in a microbubble system: Hydroxyl radical contribution and effect of salt. *Journal of Environmental Chemical Engineering*, 4(2), pp.2250-2258.

Kim, D., Nemlioglu, S., Roberts, P. and Kim, J., 2010. Ozone-contactor flow visualization and quantification using three dimensional laser induced fluorescence. *Journal - American Water Works Association*, 102(1), pp.90-99.

Kobayashi, F., Ikeura, H., Ohsato, S., Goto, T. and Tamaki, M., 2011. Disinfection using ozone microbubbles to inactivate Fusarium oxysporum f. sp. melonis and Pectobacterium carotovorum subsp. carotovorum. *Crop Protection*, 30(11), pp.1514-1518.

Kong, S., Kwon, C., and Kim, M., 2003. Ozone kinetics and diesel decomposition by ozonation in groundwater. *Korean Journal of Chemical Engineering*, 20(2), pp.293-299.

Ku, Y., Su, W., and Shen, Y., 1996. Decomposition kinetics of ozone in aqueous solution. *Industrial and Engineering Chemistry Research*, 35(10), pp.3369-3374.

Kukuzaki, M., Fujimoto, K., Kai, S., Ohe, K., Oshima, T., and Baba, Y., 2010. Ozone mass transfer in an ozone–water contacting process with Shirasu porous glass (SPG) membranes – A comparative study of hydrophilic and hydrophobic membranes. *Separation and Purification Technology*, 72(3), pp.347-356.

Kuo, P., Chian, E., and Chang, B., 1977. Identification of end products resulting from ozonation and chlorination of organic compounds commonly found in water. *Environmental Science and Technology*, *11*(13), pp.1177-1181.

NIKUNI WEBSITE. 2021. *KTMindetail of NIKUNI WEBSITE*. [online] Available at: <http://nikunijapan.com/ktm.html> [Accessed 08 October 2020].

Lage Filho, F., 2010. Ozone application in water sources: effects of operational parameters and water quality variables on ozone residual profiles and decay rates. *Brazilian Journal of Chemical Engineering*, 27(4), pp.545-554.

Lee, Y., Park, Y., Lee, G., Kim, Y., and Chon, K., 2019. Enhanced degradation of pharmaceutical compounds by a microbubble ozonation process: effects of temperature, ph, and humic acids. *Energies*, 12(22), p.4373.

Levanov, A., Isaikina, O., Gasanova, R., and Lunin, V., 2017. Coefficient of ozone mass transfer during its interaction with an aqueous solution of formic acid in a bubble column reactor. *Russian Journal of Physical Chemistry A*, 91(8), pp.1427-1431.

Levitsky, I., Tavor, D., and Gitis, V., 2016. Generation of two-phase air-water flow with fine microbubbles. *Chemical Engineering Technology*, 39(8), pp.1537–1544.

Li, H., Hu, L., Song, D., and Al-Tabbaa, A., 2013a. Subsurface transport behavior of micro-nano bubbles and potential applications for groundwater remediation. *IJERPH*, 11(1), pp.473–486.

Li, H., Hu, L., and Xia, Z., 2013b. Impact of groundwater salinity on bioremediation enhanced by micro-nano bubbles. *Materials*, 6(9), pp.3676–3687.

Li, P., and Tsuge, H., 2006. Ozone transfer in a new gas-induced contactor with microbubbles. *Journal of Chemical Engineering of Japan*, 39(11), pp.1213-1220.

Li, X., Li, P., Zu, L., and Yang, C., 2016. Gas-liquid mass transfer characteristics with microbubble aeration – I. Standard stirred tank. *Chemical Engineering and Technology*, 39(5), pp.945–952.

Lim, S., McArdell, C., and von Gunten, U., 2019. Reactions of aliphatic amines with ozone: Kinetics and mechanisms. *Water Research*, 157, pp.514-528.

Liu, S, Oshita, S., Kawabata, S., Makino, Y. and Yoshimoto, T., 2016. Identification of ROS produced by nanobubbles and their positive and negative effects on vegetable seed germination. *Langmuir*, 32, pp.11295-11302.

Liu, C., Chen, X.-X., Zhang, J., Zhou, H.-Z., Zhang, L., and Guo, Y.K., 2018. Advanced treatment of bio-treated coal chemical wastewater by a novel combination of microbubble catalytic ozonation and biological process. *Separation and Purification Technology*, 197, pp.295–301.

Liu, C., Tanaka, H., Ma, J., Zhang, L., Zhang, J., Huang, X., and Matsuzawa, Y., 2012. Effect of microbubble and its generation process on mixed liquor properties of activated sludge using Shirasu porous glass (SPG) membrane system. *Water Research*, 46(18), pp.6051-6058.

Liu, C., Tanaka, H., Zhang, J., Zhang, L., Yang, J., Huang, X., and Kubota, N., 2013. Successful application of Shirasu porous glass (SPG) membrane system for microbubble aeration in a biofilm reactor treating synthetic wastewater. *Separation and Purification Technology*, 103, pp.53-59.

Liu, S., Wang, Q., Zhai, X., Huang, Q., and Huang, P., 2010. Improved pretreatment (coagulation-floatation and ozonation) of younger landfill leachate by microbubbles. *Water Environment Research*, 82(7), pp.657-665.

López-López, A., Pic, J., and Debellefontaine, H., 2007. Ozonation of azo dye in a semi-batch reactor: A determination of the molecular and radical contributions. *Chemosphere*, 66(11), pp.2120-2126.

Lovato, M., Martín, C., and Cassano, A., 2009. A reaction kinetic model for ozone decomposition in aqueous media valid for neutral and acidic pH. *Chemical Engineering Journal*, 146(3), pp.486-497.

Magara, Y., Itoh, M., and Morioka, T., 1995. Application of ozone to water treatment and power consumption of ozone generating systems. *Progress in Nuclear Energy*, 29, pp.175-182.

Majid, A., Deendarlianto, Wiratni, Indarto, Enggar, B., Baskoro, P and Alva T., 2016. Development of an industrial-scale micro-bubble generator for the purposes of aerobic wastewater treatment. *The 9th International Conference on Multiphase Flow.*

Majid, A., Nugroho, F., Juwana, W., Budhijanto, W., Deendarlianto, and Indarto., 2018. On the performance of venturi-porous pipe microbubble generator with inlet angle of 20° and outlet angle of 12°. *American Institute of Physics Conference Proceedings*, 2001(2018), pp.1-10.

Merle, T., Pronk, W., and von Gunten, U., 2017. MEMBRO3X, a novel combination of a membrane contactor with advanced oxidation (O3/H2O2) for simultaneous micropollutant abatement and bromate minimization. *Environmental Science and Technology Letters*, 4(5), pp.180-185.

Miklos, D.B., Remy, C., Jekel, M., Linden, K., Drewes, J.E., Hübner, U., 2018. Evaluation of advanced oxidation processes for water and wastewater treatment – A critical review. *Water Research*, 139, pp.118-131.

Mitani, M., Keller, A., Sandall, O., and Rinker, R., 2005. Mass transfer of ozone using a microporous diffuser reactor system. *Ozone: Science and Engineering*, 27(1), pp.45-51.

Morooka, S., K. Ikezumi, and Y. Kato., 1978. The decomposition of ozone in aqueous solution. *Kagaku Kogaku Ronbunshu*, 4, pp.377-380.

Mueller, J., Boyle, W., and Pöpel, H., 2002. *Aeration*. CRC Press.

Mundy, B., Kuhnel, B., Hunter, G., Jarnis, R., Funk, D., Walker, S., Burns, N., Drago, J., Nezgod, W., Huang, J., Rakness, K., Jasim, S., Joost, R., Kim, R., Muri, J., Nattress, J., Oneby, M., Sosebee, A., Thompson, C., Walsh, M. and Schulz, C., 2018. A review of ozone systems costs for municipal applications. Report by the Municipal Committee – IOA Pan American Group. *Ozone: Science & Engineering*, 40(4), pp.266-274.

Muroyama, K., Imai, K., Oka, Y., and Hayashi, J., 2013. Mass transfer properties in a bubble column associated with micro-bubble dispersions. *Chemical Engineering Science*, 100, pp.464-473.

Muruganandham, M., Suri, R., Jafari, S., Sillanpää, M., Lee, G., Wu, J., and Swaminathan, M., 2014. Recent developments in homogeneous advanced oxidation processes for water and wastewater treatment. *International Journal of Photoenergy*, 2014, pp.1-21.

Nam, G., Mohamed, M. and Jung, J., 2021. Enhanced degradation of benzo[a]pyrene and toxicity reduction by microbubble ozonation. *Environmental Technology*, 42(12), pp.1853-1860.

Neta, P., and Dorfman, L., 1968. Pulse-radiolysis studies. XIII. Rate constants for the reactions of hydroxyl radicals with aromatic compounds in aqueous solutions. *Advances in Chemistry*, 81(15), pp.222-230.

Nghia, N., Van, P., Giang, P., Hanh, N., St-Hilaire, S. and Domingos, J., 2021. Control of Vibrio parahaemolyticus (AHPND strain) and improvement of water quality using nanobubble technology. *Aquaculture Research*, 52(6), pp.2727-2739.

Phaephiphat, A. and Mahakarnchanakul, W., 2018. Surface decontamination of Salmonella Typhimurium and Escherichia coli on sweet basil by ozone microbubbles. *Cogent Food and Agriculture*, 4(1), p.1558496.

Paucar, N., Kim, I., Tanaka, H., and Sato, C., 2018. Ozone treatment process for the removal of pharmaceuticals and personal care products in wastewater. *Ozone: Science and Engineering*, 41(1), pp.3-16.

Park, S., Park, C., Lee, J., and Lee, B., 2017. A simple parameterization for the rising velocity of bubbles in a liquid pool. *Nuclear Engineering and Technology*, 49(4), pp.692-699.

Parkinson, L., Sedev, R., Fornasiero, D., and Ralston, J., 2008. The terminal rise velocity of 10–100 μm diameter bubbles in water. *Journal of Colloid and Interface Science*, 322(1), pp.168-172.

Parmar, R., and Majumder, S., 2013. Microbubble generation and microbubble-aided transport process intensification—A state-of-the-art report. *Chemical Engineering and Processing: Process Intensification*, 64, pp.79-97.

Rahman, A., Darban Ahmad, K., Mahmoud, A., and Maoming, F., 2014. Nano-microbubble flotation of fine and ultrafine chalcopyrite particles. *International Journal of Mining Science and Technology*, 24(4), pp.559–566.

Rakness, K., Hunter, G., Lew, J., Mundy, B., and Wert, E., 2018. Design considerations for cost-effective ozone mass transfer in sidestream systems. *Ozone: Science and Engineering*, 40(3), pp.159-172.

Rehman, F., Medley, G., Bandulasena, H., and Zimmerman, W., 2015. Fluidic oscillator-mediated microbubble generation to provide cost effective mass transfer and mixing efficiency to the wastewater treatment plants. *Environmental Research*, 137, pp.32-39.

Rischbieter, E., Stein, H., and Schumpe, A., 2000. Ozone solubilities in water and aqueous salt solutions. *Journal of Chemical and Engineering Data*, 45(2), pp.338-340.

Roustan, M., Wang, R., and Wolbert, D., 1996. Modeling Hydrodynamics and mass transfer parameters in a continuous ozone bubble column. *Ozone: Science and Engineering*, 18(2), pp.99-115.

Rosso, D., and Stenstrom, M., 2006. Surfactant effects on a-factors in aeration systems. *Water Research*, 40(7), pp.1397–1404.

Sadatomi, M., Kawahara, A., Kano, K., and Ohtomo, A., 2005. Performance of a new micro-bubble generator with a spherical body in a flowing water tube. *Experimental Thermal and Fluid Science*, 29(5), pp.615-623.

Sadatomi, M., Kawahara, A., Matsuyama, F., and Kimura, T., 2007. An advanced microbubble generator and its application to a newly developed bubble-jet-type air-lift pump. *Multiphase Science and Technology*, 19(4), pp.323–342.

Sadatomi, M., Kawahara, A., Matsuura, H., and Shikatani, S., 2012. Micro-bubble generation rate and bubble dissolution rate into water by a simple multi-fluid mixer with orifice and porous tube. *Experimental Thermal and Fluid Science*, 41, pp.23-30.

Santana, M., Zhang, Q., and Mihelcic, J., 2014. Influence of water quality on the embodied energy of drinking water treatment. *Environmental Science and Technology*, 48(5), pp.3084-3091.

Secula, M., Barrot, Y., Cagnon, B., Versaveau, F., and Chedeville, O., 2013. Diethyl phthalate removal by continuous-flow ozonation: Response surface modeling and optimization. *Water, Air, and Soil Pollution,* 224(4).

Sein, M., Golloch, A., Schmidt, T., and von Sonntag, C., 2007. No marked kinetic isotope effect in the peroxone (H2O2/D2O2+O3) reaction: mechanistic consequences. *ChemPhysChem*, 8(14), pp.2065-2067.

Shangguan, Y., Yu, S., Gong, C., Wang, Y., Yang, W., and Hou, L., 2018. A review of microbubble and its applications in ozonation. *IOP Conference Series: Earth and Environmental Science*, 128, p.012149.

Shin, W., Mirmiran, A., Yiacoumi, S., and Tsouris, C., 1999. Ozonation using microbubbles formed by electric fields. *Separation and Purification Technology*, 15(3), pp.271-282.

Sotelo, J., Beltran, F., Benitez, F., and Beltran-Heredia, J., 1987. Ozone decomposition in water: kinetic study. *Industrial and Engineering Chemistry Research*, 26(1), pp.39-43.

Sun, Z., Chen, X., Yang, K., Zhu, N., and Lou, Z., 2020. The progressive steps for TPH stripping and the decomposition of oil refinery sludge using microbubble ozonation. *Science of the Total Environment*, 712, p.135631.

Sun, L., Mo, Z., Zhao, L., Liu, H., Guo, X., Ju, X., and Bao, J., 2017. Characteristics and mechanism of bubble breakup in a bubble generator developed for a small TMSR. *Annals of Nuclear Energy*, 109, pp.69–81.

Suwartha, N., Syamzida, D., Priadi, C., Moersidik, S., and Ali, F., 2020. Effect of size variation on microbubble mass transfer coefficient in flotation and aeration processes. *Heliyon*, 6(4), p.e03748.

Takahashi, M., Chiba, K., and Li, P., 2007. Formation of hydroxyl radicals by collapsing ozone microbubbles under strongly acidic conditions. *The Journal of Physical Chemistry B*, 111(39), pp.11443-11446.

Takahashi, N., Ichikawa, H., Torii, H., Shibata, S., Duy, N., and Phuong, P., 2012a. Ozonation of dyestuff solutions using a fine bubble generator system. *Ozone: Science and Engineering*, 34(3), pp.196-203.

Takahashi, M., Ishikawa, H., Asano, T., and Horibe, H., 2012b. Effect of microbubbles on ozonized water for photoresist removal. *The Journal of Physical Chemistry C*, 116(23), pp.12578-12583.

Talaia, M., 2007. Terminal velocity of a bubble rise in a liquid column. *World Academy of Science, Engineering and Technology*, 22, pp.264-268.

Tamaki, M., Kobayashi, F., Ikeura, H. and Sato, M., 2018. Disinfection by Ozone Microbubbles Can Cause Morphological Change of Fusarium oxysporum f. sp. melonis Spores. *The Plant Pathology Journal*, 34(4), pp.335-340.

Tanaka, S., Kastens, S., Fujioka, S., Schlüter, M., and Terasaka, K., 2020. Mass transfer from freely rising microbubbles in aqueous solutions of surfactant or salt. *Chemical Engineering Journal*, 387, p.121246.

Tang, G., Adu-Sarkodie, K., Kim, D., Kim, J., Teefy, S., Shukairy, H., and Mariñas, B., 2005. Modeling cryptosporidium parvum oocyst inactivation and bromate formation in a full-scale ozone contactor. *Environmental Science and Technology*, 39(23), pp.9343-9350.

Tekle-Röttering, A., Lim, S., Reisz, E., Lutze, H., Abdighahroudi, M., Willach, S., Schmidt, W., Tentscher, P., Rentsch, D., McArdell, C., Schmidt, T. and von Gunten, U., 2020. Reactions of pyrrole, imidazole, and pyrazole with ozone: kinetics and mechanisms. *Environmental Science: Water Research and Technology*, 6(4), pp.976-992.

Temesgen, T., Bui, T., Han, M., Kim, T., and Park, H., 2017. Micro and nanobubble technologies as a new horizon for water-treatment techniques: A review. *Advances in Colloid and Interface Science*, 246, pp.40-51.

Terasaka, K., Hirabayashi, A., Nishino, T., Fujioka, S., and Kobayashi, D., 2011. Development of microbubble aerator for waste water treatment using aerobic activated sludge. *Chemical Engineering Science*, 66(14), pp.3172-3179.

Terashima, M., So, M., Goel, R., and Yasui, H., 2016. Determination of diffuser bubble size in computational fluid dynamics models to predict oxygen transfer in spiral roll aeration tanks. *Journal of Water Process Engineering*, 12, pp.120-126.

Tizaoui, C., and Zhang, Y., 2010. The modelling of ozone mass transfer in static mixers using Back Flow Cell Model. *Chemical Engineering Journal*, 162(2), pp.557-564.

Uhm, H., Hong, Y., Lee, H., and Park, Y., 2009. Increase in the ozone decay time in acidic ozone water and its effects on sterilization of biological warfare agents. *Journal of Hazardous Materials*, 168(2-3), pp.1595-1601.

Valdés, H., Farfán, V., Manoli, J., and Zaror, C., 2009. Catalytic ozone aqueous decomposition promoted by natural zeolite and volcanic sand. *Journal of Hazardous Materials*, 165(1-3), pp.915-922.

von Gunten, U., Elovitz, M., and Kaiser, H., 1999. Calibration of full-scale ozonation systems with conservative and reactive tracers. *Journal of Water Supply: Research and Technology—AQUA*, 48(6), pp.250-256.

von Sonntag, C., 2008. Advanced oxidation processes: mechanistic aspects. *Water Science and Technology*, 58(5), pp.1015-1021.

Vyong Tkhi, L., Tarasov, V., and Popov, Y., 2009. The influence of traces on kinetics of ozone destruction in water. *Theoretical Foundations of Chemical Engineering*, 43(5), pp.846-849.

Wang, D., Yang, X., Tian, C., Lei, Z., Kobayashi, N., Kobayashi, M., Adachi, Y., Shimizu, K. and Zhang, Z., 2019. Characteristics of ultra-fine bubble water and its trials on enhanced methane production from waste activated sludge. *Bioresource Technology*, 273, pp.63-69.

Wang, W., Fan, W., Huo, M., Zhao, H., and Lu, Y., 2018. Hydroxyl radical generation and contaminant removal from water by the collapse of microbubbles under different hydrochemical conditions. *Water, Air, and Soil Pollution*, 229(3).

Wert, E., Lew, J. and Rakness, K., 2017. Effect of ozone dissolution systems on ozone exposure and bromate formation. *Journal AWWA*, 109(7).

Wolf, C., Pavese, A., von Gunten, U., and Kohn, T., 2019. Proxies to monitor the inactivation of viruses by ozone in surface water and wastewater effluent. *Water Research*, 166, p.115088.

Wu, C., Li, P., Xia, S., Wang, S., Wang, Y., Hu, J., Liu, Z. and Yu, S., 2019. The role of interface in microbubble ozonation of aromatic compounds. *Chemosphere*, 220, pp.1067-1074.

Wu, Z., Shen, H., Ondruschka, B., Zhang, Y., Wang, W., and Bremner, D., 2012. Removal of blue-green algae using the hybrid method of hydrodynamic cavitation and ozonation. *Journal of Hazardous Materials*, 235-236, pp.152-158.

Xu, X., Ge, X., Qian, Y., Zhang, B., Wang, H., and Yang, Q., 2018. Effect of nozzle diameter on bubble generation with gas self-suction through swirling flow. *Chemical Engineering Research and Design*, 138, 13–20.

Xu, Z., Mochida, K., Naito, T., and Yasuda, K., 2012. Effects of Operational Conditions on 1,4-Dioxane Degradation by Combined Use of Ultrasound and Ozone Microbubbles. *Japanese Journal of Applied Physics*, 51, p.07GD08.

Yamashita, T., and Ando, K., 2017. Aeration of water with oxygen microbubbles and its purging effect. *J. Fluid Mech.*, 825, pp.16–28.

Yao, K., Chi, Y., Wang, F., Yan, J., Ni, M., and Cen, K., 2016. The effect of microbubbles on gas-liquid mass transfer coefficient and degradation rate of COD in wastewater treatment. *Water Science and Technology,* 73(8), pp.1969–1977.

Zhang, J., Tejada-Martínez, A., Zhang, Q., and Lei, H., 2014. Evaluating hydraulic and disinfection efficiencies of a full-scale ozone contactor using a RANS-based modeling framework. *Water Research*, 52, pp.155-167.

Zhang, F., Xi, J., Huang, J., and Hu, H., 2013. Effect of inlet ozone concentration on the performance of a micro-bubble ozonation system for inactivation of Bacillus subtilis spores. *Separation and Purification Technology*, 114, pp.126-133.

Zhang, J., Huang, G., Liu, C., Zhang, R., Chen, X., and Zhang, L., 2018. Synergistic effect of microbubbles and activated carbon on the ozonation treatment of synthetic dyeing wastewater. *Separation and Purification Technology*, 201, pp.10-18.

Zheng, T., Wang, Q., Zhang, T., Shi, Z., Tian, Y., Shi, S., Smale, N. and Wang, J., 2015. Microbubble enhanced ozonation process for advanced treatment of wastewater produced in acrylic fiber manufacturing industry. *Journal of Hazardous Materials*, 287, pp.412-420.

Zimmerman, W., Tesař, V., Butler, S., and Bandulasena, H., 2008. Microbubble generation. *Recent Patents on Engineering*, 2(1), pp.1-8.

Zimmerman, W., Zandi, M., Hemaka Bandulasena, H., Tesař, V., James Gilmour, D., and Ying, K., 2011a. Design of an airlift loop bioreactor and pilot scales studies with fluidic oscillator induced microbubbles for growth of a microalgae Dunaliella salina. *Applied Energy*, 88(10), pp.3357-3369.

Zimmerman, W., Tesař, V. and Hemaka Bandulasena, H., 2011b. Towards energy efficient nanobubble generation with fluidic oscillation. *Current Opinion in Colloid and Interface Science*, 16 (4), pp.350-356,

2.8. Supplementary Information

[SI] Table 2 – S1. Microbubble definitions that have been used in the literature.

Diameter (μm)				Reference
1	10	100	1000	
100's of nm				Yasuda et al., 2008
< Several tens of μm				Chu et al. 2007; Nouri et al., 2009; Tasaki et al., 2009; Li et al., 2014; Yao et al., 2016; Zhang et al., 2018
Several tens of nm to several tens of μm				Li et al., 2013, 2013b; Chen et al., 2016; Gurung et al., 2016; Hu and Xia, 2018; Xia and Hu, 2018
<50μm				Amagai and Tabei., 2006; Takahashi et al., 2007; Hasegawa et al., 2008; Agarwal et al., 2012; Bang et al., 2011, 2012; Khuntia et al., 2012; Muroyama et al., 2013; Zheng et al., 2015; Ikeura et al., 2011; Li, X et al., 2016; Xue et al., 2016; Dayarathne et al., 2017; Li et al., 2018; Liu et al., 2018; Sun et al., 2018, 2019; Wu et al., 2019; Ye et al., 2019
	5-40μm			Srithongouthai et al., 2006
	10-50μm			Agarwal et al., 2011; Lam et al., 2012; Liu et al., 2012a, 2012b, 2013; Ebina et al., 2013; Lee et al., 2015; Jang et al., 2018; Levitsky et al., 2016; Zhang et al., 2016; Klintham et al., 2017; Basso et al., 2018; Shangguan et al., 2018; Xiong et al., 2018
	20-50μm			Yu et al., 2017
	10-60μm			Terasaka et al., 2011
	30-70μm			Etchepare et al., 2017
<80μm				Hanotu et al., 2017
1-100μm				Kurup and Naik, 2010; Uchida et al., 2011; Tesař, 2017
	10-100μm			Ramírez et al., 2017; Temesgen et al., 2017; Sancho et al., 2019
	30-100μm			Pérez-Garibay et al., 2012; Calgaroto et al., 2016
<100μm				Makuta et al., 2013; Parmar and Majumder, 2014; Gwenaelle et al., 2017; Azuma et al., 2019
		Order of 100μm		Sadatomi et al., 2007
<150μm				Kothandaraman et al., 2018
	10-200μm			Lee et al., 2019
	50-200μm			Deendarlianto et al., 2015; Majid et al., 2018
<200μm				Gigih et al., 2012; Budhijanto et al., 2015
1-Several hundreds of μm				Hosokawa et al., 2009; Maeda et al., 2011
<A few hundred of μm				Sadatomi et al., 2012; Majid et al., 2016
< Several hundreds of μm				Edzwald, 2007; Kawahara et al., 2009
1-999μm				Zimmerman et al., 2011
1-1000μm				Tesař, 2014, 2015; Jiang et al., 2016; Deendarlianto et al., 2017; Hernandez-Alvarado et al., 2017; Juwana et al., 2018
<1000μm				Uesawa et al., 2011; Wiraputra et al., 2016; Juwana et al., 2019

[SI] Table 2 – S2. Recent microbubble generator developments.

Category	Type	Scale	Gas	Bubble Diameter / µm	Application	Reference
Turbulent Flow	Spherical Body	Lab	Air	120-490	Generator performance	Sadatomi et al., 2005
				-	Fisheries aeration	Sadatomi et al., 2007
				200-2000	Seawater dissolution	Kawahara et al., 2009
				20-750	Optimisation of axial position	Gigih et al., 2013
				50-400	Organic matter decomposition	Budhijanto et al., 2015
				50-150	Removal of chemical oxygen demand	Deendarlianto et al., 2015
				50-150	Development of an industrial scale microbubble generator	Majid et al., 2016
	Orifice			600-2600	Generator performance	Sadatomi et al., 2012
				50-150	Removal of chemical oxygen demand	Deendarlianto et al., 2015
		Industrial		50-150		Majid et al., 2016
				380-1000	Oxygen transfer	Juwana et al., 2018; 2019
	Swirling Flow		Air / Ozone	-	Oxygen and ozone mass transfer	Li et al., 2006
			Oxygen	33.4-57.0	Oxygen transfer	Li et al., 2013; 2014
			Air	20	Bubble measurement	Levitsky et al., 2016
			Oxygen	470-750	Oxygen transfer	Yamashita et al., 2017
			Ozone	0.247	Degradation of methyl orange	Hu and Xia, 2018
	Venturi	Lab	Air	271-461	Bubble measurement	Xu et al., 2018
				-	Removal of chemical oxygen demand	Oliveira et al., 2009
				-	Venturi performance	Rahman et al., 2010
				6-100	Flotation of chalcopyrite	Rahman et al., 2014
				300-1150	Bubble generation characteristics	Yin et al., 2015
				375-1100	Mechanism of bubble breakup	Sun et al., 2017
				200-1350	Venturi geometry	Li et al., 2017
				150-500	Venturi performance	Deendarlianto et al., 2017
				100-300	Oxygen mass transfer	Majid et al., 2018
				260-380	Venturi performance	Huang et al., 2018
				52-225	Venturi geometry	Lee et al., 2019
Mechanical Shear	Centrifugal pump			-	Removal of Microcystis aeruginosa	Li et al., 2014b
		Pilot		-	Flotation of oily wastewater	da Silva Henauth et al., 2016
		Lab	Ozone	20-50	Ozonation of aromatic compounds	Wu et al., 2019
	Turbine pump		Air	2.6	Removal of chemical oxygen demand in wastewater	Yao et al., 2016
	Rapid mix			48.5-60.6	Aeration	Li et al., 2016
Fluidic Oscillation	20µm ceramic diffuser			20-1000	Bioreactor modelling	Al-Mashhadani et al., 2011
		Pilot		163.5-621.0	Bioreactor algae growth	Zimmerman et al., 2011b
	20µm nickel membrane	Lab		47	-	Zimmerman et al., 2011a
	20µm sparger			~300	Intensification of yeast production	Hanotu et al., 2016
	25-125µm stainless steel	Pilot		28-268	Pilot scale aerator design	Hanotu et al., 2017
	38µm diffuser	Lab		86	Microflotation for algal separation and recovery	Hanotu et al., 2012; 2014
	Sintered alumina ceramic	Lab		-	Separation of azeotropic mixtures	Abdulrazzaq et al., 2015

[SI] Table 2 – S3. Experimental conditions for microbubble and conventional bubble studies.

Generator		Bubble Diameter		k_La / min^{-1}		Column Height / cm	Liquid Volume / L	Gas Flow Rate / L min^{-1}	Ozone Gas Concentration / mg L^{-1}	Water Matrix	Reference
Microbubble	**Conventional**	**MB / µm**	**CB / mm**	**MB**	**CB**						
0.22 – 0.55 µm aeration device	500 – 1000 µm aeration device	< 50	> 1	0.23	0.11	70	1	0.5	90	pH 3 deionised water	Sun et al. (2020)
Shear force microbubble generator (Xiazhichun, China)	30 mm diameter, 0.1 mm pore size diffuser	2.35 ± 0.84	Near 3 mm	0.023	0.0055	-	20	0.5	233 (derived)	Tap water	Gao et al. (2019)
Nikuni 20NPD04S	Bubble diffuser	20 - 50	mm-size	0.34 – 0.58	0.27 – 0.37	MB: 30 CB: 60	MB: 20 CB: 5	0.5	20	pH 3 – 11 Deionised water	Wu et al. (2019)
KET-LOHR instrument (EMB Technology Co. Ltd. Korea)	40 µm cylindrical glass filter	< 50	-	1.36	1.1	160	16	1	25	50 µg L^{-1} benzo[a]pyrene	Nam et al. (2019)
25QY-2DS (Southern Pump Co.)		20 – 30		0.64 – 0.80		90	8	1.0 – 4.0	30 - 75	Deionised water	Huang et al. (2019)
Spiral liquid flow (Eco-20, Taikohgiken Ltd.)	7 mm pipe	0.25	mm-size			80	20	4	50	Deionised water	Hu and Xia (2018)
Microbubble generator							25			Coal chemical wastewater	Liu et al. (2018)
OHR Mixer F-8 (OHR Lab Corp.)	Common aerator	51.4	mm-size	0.23	0.044	31.8	10	0.3	47.5	Deionised water	Zhang et al. (2018)
Riverforest AS MK-III		< 30		0.30 – 0.41		-	20	-	0.60 – 2.2 mg s^{-1}	pH 3 – 9 0.18 mol m^{-3} diethyl phthalate	Jabesa and Ghosh (2016a)
Kikuchi ECO-Earth TCRI-A	40 µm micropore titanium plate	< 45	~ 1 mm	0.38	0.17	120	6	0.5	12	Clean water	Zheng et al. (2015)
Riverforest AS MK-III		25		0.10 – 0.24		-	20	0.102	329 - 1000	pH 6 – 9 tap water	Khuntia et al. (2013)
Microbubble generator		49.7 – 75.7		0.18 – 0.32		120	26	0.2 – 0.65	40 - 140	pH 7 with 5 x 10^7 CFU ml^{-1} B. subtilis	Zhang et al. (2013)
Cylinder pump and dispersing nozzle	Glass-bonded diffuser	15 - 40	-			-	5	1	50	Distilled water	Takahashi et al. (2012)
NITTA Awatarp	Sintered glass sparger	5 - 50	1 - 5	0.073	0.059	60	9.6	0.03	-	Water	Xu et al. (2012)
TCRI (Japan)	45 µm cylindrical porous diffuser	~ 50	-	0.30	0.20	-	8	0.2	36	Tap water	Liu et al. (2010)
Recycling pump. gyratory accelerator, injector (Kowa Engineering Co. Ltd. Japan)	45 µm cylindrical titanic porous diffuser	< 58	A few mm	0.26	0.14	-	20	0.5	132	pH 2 deionised water	Chu et al. (2007)
M2-LM/PVCm (Nanoplanet Research Institute Co.)		-		0.12 – 0.41		120	38	0.25 – 1.5	28.2	Distilled water	Li and Tsuge (2006)
Electrostatic spray	10 - 15 µm pore diffuser	~ 50	0.36	1.5	0.54	30	1.3	2.1 x 10^{-3}	10	Deionised water	Shin et al. (1999)

Chapter 3. Are Microbubbles Magic or Just Small? A Direct Comparison of Hydroxyl Radical Generation Between Microbubble and Conventional Bubble Ozonation Under Typical Operational Conditions

Alexander John[a], Adam Brookes[b], Irene Carra[a], Bruce Jefferson[a], Monika Jodkowska and Peter Jarvis[a]

[a]School of Water, Energy and Environment, Cranfield Water Science Institute, Cranfield, UK.

[b]Anglian Water, Thorpe Wood House, Peterborough, UK.

Abstract

The application of microbubbles for water treatment is an emerging technology which has been shown to significantly enhance gas-liquid contacting processes. When applied to ozonation, microbubble technology has been shown to enhance mass transfer and the speed and extent of compound removal compared with conventional bubbling techniques. One explanation as to why microbubble systems outperform conventional systems is that microbubbles shrink, collapse and spontaneously generate hydroxyl radicals which is thought to enhance the speed of compound removal. This study compared microbubble (mean diameter 37 μm) and conventional bubble (mean diameter 5.4 mm) ozonation systems under identical conditions. The experiments were normalised for effective ozone dose to determine whether microbubble ozonation generated significantly more hydroxyl radicals than conventional bubble ozonation. 4-chlorobenzoic acid was used as the hydroxyl radical probe and the proportion of hydroxyl radicals generated for a given effective ozone dose was quantified. The $^{\bullet}$OH-exposure to O_3-exposure (the R_{ct}) was used to compare the systems. The ratio of the mean $R_{ct(Microbubble)}$ to mean $R_{ct(Conventional)}$ was 0.73, 0.84 and 1.12 at pH 6, 7 and 8 respectively. Statistical assessment of the R_{ct} showed that there was no significant difference between the bubble systems. No evidence was found to support the hypothesis that microbubble systems generate more $^{\bullet}$OH. Instead, the level of $^{\bullet}$OH-exposure is linked to the effective dose and pH of the system and future designs should focus on those factors to deliver $^{\bullet}$OH based benefits.

3.1. Introduction

Recent technology advances have enabled the generation of microbubbles (1 – 100 µm) to become more widely applicable for use in drinking water treatment beyond dissolved air flotation. Previous research has shown that the use of microbubbles in place of conventionally produced fine bubbles can enhance mass transfer (Sun et al., 2020), increase gas utilisation efficiency (Zhang et al., 2018) and increase the rate and extent of compound removal (Azuma et al., 2019) during ozonation. As such, they are now being considered to replace conventional bubble (2 – 6 mm) systems (John et al., 2022).

The observed performance enhancement is commonly attributed to the large size difference between microbubbles and conventional bubbles (Temesgen et al., 2017). This size difference results in a significantly higher interfacial area (Parmar and Majumder, 2013) and a decrease in rise velocity leading to an extended contact time for the microbubble systems compared to conventional systems (Shangguan et al., 2018). These features allow for a faster and more extensive transfer of gas into the liquid phase (Suwartha et al., 2020) which can lead to enhanced treatment (John et al., 2020).

When ozone is dissolved in water it undergoes a series of pH dependent, complex self-decomposition reactions that lead, in part, to the formation of desirable hydroxyl radicals (•OH). •OH are highly oxidising and non-selective and have been shown to be beneficial to the degradation of recalcitrant compounds (John et al., 2022). A number of recent papers have proposed enhanced •OH generation from microbubbles as an additional benefit (Jothinathan et al., 2021; Li et al., 2020; Liu et al., 2020; Sun et al., 2020; Wan et al., 2020; Patel et al., 2019; Zheng et al., 2015). One proposed mechanism for this being that microbubbles shrink and collapse; rapidly causing an extreme internal temperature and pressure that results in •OH generation. This mechanism has been evidenced in bubble cavitation with a dynamic stimulus such as ultrasound (Thanh Nguyen et al., 2017; Masuda et al., 2015). However, many authors studying application of microbubbles report that their collapse and subsequent production of •OH contributes to enhanced performance without any such stimulus (Table 3 – 1). This has been reported for microbubbles that cover a size range from 1 – 450 µm. It is also the case that many microbubble studies provide limited information on bubble physical characteristics and

hence do not always report a size or compare performance directly with conventional bubbles.

It therefore remains equivocal as to whether microbubbles offer an enhanced generation of •OH over conventional systems as researchers have reported that microbubbles cannot shrink and collapse fast enough to generate •OH spontaneously (Takahashi et al., 2007; Agarwal et al., 2011; Yasui et al., 2019). The aim of the current work was to test the hypothesis that microbubbles generate an enhanced concentration of •OH compared to conventionally sized bubbles under conditions that were representative of typical operating conditions for ozone systems used in water treatment. To test this, a set of controlled experiments directly comparing •OH generation from microbubble and conventional bubbles were trialled in the same setup at three pH's which are most representative of operational ozonation pH's (6, 7, 8). The majority of research on microbubble ozonation is conducted in relatively short column (< 1 m) laboratory trails at fixed ozone input doses which generates a positive bias toward microbubble systems (John et al., 2020). The faster mass transfer associated with microbubble ozonation generates near complete transfer of the available ozone within 1 m and hence delivers a higher dissolved ozone concentration, generating a proportional increase in absolute •OH concentration. However, this does not translate to full scale systems where greater water depths are used (3 – 7 m) resulting in less difference in overall transfer (John et al., 2022). To obviate such bias, the microbubble and conventional bubble systems were operated to achieve equivalent effective dissolved ozone concentrations and thus enable direct observation of any differential •OH generation. This is rarely, if ever, done in previous studies when different sized bubbles have been compared. As such, a sub-hypothesis that the O_3-exposure was different between the microbubble and conventional bubble systems at a fixed effective dose was tested.

Table 3 – 1. Current perspective on ˙OH generation from microbubbles.

Microbubble Diameter / µm	Conventional Bubble Diameter / mm	Normalised For	Position on additional ˙OH generation	Column Height / m	Reference
10 - 50	1 - 2	Input dose	Additional ˙OH could be generated through the shrink and collapse of microbubbles.	Not stated	Jothinathan et al. (2021)
10.30 – 10.60	Not tested	No comparison with conventional	Due to pyrolytic decomposition that takes place within collapsing bubbles, ˙OH can be generated at the gas-liquid interface.	Not stated	Wan et al. (2020)
0.22 - 50	0.5 - 1	Input dose	The constant shrink and collapse of microbubbles result in a powerful pressure wave and high mechanical shear force which further eliminates pollutants.	0.7	Sun et al. (2020)
Not stated	Not stated	Input dose	Shrink and collapse of microbubbles will generate numerous hydroxyl radicals.	Conventional: 0.6 Microbubble: 0.3	Liu et al. (2020)
Not stated	Not tested	No comparison with conventional	By gradually shrinking in size, microbubbles break up in the liquid phase and produce ˙OH.	Not stated	Li et al. (2020)
44 - 450	Not tested	No comparison with conventional	˙OH can be generated due to the pyrolytic decomposition of ozone within the collapsing microbubbles.	Not stated	Patel et al. (2019)
Not stated	Not stated	Input dose	The collapse of microbubbles produces ˙OH which are associated with ion packing around the collapsed microbubbles.	0.9	Huang et al. (2019)
2.35 ± 0.84	~ 3	Input dose	Microbubble collapse can generate a shock wave that generates free radicals.	Not stated	Gao et al. (2019)
Not stated	Not stated	Input dose	When ozone microbubbles shrink it has been reported that they will burst instantaneously and generate ˙OH.	Not stated	Cheng et al. (2019)

Microbubble Diameter / μm	Conventional Bubble Diameter / mm	Normalised For	Position on additional •OH generation	Column Height / m	Reference
20 - 50	Not stated	Input dose	Higher ozone self-decomposition in microbubble systems might result from the shrink and collapse.	Conventional: 0.6 Microbubble: 0.3	Wu et al. (2019)
51.4	Not stated	Input dose	Microbubbles shrink and collapse in the liquid phase and •OH could be generated. •OH generated from collapsing microbubbles probably promote chain reactions of O_3 decomposition.	0.5	Zhang et al. (2018)
10 - 50	Not stated	Input dose	Free radicals might be generated when microbubbles collapse.	Not stated	Li et al. (2018)
0.247 ± 0.009	Not stated	Input dose	No evidence of free radical production from air microbubbles.	0.76	Hu and Xia (2018)
Not stated	Not stated	Input dose	More generation of •OH might be another cause for the increasing rate of reaction in microbubble ozonation.	0.5	Wang et al. (2017)
0.06 – 0.150 and 50	Not tested	No comparison with conventional	At pH ≤ 3, collapsed microbubbles could generate hydroxyl radicals.	Not stated	Sung et al. (2017)
2.6	Not stated	Input dose	•OH generation from collapsing microbubbles during ozonation contributed to the degradation of wastewater.	0.25 rising distance	Yao et al. (2016)
65 % of bubbles had a diameter < 30	Not tested	No comparison with conventional	•OH are very effectively generated by the collapse of O_3 microbubbles in aqueous solutions.	Not stated	Jabesa and Ghosh (2016)
< 45	Approximately 1	Input dose	The enhanced performance could be ascribed to greater amounts of •OH being generated during the collapse of O_3 microbubbles as well as the self-decomposition of O_3 at pH 8.	1.2	Zheng et al. (2015)

3.2. Materials and Methods

3.2.1. Materials

4-chlorobenzoic acid (pCBA) (≥ 99 %, Sigma Aldrich) was used as the $^{\bullet}OH$ probe. Sodium hydroxide (NaOH, Technical Grade, Fisher) and sulphuric acid (H_2SO_4, Technical Grade, Fisher) were used as pH modifiers. N,N-diethyl-1,4-phenylene diamine (DPD) photometric O_3 tests (Merck) were used to measured dissolved O_3 concentration. Potassium iodide (≥ 98 %, Merck) was used as the quenching agent. Methanol (Liquid chromatography mass spectrometry (LCMS) grade, ≥ 99.9 %, Fisher) and ultrapure water (18 MΩ, Elga Purelab) were used as mobile phases for LCMS analysis. Ammonium acetate (≥ 98 %, Sigma Aldrich) was used as a buffer for the mobile phases. Deionised water (15 MΩ, Elga Purelab) was used as the aqueous medium for the experiments.

3.2.2. Experimental Setup

Semi-batch microbubble and conventional bubble experiments were performed in an open-air cylindrical acrylic reactor (Model Products) with a height of 80 cm and a diameter of 45 cm. The experiments were conducted in 100 L of deionised water with a water height of 67 cm and the experiments were conducted in daylight.

O_3 was generated from compressed air using a corona discharge O_3 generator (C-Lasky C-L010-DT, Advanced Ozone Products) with an O_3 production of up to 2 g h^{-1} and an operational gas flow rate range of 2 – 10 L min^{-1} at atmospheric pressure. The gas flow rate was set to 2 L min^{-1} for all experiments. Microbubbles with a Sauter mean diameter (d_{32}) of 37 µm (Figure 3 – 1) were generated using a regenerative turbine microbubble generator (Nikuni KTM20N trial unit, Aeration & Mixing). The microbubble generator had a recirculating liquid flow rate of 16.6 L min^{-1} and a gas flow rate with a range of 0 – 5 L min^{-1}. The gas flow intake of the microbubble generator was set to 2 L min^{-1} for all experiments. The aqueous phase was continuously recirculated through the microbubble generator. Conventional bubbles with a d_{32} of 5.4 mm (Figure 3 – 1) were generated from a fine pore diffuser (132 mm ceramic air stone diffuser, Finest Aquatic LTD) connected directly to the O_3 generator. From the gas flow and bubble size distribution data, the quantity of bubbles generated was calculated to be 7.54 x 10^{10} bubbles min^{-1} for the

microbubble system and 2.4 x 10^4 bubbles min^{-1} for the conventional system. This equated to a bubble density of 3.77 x 10^{10} and 1.2 x 10^4 bubbles L^{-1} for the microbubble and conventional systems respectively. A separate pump (AF-1500, Hidom) recirculated the aqueous phase with a flow rate of 16.6 L min^{-1}. The pH was measured using a portable pH meter (HI-8424, Hanna Instruments), water resistant pH electrode (HI-1230B, Hanna Instruments) and temperature probe (HI-7662, Hanna Instruments). The pH was modified using sodium hydroxide or sulfuric acid. The pH was maintained ± 0.1 throughout each experiment with dropwise addition of dilute sodium hydroxide or sulfuric acid without the presence of buffer. The aqueous temperature for all experiments was 20 ± 1 ˚C (Figure 3 – 2).

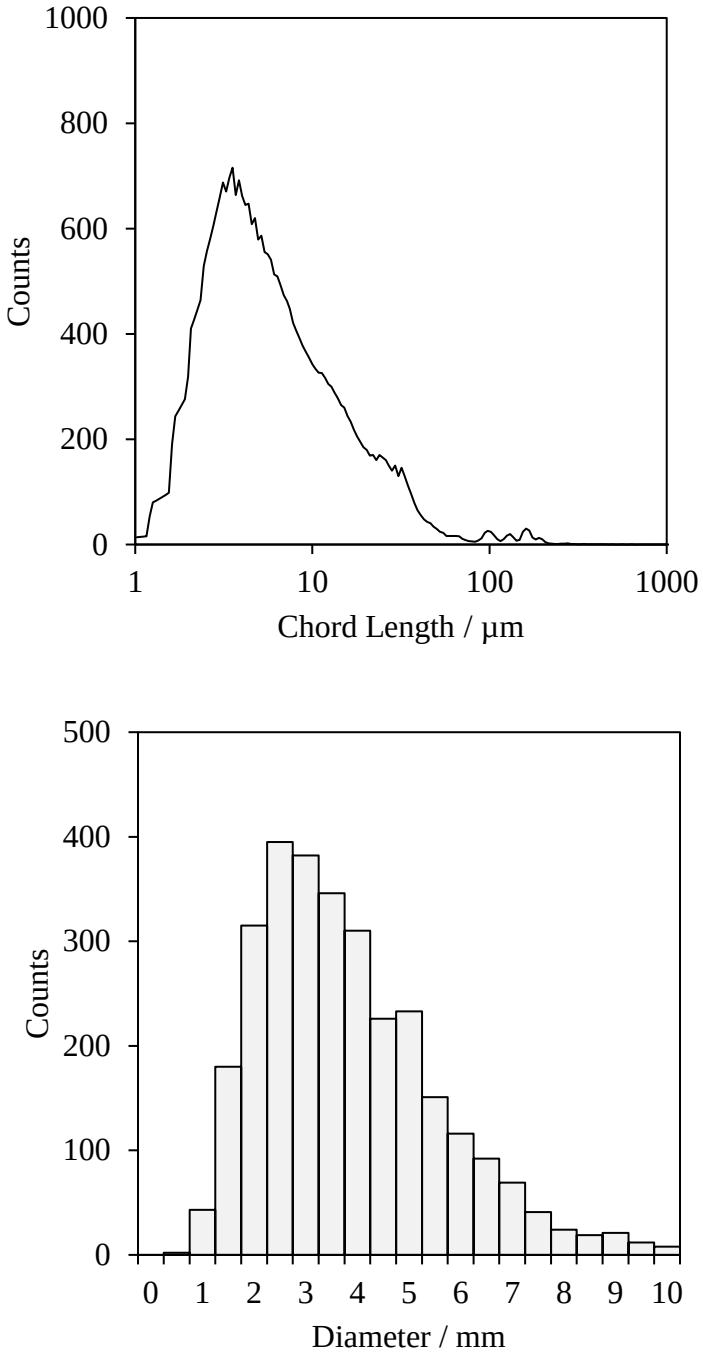

Figure 3 – 1. Size distribution of microbubbles (top) and conventional bubbles (bottom).

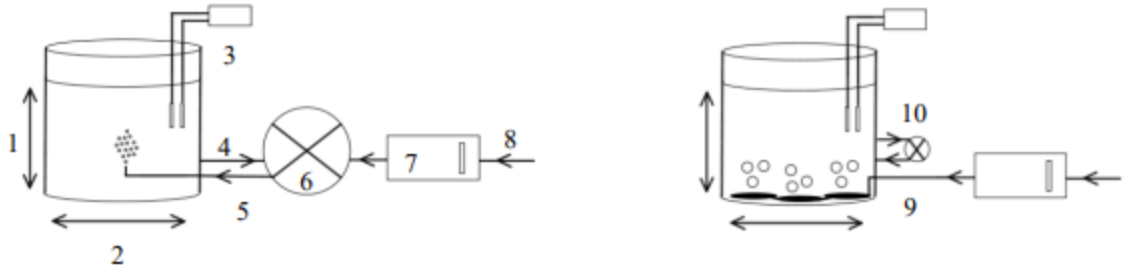

Figure 3 – 2. Experimental setup. Where (1) 0.67 m water height (2) 0.45 m diameter (3) pH and temperature probes (4) water recirculation (5) microbubble input (6) microbubble generator (7) ozone generator (8) gas supply (9) gas supply to diffusers (10) recirculation pump.

The experiments were set for a fixed effective ozone dose of 2.75 µmol L^{-1} min^{-1} to avoid any experimental bias. The ozone output power was set to 100% for the conventional bubble experiments. This equated to 130 watts of O_3 output. In order to achieve an equivalent fixed effective O_3 dose for the microbubble system, the ozone output power was reduced to 75 watts for the microbubble ozonation experiments. This accounted for the increased gas utilisation efficiency of the microbubble system and allowed for equivalent O_3-exposures for both systems. Off-gas concentration was not measured. Mixing in the reactor was achieved through recirculation of the aqueous phase at a flow rate of 16.6 L min^{-1}.

3.2.3. Analysis Method

The ˙OH concentration was measured with an indirect method using pCBA as a probe compound as previously developed (Elovitz and von Gunten, 1999) to overcome issues associated with the highly reactive and short-lived nature of ˙OH (Khuntia et al., 2015). The probe compound enables differential measurement of ˙OH over O_3 as their relative rate constants are significantly different (5.0 x 10^9 M^{-1} s^{-1} and 0.15 M^{-1} s^{-1} for ˙OH over O_3 respectively; Yang et al., 2021) such that the removal of pCBA can be solely attributed to ˙OH.

An initial concentration of pCBA of 0.056 µmol L^{-1} was used throughout. At each time interval, 20 mL of sample was withdrawn and immediately quenched with 0.2 mL potassium iodide solution to prevent further ozonation (Bader and Hoigné, 1981). 10 mL of sample was then used for dissolved O_3 measurement with the diethyl-p-phenylene diamine (DPD) O_3 test and measured using a photometer (Pharo 300, Spectroquant). The remaining 10 mL was passed through a 0.2 µm filter (Minisart, Sartorius) for LCMS analysis. The pCBA concentration was determined using LCMS (ExionLC, Triple Quad 5500+, Sciex). An Acquity C18 ethylene bridged hybrid column (1.7 µm x 2.1 mm x 50 mm) (Waters) maintained at 40 ˚C was used and the sample injection volume was 5 µL. The mobile phase flow rate was 0.45 mL min^{-1}. The mobile phase consisted of ultrapure water with 2 mMol ammonium acetate (A) and methanol with 2 mMol ammonium acetate (B). The initial mobile phase ratio was 90:10 A:B and ramped linearly to 5:95 A:B over 4 minutes before returning to 90:10 A:B for the final minute for a total run time of 5 minutes per sample. The limit of detection and limit of quantification were 0.11 and 0.33 µg L^{-1} respectively.

Bubble size was measured using focus-beam reflectance measurement (FBRM D600L, Mettler Toledo) for the microbubble system. For the conventional system, high speed video was captured (HERO8, GoPro), video frames were extracted (VLC Media Player, VideoLAN) and processed with image processing software (ImageJ).

The integrated form of the rate equation shows that pCBA removal is related to the time-integral of •OH concentration; known as •OH-exposure (Elovitz and von Gunten, 1999):

$$\ln\left(\frac{[pCBA]}{[pCBA]_0}\right) = -k_{\bullet OH(pCBA)} \int [\bullet OH]\, dt \qquad \text{Equation 3 – 1}$$

Where $[pCBA]$ is pCBA concentration (mol L^{-1}), $[pCBA]_0$ is the initial pCBA concentration (mol L^{-1}), $k_{\bullet OH(pCBA)}$ is the rate constant for the reaction of pCBA with •OH (L mol^{-1} s^{-1}) and $\int [\bullet OH]\, dt$ is the time integral of $[\bullet OH]$ (mol L^{-1} s). Therefore, the removal of pCBA over time is an indirect measurement of •OH generation.

To test the main hypothesis, the ratio of •OH measured to O_3 dose delivered was compared (Equation 3 – 2):

$$R_{ct} = \frac{\int [\bullet OH] dt}{\int [O_3] dt}$$ Equation 3 – 2

Where $\int [O_3] dt$ is the time-integrated dissolved O_3 concentration (mol L^{-1} s) and R_{ct} is the ratio of $^{\bullet}OH$-exposure to O_3-exposure. R_{ct} can be calculated from a graphical plot of the change in pCBA concentration over time against the time-integrated dissolved O_3 concentration (Equation 3 – 3):

$$\ln\left(\frac{[pCBA]}{[pCBA]_0}\right) = -k_{\bullet OH(pCBA)} R_{ct} \int [O_3]\, dt$$ Equation 3 – 3

3.3. Results and Discussion

The pseudo-first order rate constant for the removal of pCBA ($k_{\bullet OH(pCBA)}$) increased as pH increased for both the microbubble and conventional bubble systems ([SI] Figure 3 – S1). To illustrate, at pH 6, 7 and 8 the value of $k_{\bullet OH(pCBA)}$ was 0.07 ± 0.004, 0.48 ± 0.09 and 0.86 ± 0.07 min^{-1} for the microbubble system and 0.09 ± 0.01, 0.57 ± 0.1 and 0.97 ± 0.09 min^{-1} for the conventional bubble system. If the main hypothesis was true then $R_{ct(Microbubble)}$ would be greater than $R_{ct(Conventional)}$ due to enhanced $^{\bullet}OH$ generation related to microbubble collapse. This was tested at three different pH levels to reflect changes in the O_3-exposure which decreased with increasing pH due to the associated change in the rate of O_3 self-decomposition ([SI] Figure 3 - S2). After 10 minutes of ozonation, the O_3-exposure for the microbubble system was 173.8 ± 11.8, 133.5 ± 11.7 and 102.3 ± 4.9 µmol L^{-1} min at pH 6, 7 and 8 respectively. The comparative data for the conventional bubble system was 194.4 ± 21.6, 154.5 ± 7.5 and 116.0 ± 14.8 µmol L^{-1} min. The difference in O_3-exposure between the two bubble systems at each pH was not significantly different based on a two-tailed Mann-Whitney U-test with a confidence interval of 95 %. The p-values at pH 6, 7 and 8 were 0.40, 0.10 and 0.38 such that the sub-hypothesis that the O_3-exposures were different between microbubble and conventional bubble systems (h_1) was rejected and hence any difference in $^{\bullet}OH$ concentration could be associated with enhanced generation.

The R_{ct} was calculated from the change in pCBA concentration over time against the time-integrated dissolved O_3 concentration (Figure 3 – 3). For microbubble ozonation, R_{ct} values of 1.77 x 10^{-8} ± 3.91, 2.17 x 10^{-7} ± 4.98 x 10^{-8} and 4.79 x 10^{-7} ± 7.12 x 10^{-8} were obtained at pH 6, 7 and 8 respectively. In comparison, the equivalent R_{ct} values for the conventional bubble system were 2.40 x 10^{-8} ± 4.49 x 10^{-9}, 2.59 x 10^{-7} ± 3.39 x 10^{-8} and 4.27 x 10^{-7} ± 9.37 x 10^{-8} at pH 6, 7 and 8 respectively. Consequently, the ratio of mean $R_{ct(Microbubble)}$ to mean $R_{ct(Conventional)}$ was 0.73, 0.84 and 1.12 at pH 6, 7 and 8 respectively. Statistical assessment of the R_{ct} value indicated no significant difference could be observed based on the Mann-Whitney U-test at a 95 % confidence interval. The p-values obtained were 0.16, 0.51 and 1.0 for the comparison of microbubble and conventional bubble R_{ct} values at pH 6, 7 and 8 respectively. Since $p > 0.05$ for all comparison, h_1 was rejected and hence the R_{ct} values for each comparison were the same.

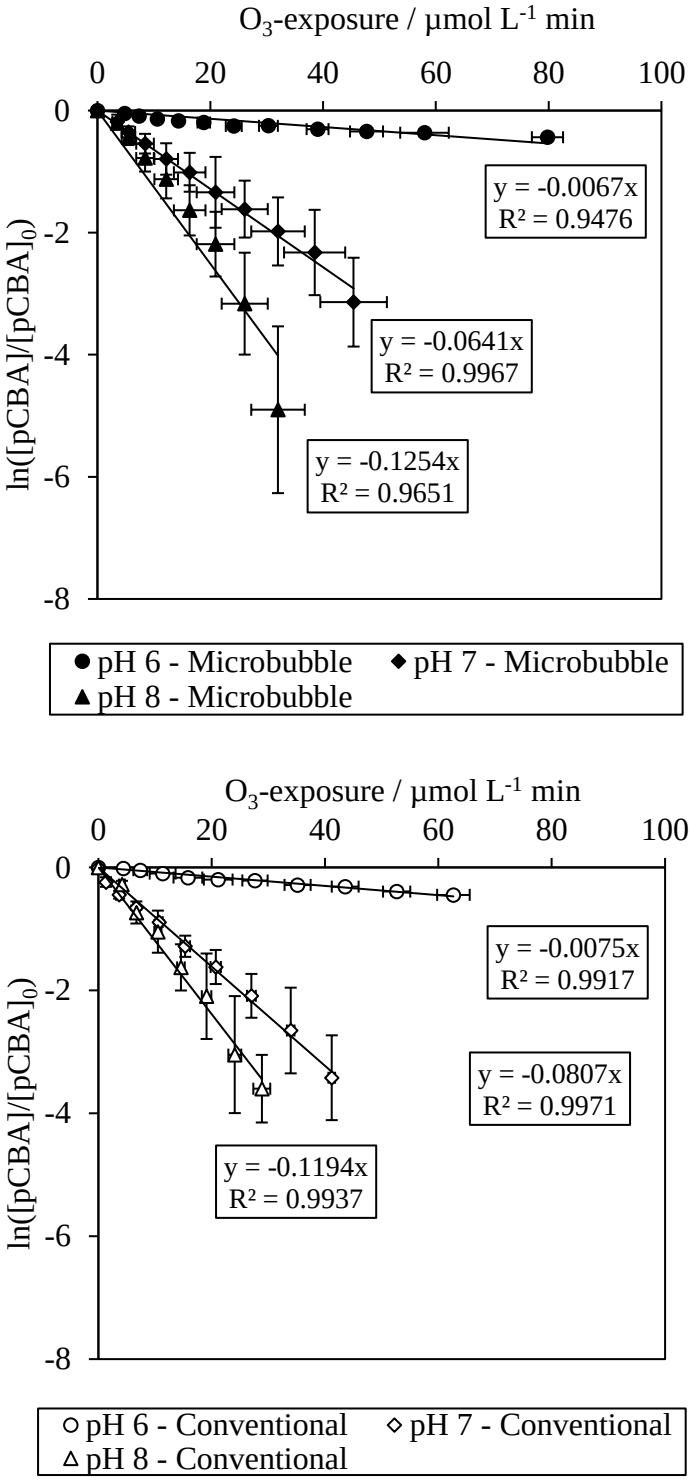

Figure 3 – 3. Plots of $\ln\left(\frac{[pCBA]}{[pCBA]_0}\right)$ vs. $\int[O_3]dt$ at pH 6, 7 and 8 for microbubble (top) and conventional bubble (bottom) ozonation of pCBA.

The impact of R_{ct} and O_3-exposure data on the resultant •OH-exposures revealed an increase as a function of pH with the biggest change occurring as the water increased from slightly acidic to neutral (Figure 3 – 4). To illustrate, •OH-exposure was 3.1 x 10^{-12} ± 1.8 x 10^{-13} mol L^{-1} min for the microbubble system and 4.6 x 10^{-12} ± 0.6 x 10^{-12} mol L^{-1} min for the conventional system at pH 6. In the case of the conventional bubble systems, this increased to 3.9 x 10^{-11} ± 4.5 x 10^{-12} mol L^{-1} min and 4.8 x 10^{-11} ± 1.0 x 10^{-11} mol L^{-1} min for pH 7 and 8 respectively. The corresponding data for the microbubble system was 3.2 x 10^{-11} ± 9.0 x 10^{-12} and 4.1 x 10^{-11} ± 5.7 x 10^{-12} mol L^{-1} min. This represented an increase in mean values of 10.2 times and 13.2 times compared to pH 6 for the microbubble system and 8.4 and 10.4 times for the conventional bubble system. Overall, this confirms the benefit of operating away from slightly acidic conditions when wanting to maximise •OH-exposure. •OH production from ozonation is generally accepted to proceed solely through O_3 self-decomposition in pure water systems (Gardoni et al., 2012). O_3 self-decomposition is not fully understood, however there are two generally accepted self-decomposition pathways (John et al., 2020). Both of these reaction routes are initiated by the hydroxide ion and, as such, these results lend support to the notion that •OH production is primarily a consequence of the speed of O_3 self-decomposition. This implies that as the pH increased, the speed of O_3 self-decomposition increased as the concentration of hydroxide ions increased. This culminated in the expected observation that as pH increased, •OH production increased and thus •OH-exposure also increased.

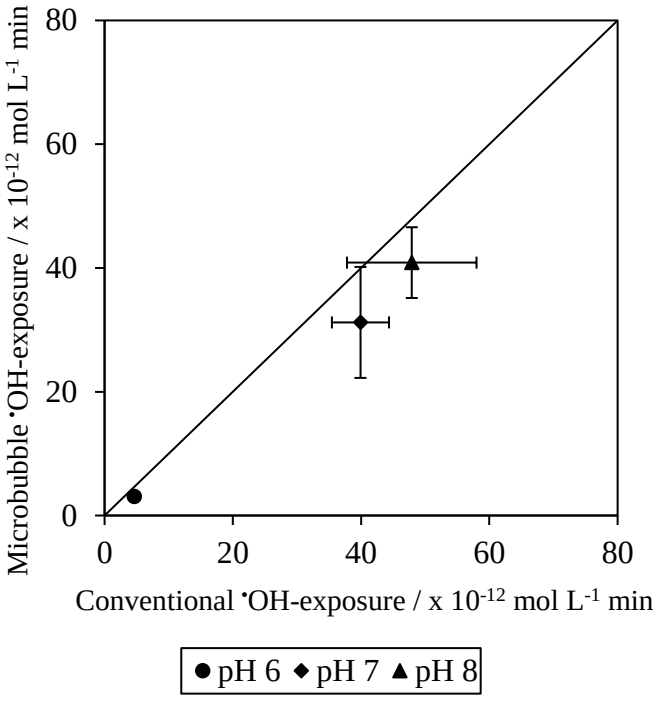

Figure 3 – 4. Parity plot of $\int[\bullet OH]dt$ for microbubble vs. conventional bubble ozonation at pH 6, 7 and 8.

Overall, statistical testing of the data with a Mann-Whitney U-test ($p < 0.05$) showed no significant difference in •OH generation between microbubble and conventional systems and so the hypothesis can be rejected. The Mann-Whitney U-test was used in order to assess whether the difference in observed $\int[\bullet OH]dt$ values between the microbubble system and conventional bubble system were statistically significant. It was found that, at the 95 % confidence level, the hypothesis that either microbubble or conventional bubble ozonation produced a higher proportion of •OH for a given O_3 dose cannot be accepted at any of the tested pH's and it must be assumed that the $\int[\bullet OH]dt$ values are equal.

A large proportion of the microbubble-ozonation literature suggests that •OH generated from collapsing microbubbles is an important component in enhancing the performance of microbubble systems. The current research has shown this is not an important mechanism under normal operational conditions for ozone treatment (pH 6-8). Some

researchers have reported spontaneous •OH generation from collapsing microbubbles but only under specific, strongly acidic conditions for which the mechanism is not fully understood (Takahashi et al., 2007; Li et al., 2009; Khuntia et al., 2016; Minamoto et al., 2021). However, these researchers did not observe ˙OH generation at slightly acidic, neutral or alkaline pH. It has not been fully explained as to why strongly acidic conditions are required, however it has been proposed that the addition of strong acid causes a change in the electrical properties of the gas-liquid interface which does not occur under slightly acidic, neutral or alkaline conditions. Additional ˙OH generation from collapsing microbubbles under neutral or alkaline conditions has not been observed in other studies (Hu and Xia, 2018). Even when nanobubbles as small as 40 nm have been used, under normal operational pH conditions no ˙OH was detected and the addition of strong acid was required to trigger ˙OH generation (Takahashi et al., 2021). Spontaneous production of ˙OH from bubble collapse is only expected to be seen for bubbles in the low nm diameter size range (Liu et al., 2016) or where there is the presence of acoustic stimuli, such as ultrasound (Wu et al., 2013).

These results support the view that the quantity of ˙OH produced is proportional to the effective O_3 dose and that any reported enhancement of ˙OH when using microbubbles is explained by that. Accordingly, the greater O_3 mass transfers afforded in the laboratory set-ups for microbubble systems generates an artefact that may not translate into full scale practice, where overall gas utilisation efficiencies will be more closely matched. However, the ability to transfer high doses into small volumes of water through microbubble systems offers the possibility of alternative designs that benefit from such outcomes and where the dose related enrichment of ˙OH could be positively utilised.

3.4. Conclusions

The presented data here has provided evidence to show that the amount of ˙OH produced through microbubble and conventional bubble ozonation are the same for equivalent O_3-exposure. This study has not found evidence to support the view that microbubble ozonation produces more ˙OH than conventional bubble ozonation when effective O_3 doses are equivalent. The evidence presented implies that the collapse of microbubbles does not cause the spontaneous generation of ˙OH under the tested conditions, within pH

ranges between 6 – 8 that would be considered typical for most ozone applications in water treatment. This study supports the notion that •OH production is directly linked to the O_3 self-decomposition pathway and that other mechanisms for •OH production such as microbubble collapse are either negligible or not present under the pH conditions tested and for the prevailing bubble size distribution.

3.5. Acknowledgements

This research is gratefully supported by the Engineering and Physical Sciences Research Council (EPSRC) through their funding of the STREAM Industrial Doctorate Centre (EP/G037094/1) and from the project sponsor Anglian Water.

3.6. References

Agarwal, A., Ng, W. and Liu, Y., 2011. Principle and applications of microbubble and nanobubble technology for water treatment. *Chemosphere*, 84(9), pp.1175-1180.

Azuma, T., Otomo, K., Kunitou, M., Shimizu, M., Hosomaru, K., Mikata, S., Mino, Y. and Hayashi, T., 2019. Removal of pharmaceuticals in water by introduction of ozonated microbubbles. *Separation and Purification Technology*, 212, pp.483-489.

Bader, H. and Hoigné, J., 1981. Determination of ozone in water by the indigo method. *Water Research*, 15(4), pp.449-456.

Cheng, W., Jiang, L., Quan, X., Cheng, C., Huang, X., Cheng, Z. and Yang, L., 2019. Ozonation process intensification of p-nitrophenol by in situ separation of hydroxyl radical scavengers and microbubbles. *Water Science and Technology*, 80(1), pp.25-36.

Elovitz, M. and von Gunten, U., 1999. Hydroxyl radical/ozone ratios during ozonation processes. I. the R_{ct} concept. *Ozone: Science and Engineering*, 21(3), pp.239-260.

Gao, Y., Duan, Y., Fan, W., Guo, T., Huo, M., Yang, W., Zhu, S. and An, W., 2019. Intensifying ozonation treatment of municipal secondary effluent using a combination of microbubbles and ultraviolet irradiation. *Environmental Science and Pollution Research*, 26(21), pp.21915-21924.

Gardoni, D., Vailati, A. and Canziani, R., 2012. Decay of ozone in water: a review. *Ozone: Science and Engineering*, 34(4), pp.233-242.

Hu, L. and Xia, Z., 2018. Application of ozone micro-nano-bubbles to groundwater remediation. *Journal of Hazardous Materials*, 342, pp.446-453.

John, A., Brookes, A., Carra, I., Jefferson, B. and Jarvis, P., 2022. Microbubbles and their application to ozonation in water treatment: A critical review exploring their benefit and future application. *Critical Reviews in Environmental Science and Technology*, pp.1-43.

Jabesa, A. and Ghosh, P., 2016. Removal of diethyl phthalate from water by ozone microbubbles in a pilot plant. *Journal of Environmental Management*, 180, pp.476-484.

Jothinathan, L., Cai, Q., Ong, S. and Hu, J., 2021. Organics removal in high strength petrochemical wastewater with combined microbubble-catalytic ozonation process. *Chemosphere*, 263, p.127980.

Khuntia, S., Majumder, S. and Ghosh, P., 2015. Quantitative prediction of generation of hydroxyl radicals from ozone microbubbles. *Chemical Engineering Research and Design*, 98, pp.231-239.

Khuntia, S., Majumder, S. and Ghosh, P., 2016. Catalytic ozonation of dye in a microbubble system: Hydroxyl radical contribution and effect of salt. *Journal of Environmental Chemical Engineering*, 4(2), pp.2250-2258.

Lee, Y., Park, Y., Lee, G., Kim, Y. and Chon, K., 2019. Enhanced degradation of pharmaceutical compounds by a microbubble ozonation process: effects of temperature, ph, and humic acids. *Energies*, 12(22), p.4373.

Li, C., Yuan, S., Jiang, F., Xie, Y., Guo, Y., Yu, H., Cheng, Y., Qian, H. and Yao, W., 2020. Degradation of fluopyram in water under ozone enhanced microbubbles: Kinetics, degradation products, reaction mechanism, and toxicity evaluation. *Chemosphere*, 258, p.127216.

Li, P., Takahashi, M. and Chiba, K., 2009. Degradation of phenol by the collapse of microbubbles. *Chemosphere*, 75(10), pp.1371-1375.

Li, P., Wu, C., Yang, Y., Wang, Y., Yu, S., Xia, S. and Chu, W., 2018. Effects of microbubble ozonation on the formation of disinfection by-products in bromide-containing water from Tai Lake. *Separation and Purification Technology*, 193, pp.408-414.

Liu, Y., Wang, S., Shi, L., Lu, W. and Li, P., 2020. Enhanced degradation of atrazine by microbubble ozonation. *Environmental Science: Water Research and Technology*, 6(6), pp.1681-1687.

Liu, S, Oshita, S., Kawabata, S., Makino, Y. & Yoshimoto, T., 2016. Identification of ROS produced by nanobubbles and their positive and negative effects on vegetable seed germination. *Langmuir*, 32, pp. 11295-11302.

Masuda, N., Maruyama, A., Eguchi, T., Hirakawa, T. and Murakami, Y., 2015. Influence of microbubbles on free radical generation by ultrasound in aqueous solution: dependence of ultrasound frequency. *The Journal of Physical Chemistry B*, 119(40), pp.12887-12893.

Minamoto, C., Fujiwara, N., Shigekawa, Y., Tada, K., Yano, J., Yokoyama, T., Minamoto, Y. and Nakayama, S., 2021. Effect of acidic conditions on decomposition of methylene blue in aqueous solution by air microbubbles. *Chemosphere*, 263, p.128141.

Parmar, R. and Majumder, S., 2013. Microbubble generation and microbubble-aided transport process intensification—A state-of-the-art report. *Chemical Engineering and Processing: Process Intensification*, 64, pp.79-97.

Patel, S., Majumder, S., Das, P. and Ghosh, P., 2019. Ozone microbubble-aided intensification of degradation of naproxen in a plant prototype. *Journal of Environmental Chemical Engineering*, 7(3), p.103102.

Shangguan, Y., Yu, S., Gong, C., Wang, Y., Yang, W. and Hou, L., 2018. A review of microbubble and its applications in ozonation. *IOP Conference Series: Earth and Environmental Science*, 128, p.012149.

Sun, Z., Chen, X., Yang, K., Zhu, N. and Lou, Z., 2020. The progressive steps for TPH stripping and the decomposition of oil refinery sludge using microbubble ozonation. *Science of the Total Environment*, 712, p.135631.

Sung, M., Teng, C. and Yang, T., 2017. Dissolution enhancement and mathematical modeling of removal of residual trichloroethene in sands by ozonation during flushing with micro-nano-bubble solution. *Journal of Contaminant Hydrology*, 202, pp.1-10.

Suwartha, N., Syamzida, D., Priadi, C., Moersidik, S. and Ali, F., 2020. Effect of size variation on microbubble mass transfer coefficient in flotation and aeration processes. *Heliyon*, 6(4), p.e03748.

Takahashi, M., Chiba, K. and Li, P., 2007. Free-radical generation from collapsing microbubbles in the absence of a dynamic stimulus. *The Journal of Physical Chemistry B*, 111(6), pp.1343-1347.

Takahashi, M., Shirai, Y. and Sugawa, S., 2021. Free-radical generation from bulk nanobubbles in aqueous electrolyte solutions: esr spin-trap observation of microbubble-treated water. *Langmuir*, 37(16), pp.5005-5011.

Temesgen, T., Bui, T., Han, M., Kim, T. and Park, H., 2017. Micro and nanobubble technologies as a new horizon for water-treatment techniques: A review. *Advances in Colloid and Interface Science*, 246, pp.40-51.

Wan, X., Zhang, L., Sun, Z., Yu, W. and Xie, H., 2020. Treatment of high concentration acid plasticizer wastewater by ozone microbubble oxidation. *Water, Air and Soil Pollution*, 231(7).

Wang, H., Wang, Y., Lou, Z., Zhu, N. and Yuan, H., 2017. The degradation processes of refractory substances in nanofiltration concentrated leachate using micro-ozonation. *Waste Management*, 69, pp.274-280.

Wu, T.Y., Guo, N., The, C.Y., and Hay, J.X.W., 2013. Theory and fundamentals of ultrasound. in: advances in ultrasound technology for environmental remediation. Springer Briefs in Molecular Science. Springer, Dordrecht.

Wu, C., Li, P., Xia, S., Wang, S., Wang, Y., Hu, J., Liu, Z. and Yu, S., 2019. The role of interface in microbubble ozonation of aromatic compounds. *Chemosphere*, 220, pp.1067-1074.

Yang, X., Liu, Z., Manhaeghe, D., Yang, Y., Hogie, J., Demeestere, K. and Van Hulle, S., 2021. Intensified ozonation in packed bubble columns for water treatment: Focus on mass transfer and humic acids removal. *Chemosphere*, 283, p.131217.

Yao, K., Chi, Y., Wang, F., Yan, J., Ni, M. and Cen, K., 2016. The effect of microbubbles on gas-liquid mass transfer coefficient and degradation rate of COD in wastewater treatment. *Water Science and Technology*, 73(8), pp.1969-1977.

Yasui, K., Tuziuti, T. and Kanematsu, W., 2019. Mechanism of OH radical production from ozone bubbles in water after stopping cavitation. *Ultrasonics Sonochemistry*, 58, p.104707.

Zhang, J., Huang, G., Liu, C., Zhang, R., Chen, X. and Zhang, L., 2018. Synergistic effect of microbubbles and activated carbon on the ozonation treatment of synthetic dyeing wastewater. *Separation and Purification Technology*, 201, pp.10-18.

Zheng, T., Zhang, T., Wang, Q., Tian, Y., Shi, Z., Smale, N. and Xu, B., 2015. Advanced treatment of acrylic fiber manufacturing wastewater with a combined microbubble-ozonation/ultraviolet irradiation process. *RSC Advances*, 5(95), pp.77601-77609.

3.7. Supplementary Information

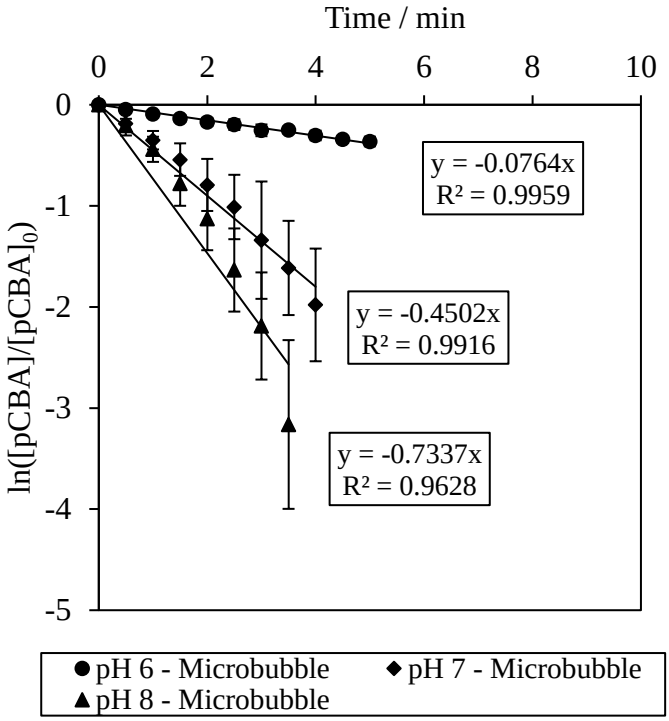

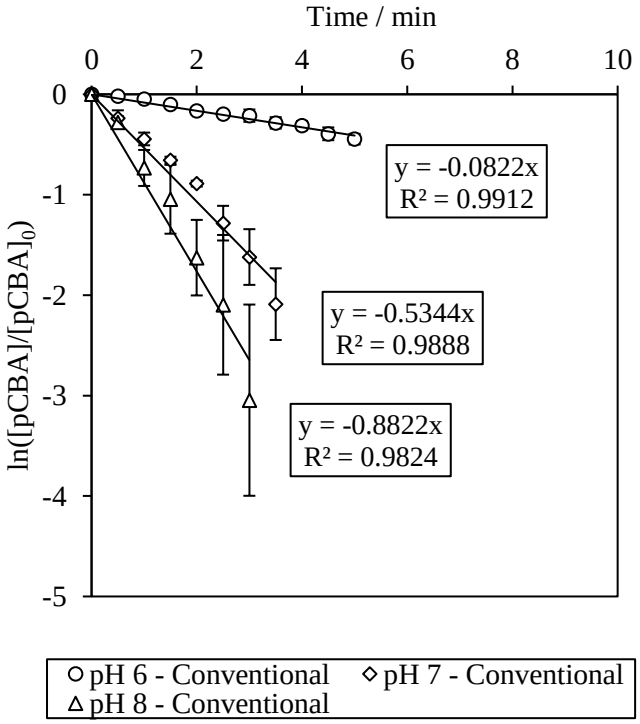

[SI] Figure 3 – S1. pCBA removal profiles for microbubble (top) and conventional bubble (bottom) ozonation at pH 6, 7 and 8.

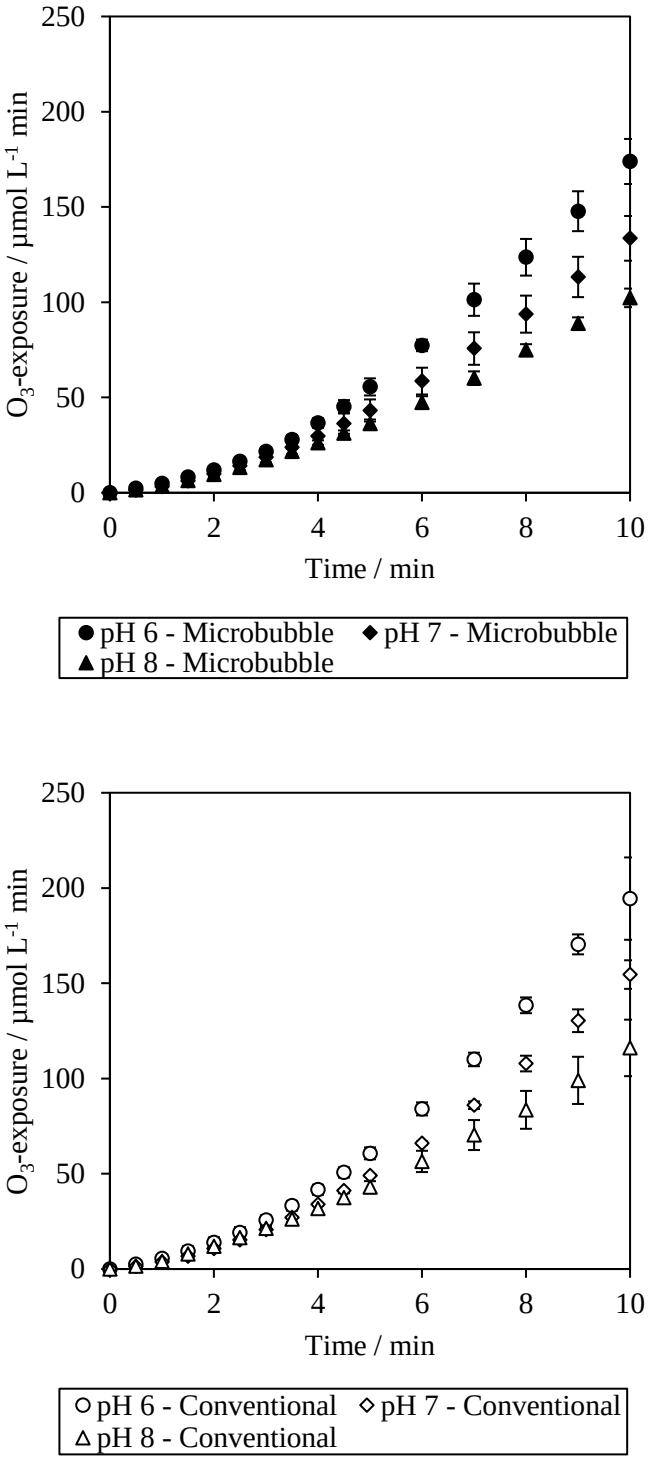

[SI] Figure 3 – S2. Ozone exposure profiles for microbubble (top) and conventional bubble (bottom) ozonation at pH 6, 7 and 8.

Chapter 4. Intensification of Ozonation Using Microbubbles – Micropollutant Removal, Mass Transfer and Bromate Formation

Alexander John[a], Irene Carra[a], Bruce Jefferson[a], Adam Brookes[b], Peter Jarvis[a]*

[a]School of Water, Energy and Environment, Cranfield Water Science Institute, Cranfield, UK.

[b]Anglian Water, Thorpe Wood House, Peterborough, UK.

*Corresponding author

Abstract

Microbubble technology is a promising development in the optimisation of gas-liquid contacting processes. When applied to ozonation, microbubbles have demonstrated significant enhancements to mass transfer, dissolved ozone residual and the speed and extent of compound removal. However, the mechanism by which microbubbles enhance performance when compared to conventional bubbles is not well understood, with numerous disparate explanations in the literature. To elucidate the critical components that drive such enhancements, the performance of microbubbles (Sauter mean diameter 37 µm) and conventional bubbles (5.4 mm) were compared under identical conditions in terms of volumetric mass transfer coefficient, steady state dissolved ozone concentration, rate constant for ozone self-decomposition and the rate constant for degradation of two pesticides: mecoprop and metaldehyde. Overall, the enhancement observed in performance can be attributed to the increase in the volumetric mass transfer coefficient through the combination of an increase in bubble specific interfacial area and a decrease in the mass transfer coefficient. The increase in area outweighed the decrease in mass transfer coefficient such that an overall enhancement factor of 1.6 was observed. All other differences were an artefact of the enhanced mass transfer leading to higher dissolved ozone concentrations when operating at a fixed input dose. When normalised to effective ozone dose, no enhancement in hydroxyl radical production, bromate formation or the impact of background constituent could be observed.

4.1. Introduction

Over the past decade, microbubble technology has emerged as a promising route towards the enhancement of a number of processes that utilise bubbles including vegetable growth (Tamaki et al., 2020), the ripening and removal of residual pesticides on fruit products (Li et al., 2021; Pongprasert et al., 2020), fisheries aeration (Heriyati et al., 2021), biodiesel production (Ahmad et al., 2019) and in gas-liquid contacting processes for water and wastewater treatment (Marbelia et al., 2020; Thomas et al., 2020). For instance, ozonation is an extensively used process in water treatment due to its oxidising and disinfection capabilities (Seridou et al., 2021). Molecular ozone (O_3) is an unstable, powerful oxidant with a standard oxidation potential of 2.07 V (Jin et al., 2023). When ozone dissolves in water, it undergoes a series of complex self-decomposition reactions in which numerous short-lived radicals, including the hydroxyl radical, are formed. Hydroxyl radicals are a non-selective, powerful oxidant with a standard oxidation potential of 2.8 V (Wang et al., 2018) which makes their production desirable in oxidative processes. Accordingly, in ozone-based water treatment, the removal of contaminants proceeds through either direct reactions with molecular ozone or through indirect reactions with hydroxyl radicals. Ozonation is particularly useful in the removal of colour (Khuntia et al., 2016), aromatic organic compounds (Nam et al., 2021), pharmaceuticals (Azuma et al., 2019; Paucar et al., 2019), pesticides (Ikehata and El-Din, 2005) and a wide variety of other micropollutants (Derco et al., 2021). Whilst highly effective, the operational cost of ozonation is significant due to its relatively low mass transfer efficiency (Huang et al., 2020; Jodzis and Zięba, 2018), low solubility (Yang et al., 2021), losses through off-gas (Zhang et al., 2018) and its inability to be stored due to its instability (John et al., 2022).

Ozone is conventionally delivered into water through transfer from bubbles in the millimetre-size range. As such, one potential route for enhancing the process is to reduce bubble size to within the range 1 – 100 μm (microbubbles) using recently developed generator technology. Such devices generate microbubbles through either turbulent flow, mechanical shear, pressurised dissolution or forced bubble detachment (John et al., 2022). Reported studies using microbubbles have confirmed that they offer: Increased interfacial area (Temesgen et al., 2017); lower rise velocity (Swart et al., 2020); enhanced gas utilisation efficiency (Zheng et al., 2015; Muroyama et al., 2013), increased rate of mass

transfer (Wu et al., 2019); and, increased rate of contaminant removal (Cheng et al., 2019; Lee et al., 2019) when compared with conventional bubbles (Table 4 – 1). For instance, the volumetric mass transfer coefficient has been reported to be as much as 5.2 times higher for microbubbles when compared to conventional bubbles (Zheng et al., 2015). Hu and Xia (2018) reported a steady state dissolved ozone concentration that was 15.8 times higher with microbubble ozonation compared with a conventional system. Numerous authors have reported enhancements in the removal of a variety of compounds with enhancement ratios ranging from 1.63 (Khuntia et al., 2016) to 30 (Hu and Xia, 2018). However, the mechanism by which performance is enhanced is not well understood. Several mechanisms have been proposed to suggest that microbubble ozonation enhances hydroxyl radical production through microbubble collapse (Zheng et al., 2015), faster ozone self-decomposition (Zhang et al., 2018), slower ozone self-decomposition (Nam et al., 2021) and increased ozone consumption (Wu et al., 2019). These factors have also been proposed to increase risks in relation to the formation of bromate when used to treat bromide containing waters (Li et al., 2018). However, recent literature has explored this suggestion and revealed no discernible evidence for enhanced radical production when comparing microbubble and conventional ozonation systems (John et al., 2022b; Chapter 3). Instead, the difference reported was a function of the enhanced mass transfer observed in microbubble systems leading to higher dissolved ozone concentrations. Accordingly, any difference is accounted for when comparing both based on effective ozone dose rather than applied dose.

The lack of clarity over the mechanisms by which microbubble systems enhance performance limits the opportunity to optimise such systems or provide robust design procedures. Therefore, the aim of the current work was to understand the controlling mechanism(s) by which microbubbles enhance the performance of ozonation. To achieve this a set of controlled experiments directly comparing the removal of the micropollutants mecoprop and metaldehyde were carried out for both microbubble and conventional bubble ozonation in synthetic and real water sources. In order to assess the mechanism by which the performance was enhanced, a series of controlled mass transfer tests were also conducted. A variety of parameters including the volumetric mass transfer coefficient, steady state dissolved ozone concentration and rate of ozone decomposition were assessed for both microbubble and conventional bubble ozonation at three pH’s

which were representative of typical ozonation pH's (6, 7, 8). A secondary objective was to test the hypothesis that the use of microbubbles during ozonation leads to increased formation of bromate in the ozonation of real bromide containing waters compared with conventional bubbles. This was achieved by undertaking comparative experiments using a part-treated real water from an operational water treatment works that was consistent with a matrix that would be treated by ozonation. Experiments were normalised for both input ozone dose and effective ozone dose in order to determine the extent to which the enhanced mass transfer contributed towards bromate formation and whether bromate formation was dose-dependent or whether another mechanism was involved.

Table 4 – 1. Direct comparison of a variety of parameters for microbubble (MB) and conventional bubble (CB), where $k_L a$ is the volumetric mass transfer coefficient (min^{-1}), k_D is the rate constant for ozone self-decomposition (min^{-1}), C_s is the steady state dissolved ozone concentration ($mg\ L^{-1}$) k_a is the rate constant for target compound removal (min^{-1}) and R is the ratio of microbubble to conventional.

Bubble Diameter		**k_La / min^{-1}**			**k_D / min^{-1}**			**C_s / $mg\ L^{-1}$**			**k_a / min^{-1}**			**Reference**
MB / μm	**CB / mm**	**MB**	**CB**	**R**	**MB**	**CB**	**R**	**MB**	**CB**	**R**	**MB**	**CB**	**R**	
< 50	-	1.38	1.15	1.2	-	-	-	1.2	1.11	1.08	-	-	-	Nam et al. (2021)
< 50	> 1	-	-		-	-	-	35	24	1.46	-	-	-	Sun et al. (2020)
2.35 ± 0.84	~ 3	0.058	0.046	1.26	-	-	-	-	-	-	-	-	-	Gao et al. (2019)
20 – 50	mm-size	0.54	0.35	1.54	0.030	0.023	1.3	2.8	2.3	1.22	0.1	0.032	3.13	Wu et al. (2019)
0.25	mm-size	-	-	-	-	-	-	10.09	0.64	15.8	0.24	0.008	30	Hu and Xia (2018)
51.4	mm-size	0.23	0.044	5.2	0.049	0.013	3.77	5.7	5.5	1.04	0.11	0.061	1.80	Zhang et al. (2018)
-	-	-	-	-	-	-	-	-	-	-	0.39	0.24	1.63	Khuntia et al. (2016)
< 45	~ 1	0.34	0.23	1.48	-	-	-	9.6	8.4	1.14	-	-	-	Zheng et al. (2015)
15 – 40	-	-	-	-	-	-	-	24	9	2.67	0.099	0.032	3.09	Takahashi et al. (2012)
5 – 50	1 – 5	0.095	0.109	0.87	-	-	-	2.5	2.2	1.14	0.0025	0.001	2.5	Xu et al. (2012)
~ 50	-	0.32	0.25	1.28	-	-	-	-	-	-	-	-	-	Liu et al. (2010)
< 58	A few mm	-	-	-	-	-	-	15	14	1.07	0.16	0.091	1.76	Chu et al. (2007)

4.1.1. Theory

The rate of degradation of a compound during ozonation in a bubble contactor is a function of four components: the volumetric mass transfer coefficient, the rate constant for ozone self-decomposition, the hydroxyl radical production and the rate constant for the removal of a particular contaminant (Equation 4 – 1).

$$\varepsilon(r_a) = f[\alpha(k_L a), \beta(k_D), \gamma\left(k_{a_{(O_3)}}\right), \delta\left(k_{a_{(\bullet OH)}}\right)] \quad \text{Equation 4 – 1}$$

Where r_a is the overall rate of removal, $k_L a$ is the volumetric mass transfer coefficient (min^{-1}), k_D is the rate constant of ozone self-decomposition (min^{-1}), $k_{a_{(O_3)}}$ is the rate constant for the reaction of contaminant a with molecular ozone (min^{-1}), $k_{a_{(\bullet OH)}}$ is the rate constant for the reaction of contaminant a with hydroxyl radicals (min^{-1}) and α, β, γ, δ are the ratio of the contributions from microbubble and conventional bubble and ε is the overall enhancement observed in the experiments. The purpose of this work was to identify the difference between the use of microbubble and conventional bubble ozonation with regards to how the different factors contribute to the overall removal enhancement.

The volumetric mass transfer coefficient is comprised of the liquid side mass transfer coefficient, k_L, and the specific gas to liquid interfacial area, a. In a semi-batch ozonation system (as used in the current study), the mass balance can be described by:

$$\frac{dC}{dt} = k_L a(C^* - C) + k_D C \quad \text{Equation 4 – 2}$$

Where $k_L a$ is the volumetric mass transfer coefficient (min^{-1}), C^* is the steady state equilibrium dissolved ozone concentration (mg L^{-1}), C is dissolved ozone concentration (mg L^{-1}) and k_D is the first order rate constant for ozone self-decomposition (min^{-1}). When mass transfer reaches equilibrium, the mass balance can be described by (Wu et al., 2019):

$$0 = k_L a(C^* - C_s) + k_D C_s \quad \text{Equation 4 – 3}$$

Where C_s is the steady state dissolved ozone concentration (mg L^{-1}). Through substitution, $k_L a$ can be determined graphically:

$$\frac{dC}{dt} = (k_L a - k_D)(C_s - C) \qquad \text{Equation 4 – 4}$$

Therefore, $k_L a$ can be found from the measurement of the increase in dissolved ozone concentration over time until a steady state has been reached. A plot of ln $(C_s - C)$ against time has the gradient $(k_L a - k_D)$ which allows for $k_L a$ to be calculated provided that k_D is known. k_D can be determined experimentally after steady state has been reached. Once at steady state, the ozone generator and either the microbubble generator or separate recirculation pump were turned off. The decrease in ozone concentration against time can be measured and the k_D found from a plot of $\ln(C) = k_D . t$. In the absence of contaminants, it can be assumed that the only reaction route for ozone dissolved in deionised water is its self-decomposition, which follows a first order process (Roustan et al., 1996). The $k_L a$ term can be further analysed by separately calculating the interfacial area from the known bubble size distribution and total bubble volume:

$$a = \frac{6\varepsilon}{d_{32}(1 - \varepsilon)} \qquad \text{Equation 4 – 5}$$

Where a is the interfacial area (m^{-1}) and ε is gas hold up (a.u.). An experimental mass transfer coefficient can then be derived:

$$k_L = \frac{k_L a}{a} \qquad \text{Equation 4 – 6}$$

Where k_L is the mass transfer coefficient (m s^{-1}).

4.2. Materials and Methods

4.2.1. Materials

Metaldehyde (Technical grade, Sigma Aldrich) and mecoprop (Analytical grade, Sigma Aldrich) were used as the target micropollutant compounds. Sulphuric acid (H_2SO_4, technical grade, Fisher) and sodium hydroxide (NaOH, technical grade, Fisher) were used for pH adjustment. Potassium iodide (≥ 98 %, Merck) was used as the O_3 quenching agent. N,N-diethyl-1,4-phenylene diamine (DPD) photometric O_3 tests (Merck) were used to measure the dissolved O_3 concentration. Methanol (Liquid chromatography mass spectrometry (LCMS) grade, ≥ 99.9 %, Fisher) and ultrapure water (18 MΩ, Elga Purelab) were used as the mobile phases for LCMS analysis. Ammonium formate (Technical grade, Sigma Aldrich) was used as the mobile phase buffer for LCMS analysis. Deionised water (15 MΩ, Elga Purelab) and part-treated pre-ozone natural water (East of England) was used as the aqueous medium for the experiments.

4.2.2. Experimental Setup

Microbubble and conventional bubble experiments were conducted in an open-air cylindrical acrylic reactor (Model Products) with a height of 80 cm and an inner diameter of 45 cm. When filled with 100 L of liquid, the water height was 62 cm. The experiments were conducted in semi-batch mode and the experiments were conducted in daylight (Figure 4 – 1).

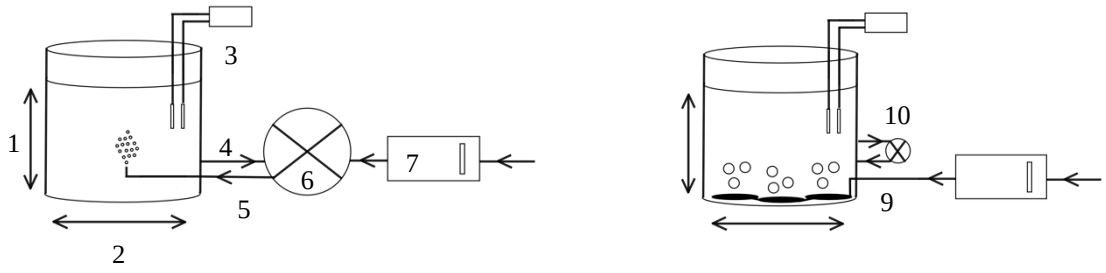

Figure 4 – 1. Experimental setup. Where (1) 0.67 m water height (2) 0.45 m diameter (3) pH and temperature probes (4) water recirculation (5) microbubble input (6) microbubble generator (7) ozone generator (8) gas supply (9) gas supply to diffusers (10) recirculation pump.

Ozone gas was produced from compressed air using a corona discharge ozone generator (C-Lasky C-L010-DT, Advanced Ozone Products) with an operational gas flow rate of 2 – 10 L min^{-1}. The ozone gas output of the generator was up to 2 g h^{-1}. For all experiments, the gas flow rate of the ozone generator was set to 2 L min^{-1}. Microbubbles were generated using a regenerative turbine microbubble generator (Nikuni KTM20N trial unit, Aeration & Mixing). The microbubble generator had a recirculating liquid flow rate of 16.6 L min^{-1} to aid mixing and a gas flow meter with a range of 0 – 5 L min^{-1}. The gas flow intake of the microbubble generator was set to 2 L min^{-1} for all experiments for optimal operation of the microbubble generator. The aqueous phase was continuously recirculated through the microbubble generator. Conventional bubbles were generated from a fine pore diffuser (132 mm ceramic air stone diffuser, Finest Aquatic LTD) connected directly to the ozone generator. In order to match the configuration of the microbubble generator as closely as possible, a separate liquid pump (AF-1500, Hidom) with a flow rate of 16.6 L min^{-1} was used to recirculate and mix the aqueous phase for the conventional bubble experiments. Off-gas concentration was not measured.

The pH was measured using a portable pH meter (HI-8424, Hanna Instruments), water resistant pH electrode (HI-1230B, Hanna Instruments) and temperature probe (HI-7662, Hanna Instruments). The pH was modified using sodium hydroxide or sulfuric acid. The pH was maintained ± 0.1 throughout each experiment with dropwise addition of dilute sodium hydroxide or sulfuric acid without buffer. The aqueous temperature for all experiments was 20 ± 1 ˚C. For experiments normalised for input dose, ozonation was delivered with 100 % output from the ozone generator which equated to 130 watts of ozone output. For the experiments that were normalised for effective ozone dose, the conventional bubble system received an input dose which equated to 130 watts of ozone output and the microbubble system received an equivalent effective ozone dose with 75 watts of ozone output.

For the single micropollutant removal experiments, an initial concentration of 0.056 µmol L^{-1} of metaldehyde or mecoprop was used throughout (equivalent to 10 and 12 µg L^{-1} respectively). Metaldehyde was selected due to its low reactivity with molecular ozone, persistence and its regulatory concern (Tang et al., 2016). In contrast, mecoprop was selected due to its relatively high affinity for molecular ozone (Gulde et al., 2021) and allows for the comparison of both fast- and slow- reaction speeds with molecular ozone.

The concentration of 0.056 µmol L^{-1} was selected in order to have a sufficiently high initial concentration for measurement and also low enough to be relatively representative of concentrations found in natural waters. A 20 mL aliquot was removed at pre-defined time intervals and immediately quenched with 200 µL potassium iodide solution to cease ozonation. 10 mL of sample was used for dissolved ozone measurement with the DPD ozone test and measured using a spectrophotometer (Pharo 300, Spectroquant). A portion of the retained sample was filtered through a 0.2 µm syringe filter (Minisart, Sartorius) for LCMS analysis. All experiments were performed in triplicate. For the part-treated pre-ozone experiments, 120 mL of sample was removed at pre-defined time intervals and immediately quenched with 1.2 mL potassium iodide. 10 mL of sample was used for dissolved ozone measurement using the DPD ozone test and measured using the spectrophotometer. 10 mL of sample was filtered through a 0.2 µm syringe filter for LCMS analysis. The remaining 100 mL of sample was stored in labelled sample bottles and delivered to an external laboratory for bromate analysis.

4.2.3. LCMS Methods

Mecoprop concentration was determined using LCMS (ExionLC, Triple Quad 5500+, Sciex). An Acquity C18 ethylene bridged hybrid column (1.7 µm x 2.1 mm x 50 mm) (Waters) maintained at 60 ˚C was used and the sample injection volume was 10 µL. The mobile phase flow rate was 0.45 mL min^{-1}. The mobile phase consisted of ultrapure water with 2 mmol L^{-1} ammonium formate (A) and methanol with 2 mmol L^{-1} ammonium formate (B). The initial mobile phase ratio was 95:5 A:B. It was ramped linearly to 5:95 A:B over 3 minutes and held for 30 seconds before returning to 95:5 A:B for the final 30 seconds for a total run time of 4 minutes per sample. Metaldehyde concentration was determined using LCMS (ExionLC, Triple Quad 5500+, Sciex). An Acquity C18 ethylene bridged hybrid column (1.7 µm x 2.1 mm x 50 mm) (Waters) maintained at 60 ˚C was used and the sample injection volume was 10 µL. The mobile phase flow rate was 0.45 mL min^{-1}. The mobile phase consisted of ultrapure water with 2 mmol L^{-1} ammonium formate (A) and methanol with 2 mmol L^{-1} ammonium formate (B). The initial mobile phase ratio was 95:5 A:B. It was ramped linearly to 5:95 A:B over 2 minutes and held for 24 seconds before returning to 95:5 A:B over 6 seconds and maintained for 90 seconds for a total run time of 4 minutes per sample.

4.2.4. Measurement of Bubble Size Distribution

Microbubble size distribution was measured using focus-beam reflectance measurement (FBRM 600L, Mettler Toledo) continuously over a period of 30 minutes. A minimum of 30,000 counts were collected and the instrument range was 1 – 4000 µm.

Conventional bubble size distribution was measured using high speed video (HERO8, GoPro) mounted to a camera tripod (JB01511-BWW, Joby) with a waterproof LED video light (XShot, Suptig) which was submerged into the water. The camera was focussed on a precision ruler with 1 mm spacing (Precision ruler, Dorcrafts) which acted as a size reference. Video was shot at 240 frames per second for 10 minutes. The video was slowed to 30 frames per second and desaturated using video editing software (GoPro Studio, GoPro). Image frames from the video were extracted using a media software (VLC Media Player, VLAN). The image frames were processed manually using image processing software (ImageJ) and the diameter of in-focus bubbles was measured against the size reference. A minimum of 1000 individual in-focus bubbles were measured for each run for a total of 3000 measurements.

The Sauter mean diameter for the microbubble and conventional bubble distributions were calculated as follows (Abbasian-arani et al., 2020):

$$d_{32} = \frac{\sum n_i d_i^3}{\sum n_i d_i^2} \qquad \text{Equation 4 – 7}$$

Where d_{32} is the Sauter mean diameter (m) and n_i is the number of bubbles with diameter d_i. Bubble size distributions were measured at pH 7.

4.3. Results and Discussion

4.3.1. Performance of Microbubble Ozonation in a Synthetic Matrix

The rate of removal of both mecoprop and metaldehyde increased as pH increased for both the microbubble and conventional bubble ozonation (Figure 4 – 2). In the case of mecoprop, a pesticide known to be degraded by ozonation, the residual concentration was below 5% of the initial concentration after 15, 10, and 10 minutes for the microbubble

systems compared to 20, 15 and 15 minutes for the conventional system for pH values of 6, 7 and 8 respectively. Greater differences were observed in the case of metaldehyde, a pesticide known to be recalcitrant to ozone but degradable by hydroxyl radicals. In this case the residual concentration after 45 minutes was 58%, 46% and 5% of the initial concentration for the microbubble systems at pHs of 6, 7 and 8 respectively. The corresponding values for the conventional system were 75, 66 and 32% respectively. Overall, the use of the microbubble systems led to either faster removal (mecoprop) or better overall removal (metaldehyde).

The pseudo-first order rate constant for the removal of mecoprop at pH 6, 7 and 8 was 0.31 ± 0.01, 0.34 ± 0.02 and 0.37 ± 0.04 min^{-1} respectively for the microbubble system and 0.17 ± 0.02, 0.21 ± 0.02 and 0.25 ± 0.02, respectively for the conventional systems. The corresponding enhancement factors for each pH condition was 1.8, 1.6 and 1.5 times (Figure 4 – 3). Due to its low reactivity with molecular ozone, the pseudo-first order rate constant for the removal of metaldehyde was much lower than that of mecoprop. To illustrate, the values at pH 6, 7 and 8 were 0.012 ± 0.002, 0.017 ± 0.004 and 0.042 ± 0.004 respectively for the microbubble system and 0.006 ± 0.001, 0.009 ± 0.002 and 0.021 ± 0.003 for the conventional system. The corresponding enhancement factors due to using microbubbles was slightly higher than for mecoprop, with values of 2.0, 1.9 and 2.0 times. The current enhancement factors are at the low end of those previously reported (Table 4 – 1). To illustrate, Wu et al. (2019) observed an average rate constant enhancement of 3.4 and 2.8 times for the microbubble ozonation of phenol and nitrobenzene, respectively, across the pH range 3 – 11. Takahashi et al. (2012) observed a rate constant enhancement of 1.1 – 3.1 times in favour of microbubble ozonation in the removal of four different dyes. All these previous studies use a common input dose and attribute the observed enhancement to increased $^{\bullet}OH$ production (Sun et al., 2020; Wu et al., 2019; Hu and Xia, 2018; Zhang et al., 2018; Wang et al., 2017; Yao et al., 2016; Zheng et al., 2015). However, the microbubble systems will exhibit a substantially higher surface area for mass transfer and so the effective dose will be higher in the microbubble system.

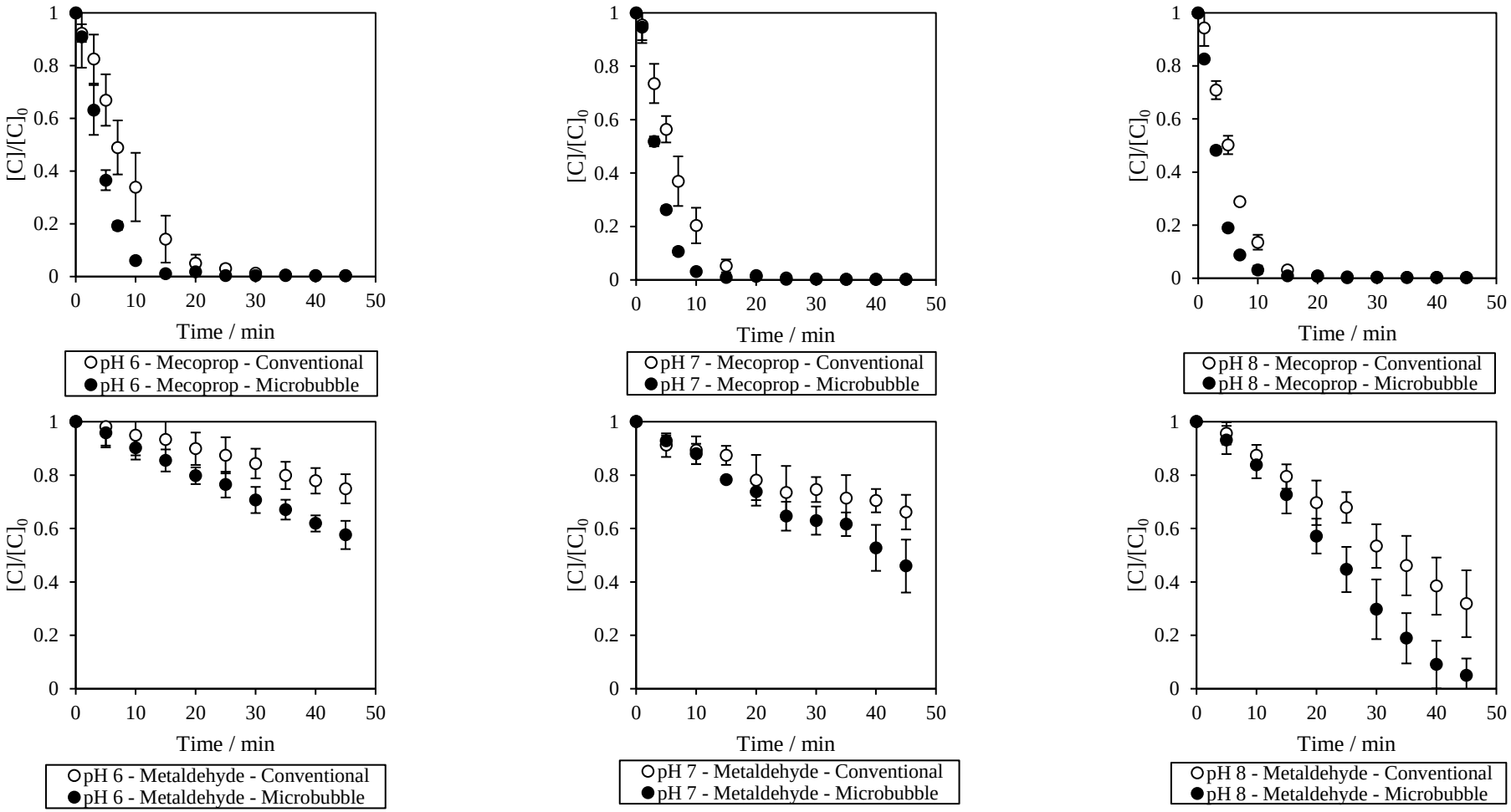

Figure 4 – 2. Removal profile of mecoprop (top) and metaldehyde (bottom) with microbubble and conventional bubble ozonation at pH 6 (left), 7 (middle) and 8 (right).

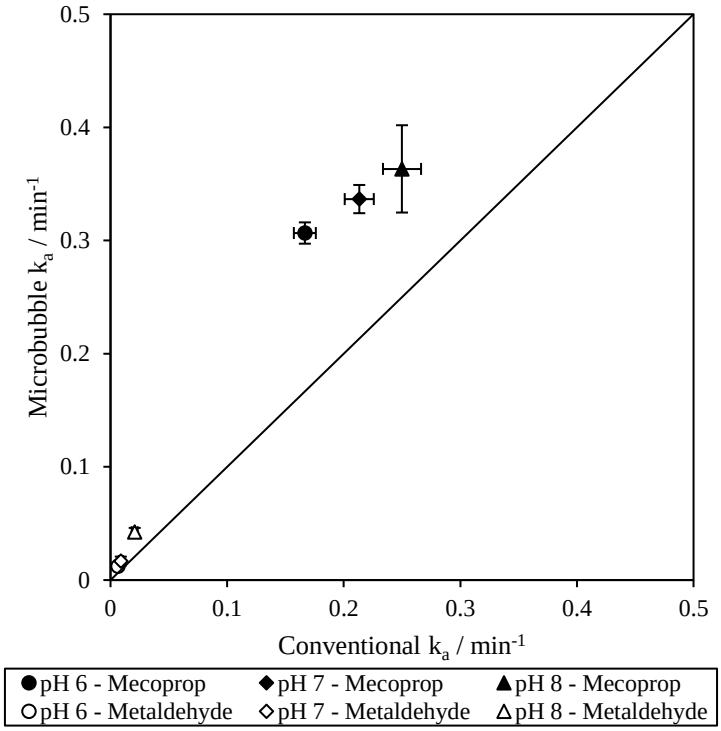

Figure 4 – 3. Pseudo first-order rate constants for the removal of metaldehyde and mecoprop for microbubble and conventional bubble ozonation at pH 6, 7, 8.

To consider this, the data was replotted using the time integral of dissolved ozone concentration (ozone exposure) (Figure 4 – 4). In all cases the comparison of the two systems revealed approximately the same extent and rate of removal for the micropollutants for a given pH. No discernible difference in removal was observed with respect to pH for mecoprop, a point that was consistent with its high reactivity towards molecular ozone ($k_{O_3} \approx 100$ M^{-1} s^{-1}) (Gulde et al., 2021). However, a clear increase in removal was observed as pH increased for metaldehyde. This was consistent with an increase in $^{\bullet}$OH production which occurs when more hydroxide ions are present in the water. Hydroxyl radical attack is known to be the predominant mechanism of removal of metaldehyde in ozone systems (Tang et al., 2016). Importantly, there was no statistical difference in the removal data observed for conventional and microbubble systems at any of the pH investigated, suggesting no appreciable change in $^{\bullet}$OH production for either system. This aligns with the outcomes from a previous study by the authors that directly

measured •OH production for both systems that concluded microbubble ozonation does not form proportionally higher quantities of •OH compared with conventional bubble ozonation for a given dissolved ozone dose (Chapter 3; John et al., 2022b). Consequently, the improvements previously reported are a reflection of improvements in mass transfer such that the target dissolved ozone dose can be achieved using a reduced input dose. In the current case, this equates to a reduction in input dose of 1.9 – 2.5 times indicating the potential savings that may be possible if switching to microbubble systems when dosing ozone. Regarding the respective mechanisms that are responsible for the observed enhancement, the data above indicates that the γ and δ terms of equation 4 – 1 are equal to 1 and that microbubbles enhance performance through some function of k_L, a, $k_L a$ and / or k_D.

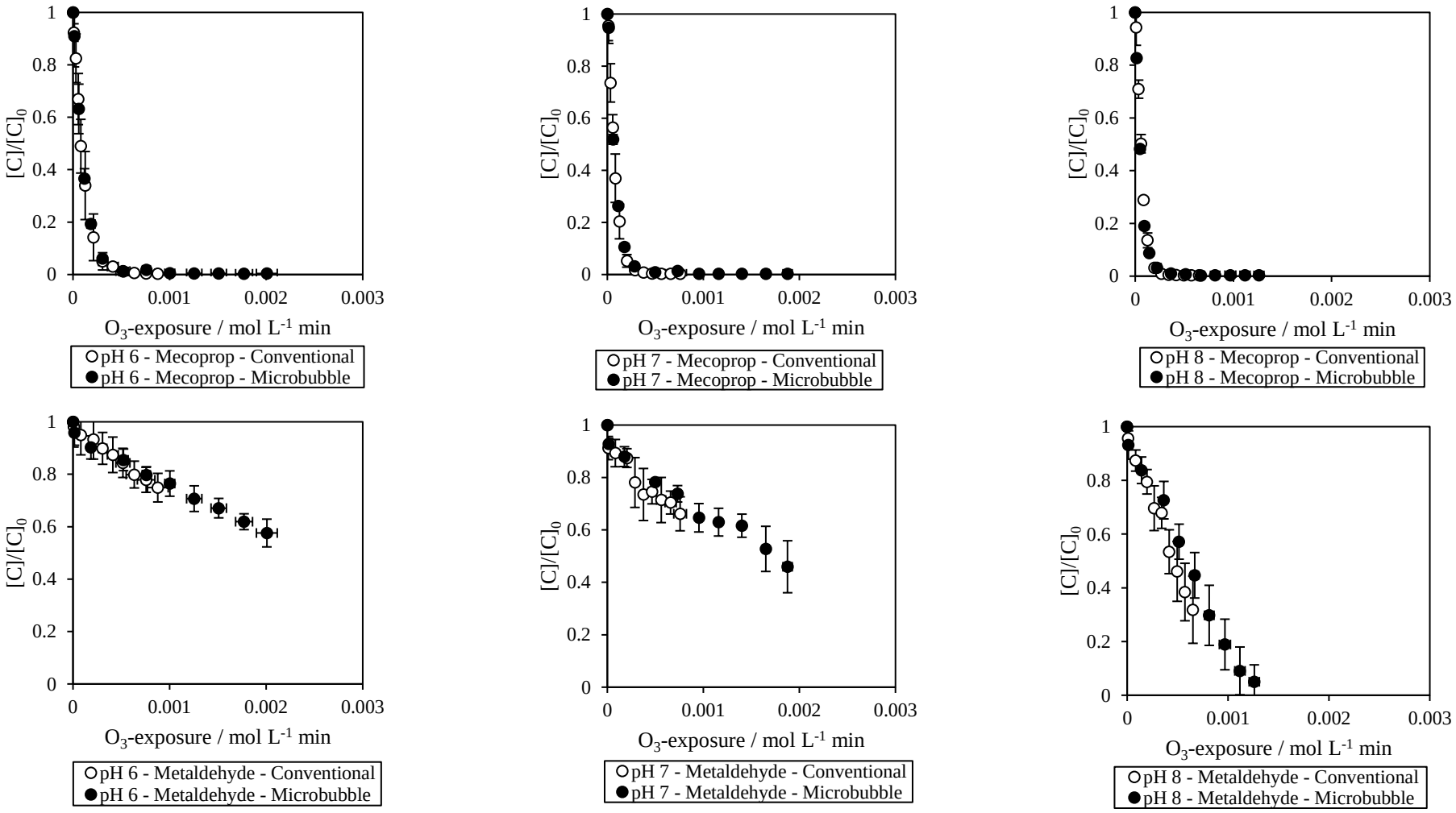

Figure 4 – 4. Removal profile of mecoprop (top) and metaldehyde (bottom) normalised against O_3-exposure for microbubble and conventional bubble ozonation at pH 6 (left), 7 (middle) and 8 (right).

4.3.2. Mass Transfer

4.3.2.1. Steady State Concentration and Self-Decomposition

In order to further explore the mechanism by which microbubbles enhance ozonation performance, mass transfer tests were conducted. The increase in dissolved ozone concentration for a fixed input dose was measured over time until a steady state was reached. For conventional bubble ozonation, C_s values of 1.21 ± 0.03, 0.98 ± 0.04 and 0.83 ± 0.03 mg L^{-1} were obtained at pH 6, 7, and 8 respectively (Figure 4 – 5). For microbubble ozonation, the C_s values at pH 6, 7 and 8 were 2.56 ± 0.07, 2.27 ± 0.11 and 1.43 ± 0.04 mg L^{-1}. The increase in dissolved ozone at steady state for the microbubble systems represented an enhancement of 2.1, 2.3 and 1.7 times respectively. Previous literature supports the observation of an increase in dissolved ozone concentration for a given input dose but with lower ratios that were between 1.1 and 1.7 (Chu et al., 2007; Zheng et al., 2015; Wu et al., 2019). However, differences are to be expected since C_s is influenced by many factors including gas phase ozone input concentration, pH, consumption from reactions with contaminants, gas utilisation efficiency and self-decomposition (Lage Filho, 2010).

Self-decomposition is particularly important due to its link to hydroxyl radical production, which involves a complex series of reactions which are pH dependent (Gardoni et al., 2012). To explore this aspect, k_D was determined experimentally by monitoring the decrease in ozone concentration over time (Figure 4 – 6). Self-decomposition rate constants of 0.0016 ± 0.0005, 0.0051 ± 0.0015 and 0.013 ± 0.001 min^{-1} were observed at pHs 6,7 and 8 respectively in the conventional bubble system. These compared to 0.0019 ± 0.0006, 0.0053 ± 0.0012 and 0.013 ± 0.0008 min^{-1} for the microbubble system indicating no discernible difference due to bubble size. This was confirmed statistically using a Mann-Whitney U-test with a 95 % confidence interval such that k_D values were the same irrespective of ozone delivery method, but vary with pH as expected (Mao et al., 2021). These observations contradict previous reported trials that considered ozone self-decomposition (Wu et al., 2019; Zhang et al., 2018). For instance, Zhang et al. (2018) noted an increase in the rate of ozone self-decomposition from 0.013 min^{-1} to 0.049 min^{-1} when microbubbles were used in place of conventional bubbles; an increase of 3.7 times. Here, the authors explained the increase in k_D as a result of the

increased production of •OH due to collapsing microbubbles which caused an increase in ozone self-decomposition. A decrease in k_D has also been reported (Nam et al., 2021), with the authors' observing almost no decomposition for microbubbles. In this work, the authors attributed the limited decomposition to the long stagnation time of microbubbles. Evidently, these two observations from the literature infer opposing microbubble behaviour which suggests that some other experimental difference may have been causing the different observations in k_D. In the current case, no difference in self-decomposition was observed such that the exponent β in equation 4 – 1 was equal to 1.

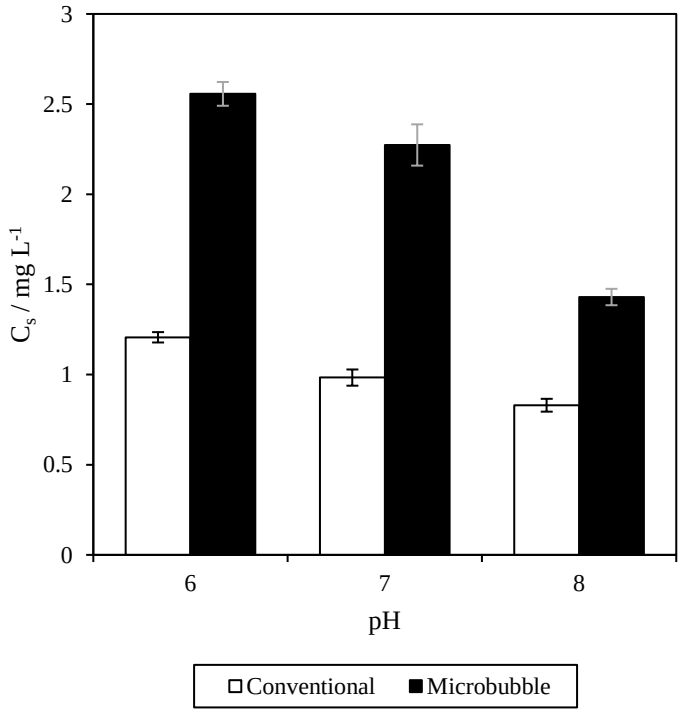

Figure 4 – 5. Steady state dissolved O_3 concentration for microbubble and conventional bubble ozonation at pH 6, 7, 8.

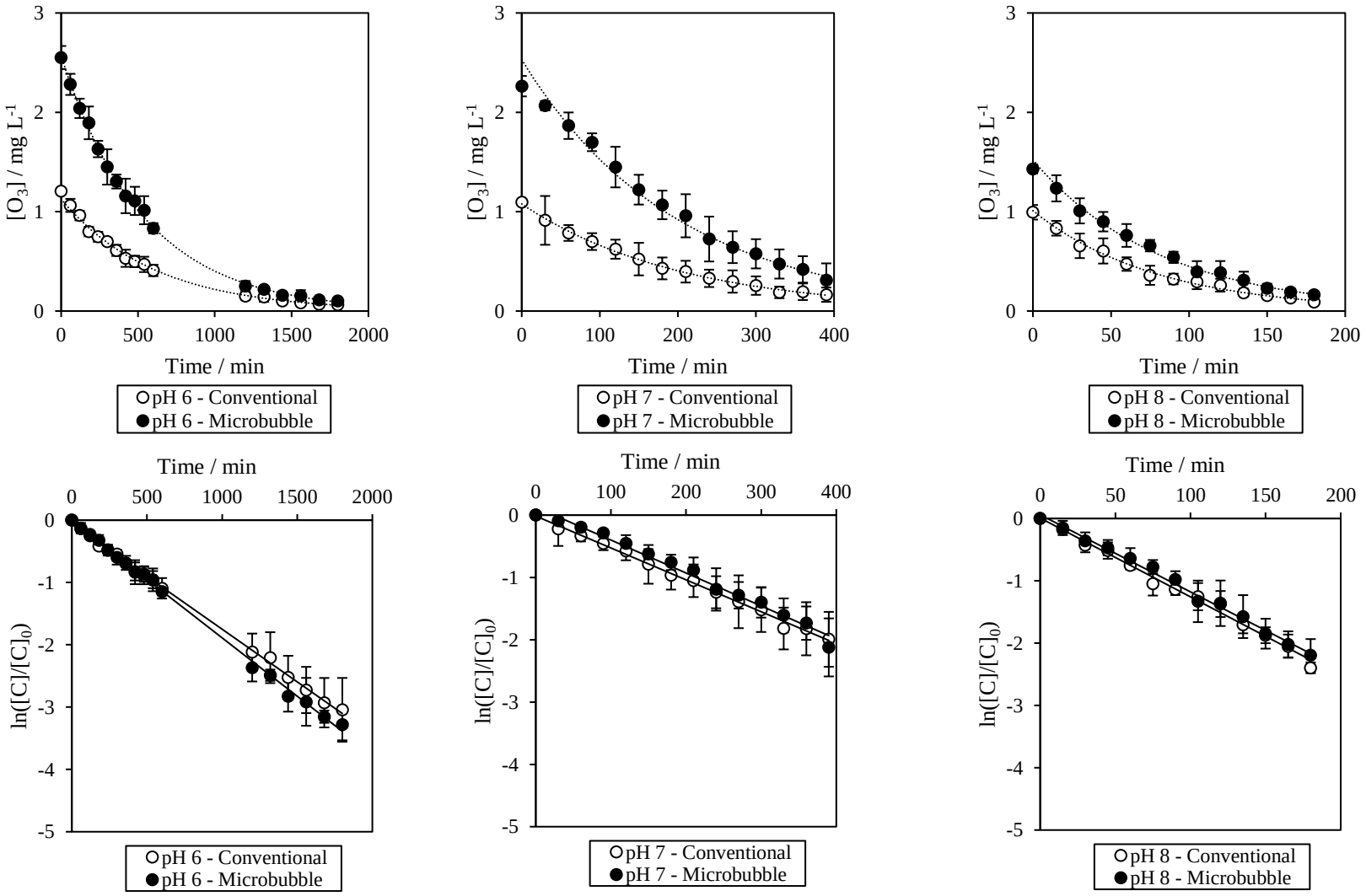

Figure 4 – 6. O_3 self-decomposition profiles (top) and first order rate constants (bottom) for microbubble and conventional bubble ozonation at pH 6 (left), 7 (middle) and 8 (right).

4.3.2.2. Volumetric Mass Transfer Coefficients

The volumetric mass transfer coefficient ($k_L a$) was 0.067 ± 0.009, 0.091 ± 0.005 and 0.15 ± 0.03 min^{-1} for the conventional system and 0.12 ± 0.004, 0.15 ± 0.02 and 0.30 ± 0.03 min^{-1} for the microbubble system as the pH changed from 6 to 7 to 8 respectively (Figure 4 – 7). The corresponding enhancement factors were 1.7, 1.6 and 2.0 for the microbubbles when compared to the conventional bubble system. The enhancement factors reported here are at the high end of the range previously reported between 1.2 and 1.8 (Nam et al., 2021; Wu et al., 2019; Zheng et al., 2015; Liu et al., 2010).

The $k_L a$ itself consists of two components: the mass transfer coefficient, k_L, and the specific gas-to-liquid interfacial area, a. The size distribution of the microbubble system was only measured at pH 7 and was found to have a relatively narrow distribution with 50 % of the microbubbles having a diameter of < 4.9 µm. The 25^{th} and 75^{th} percentile bubble diameters were 3.1 and 10.0 µm respectively. The Sauter mean diameter was 37 µm with its value reflecting the presence of a relatively lower number of larger bubbles but is the most appropriate diameter model for systems with active surfaces (Wang et al., 2020).

The interfacial areas of the microbubble and conventional bubble systems were calculated from the interfacial area distributions derived from the bubble size measurement and a gas holdup estimation of 0.0015 a.u. (Maceiras et al., 2010), with values of 243 and 1.7 m^{-1} for the microbubble and conventional bubble systems respectively, a difference of 143 times (Supplementary Information [SI] Figure 4 – S1). Utilising the values for interfacial area, experimental values of k_L were calculated as 9.65 x 10^{-6} and 8.2 x 10^{-4} m s^{-1} for microbubble and conventional bubble ozonation, respectively at pH 7. The observed increase in k_L for the conventional system compared to microbubble system is congruent with the work of Kawahara et al., (2009) who noted that k_L increased with an increase in bubble diameter and attributed this to bubble-induced turbulence. This also aligns with the expected reduction in rise velocity (relative to that expected of a spherical bubble) for bubbles over 2 mm due to oscillations, deformation of the bubble and an increase in drag which slows the bubble and increases residence time (Clift et al., 1978).

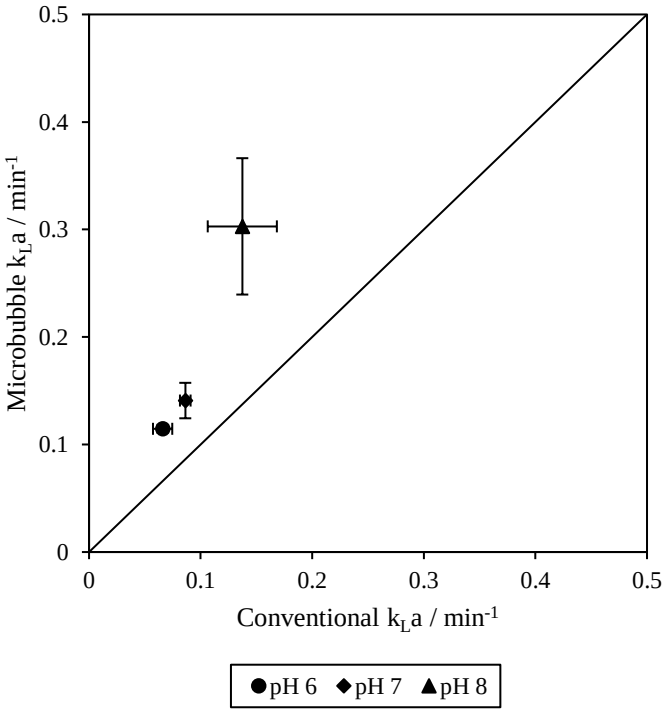

Figure 4 – 7. Parity plot of volumetric mass transfer coefficient for microbubble ozonation against conventional bubble ozonation for pH 6, 7, 8.

Further consideration of how k_L is influenced by the bubble size can be elucidated through the use of established bubble mass transfer models such as those of Higbie (Equation 4 – 8) and Frössling (Equation 4 – 9):

$$k_{L(H)} = \sqrt{\frac{4D_L u_B}{\pi d_{32}}} \qquad \text{Equation 4 – 8}$$

$$k_{L(F)} = 0.6\sqrt{\frac{u_B}{d_{32}}} D_L{}^{\frac{2}{3}} v_L{}^{-\frac{1}{6}} \qquad \text{Equation 4 – 9}$$

Where k_L is the mass transfer coefficient (m s^{-1}), D_L is the diffusion coefficient (m s^{-2}), u_B is the bubble slip velocity (m s^{-1}), d_{32} is the Sauter mean diameter (m) and v_L is the kinematic viscosity of the liquid (m^2 s^{-1}). The two models differ in how they consider the bubble, with the Higbie model being more appropriate for larger bubbles that have fluid like properties with

mobile interfaces and the Frössling model which is more appropriate for smaller bubbles that behave like rigid spheres (Kawahara et al., 2009).

The value of k_L derived for microbubbles was 1.11 x 10^{-4} m s^{-1} for the Higbie model and 2.04 x 10^{-5} m s^{-1} for the Frössling model. This compared to 1.45 x 10^{-8} m s^{-1} obtained from the experimental data. The equivalent values for the conventional system were 9.08 x 10^{-6} m s^{-1} for the Higbie model and 1.96 x 10^{-6} m s^{-1} for the Frössling model, with an experimental value of 1.29 x 10^{-6} m s^{-1}. The large difference between experimental and theoretical k_L for microbubble systems has been previously reported (Kawahara et al., 2009) and has been attributed to bubble-induced turbulence which is also reported to be proportional to the bubble diameter and bubble rise velocity (Sato et al., 1981) and the associated impact on the boundary layer thickness. Kawahara et al (2009) proposed a modification to the Higbie and Frössling models in order to correlate with the experimental k_L:

$$f_H = \frac{k_{L(E)}}{k_{L(H)}} \qquad \text{Equation 4 – 10}$$

$$f_F = \frac{k_{L(E)}}{k_{L(F)}} \qquad \text{Equation 4 – 11}$$

Where f is the ratio of the experimental k_L to theoretical k_L. By plotting f against the Ohnesorge number, Z, (Equation 4 – 12), a correlation can be derived.

$$Z = \frac{\mu_L}{\sqrt{\rho_L d_{32} \sigma}} \qquad \text{Equation 4 – 12}$$

Where Z is the Ohnesorge number, μ_L is the superficial liquid velocity (m s^{-1}), ρ_L is the density of the liquid (kg m^{-3}), d_{32} is the Sauter mean diameter (m) and σ is the surface tension (N m^{-1}). Kawahara et al. (2009) presented correlations based on fifteen data points representing different salt concentrations for the dissolution of oxygen as $f_H = 1.10 \times 10^{-7} Z^{-2.74}$ and $f_F = 6.87 \times 10^{-7} Z^{-2.71}$ which resulted in modified models of:

$$k'_{L(H)} = 1.1 \times 10^{-7} Z^{-2.74} \sqrt{\frac{4 D_L u_B}{\pi d_{32}}} \qquad \text{Equation 4 – 13}$$

$$k'_{L(F)} = 6.87 \times 10^{-7} Z^{-2.71}\, 0.6 \sqrt{\frac{u_B}{d_{32}}} D_L{}^{\frac{2}{3}} v_L{}^{-\frac{1}{6}}$$ Equation 4 – 14

The estimated mass transfer coefficients agreed with their data to within 13 %. Application of the modified models to the current data sets revealed a much closer fit to the experimental data than was seen with the original models, and in particular the observed enhancement factors (Table 4 – 2). The predicted values showed a close fit for the microbubble system, while the fit for the conventional system was two orders of magnitude higher for both of the modified mass transfer models. However, the difference between the predictions and the experimental data was still almost two orders of magnitude for the microbubble system. In practice it is likely that bespoke correlations are required for different systems (ozone v air) and different approaches for measuring the bubble volume and size distribution. This was not possible for the current case as the bubble size was only measured at pH 7. Hence, this is suggested as an area for further work, especially involving changing bubble size in order to establish the optimum bubble size for ozonation systems.

Table 4 – 2. Mass transfer coefficients according to experimental data and mass transfer models.

Mass Transfer Model	Microbubble k_L / m s^{-1}	Conventional k_L / m s^{-1}	Enhancement
Experimental (this study)	9.65 x 10^{-6}	8.2 x 10^{-4}	0.012
Higbie	1.11 x 10^{-4}	9.08 x 10^{-6}	12.22
Modified Higbie	2.37 x 10^{-7}	9.77 x 10^{-6}	0.024
Frössling	2.04 x 10^{-5}	1.69 x 10^{-6}	12.07
Modified Frössling	2.63 x 10^{-7}	9.52 x 10^{-6}	0.028

4.3.3. Influence of Microbubble Ozonation on Micropollutant Removal and Bromate Formation in Natural Water

In order to determine the performance of the microbubble system for the removal of a micropollutant in a complex matrix, 0.056 µmol L^{-1} of mecoprop was spiked into a part-treated pre-ozone natural water source. The background matrix contained 4.1 ± 0.2 mg dissolved organic carbon (DOC) and 100 – 150 µg L^{-1} of bromide. All experiments were performed using water retrieved from the same batch.

The rate constants for the removal of mecoprop in the natural water source using conventional sized bubbles was 0.12 ± 0.01 min^{-1} at pH 6 (Figure 4 – 8). This value was 70 % of that measured during the synthetic experiments (0.17 ± 0.02 min^{-1}). This compared to 0.22 ± 0.02 min^{-1} for the microbubble system in the natural water source and 0.31 ± 0.01 min^{-1} for the synthetic matrix. The enhancement factors for microbubbles over conventional bubbles was 1.8 for both matrices, indicating that the presence of other contaminants had not altered the benefit of using a microbubble system for enhanced mass transfer. This was supported by the fact that there was no detected removal of DOC for any of the tests. The findings that the microbubble system enhanced removal by transferring more ozone into the water was confirmed from analysis of the ozone exposure in the water, which was 1304 ± 75 µmol L^{-1} min for the microbubble system and 832 ± 7.5 µmol L^{-1} min for the conventional systems; a ratio of 1.6, a value similar to the enhancement factor.

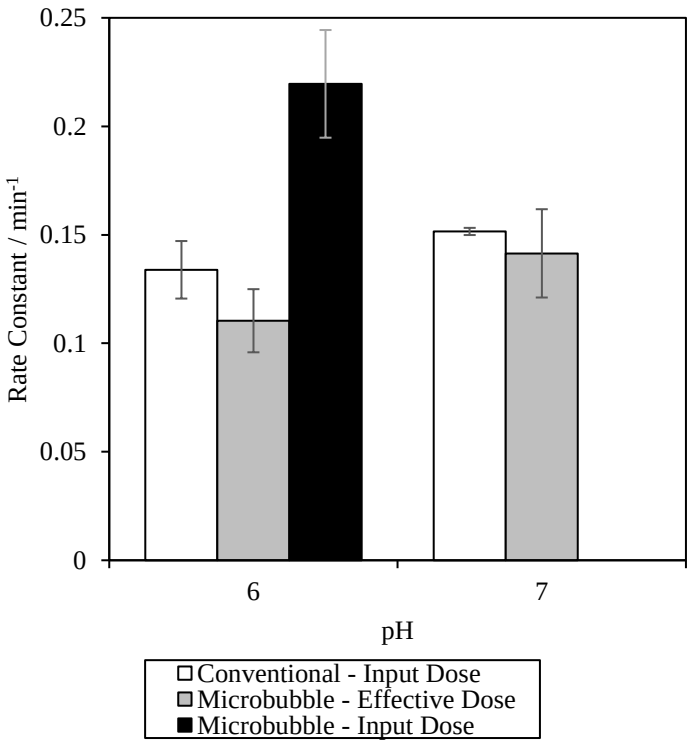

Figure 4 – 8. Rate constants for the removal of mecoprop in part-treated pre-O_3 natural water for conventional bubble ozonation (white), microbubble ozonation normalised for effective O_3 dose (grey) and microbubble ozonation normalised for input O_3 dose (black) at pH 6 and 7.

The total ozone exposure received was 832 ± 8, 811 ± 39 and 1304 ± 75 µmol L^{-1} min for conventional bubble ozonation, microbubble ozonation normalised for effective ozone dose and microbubble ozonation normalised for input ozone dose respectively at pH 6. At pH 7, the conventional bubble ozone exposure was 651 ± 77 µmol L^{-1} min and the microbubble ozone exposure was 711 ± 51 µmol L^{-1} min when normalised for effective ozone dose. The corresponding bromate concentrations were 0.054 ± 0.002 µmol L^{-1} for conventional bubble ozonation, 0.049 ± 0.001 µmol L^{-1} for microbubble ozonation normalised for effective ozone dose and 0.088 ± 0.015 µmol L^{-1} for microbubble ozonation normalised for input dose at pH 6. For pH 7, the bromate concentration for conventional bubble ozonation was 0.19 ± 0.02 µmol L^{-1} and the bromate concentration for microbubble ozonation normalised for effective ozone dose was 0.21 ± 0.02 µmol L^{-1} (Figure 4 – 9). The results showed that, when normalised for input dose, the total bromate formation was 1.64 times higher for the microbubble system. However, the effective ozone exposure was 1.57 times higher. When normalised for effective ozone dose, there was no significant difference in the extent of bromate formation between the microbubble and conventional bubble systems. Such observation are aligned to the fact that the bromate concentration is dependent on the dissolved ozone concentration. The impact of using microbubble systems is that more ozone transfer is achieved a given input dose. Consequently, when comparing microbubble and conventional bubble systems at a fixed input dose, the microbubble systems will generate more bromate. However, the use of microbubble systems will enable reduced input doses to achieve the same levels of treatment and hence no difference in bromate levels should be expected under typical operation.

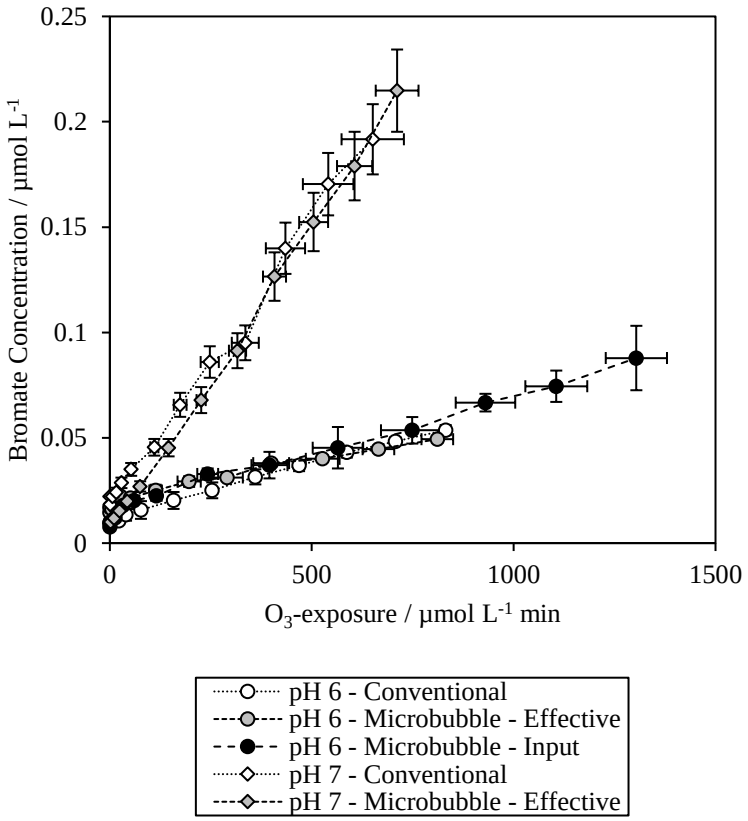

Figure 4 – 9. Plot of bromate concentration / µmol L^{-1} vs. O_3 exposure / µmol L^{-1} min in part-treated, pre-O_3 natural water for conventional bubble ozonation, microbubble ozonation normalised for effective O_3 dose and microbubble ozonation normalised for input O_3 dose at pH 6 and 7.

4.4. Conclusion

The work has sought to understand what drives the reported enhancements that occur when using microbubbles compared to conventional bubbles in systems for reactive mass transfer applications, such as ozonation as used in water treatment. Comparison of the different

components revealed that the overall enhancement is predominately driven by an enhancement in the overall volumetric mass transfer coefficient ($k_L a$). This is made up of two components: a reduction in the mass transfer coefficient (k_L) and an increase in the specific interfacial surface area (a). In the case of a regenerative turbine microbubble generator delivering ozone microbubbles, the k_L was 0.012 the value of that seen for conventional bubbles, while the enhancement in a was 143 for microbubbles, leading to an overall enhancement of 1.6. Thus, the increase in transfer area for microbubbles outweighs the reduction in mass transfer coefficient. No enhancement was observed when performance was normalised to a fixed effective ozone dose in terms of ozone self-decomposition, hydroxyl radical production or the specific micropollutant reaction rate constants associated with either ozone or hydroxyl radicals. However, when normalised to input dose the improvement in microbubble performance was related to an increase in the steady state dissolved ozone concentration.

Comparison between experiments carried out in synthetic water compared to real waters revealed the background constituents in the real water did not preferentially impact the performance of either the microbubble or conventional bubble systems such that the enhancement factors remained the same. Further, when normalised to effective dose both systems produced the same levels of bromate. The work indicates that future focus should be on understanding the optimum bubble size of any given application based on its impact on both k_L and a.

4.5. Acknowledgements

This research is gratefully supported by the Engineering and Physical Sciences Research Council (EPSRC) through their funding of the STREAM Industrial Doctorate Centre (EP/ G037094/1) and from the project sponsor Anglian Water.

4.6. References

Abbasian-arani, M., Hatamipour, M. and Rahimi, A., 2021. Experimental determination of gas holdup and volumetric mass transfer coefficient in a jet bubbling reactor. *Chinese Journal of Chemical Engineering*, 34, pp.61-67.

Abufalgha, A., Clarke, K. and Pott, R., 2020. Characterisation of bubble diameter and gas hold-up in simulated hydrocarbon-based bioprocesses in a bubble column reactor. *Biochemical Engineering Journal*, 158, p.107577.

Ahmad, N., Javed, F., Awan, J., Ali, S., Fazal, T., Hafeez, A., Aslam, R., Rashid, N., Rehman, M., Zimmerman, W. and Rehman, F., 2019. Biodiesel production intensification through microbubble mediated esterification. *Fuel*, 253, pp.25-31.

Azuma, T., Otomo, K., Kunitou, M., Shimizu, M., Hosomaru, K., Mikata, S., Mino, Y. and Hayashi, T., 2019. Removal of pharmaceuticals in water by introduction of ozonated microbubbles. *Separation and Purification Technology*, 212, pp.483-489.

Bai, M., Liu, Z., Zhang, J. and Lu, L., 2021. Prediction and experimental study of mass transfer properties of micronanobubbles. *Industrial and Engineering Chemistry Research*, 60(22), pp.8291-8300.

Castro-Gutierrez, V., Pickering, L., Cambronero-Heinrichs, J., Holden, B., Haley, J., Jarvis, P., Jefferson, B., Helgason, T., Moir, J. and Hassard, F., 2022. Bioaugmentation of pilot-scale slow sand filters can achieve compliant levels for the micropollutant metaldehyde in a real water matrix. *Water Research*, 211, p.118071.

Cheng, W., Jiang, L., Quan, X., Cheng, C., Huang, X., Cheng, Z. and Yang, L., 2019. Ozonation process intensification of p-nitrophenol by in situ separation of hydroxyl radical scavengers and microbubbles. *Water Science and Technology*, 80(1), pp.25-36.

Chu, L., Xing, X., Yu, A., Zhou, Y., Sun, X. and Jurcik, B., 2007. Enhanced ozonation of simulated dyestuff wastewater by microbubbles. *Chemosphere*, 68(10), pp.1854-1860.

Clift, R., Grace, J.R., Weber, M.E., 1978. Bubbles, Drops, and Particles. *Academic Press*.

Derco, J., Gotvajn, A., Čižmárová, O., Dudáš, J., Sumegová, L. and Šimovičová, K., 2021. Removal of micropollutants by O_3-based processes. *Processes*, 9(6), p.1013.

Dong, J., Yao, J., Tao, J., Shi, X. and Wei, F., 2022. Degradation of Methyl Orange by ozone microbubble process with packing in the bubble column reactor. *Environmental Technology*, pp.1-13.

Gao, Y., Duan, Y., Fan, W., Guo, T., Huo, M., Yang, W., Zhu, S. and An, W., 2019. Intensifying ozonation treatment of municipal secondary effluent using a combination of

microbubbles and ultraviolet irradiation. *Environmental Science and Pollution Research*, 26(21), pp.21915-21924.

Gardoni, D., Vailati, A. and Canziani, R., 2012. Decay of ozone in water: a review. *O3: Science and Engineering*, 34(4), pp.233-242.

Gulde, R., Clerc, B., Rutsch, M., Helbing, J., Salhi, E., McArdell, C. and von Gunten, U., 2021. Oxidation of 51 micropollutants during drinking water ozonation: Formation of transformation products and their fate during biological post-filtration. *Water Research*, 207, p.117812.

Heriyati, E., Rustadi, R., Isnansetyo, A., Triyatmo, B. and Istiqomah, I., 2021. Microbubble aerator test and harvest target prediction based on oxygen consumption of red tilapia (Oreochromis sp.). *Aquaculture, Aquarium, Conservation & Legislation - International Journal of the Bioflux Society*, 4(5), pp.3006-3022.

Hu, L. and Xia, Z., 2018. Application of ozone micro-nano-bubbles to groundwater remediation. *Journal of Hazardous Materials*, 342, pp.446-453.

Huang, X., Quan, X., Cheng, W., Cheng, C., Cheng, Z., Yang, L. and Jiang, L., 2020. Enhancement of O3 mass transfer by stainless steel wire mesh and its effect on hydroxyl radical generation. *Ozone: Science and Engineering*, 42(4), pp.347-356.

Ikehata, K. and Gamal El-Din, M., 2005. Aqueous pesticide degradation by ozonation and ozone-based advanced oxidation processes: a review (part II). *Ozone: Science and Engineering*, 27(3), pp.173-202.

International Organization for Standardization. (2017). ISO/TC 281: Fine bubble technology. ISO. Retrieved December 20, 2021, from https://www.iso.org/committee/4856666.html

Jin, X., Wu, C., Fu, L., Tian, X., Wang, P., Zhou, Y. and Zuo, J., 2022. Development, dilemma and potential strategies for the application of nanocatalysts in wastewater catalytic ozonation: A review. *Journal of Environmental Sciences*, 124, pp.330-349.

Jodzis, S. and Zięba, M., 2018. Energy efficiency of an ozone generation process in oxygen. Analysis of a pulsed DBD system. *Vacuum*, 155, pp.29-37.

John, A., Brookes, A., Carra, I., Jefferson, B. and Jarvis, P., 2022. Microbubbles and their application to ozonation in water treatment: A critical review exploring their benefit and future application. *Critical Reviews in Environmental Science and Technology*, 52(9), pp.1561-1603.

John, A., Carra, I., Jefferson, B., Jodkowska, M., Brookes, A. and Jarvis, P., 2022. Are microbubbles magic or just small? A direct comparison of hydroxyl radical generation between microbubble and conventional bubble ozonation under typical operational conditions. *Chemical Engineering Journal*, 435, p.134854.

Kawahara, A., Sadatomi, M., Matsuyama, F., Matsuura, H., Tominaga, M. and Noguchi, M., 2009. Prediction of micro-bubble dissolution characteristics in water and seawater. *Experimental Thermal and Fluid Science*, 33(5), pp.883-894.

Khuntia, S., Majumder, S. and Ghosh, P., 2016. Catalytic ozonation of dye in a microbubble system: Hydroxyl radical contribution and effect of salt. *Journal of Environmental Chemical Engineering*, 4(2), pp.2250-2258.

Lage Filho, F., 2010. O3 application in water sources: effects of operational parameters and water quality variables on O3 residual profiles and decay rates. *Brazilian Journal of Chemical Engineering*, 27(4), pp.545-554.

Lee, Y., Park, Y., Lee, G., Kim, Y. and Chon, K., 2019. Enhanced degradation of pharmaceutical compounds by a microbubble ozonation process: effects of temperature, ph, and humic acids. *Energies*, 12(22), p.4373.

Li, C., Xie, Y., Guo, Y., Cheng, Y., Yu, H., Qian, H. and Yao, W., 2021. Effects of O3-microbubble treatment on the removal of residual pesticides and the adsorption mechanism of pesticides onto the apple matrix. *Food Control*, 120, p.107548.

Li, P., Wu, C., Yang, Y., Wang, Y., Yu, S., Xia, S. and Chu, W., 2018. Effects of microbubble ozonation on the formation of disinfection by-products in bromide-containing water from Tai Lake. *Separation and Purification Technology*, 193, pp.408-414.

Liu, S., Wang, Q., Zhai, X., Huang, Q. and Huang, P., 2010. Improved pretreatment (coagulation-floatation and ozonation) of younger landfill leachate by microbubbles. *Water Environment Research*, 82(7), pp.657-665.

Maceiras, R., Álvarez, E. and Cancela, M.A. 2010. Experimental interfacial area measurements in a bubble column. *Chemical Engineering Journal*. 163(3), pp. 331–336.

Marbelia, L., Wan Noor, A., Paramesti, A., Damarjati, B., Widyaparaga, A., Deendarlianto, Bilad, M. and Budhijanto, W., 2020. A comparative study of conventional aerator and

microbubble generator in aerobic reactors for wastewater treatment. *IOP Conference Series: Materials Science and Engineering*, 778(1), p.012132.

Mao, Y., Qi, S., Guo, X., Yang, H. and Xie, Y., 2021. Optimization of O3 dosage in an O3 contact tank using a numerical model. *Environmental Science and Pollution Research*, 28(33), pp.44987-44997.

Muroyama, K., Imai, K., Oka, Y. and Hayashi, J., 2013. Mass transfer properties in a bubble column associated with micro-bubble dispersions. *Chemical Engineering Science*, 100, pp.464-473.

Nam, G., Mohamed, M. and Jung, J., 2021. Enhanced degradation of benzo[a]pyrene and toxicity reduction by microbubble ozonation. *Environmental Technology*, 42(12), pp.1853-1860.

Parkinson, L., Sedev, R., Fornasiero, D. and Ralston, J., 2008. The terminal rise velocity of 10–100 μm diameter bubbles in water. *Journal of Colloid and Interface Science*, 322(1), pp.168-172.

Paucar, N., Kim, I., Tanaka, H. and Sato, C., 2019. O3 treatment process for the removal of pharmaceuticals and personal care products in wastewater. *Ozone: Science and Engineering*, 41(1), pp.3-16.

Pongprasert, N., Srilaong, V. and Sugaya, S., 2020. An alternative technique using ethylene micro-bubble technology to accelerate the ripening of banana fruit. *Scientia Horticulturae*, 272, p.109566.

Roustan, M., Wang, R. and Wolbert, D., 1996. Modeling hydrodynamics and mass transfer parameters in a continuous o3 bubble column. *Ozone: Science and Engineering*, 18(2), pp.99-115.

Sato, Y., Sadatomi, M. and Sekoguchi, K., 1981. Momentum and heat transfer in two-phase bubble flow—I. Theory. *International Journal of Multiphase Flow*, 7(2), pp.167-177.

Seridou, P. and Kalogerakis, N., 2021. Disinfection applications of O3 micro- and nanobubbles. *Environmental Science: Nano*, 8(12), pp.3493-3510.

Sun, Z., Chen, X., Yang, K., Zhu, N. and Lou, Z., 2020. The progressive steps for TPH stripping and the decomposition of oil refinery sludge using microbubble ozonation. *Science of The Total Environment*, 712, p.135631.

Swart, B., Zhao, Y., Khaku, M., Che, E., Maltby, R., Chew, Y. and Wenk, J., 2020. In situ characterisation of size distribution and rise velocity of microbubbles by high-speed photography. *Chemical Engineering Science*, 225, p.115836.

Takahashi, N., Ichikawa, H., Torii, H., Shibata, S., Duy, N. and Phuong, P., 2012. Ozonation of dyestuff solutions using a fine bubble generator system. *Ozone: Science and Engineering*, 34(3), pp.196-203.

Tang, L.L., DeNardo, M.A., Gayathri, C., Gil, R.R., Kanda, R. and Collins, T.J., 2016. TAML/H_2O_2 oxidative degradation of metaldehyde: pursuing better water treatment for the most persistent pollutants. *Environmental Science and Technology*, 50(10), pp.5261–5268.

Tamaki, M., Ikeura, H. and Enmei, N., 2020. Growth response of hydroponic leaf lettuce and komatsuna to O3 microbubble treatment. *Journal of Plant Nutrition*, 43(10), pp.1369-1377.

Temesgen, T., Bui, T., Han, M., Kim, T. and Park, H., 2017. Micro and nanobubble technologies as a new horizon for water-treatment techniques: A review. *Advances in Colloid and Interface Science*, 246, pp.40-51.

Thomas, B., Ohde, D., Matthes, S., Engelmann, C., Bubenheim, P., Terasaka, K., Schlüter, M. and Liese, A., 2020. Comparative investigation of fine bubble and macrobubble aeration on gas utility and biotransformation productivity. *Biotechnology and Bioengineering*, 118(1), pp.130-141.

Wang, B., Yang, G., Tian, H., Li, X., Yang, G., Shi, Y., Zhou, Z., Zhang, F. and Zhang, Z., 2020. A new model of bubble Sauter mean diameter in fine bubble-dominated columns. *Chemical Engineering Journal*, 393, p.124673.

Wang, H., Wang, Y., Lou, Z., Zhu, N. and Yuan, H., 2017. The degradation processes of refractory substances in nanofiltration concentrated leachate using micro-ozonation. *Waste Management*, 69, pp.274-280.

Wang, W., Fan, W., Huo, M., Zhao, H. and Lu, Y., 2018. Hydroxyl radical generation and contaminant removal from water by the collapse of microbubbles under different hydrochemical conditions. *Water, Air and Soil Pollution*, 229(3).

Wu, C., Li, P., Xia, S., Wang, S., Wang, Y., Hu, J., Liu, Z. and Yu, S., 2019. The role of interface in microbubble ozonation of aromatic compounds. *Chemosphere*, 220, pp.1067-1074.

Xu, Z., Mochida, K., Naito, T., and Yasuda, K., 2012. Effects of operational conditions on 1,4-dioxane degradation by combined use of ultrasound and ozone microbubbles. *Japanese Journal of Applied Physics*, 51, p.07GD08.

Yang, X., Liu, Z., Manhaeghe, D., Yang, Y., Hogie, J., Demeestere, K. and Van Hulle, S., 2021. Intensified ozonation in packed bubble columns for water treatment: Focus on mass transfer and humic acids removal. *Chemosphere*, 283, p.131217.

Yao, K., Chi, Y., Wang, F., Yan, J., Ni, M. and Cen, K., 2016. The effect of microbubbles on gas-liquid mass transfer coefficient and degradation rate of COD in wastewater treatment. *Water Science and Technology*, 73(8), pp.1969-1977.

Zhang, J., Huang, G., Liu, C., Zhang, R., Chen, X. and Zhang, L., 2018. Synergistic effect of microbubbles and activated carbon on the ozonation treatment of synthetic dyeing wastewater. *Separation and Purification Technology*, 201, pp.10-18.

Zheng, T., Wang, Q., Zhang, T., Shi, Z., Tian, Y., Shi, S., Smale, N. and Wang, J., 2015. Microbubble enhanced ozonation process for advanced treatment of wastewater produced in acrylic fiber manufacturing industry. *Journal of Hazardous Materials*, 287, pp.412-420.

4.7. Supplementary Information

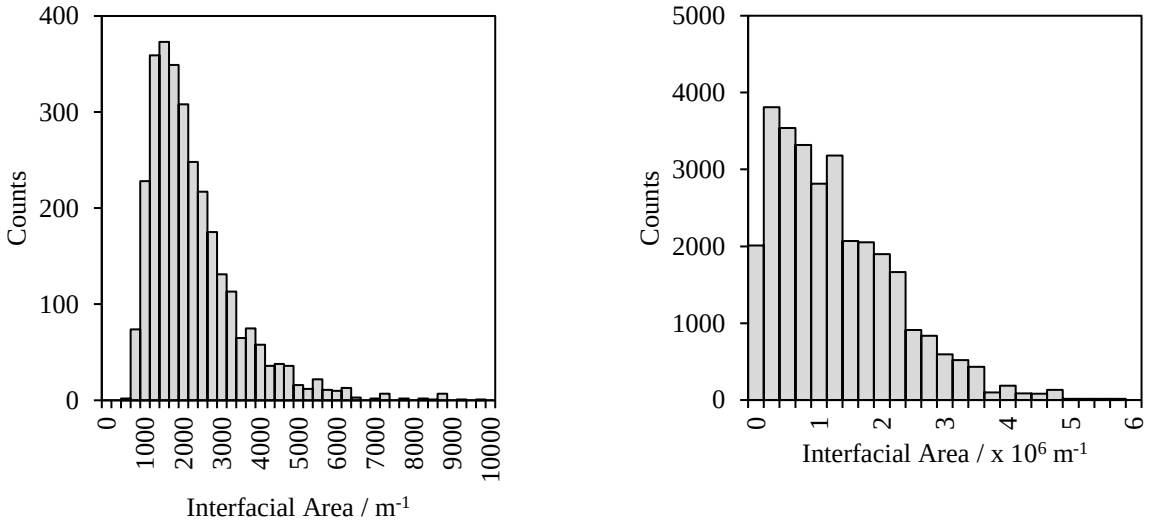

[SI] Table 4 – S1. Interfacial area distributions for microbubble (left) and conventional bubble (right) ozonation at pH 7 and a gas flow rate of 2 L min^{-1}.

Chapter 5. Size Distributions of Micro-nano Bubbles (MNBs) Generated by a Regenerative Turbine Microbubble Generator using Ozone: Significance and Potential Importance of the Nanobubble Fractions

Alexander John[a], Adam Brookes[b], Irene Carra[a], Bruce Jefferson[a] and Peter Jarvis[a]

[a]School of Water, Energy and Environment, Cranfield Water Science Institute, Cranfield, UK.

[b]Anglian Water, Thorpe Wood House, Peterborough, UK.

Abstract

The use of microbubbles in gas-liquid contacting processes is gaining traction as a viable way to improve performance over conventional bubble-liquid contactor systems. The generation of microbubbles usually results in a distribution of bubbles containing both micro- and nanobubbles. Of which, nanobubbles have recently come to light as a potential way to enhance performance even further. Nanobubbles are defined as bubbles with a diameter of 1 – 1000 nm and have a very large specific surface area. They are thought to have a high surface and internal energy for mass transfer, which has facilitated a lot of interest in a variety of applications. However, there has been significant debate about the existence of stable, bulk nanobubbles as there is currently no definitive method to confirm whether nanoscale observations are truly nanobubbles or other nano-entities such as particles or droplets. In addition, it is unclear what the relative importance of the two bubble size fractions is, and whether there is a risk of stable nanobubbles causing concern downstream of where they are generated. This lack of knowledge is impeding the deployment of systems in water treatment applications as well as the establishment of bubble sizes required to deliver optimum performance. This study uses ozone to measure the micro and nanobubble size distributions produced by a regenerative turbine microbubble generator to determine the relative contribution of each fraction and assess the potential risk of stable bulk nanobubbles. Sauter mean diameters of 217 nm and 37 µm were reported for the nano and micro bubbles, respectively. Half of the measured bubbles were less than 5000 nm in size. In order to optimise the overall process, emphasis

should be placed on understanding how to manage the size distribution of the microbubble fraction as the risk of residual ozone from nanobubble survival was deemed insignificant with an estimated maximum contribution to ozone residual of 3.2 µg L^{-1} under normal conditions.

5.1. Introduction

The application of microbubbles to gas-liquid contacting processes is becoming established as a viable way to enhance performance in comparison to conventional bubble-liquid contactor systems (Levistky et al., 2022; John et al., 2022; Singh et al., 2021; Movahed and Sarmah, 2021; Tesmegen et al., 2017). Microbubbles are defined as bubbles with a diameter of 1 – 100 µm (ISO 20480-1:2017) and have a number of favourable properties compared with the larger bubbles formed in conventional gas liquid systems using porous diffusers which are typically 2 – 6 mm (Baquero-Rodriguez et al., 2018; Behnisch et al., 2018; Garrido-Baserba et al., 2018; Terashima et al., 2016). The large difference in size between microbubbles and conventional bubbles means that microbubbles have a significantly lower buoyancy, lower rise velocity (Shangguan et al., 2018) and a much higher specific gas-to-liquid interfacial area (Parmar and Majumder, 2013) and hence faster mass transfer (Suwartha et al., 2020) compared with conventional bubbles. For instance, in the case of ozonation used in drinking water treatment, the comparison between microbubbles and conventional bubbles systems has revealed an average enhancement factor in the absorption coefficient ($k_L a$) of 2.5 when aggregated across multiple studies (John et al., 2022) and this translates to higher dissolved ozone concentrations and hence more effective treatment. However, many of the studies do not report the associated bubble size distributions making interpretation of the importance of the key bubble sizes impossible.

The generation of microbubbles from most devices usually results in the formation of both micro- and nanobubbles (MNBs). The latter have recently come to attention as a route to potentially enhance performance further. Nanobubbles, defined as bubbles with a diameter of 1 – 1000 nm, have an extremely large specific surface area and are believed to have a high surface and internal energy for the facilitation of mass transfer (Atkinson et al., 2019; Lyu et al., 2019). In addition, nanobubbles have been reported to be extremely

stable and long-lived in the order of weeks and months (Sun et al., 2022). Overall, this has generated significant interest for applications in agriculture (Wang et al., 2021), aquaculture (Farid et al., 2022), cleaning (Ulatowski et al., 2020), environmental remediation (Tang et al., 2021) and water treatment (specifically ozonation systems used in drinking water treatment), as well as an emerging option to replace existing microbubble use in medicine for ultrasonic imaging and therapeutic purposes (Sun et al., 2022; Rak et al., 2019). However, since the existence of nanobubbles was first proposed in 1981, significant debate remains about the existence of stable, bulk nanobubbles since there is currently no definitive method to confirm whether nanoscale observations are truly nanobubbles or other nano-entities such as particles or droplets (Jadhav and Barigou, 2020). Further, the established Epstein-Plesset theory on single-bubble lifetime predicts that bulk nanobubbles in gas saturated liquids should remain stable for milliseconds (Epstein and Plesset, 1950). The theory is based on the combination of the Young-Laplace equation that describes how the pressure inside a bubble increases as bubble size decreases and Henry's law which states that the solubility of a gas in a liquid is proportional to the pressure inside the bubble. Therefore, nanobubbles should be either inherently unstable or made unstable through natural perturbations (Rak et al., 2019). Accordingly, a number of works have questioned the existence of nanobubbles (Alheshibri and Craig, 2018; Alheshibri and Craig, 2019; Alheshibri et al., 2019; Rak et al., 2019; Leroy and Norisuye, 2016; Sedlák and Rak, 2013; Häbich et al., 2010) whilst numerous other works have demonstrated their existence and long-term stability (Jadhav and Barigou, 2021; Fang et al., 2020; Kanematsu et al., 2020; Manning, 2020; Zhang et al., 2020; Jin et al., 2019; Nirmalkar et al., 2019). Nonetheless, the generation of nanobubbles has gained considerable interest with respect to gas-liquid contacting processes and several works have reported nanometre-range objects that they ascribed as bubbles (Table 5 – 1).

To date, it is unclear on the relative significance of the two bubble size fractions (micro and nano) and whether there is a risk of stable nanobubbles causing concern downstream of the principal reactor where they are being generated. This lack of knowledge is inhibiting deployment of systems in water treatment applications and the establishment of key bubble sizes required to deliver optimum performance. Perhaps the most prominent application for MNBs in water treatment is related to the use of ozone to

oxidise organic components. The technology has been widely established since the 1980s and, in many countries, plants are reaching the end of their design lives, offering potential opportunity for rapid uptake of MNB systems. Consequently, the current paper measures micro and nano bubble size distributions produced from a regenerative turbine microbubble generator using ozone to establish the relative contribution from each fraction and assess the potential risk of stable bulk nanobubbles.

Table 5 – 1. Generation, measurement techniques, reported diameters and concentration of nanobubbles.

Micro-nanobubble Generator	Diameter	Concentration / # ml^{-1}	Method	Reference
Fine-bubble generator (Langpai Technology Co., Ltd.)	MB: Majority < 10 µm NB: 50 – 500 nm	3×10^7 – 14×10^7	Focused beam reflectance measurement for micron sized bubbles (G400, Mettler-Toledo) Nanoparticle tracking analysis for nanometre bubbles (NS300, Nanosight)	Zhou et al. (2022)
140 nm tubular ceramic membrane (MSKTB01014UM, Sterlitech)	200 – 700 nm	Approximately 10^6	Zetasizer (Nano ZS, Malvern Instruments) Nanoparticle tracking analysis (NS300, Nanosight)	Xue et al. (2022)
380 kPa recirculation pump with micro-nano-sized nozzle (BT-50FR, Riverforest Co.)	Between 30 – 300 nm, 75 % < 122 nm, median 68.1 nm	Not reported	Zetasizer (Nano ZS, Malvern Instruments)	Althgun Hewage et al. (2021)
Nanobubble generator (aQua+075MO, AquaPro Solutions Ltd.)	Majority < 130 nm	$2.39 \times 10^7 \pm 1.01 \times 10^7$ – $3.03 \times 10^7 \pm 1.11 \times 10^6$	Nanoparticle tracking analysis (NS300, Malvern Panalytical Ltd.)	Jhunkeaw et al. (2021)
140 nm tubular ceramic membrane (MSKTB0104UM, Starlitech)	199 – 294 nm	4.3×10^7 – 6×10^8	Zetasizer (Nano ZS, Malvern Instruments) Nanoparticle tracking analysis (NS300, Nanosight)	Shi et al. (2021)
Ultrafine bubble generator (Asupu, Japan)	Average 650 nm	Not reported	Coulter multisizer 4e (Beckman Coulter, US)	Fan, Desai et al. (2021)
Generator with high speed rotation and pressurised dissolution	1.08 ± 0.37 µm	4.93×10^7	Coulter multisizer 4e (Beckman Coulter, US)	Fan, Li et al. (2021)
Micro-nanobubble generator (XZCP-K-0.75, Xiazhichun)	Sauter mean diameter 2.7 µm, 30 % < 1 µm	1.84×10^5	Coulter multisizer 4e (Beckman Coulter, US)	Fan, Cui et al. (2021)
Nanobubble generator (XZCP-K-0.75, Xiazhichun)	Median diameter 580 nm	2.16×10^5	Coulter multisizer 4e (Beckman Coulter, US)	Fan, An et al. (2021)
Microbubble-nanobubble nozzle (BT-50FT, Riverforest Co.)	100 – 300 nm	Not reported	Nano Zetasizer (DTS1070, Malvern Instruments)	Althgun Hewage et al. (2020)
Nanobubble generator (Zhongnong Tianlu Micro-nano Bubble Water Technology Co. Ltd., China)	100 – 500 nm Mean diameter 185 – 210 nm	$2.29 – 2.51 \times 10^8$	Nanoparticle tracking analysis (NS500, Malvern Instruments Ltd.)	Wang et al. (2020)
Micro-nanobubble generator (Xiazhichun, China)	Average 3.38 ± 0.73 µm	$2.41 \pm 1.45 \times 10^5$	Coulter multisizer 4e (Beckman Coulter, US)	Fan et al. (2020)
Micro-nano-bubble nozzle (BT-50FR, Riverforest Co.)	100 – 200 nm	Not reported	Zetasizer (Nano, Malvern Instruments)	Batagoda et al. (2019)
Nanobubble generator (KTM, Nikuni Co., Ltd.)	87 % < 200 nm	4.1×10^7 – 7.5×10^8	ZetaView PMX 120 (Particle Metrix, Germany)	Wu et al. (2019)
Micro-nanobubble generator (Asupu, Japan)	Average 3.44 µm	Not reported	Coulter multisizer 4e (Beckman Coulter, US)	Fan et al. (2019)
Micronano sized nozzle (BT-50FR, Riverforest Co.)	191 – 220 nm	Not reported	Zetasizer (Nano ZS, Malvern Instruments)	Meegoda et al. (2019)

5.2. Materials and Methods

5.2.1. Bubble Generation

MNBs and conventional bubble measurements were conducted in semi-batch mode in 100 L of deionised water inside a cylindrical acrylic reactor with a height of 80 cm, diameter of 45 cm and a water height of 62 cm (Figure 5 – 1).

For the ozonation experiments, O_3 gas was generated from compressed air using a corona discharge O_3 generator (C-Lasky C-L010-DT, Advanced Ozone Products) with an operational gas flow rate of 2 – 10 L min^{-1}. The O_3 gas output of the generator was up to 2 g h^{-1}. For all experiments, the gas flow rate of the O_3 generator was set to 2 L min^{-1}. For aeration experiments, ambient air was supplied to the microbubble generator through automatic suction.

MNBs were formed using a regenerative turbine microbubble generator (Nikuni KTM20N trial unit, Aeration & Mixing). The microbubble generator had a recirculating liquid flow rate of 16.6 L min^{-1} and a gas flow meter with a range of 0 – 5 L min^{-1}. The gas flow intake of the microbubble generator was set to 1 – 3 L min^{-1} depending on the required gas flow rate. The aqueous phase was continuously recirculated through the microbubble generator. Conventional bubbles were generated from a fine pore diffuser (132 mm ceramic air stone diffuser, Finest Aquatic LTD) connected directly to the O_3 generator.

Figure 5 – 1. Microbubble generation experimental apparatus.

5.2.2. Preparation of Nanosphere Calibration Standards

A nanoparticle tracking analysis (NTA) instrument (Nanosight LM-20, Malvern Instruments) was used to measure nanobubbles. The ability of the NTA to detect and measure nano-sized entities was tested using calibration standards for a range of particle sizes and concentrations. Polystyrene-latex nanospheres of sizes 100nm, 200nm and 400nm (NTA4088, NTA4089, NTA4091, Malvern Instruments) were analysed. The concentration of nanosphere preparations was calculated by the known parameters of nanosphere diameter, nanosphere density and percentage solids of nanosphere. For each of the nanosphere sizes, suspensions of 1 x 10^7, 1 x 10^8 and 1 x 10^9 # mL^{-1} were prepared according to the following equation:

$$c = 6 * 10^{10} \frac{W}{d^3 \pi \rho} \qquad \text{Equation 5 – 1}$$

Where c is particle concentration (# mL^{-1}), ρ is density of nanospheres (kg m^{-3}), W is percent solids of nanosphere fraction and d is nanosphere diameter (m). Blanks consisting of ultrapure water and water that had run through the microbubble generator without

aeration were also analysed to determine whether contaminant nanoparticles were detectable.

5.2.3. Nanoparticle Tracking Analysis

The size distribution and number count of the nanobubbles was measured using the NTA. Dispersed objects are viewed as bright dots against a dark background and video recorded utilising illumination from a 642 nm red laser delivered at 90° to the observation window. Particles appear as bright dots against a dark background. The video files are utilised to measure the mean square of the motion which is then converted into a hydraulic radius according to the Stokes-Einstein equation (Dragovic et al., 2011; Saveyn et al., 2010):

$$D = \frac{(x,y)^2}{2t} \qquad \text{Equation 5 – 2}$$

$$D = \frac{2k_B T}{3r_h \pi \eta} \qquad \text{Equation 5 – 3}$$

Where D is the diffusion coefficient ($m^2\ s^{-1}$), $(x,y)^2$ is the mean squared displacement of the particle ($m^2\ s^{-1}$), t is time (s), k_B is the Boltzmann constant ($m^2\ kg\ s^{-2}\ K^{-1}$), T is temperature (K), r_h is hydrodynamic radius of the particle (m) and η is the dynamic viscosity of the liquid ($kg\ m^{-1}\ s^{-1}$).

For each sample, 5 mL was collected in a brand new 5 mL syringe. To load the sample, the sample chamber was removed and oriented sideways so that the sample chamber could be filled from bottom to top. The sample was added slowly so that the viewing pane was free from any voids. After measurement, the sample was removed using the syringe. Between runs, the sample chamber was flushed three times with ultrapure water followed by three rinses with the sample. The sample chamber was never dismantled for manual cleaning as it was easy to introduce contamination to the viewing window.

The method is known to be sensitive to the settings for recording and analysis and in particular the detection threshold in which the software excludes certain greyscale values

from being tracked (Eklund et al., 2021). In order to determine optimal processing, each set of 10 captures was processed using 24 different detection thresholds from 2 to 50.

5.2.4. Microbubble and Conventional Bubble Size Distributions

The size distribution of the microbubbles was measured using focus-beam reflectance measurement (FBRM) (600L, Mettler Toledo). The probe was placed centrally in the bubble column and measured continuously over a period of 30 minutes whilst the microbubble generator was running. The measurable range of the instrument was 1 – 4000 µm and a minimum of 30,000 counts were collected per run. For the size distribution of the conventional bubbles, high speed video was recorded using a waterproof high-speed camera (HERO8, GoPro). The camera was submerged in the water to avoid distortion from the cylindrical reactor. The camera was focussed on a precision ruler with 1 mm spacing (Precision ruler, Dorcrafts) which acted as a size reference. The region was illuminated by a waterproof LED video light (XShot, Suptig) which was mounted to the camera tripod (JB01511-BWW, Joby). Video was shot at 240 frames per second for 10 minutes. The video was slowed down to 30 frames per second and desaturated using video editing software (GoPro Studio, GoPro). Image frames from the video were extracted using a media software (VLC Media Player, VLAN). The image frames were processed manually using image processing software (ImageJ). The reference was measured in each frame and in-focus bubbles were measured against it. A minimum of 1000 individual in-focus bubbles were measured for each run.

Once the distributions were collected, the Sauter mean diameter for the microbubble and conventional bubble distributions were calculated as follows (Abbasian-arani et al., 2020):

$$d_{32} = \frac{\sum n_i d_i^3}{\sum n_i d_i^2} \qquad \text{Equation 5 – 4}$$

Where d_{32} is the Sauter mean diameter (m) and n_i is the number of bubbles with diameter d_i.

5.3. Results and Discussion

5.3.1. Diameter Measurement of Polystyrene Latex Spheres

For each diameter and concentration combination, the measured diameter appeared to increase as the processing detection threshold was increased. The variance in measured diameter also increased due to the different detection thresholds as the particle number increased. For instance, with the 100 nm spheres, the difference between detection thresholds of 2 and 48 was 12.9 nm for a particle concentration of 1 x 10^7 # mL^{-1} and increased to 14.2 and 33.7 nm for particle concentrations of 1 x 10^8 and 1 x 10^9 # mL^{-1}, respectively. For the 200 nm spheres, the difference in measured diameter was 4.0 nm with a particle concentration of 1 x 10^7 # mL^{-1} which increased to 15.6 and 11.1 nm with particle concentrations of 1 x 10^8 and 1 x 10^9 # mL^{-1}. For the 400 nm spheres, the variance was much higher between the different detection thresholds; with a particle concentration of 1 x 10^7 # mL^{-1}, the difference in measured diameter was 52.8 nm. This increased to 69.3 and 102.8 nm for particle concentrations of 1 x 10^8 and 1 x 10^9 # mL^{-1}, respectively.

Taking an average value from multiple detection thresholds provides the benefit that it removes any influence of the operator, as the ability to select the most optimal detection threshold is removed. When the results from all detection thresholds were averaged, the measured diameters for the 100 nm spheres were 103.9 ± 3.7, 106.8 ± 4.1 and 112.1 ± 11.0 nm at particle concentrations of 1 x10^7, 1 x 10^8 and 1 x 10^9 # mL^{-1}. For the 200 nm spheres, measured diameters of 208.0 ± 7.4, 202.9 ± 4.9 and 185.5 ± 5.3 nm were found at particle concentrations of 1 x 10^7, 1 x 10^8 and 1 x 10^9 # mL^{-1}. For the 400 nm spheres, measured diameters of 381.5 ± 12.7, 368.9 ± 12.6 and 356.0 ± 24.1 nm were obtained for particle concentrations of 1 x 10^7, 1 x 10^8 and 1 x 10^9 # mL^{-1}. Consequently, the measurement of nano-entity size using the NTA system can be considered to be within 10 % of the reported diameter (Figure 5 – 2). These results are similar to previous work by Usfoor et al. (2020) who found that larger diameter nanoparticles were consistently

underestimated using NTA and by Bachurski et al. (2019) who noted that NTA overestimated diameter for 100 nm spheres.

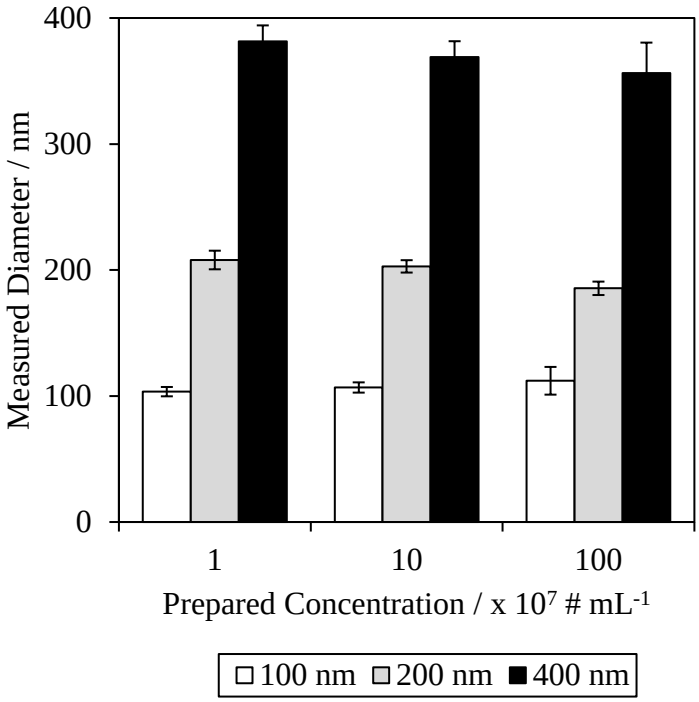

Figure 5 – 2. Measured diameter (nm) vs. prepared particle concentration (x 10^{7} # mL^{-1}) for 100, 200 and 400 nm polystyrene latex spheres.

5.3.2. Concentration Measurement of Polystyrene Latex Spheres

Every concentration measurement varied by at least one order of magnitude across the full range of detection thresholds. To illustrate, when prepared to a concentration of 1 x 10^{7} # mL^{-1}, the measured concentration for the 100 nm polystyrene latex spheres decreased from 1.08 x 10^{8} # mL^{-1} at detection threshold 2 to 8.60 x 10^{6} # mL^{-1} at detection threshold 48. Similar decreases in number count were observed for the 1 x 10^{8} and 1 x 10^{9} # mL^{-1} calibration standards (Figure 5 – 3). The same was true for the larger sized calibration particles although the level of variation appeared similar for all sizes. For example, in the case of the 400 nm particles, the measured concentration of the 1 x 10^{7} # mL^{-1} standard was 1.73 x 10^{8} # mL^{-1} at a detection threshold of 2 and 9.27 x 10^{6} # mL^{-1} at a detection threshold of 48.

Despite the variation in measured concentrations, an optimal detection threshold was found for every combination of diameter and concentration (Supplementary Information [SI] Table S5 – 1). The major problem with this, however, is that the optimal detection threshold was different for every combination of diameter and concentration. Therefore, it would be virtually impossible to confidently measure the concentration of an unknown sample based on a single detection threshold and there could easily be over an order of magnitude of over- or under- measurement. Averaging across the detection thresholds 2 – 50 was not a perfect solution, however this reduced the variability that an operator could introduce into the results. To illustrate, for the 100 nm spheres at a prepared concentration of 1×10^7 # mL^{-1}, the measured concentration spanned across three orders of magnitude from 8.18×10^6 to 3.85×10^9 # mL^{-1}. By averaging across all detection thresholds, the measured concentration was $2.67 \times 10^7 \pm 4.24 \times 10^6$ # mL^{-1} which was much closer to the actual value.

In the current case, averaging across all detection thresholds resulted in measured concentration for the 100 nm polystyrene latex spheres at prepared concentrations of 1×10^7, 1×10^8 and 1×10^9 # mL^{-1} were $2.67 \times 10^7 \pm 4.24 \times 10^6$, $1.81 \times 10^8 \pm 9.00 \times 10^6$ and $6.84 \times 10^8 \pm 1.84 \times 10^7$ # mL^{-1} respectively. For the 200 nm spheres, measured concentrations of $1.42 \times 10^7 \pm 2.4 \times 10^6$, $1.29 \times 10^8 \pm 1.06 \times 10^7$ and $7.57 \times 10^8 \pm 2.06 \times 10^7$ # mL^{-1} were found for prepared concentrations of 1×10^7, 1×10^8 and 1×10^9 # mL^{-1} respectively. Measured concentrations of $3.77 \times 10^7 \pm 6.44 \times 10^6$, $1.19 \times 10^8 \pm 5.08 \times 10^6$ and $4.39 \times 10^8 \pm 9.06 \times 10^6$ # mL^{-1} were found for the 400 nm spheres at prepared concentrations of 1×10^7, 1×10^8 and 1×10^9 # mL^{-1}, respectively. Overall, the measured number concentrations could be viewed to be accurate within one order of magnitude.

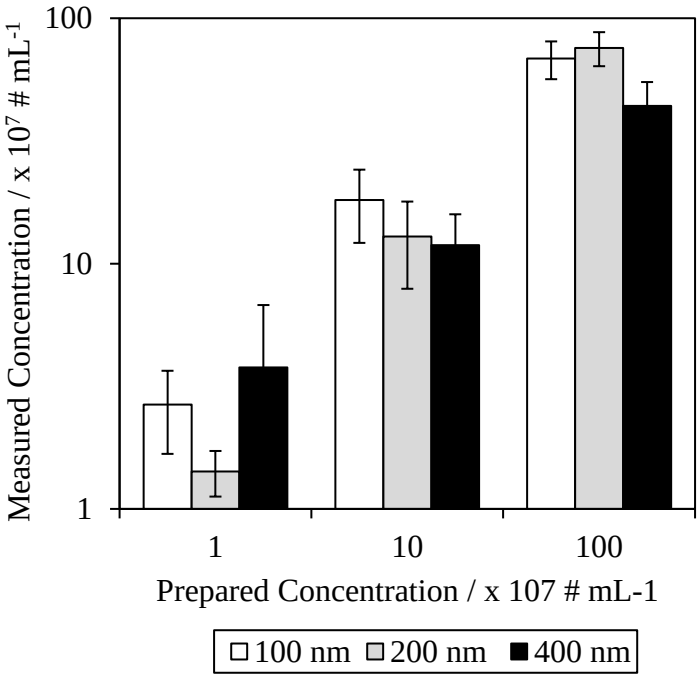

Figure 5 – 3. Averaged measured concentrations across detection thresholds 2 – 50 for prepared concentrations of 1 x 10^7, 1 x 10^8 and 1 x 10^9 # mL^{-1} for 100, 200 and 400 nm polystyrene latex spheres.

5.3.3. Size Distributions of MNBs

At gas flow rates 1, 2 and 3 L min^{-1}, the real-time size distribution of the ozone microbubbles was almost identical (Figure 5 – 4). The vast majority of the size distribution was between 1 – 100 µm, skewed towards the smaller sizes with 50 % of bubbles < 5 µm. The Sauter mean diameter was 37 µm. This suggests that the regenerative turbine microbubble generator process produces a consistent size distribution irrespective of the gas flow rate. The mean diameters reported here are congruent with the work of Zhou et al. (2022) who reported that the majority of microbubbles formed with a fine bubble generator were less than 10 µm in size when measured using FBRM. Similar mean sizes between 1 and 10 µm have also been reported from both micro-nanobubble

generators and high-speed rotation devices following measurement using a Coulter counter (Table 5 – 1).

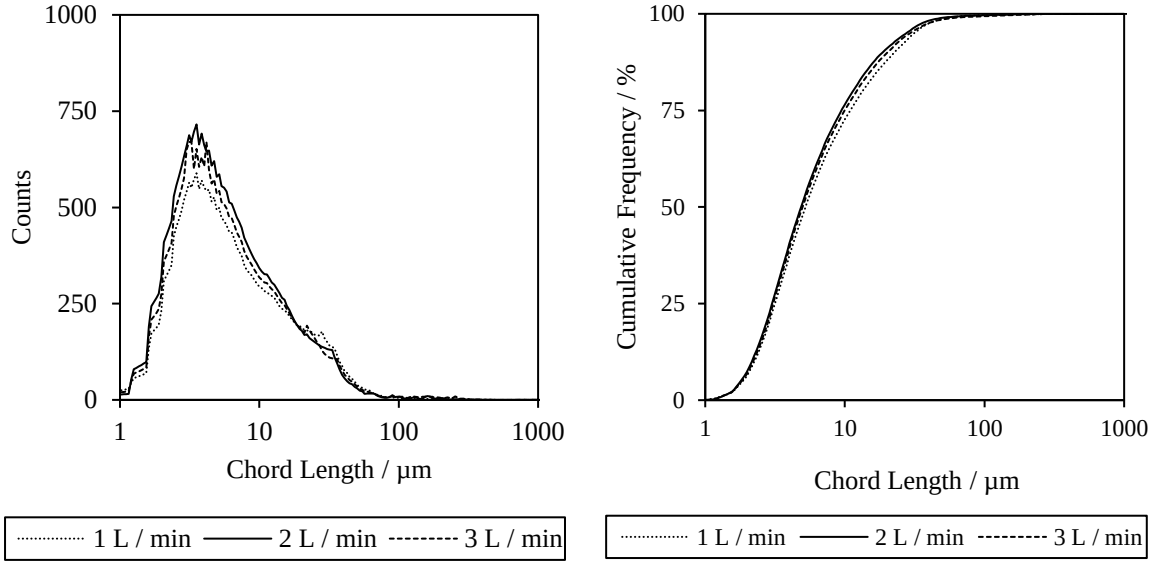

Figure 5 – 4. Size distribution (left) and cumulative frequency (right) of microbubbles measured using focussed-beam reflectance measurement during ozonation at gas flow rates 1, 2 and 3 L min^{-1}.

The nanobubble fraction was measured by NTA, with the sizes averaged across detection thresholds 2 – 50 in order to remove any operator influence in the processing. The maximum detectable diameter with NTA was 1000 nm so it was assumed that micron-sized objects were excluded. The resulting size distribution was relatively uniform with an average diameter of 217 ± 38 nm and 25^{th}, 50^{th} and 75^{th} percentile diameters of 182, 211 and 231 nm (Figure 5 – 5). The breadth of the distribution was very narrow, with the majority of the bubbles sized below 130 nm. Comparison to other generators and sizing instruments reveals a broad range of sizes similar to those reported here (Table 5 – 1). The average size measured in the current study was higher than those previously reported for bubbles generated by a range of methods including continuous high shear rotor stator device (similar to the one used in the current work), acoustic cavitation and water-ethanol mixing (Jadhav and Barigou, 2020). In these examples, NTA was used for bubble measurement with reported mean sizes between 95 and 125 nm, with the larger sizes

being generated by the high shear device. Interestingly, the bubble size data generated by the Coulter counter reported higher mean sizes reflecting the difficultly in directly comparing data measured by different instruments.

The average concentration of nanobubbles across all captures and detection thresholds was $2.9 \times 10^7 \pm 1.2 \times 10^7$ # mL^{-1} which was towards the high end of the previously reported concentrations, which varied between 1.84×10^5 and 7.5×10^8 # mL^{-1} (Table 5 – 1). The previously reported work using a high shear device and nanoparticle tracking reported an initial bubble number density of 2.4×10^8 # mL^{-1}, albeit with a smaller mean diameter (Jadhav and Barigou, 2020).

The NTA instrument does not differentiate between particles, droplets and bubbles and so it was not possible to confirm whether the measured distribution were nanobubbles. Indeed, the question as to whether the measured items are actually bubbles is an active area of debate with compelling evidence for both positions (Sun et al., 2022). The source of potential nanoparticles when using devices such as the regenerative turbine microbubble generator includes contamination in the water such from organic or inorganic particles, or from release of metallic nanoparticles from the device. This has been confirmed in the case of ultrasonic cavitation, where titanium and vanadium nanoparticles were measured (Rak et al., 2019). However, in other studies, no such organic or inorganic materials have been detected, while the amount of dissolved gas has a direct bearing on the number count and differences in pressure impacts bubble size (Jadhav and Barigou, 2020). Interestingly, in the case of experiments using acoustic cavitation or water-ethanol mixing under a partial vacuum, an order of magnitude reduction in numbers was observed which indicates that such entities must be gas filled (Jadhav and Barigou, 2020). Overall, it remains unclear as to the exact nature of the nano-entities but is likely to be a combination of bubbles and non-bubbles (particles and droplets); the proportions of which will be system dependent. In the case of the current trials, measurement of blanks and non-aerated water revealed that any other nanoparticles, if present, were sufficiently low in concentration to be below the limit of detection for the NTA ($< 10^6$ # mL^{-1}). This does not mean that nanoparticles were not present, it instead means that any detected particles, believed to be nanobubbles, were a result of the aeration process.

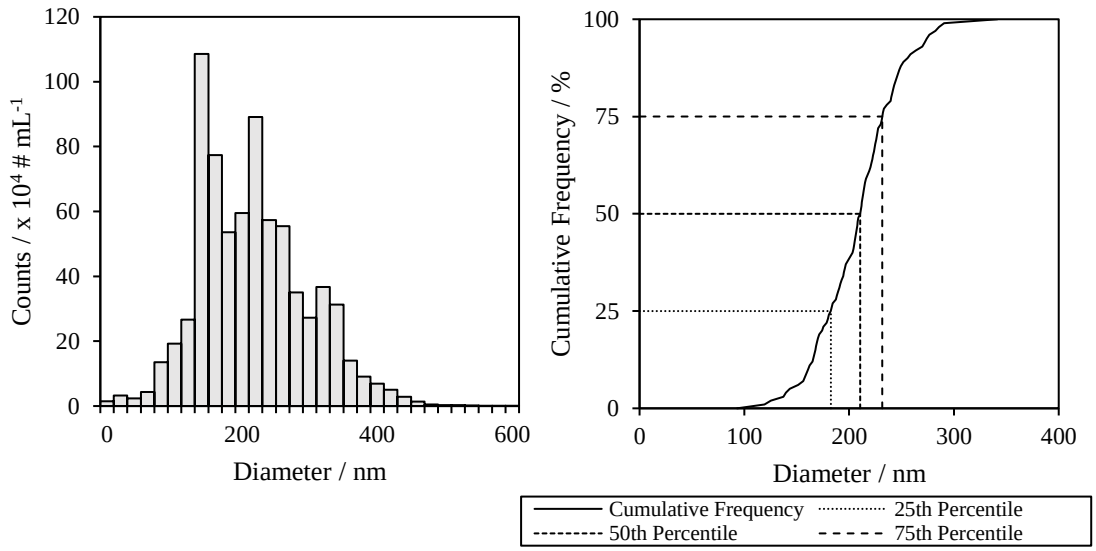

Figure 5 – 5. Size distribution (left) and cumulative frequency (right) of residual ozone nanobubbles measured using nanoparticle tracking analysis with an original ozone gas flow rate of 2 L min^{-1}.

Direct comparison between the size distributions of the micro- and nanobubbles is complex as they have been measured by different instruments and so have different inherent biases and what is measured (hydraulic diameter versus chord length). However, the distributions can be broadly compared to explore the relative contribution both fractions will have in relation to mass transfer in gas-liquid systems such as ozone contactors used in water treatment (John et al., 2022). The microbubble fraction ranged between 1 and 100 μm with a mean diameter of 37 μm, while the nanobubble fraction ranged between 100 and 400 nm with a mean diameter of 217 nm. For context, the conventional bubble fraction ranged between 1 – 10 mm with a mean diameter of 5.4 mm (Chapter 3, Figure 3 – 2). Accordingly, the difference in size for micro- and nanobubbles was between 1 or 2 orders of magnitude suggesting the differences is potentially less significant than previously thought for this type of MNB generator. Eklund et al. (2021) illustrated the difference by comparing the properties of a 100 nm (nanobubble) and a 1 μm (1000 nm) (microbubble) bubbles, i.e. the smaller end of each size range, at a typical nanobubble concentration of 10^8 # mL^{-1}. The bubble volume fraction relative to the liquid

was 10^{-7} and 10^{-4}, respectively and so reasonably low in both cases. If no Laplace pressure in the bubbles is assumed this then translates to gas concentrations of 0.0001 mg L^{-1} and 0.1 mg L^{-1} respectively. Adjusting to account for the Laplace pressure, assuming standard conditions, would increase the gas concentration in the nanobubbles by an order of magnitude to 0.001 mg L^{-1} meaning that the majority of any transferred gas will be associated with the microbubble fraction. In the current case, this was further weighted towards the microbubble fraction with, for instance, one individual 37 μm microbubble containing the same volume of gas as five million 217 nm nanobubbles. The smaller size of the nanobubbles will translate to a higher specific surface area, with values of 1.62 x 10^5 m^{-1} for the microbubble and 2.76 x 10^7 m^{-1} for the nanobubble in the current case. The specific surface area of the comparative conventional bubble system was 1111 m^{-1}. This should translate to a faster rate of mass transfer and hence enhanced performance as bubble size decreases. However, even for the microbubbles the enhanced specific surface area compared to conventional systems means that almost complete gas transfer would occur within 1 - 2 m of water depth. To illustrate, a gas transfer efficiency of 96 % was reported in a 32 cm deep tank for microbubbles with a mean size of 51 μm (Zhang et al., 2018). In most water treatment applications ozone tank depths exceed 3 m and can be a deep as 7 - 8 m (John et al., 2022). Consequently, the benefits of enhanced mass transfer are realised with microbubbles and indeed could be larger than those currently considered. Further, the benefits of nanobubbles on enhanced mass transfer can only be realised in shallow tank depths and hence require new reactor designs to be developed. In addition, it has been proposed in ozone systems that MNBs produce more hydroxyl radicals enabling better and faster reactions. However, previous research has shown no statistically significant difference in radical formation when MNBs were compared to conventional bubbles (2 - 6 mm) when normalised for dissolved ozone concentration (John et al., 2022b). Previously reported enhancements reflect increased mass transfer due to the much higher specific surface areas associated with MNBs.

5.3.4. Longevity of Residual Nanobubbles

The other advantage stated for bulk nanobubbles is their stability over prolonged times. To test for the longevity of the residual nanobubbles from the current system, samples

were measured continuously for 18 hours using a custom script on the NTA system which automatically captured measurements every hour. Residual nanobubbles were detected consistently across the analysis period. The diameter of the residual nanobubbles immediately after the cessation of microbubble generation was 208.1 ± 24.9 nm and the measured concentration was $7.17 \times 10^7 \pm 1.93 \times 10^7$ # mL^{-1}. Over the course of the 18 hours, there was very little change in the diameter or concentration. The measured diameter did not appear to increase or decrease significantly and remained relatively static for the duration of the measurements (Figure 5 – 6). The same was true for the measured concentration (Figure 5 – 7). After the 18-hour period, there was a slight decrease in measured concentration to $2.09 \times 10^7 \pm 5.54 \times 10^6$ # mL^{-1}, although this was within the uncertainty ranges for the measurements. Previously reported data from a similar system extended the trial to 140 days and showed that the number concentration decreased slightly over this time but the size distribution decreased, with the majority of the bubbles being between 50 and 100 nm for the measurement taken after the first day (Jadhav and Barigou, 2020). While the stability of bulk nanoparticles remains an open area of debate, a number of theories have been proposed to help explain the deviation from the established Epstein-Plesset theory which suggests nanobubbles in saturated liquids should be stable for no more than a few milliseconds (Rak et al., 2019). These include: the skin model and the armoured bubble model, where surfactant and organic layers on the outside of bubbles stabilise them; the electrostatic repulsion model related to the very high magnitude zeta potential that nanobubbles are reported to have; and a dynamic equilibrium model (Sun et al., 2022). Surface coating in real waters is likely but the exact extent and type will vary. Such surface accumulation can reduce the surface tension, and hence the Laplace pressure, such that the bubble can exist in equilibrium with the surrounded saturated liquid. It may be the case that there will be significant transfer into complex matrices leading to a reduction in bubble size. The dynamic equilibrium model proposes patchwork hydrophobic zones on the bubbles that aids diffusion into the bubble, while gas can diffuse out into the liquid through the uncovered areas. The net is no overall transfer and hence the bubbles are stable (Yasui et al., 2016). No one model currently explains the phenomena observed and there is often limited direct evidence such that no common explanatory model currently exists (Sun et al., 2022). One important aspect is

common to a number of these ideas: there is no net gas transfer and hence the nanobubbles are unlikely to contribute to overall transfer and performance enhancement.

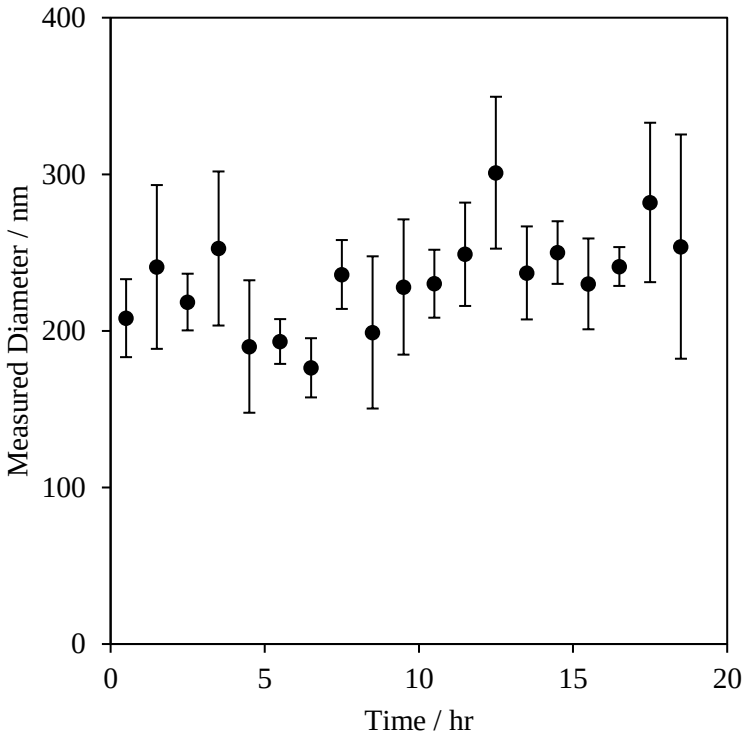

Figure 5 – 6. Measured diameter of residual nanobubbles over an 18-hour period from the generation of air microbubbles.

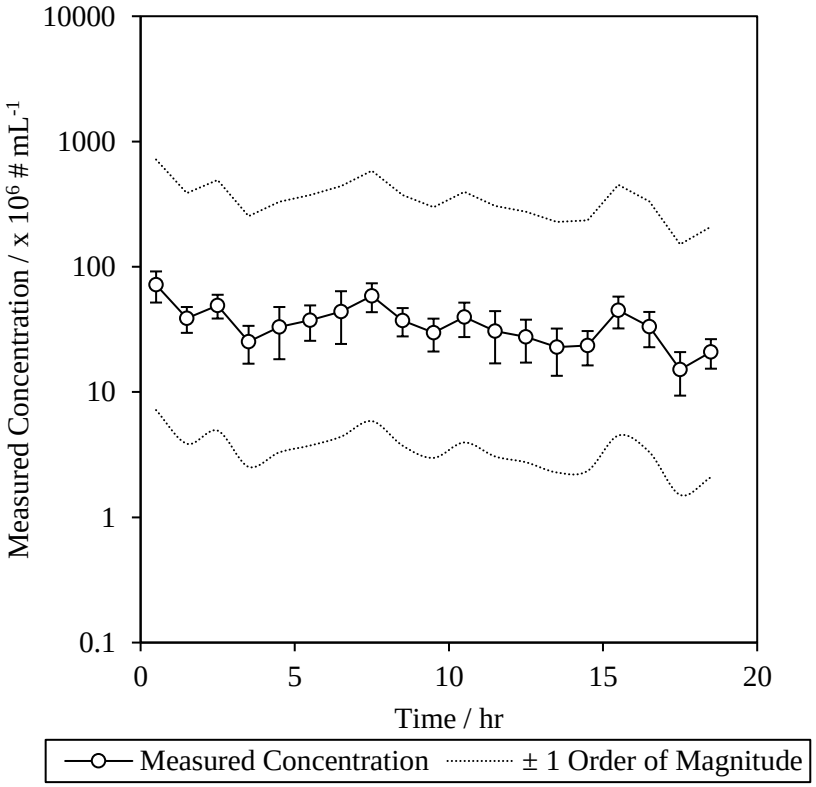

Figure 5 – 7. Measured concentration of residual nanobubbles over an 18-hour period from the generation of air microbubbles.

Overall, the work indicates that, despite the debate as to whether they exist or not, nanobubbles are unlikely to be the key component that delivers enhancement in gas-liquid treatment systems used in water treatment. Instead, and particularly in the case of ozone, the fate of the nanobubbles represents a potential concern as they will likely exit the ozone contactor into the downstream processes. It is likely that nanobubbles are also formed in conventional bubble contactors. The conventional bubble generator produces bubbles in the micro-range and it is possible that bubbles in the nano-range are also formed. Although, given that the overwhelming majority of the gas volume is entrained within millimetre bubbles, it is entirely reasonable to assume that the number of nanobubbles produced is minimal. Residual dissolved ozone is typically removed by granular activated carbon to ensure no residual in the later stages to minimise ozone off-gassing post-contactors (Mitra et al. (2017). However, the fate of stabilised nanobubbles is unknown and represents an area of urgent need for investigation. The likely surface coating and the

high negative zeta potentials associated with nanobubbles means that they will likely have a very low attachment efficiency (Kim et al., 2020) and hence could pass through these post ozone stages. Calculation of the maximum potential impact based on our current data of a mean diameter of 217 nm and a bubble concentration of 2.89 x 10^7 # mL^{-1}, translates into a potential quantity of molecular ozone of 0.32 µg L^{-1}. Factoring in the observed uncertainty, an ozone concentration range between 0.032 – 3.2 µg L^{-1} may be possible. However it must be noted that conventional gas bubble theories may not apply to nanobubbles and so further confirmation is required. Most ozone generators do not output 100 % ozone gas. For example, a typical ozone output for a pure oxygen feed gas is 6 – 13 % (Vezzù et al., 2019) and significantly lower for air-fed fed systems. Therefore, the potential quantity of molecular ozone within nanobubbles is likely to be much lower than stated. Current legislation for ozonation is focussed around the formation of bromate from the ozonation of bromide-containing waters. Bromate is a potential human carcinogen with a regulatory limit of 10 µg L^{-1} (Soltermann et al., 2017). Undissolved and unquenched gaseous ozone passing through to post-ozone stages risks the formation of additional bromate, however the gaseous ozone volume entrained within the nanobubbles is sufficiently low to not be a cause for concern.

5.4. Conclusion

The work has compared the nanobubble and microbubble fractions of a MNB distribution generated using a regenerative turbine microbubble generator with ozone. Mean bubbles sizes of 217 nm and 37 µm were reported for each fraction, respectively, both with reasonably distributed size ranges. Further, 50 % of the microbubbles were less than 5000 nm in size, such that the two distributions differed by around one to two orders of magnitude. Interpretation of the findings, with regards to water treatment using an ozone gas liquid contactor, indicated that the nanobubble fraction is unlikely to be a significant contributor to the efficiency and effectiveness of the process and that the majority of the performance is delivered through the microbubble fraction. This suggests that more focus should be placed on understanding how to control the size distribution of the microbubble fraction in order to optimise the overall process. The nanobubbles were observed to remain stable in terms of number and size for 18 hours. This further supports the

negligible impact of the nanobubble fraction on treatment but raises concerns as to their fate as they are likely to exit the contactors. Based on the measured data, the risk for residual ozone through nanobubble survival was considered negligible, with an estimated maximum ozone residual of 3.2 μg L^{-1} predicted under typical water treatment conditions. However, work is required to confirm the fate of nanobubble through downstream processes such as GAC.

5.5. Acknowledgements

This research is gratefully supported by the Engineering and Physical Sciences Research Council (EPSRC) through their funding of the STREAM Industrial Doctorate Centre (EP/G037094/1) and from the project sponsor Anglian Water.

5.6. References

Abbasian-arani, M., Hatamipour, M. and Rahimi, A., 2021. Experimental determination of gas holdup and volumetric mass transfer coefficient in a jet bubbling reactor. *Chinese Journal of Chemical Engineering*, 34, pp.61-67.

Alheshibri, M. and Craig, V., 2019. Generation of nanoparticles upon mixing ethanol and water; Nanobubbles or Not? *Journal of Colloid and Interface Science*, 542, pp.136-143.

Alheshibri, M. and Craig, V., 2018. Differentiating between nanoparticles and nanobubbles by evaluation of the compressibility and density of nanoparticles. *The Journal of Physical Chemistry C*, 122(38), pp.21998-22007.

Alheshibri, M., Jehannin, M., Coleman, V. and Craig, V., 2019. Does gas supersaturation by a chemical reaction produce bulk nanobubbles? *Journal of Colloid and Interface Science*, 554, pp.388-395.

Aluthgun Hewage, S., Batagoda, J.H. and Meegoda, J.N. (2020). In situ remediation of sediments contaminated with organic pollutants using ultrasound and ozone nanobubbles. *Environmental Engineering Science*, 37(8), pp.521–534.

Aluthgun Hewage, S., Batagoda, J. and Meegoda, J., 2021. Remediation of contaminated sediments containing both organic and inorganic chemicals using ultrasound and ozone nanobubbles. *Environmental Pollution*, 274, p.116538.

Atkinson, A., Apul, O., Schneider, O., Garcia-Segura, S. and Westerhoff, P., 2019. Nanobubble technologies offer opportunities to improve water treatment. *Accounts of Chemical Research*, 52(5), pp.1196-1205.

Bachurski, D., Schuldner, M., Nguyen, P., Malz, A., Reiners, K., Grenzi, P., Babatz, F., Schauss, A., Hansen, H., Hallek, M. and Pogge von Strandmann, E., 2019. Extracellular vesicle measurements with nanoparticle tracking analysis – An accuracy and repeatability comparison between NanoSight NS300 and ZetaView. *Journal of Extracellular Vesicles*, 8(1), p.1596016.

Baquero-Rodríguez, G., Lara-Borrero, J., Nolasco, D. and Rosso, D., 2018. A critical review of the factors affecting modeling oxygen transfer by fine-pore diffusers in activated sludge. *Water Environment Research*, 90(5), pp.431-441.

Batagoda, J., Hewage, S. and Meegoda, J., 2019. Remediation of heavy-metal-contaminated sediments in USA using ultrasound and ozone nanobubbles. *Journal of Environmental Engineering and Science*, 14(2), pp.130-138.

Behnisch, J., Ganzauge, A., Sander, S., Herrling, M. and Wagner, M., 2018. Improving aeration systems in saline water: measurement of local bubble size and volumetric mass transfer coefficient of conventional membrane diffusers. *Water Science and Technology*, 78(4), pp.860-867.

Eklund, F., Alheshibri, M. and Swenson, J., 2021. Differentiating bulk nanobubbles from nanodroplets and nanoparticles. *Current Opinion in Colloid and Interface Science*, 53, p.101427.

Epstein, P. and Plesset, M., 1950. On the stability of gas bubbles in liquid-gas solutions. *The Journal of Chemical Physics*, 18(11), pp.1505-1509.

Fan, W., An, W., Huo, M., Xiao, D., Lyu, T. and Cui, J., 2021. An integrated approach using ozone nanobubble and cyclodextrin inclusion complexation to enhance the removal of micropollutants. *Water Research*, 196, p.117039.

Fan, W., An, W., Huo, M., Yang, W., Zhu, S. and Lin, S., 2020. Solubilization and stabilization for prolonged reactivity of ozone using micro-nano bubbles and ozone-saturated solvent: A promising enhancement for ozonation. *Separation and Purification Technology*, 238, p.116484.

Fan, W., Cui, J., Li, Q., Huo, Y., Xiao, D., Yang, X., Yu, H., Wang, C., Jarvis, P., Lyu, T. and Huo, M., 2021. Bactericidal efficiency and photochemical mechanisms of micro/nano bubble–enhanced visible light photocatalytic water disinfection. *Water Research*, 203, p.117531.

Fan, W., Desai, P., Zimmerman, W., Duan, Y., Crittenden, J., Wang, C. and Huo, M., 2021. Optical density inferences in aqueous solution with embedded micro/nano bubbles: A reminder for the emerging green bubble cleantech. *Journal of Cleaner Production*, 294, p.126258.

Fan, W., Li, Y., Wang, C., Duan, Y., Huo, Y., Januszewski, B., Sun, M., Huo, M. and Elimelech, M., 2021. Enhanced photocatalytic water decontamination by micro–nano bubbles: measurements and mechanisms. *Environmental Science and Technology*, 55(10), pp.7025-7033.

Fan, W., Zhou, Z., Wang, W., Huo, M., Zhang, L., Zhu, S., Yang, W. and Wang, X., 2019. Environmentally friendly approach for advanced treatment of municipal secondary effluent by integration of micro-nano bubbles and photocatalysis. *Journal of Cleaner Production*, 237, p.117828.

Fang, Z., Wang, X., Zhou, L., Zhang, L. and Hu, J., 2020. Formation and stability of bulk nanobubbles by vibration. *Langmuir*, 36(9), pp.2264-2270.

Farid, M., Choi, P., Kharraz, J., Lao, J., St-Hilaire, S., Ruan, Y., Lam, P. and An, A., 2022. Hybrid nanobubble-forward osmosis system for aquaculture wastewater treatment and reuse. *Chemical Engineering Journal*, 435, p.135164.

Garrido-Baserba, M., Asvapathanagul, P., Park, H., Kim, T., Baquero-Rodriguez, G., Olson, B. and Rosso, D., 2018. Impact of fouling on the decline of aeration efficiency under different operational conditions at WRRFs. *Science of The Total Environment*, 639, pp.248-257.

Häbich, A., Ducker, W., Dunstan, D. and Zhang, X., 2010. Do stable nanobubbles exist in mixtures of organic solvents and water? *The Journal of Physical Chemistry B*, 114(20), pp.6962-6967.

Jadhav, A. and Barigou, M., 2020. Bulk nanobubbles or not nanobubbles: That is the question. *Langmuir*, 36(7), pp.1699-1708.

Jadhav, A. and Barigou, M., 2021. Response to "Comment on bulk nanobubbles or not nanobubbles: That is the question". *Langmuir*, 37(1), pp.596-601.

Jhunkeaw, C., Khongcharoen, N., Rungrueng, N., Sangpo, P., Panphut, W., Thapinta, A., Senapin, S., St-Hilaire, S. and Dong, H., 2021. Ozone nanobubble treatment in freshwater effectively reduced pathogenic fish bacteria and is safe for Nile tilapia (Oreochromis niloticus). *Aquaculture*, 534, p.736286.

Jin, J., Feng, Z., Yang, F. and Gu, N., 2019. Bulk nanobubbles fabricated by repeated compression of microbubbles. *Langmuir*, 35(12), pp.4238-4245.

John, A., Brookes, A., Carra, I., Jefferson, B. and Jarvis, P., 2022. Microbubbles and their application to ozonation in water treatment: A critical review exploring their benefit and future application. *Critical Reviews in Environmental Science and Technology*, 52(9), pp.1561-1603.

John, A., Carra, I., Jefferson, B., Jodkowska, M., Brookes, A. and Jarvis, P., 2022. Are microbubbles magic or just small? A direct comparison of hydroxyl radical generation between microbubble and conventional bubble ozonation under typical operational conditions. *Chemical Engineering Journal*, p.134854.

Kanematsu, W., Tuziuti, T. and Yasui, K., 2020. The influence of storage conditions and container materials on the long term stability of bulk nanobubbles — Consideration from a perspective of interactions between bubbles and surroundings. *Chemical Engineering Science*, 219, p.115594.

Kim, M., Han, M., Kim, T., Lee, J. and Kwak, D., 2020. Effect of nanobubbles for improvement of water quality in freshwater: Flotation model simulation. *Separation and Purification Technology*, 241, p.116731.

Leroy, V. and Norisuye, T., 2016. Investigating the existence of bulk nanobubbles with ultrasound. *ChemPhysChem*, 17(18), pp.2787-2790.

Levitsky, I., Tavor, D. and Gitis, V., 2022. Micro and nanobubbles in water and wastewater treatment: A state-of-the-art review. *Journal of Water Process Engineering*, 47, p.102688.

Lyu, T., Wu, S., Mortimer, R. and Pan, G., 2019. Nanobubble technology in environmental engineering: revolutionization potential and challenges. *Environmental Science and Technology*, 53(13), pp.7175-7176.

Manning, G., 2020. On the thermodynamic stability of bubbles, immiscible droplets, and cavities. *Physical Chemistry Chemical Physics*, 22(31), pp.17523-17531.

Meegoda, J., Hewage, S. and Batagoda, J., 2019. Application of the diffused double layer theory to nanobubbles. *Langmuir*, 35(37), pp.12100-12112.

Miller, C., 1924. The Stokes-Einstein law for diffusion in solution. *Proceedings of the Royal Society of London. Series A, Containing Papers of a Mathematical and Physical Character*, 106(740), pp.724-749.

Mitra, S., Johnston, R., Scott, K., Lin, R., Wyatt, F., Coffey, B. and Rakness, K., 2017. Ozone plant operations under drought conditions. *Ozone: Science and Engineering*, 39(3), pp.202-208.

Movahed, S. and Sarmah, A., 2021. Global trends and characteristics of nano- and micro-bubbles research in environmental engineering over the past two decades: A scientometric analysis. *Science of the Total Environment*, 785, p.147362.

Nirmalkar, N., Pacek, A. and Barigou, M., 2019. Bulk nanobubbles from acoustically cavitated aqueous organic solvent mixtures. *Langmuir*, 35(6), pp.2188-2195.

Parmar, R. and Majumder, S., 2013. Microbubble generation and microbubble-aided transport process intensification—A state-of-the-art report. *Chemical Engineering and Processing: Process Intensification*, 64, pp.79-97.

Rak, D., Ovadová, M. and Sedlák, M., 2019. (Non)Existence of bulk nanobubbles: the role of ultrasonic cavitation and organic solutes in water. *The Journal of Physical Chemistry Letters*, 10(15), pp.4215-4221.

Sedlák, M. and Rak, D., 2013. Large-scale inhomogeneities in solutions of low molar mass compounds and mixtures of liquids: supramolecular structures or nanobubbles? *The Journal of Physical Chemistry B*, 117(8), pp.2495-2504.

Shangguan, Y., Yu, S., Gong, C., Wang, Y., Yang, W. and Hou, L., 2018. A review of microbubble and its applications in ozonation. *IOP Conference Series: Earth and Environmental Science*, 128, p.012149.

Shi, X., Xue, S., Marhaba, T. and Zhang, W., 2021. Probing internal pressures and long-term stability of nanobubbles in water. *Langmuir*, 37(7), pp.2514-2522.

Singh, B., Shukla, N., Cho, C., Kim, B., Park, M. and Kim, K., 2021. Effect and application of micro- and nanobubbles in water purification. *Toxicology and Environmental Health Sciences*, 13(1), pp.9-16.

Soltermann, F., Abegglen, C., Tschui, M., Stahel, S. and von Gunten, U., 2017. Options and limitations for bromate control during ozonation of wastewater. *Water Research*, 116, pp.76-85.

Sun, L., Zhang, F., Guo, X., Qiao, Z., Zhu, Y., Jin, N., Cui, Y. and Yang, W., 2022. Research progress on bulk nanobubbles. *Particuology*, 60, pp.99-106.

Suwartha, N., Syamzida, D., Priadi, C., Moersidik, S. and Ali, F., 2020. Effect of size variation on microbubble mass transfer coefficient in flotation and aeration processes. *Heliyon*, 6(4), p.e03748.

Tang, Y., Zhang, M., Zhang, J., Lyu, T., Cooper, M. and Pan, G., 2021. Reducing arsenic toxicity using the interfacial oxygen nanobubble technology for sediment remediation. *Water Research*, 205, p.117657.

Temesgen, T., Bui, T., Han, M., Kim, T. and Park, H., 2017. Micro and nanobubble technologies as a new horizon for water-treatment techniques: A review. *Advances in Colloid and Interface Science*, 246, pp.40-51.

Terashima, M., So, M., Goel, R. and Yasui, H., 2016. Determination of diffuser bubble size in computational fluid dynamics models to predict oxygen transfer in spiral roll aeration tanks. *Journal of Water Process Engineering*, 12, pp.120-126.

Ulatowski, K., Sidorski, M. and Sobieszuk, P., 2020. Oil-contaminated surface cleaning using oxygen and nitrogen nanobubbles. *Journal of Physics: Conference Series*, 1681(1), p.012017.

Usfoor, Z., Kaufmann, K., Rakib, A., Hergenröder, R. and Shpacovitch, V., 2020. Features of sizing and enumeration of silica and polystyrene nanoparticles by nanoparticle tracking analysis (NTA). *Sensors*, 20(22), p.6611.

Vezzù, G., Lopez, J., Freilich, A. and Becker, K., 2009. Optimization of large-scale ozone generators. *IEEE Transactions on Plasma Science*, 37(6), pp.890-896.

Wang, L., Ali, J., Wang, Z., Oladoja, N., Cheng, R., Zhang, C., Mailhot, G. and Pan, G., 2020. Oxygen nanobubbles enhanced photodegradation of oxytetracycline under visible light: Synergistic effect and mechanism. *Chemical Engineering Journal*, 388, p.124227.

Wang, Y., Wang, S., Sun, J., Dai, H., Zhang, B., Xiang, W., Hu, Z., Li, P., Yang, J. and Zhang, W., 2021. Nanobubbles promote nutrient utilization and plant growth in rice by upregulating nutrient uptake genes and stimulating growth hormone production. *Science of the Total Environment*, 800, p.149627.

Wu, Y., Lyu, T., Yue, B., Tonoli, E., Verderio, E., Ma, Y. and Pan, G., 2019. Enhancement of tomato plant growth and productivity in organic farming by agri-nanotechnology using nanobubble oxygation. *Journal of Agricultural and Food Chemistry*, 67(39), pp.10823-10831.

Xue, S., Zhang, Y., Marhaba, T. and Zhang, W., 2022. Aeration and dissolution behavior of oxygen nanobubbles in water. *Journal of Colloid and Interface Science*, 609, pp.584-591.

Yasui, K., Tuziuti, T., Kanematsu, W. and Kato, K., 2016. Dynamic equilibrium model for a bulk nanobubble and a microbubble partly covered with hydrophobic material. *Langmuir*, 32(43), pp.11101-11110.

Zhang, H., Guo, Z. and Zhang, X., 2020. Surface enrichment of ions leads to the stability of bulk nanobubbles. *Soft Matter*, 16(23), pp.5470-5477.

Zhang, J., Huang, G., Liu, C., Zhang, R., Chen, X. and Zhang, L., 2018. Synergistic effect of microbubbles and activated carbon on the ozonation treatment of synthetic dyeing wastewater. *Separation and Purification Technology*, 201, pp.10-18.

Zhou, S., Nazari, S., Hassanzadeh, A., Bu, X., Ni, C., Peng, Y., Xie, G. and He, Y., 2022. The effect of preparation time and aeration rate on the properties of bulk micro-nanobubble water using hydrodynamic cavitation. *Ultrasonics Sonochemistry*, 84, p.105965.

5.7. Supplementary Information

[SI] Table 5 – S1. Measured concentrations for 100, 200 and 400 nm polystyrene latex spheres at prepared concentrations of 1 x 10^7, 1 x 10^8 and 1 x 10^9 # ml^{-1} with the optimal detection threshold in bold.

DT	100 nm / # ml^{-1}			200 nm / # ml^{-1}			400 nm / # ml^{-1}		
	1 x 10^7	**1 x 10^8**	**1 x 10^9**	**1 x 10^7**	**1 x 10^8**	**1 x 10^9**	**1 x 10^7**	**1 x 10^8**	**1 x 10^9**
2	1.08 x 10^8 ± 1.48 x 10^7	6.40 x 10^8 ± 1.85 x 10^7	3.85 x 10^9 ± 6.51 x 10^7	3.88 x 10^7 ± 5.78 x 10^6	3.86 x 10^8 ± 2.76 x 10^7	2.49 x 10^9 ± 6.38 x 10^7	1.73 x 10^8 ± 1.81 x 10^7	4.59 x 10^8 ± 1.30 x 10^7	1.87 x 10^9 ± 3.01 x 10^7
4	6.36 x 10^7 ± 9.21 x 10^6	4.74 x 10^8 ± 1.48 x 10^7	2.70 x 10^9 ± 3.99 x 10^7	3.27 x 10^7 ± 4.47 x 10^6	3.09 x 10^8 ± 2.17 x 10^7	2.24 x 10^9 ± 2.63 x 10^7	7.31 x 10^7 ± 1.21 x 10^7	3.24 x 10^8 ± 1.02 x 10^7	**1.05 x 10^9 ± 1.59 x 10^7**
6	5.84 x 10^7 ± 8.05 x 10^6	4.46 x 10^8 ± 1.44 x 10^7	2.44 x 10^9 ± 3.58 x 10^7	3.13 x 10^7 ± 4.26 x 10^6	2.90 x 10^8 ± 2.01 x 10^7	2.05 x 10^9 ± 2.71 x 10^7	6.92 x 10^7 ± 1.15 x 10^7	3.02 x 10^8 ± 1.05 x 10^7	9.60 x 10^8 ± 1.48 x 10^7
8	4.92 x 10^7 ± 6.81 x 10^6	3.96 x 10^8 ± 1.37 x 10^7	2.01 x 10^9 ± 2.72 x 10^7	2.84 x 10^7 ± 3.78 x 10^6	2.66 x 10^8 ± 1.86 x 10^7	1.79 x 10^9 ± 2.86 x 10^7	6.41 x 10^7 ± 1.04 x 10^7	2.71 x 10^8 ± 9.98 x 10^6	8.44 x 10^8 ± 1.42 x 10^7
10	4.13 x 10^7 ± 5.61 x 10^6	3.44 x 10^8 ± 1.31 x 10^7	1.55 x 10^9 ± 2.22 x 10^7	2.65 x 10^7 ± 3.87 x 10^6	2.39 x 10^8 ± 1.68 x 10^7	1.55 x 10^9 ± 2.87 x 10^7	5.91 x 10^7 ± 9.90 x 10^6	2.40 x 10^8 ± 9.80 x 10^6	7.32 x 10^8 ± 1.34 x 10^7
12	3.63 x 10^7 ± 4.60 x 10^6	2.99 x 10^8 ± 1.23 x 10^7	**1.05 x 10^9 ± 2.35 x 10^7**	2.39 x 10^7 ± 3.70 x 10^6	2.13 x 10^8 ± 1.52 x 10^7	1.33 x 10^9 ± 2.80 x 10^7	5.44 x 10^7 ± 9.21 x 10^6	2.10 x 10^8 ± 8.97 x 10^6	6.35 x 10^8 ± 1.26 x 10^7
14	3.34 x 10^7 ± 4.26 x 10^6	2.63 x 10^8 ± 1.18 x 10^7	8.57 x 10^8 ± 2.66 x 10^7	2.14 x 10^7 ± 3.37 x 10^6	1.90 x 10^8 ± 1.40 x 10^7	1.14 x 10^9 ± 2.68 x 10^7	5.02 x 10^7 ± 8.64 x 10^6	1.85 x 10^8 ± 8.18 x 10^6	5.59 x 10^8 ± 1.13 x 10^7
16	2.96 x 10^7 ± 3.85 x 10^6	2.35 x 10^8 ± 1.14 x 10^7	6.54 x 10^8 ± 2.81 x 10^7	1.92 x 10^7 ± 3.11 x 10^6	1.73 x 10^8 ± 1.29 x 10^7	**9.96 x 10^8 ± 2.59 x 10^7**	4.68 x 10^7 ± 8.15 x 10^6	1.64 x 10^8 ± 7.38 x 10^6	5.04 x 10^8 ± 1.02 x 10^7
18	2.66 x 10^7 ± 3.49 x 10^6	2.10 x 10^8 ± 1.12 x 10^7	5.05 x 10^8 ± 2.81 x 10	1.73 x 10^7 ± 2.84 x 10^6	1.57 x 10^8 ± 1.22 x 10^7	8.70 x 10^8 ± 2.45 x 10^7	4.31 x 10^7 ± 7.98 x 10^6	1.45 x 10^8 ± 6.70 x 10^6	4.59 x 10^8 ± 9.34 x 10^6
20	2.37 x 10^7 ± 3.17 x 10^6	1.86 x 10^8 ± 1.09 x 10^7	3.85 x 10^8 ± 2.69 x 10^7	1.54 x 10^7 ± 2.59 x 10^6	1.43 x 10^8 ± 1.15 x 10^7	7.59 x 10^8 ± 2.25 x 10^7	3.98 x 10^7 ± 7.25 x 10^7	1.26 x 10^8 ± 6.41 x 10^6	4.20 x 10^8 ± 8.99 x 10^6
22	2.13 x 10^7 ± 2.93 x 10^6	1.64 x 10^8 ± 1.06 x 10^7	2.88 x 10^8 ± 2.58 x 10^7	1.37 x 10^7 ± 2.35 x 10^6	1.29 x 10^8 ± 1.09 x 10^7	6.56 x 10^8 ± 2.05 x 10^7	3.65 x 10 ± 6.41 x 10^6	**1.07 x 10^8 ± 6.11 x 10^6**	3.85 x 10^8 ± 8.39 x 10^6
24	2.03 x 10^7 ± 3.54 x 10^6	1.41 x 10^8 ± 1.05 x 10^7	2.07 x 10^8 ± 2.39 x 10^7	1.21 x 10^7 ± 2.15 x 10^6	**9.98 x 10^7 ± 1.05 x 10^7**	5.61 x 10^8 ± 1.87 x 10^7	3.30 x 10^7 ± 5.98 x 10^6	8.86 x 10^7 ± 5.56 x 10^6	3.53 x 10^8 ± 7.77 x 10^6
26	1.83 x 10^7 ± 3.40 x 10^6	1.21 x 10^8 ± 1.03 x 10^7	1.47 x 10^8 ± 2.11 x 10^7	**1.08 x 10^7 ± 1.99 x 10^6**	9.10 x 10^7 ± 1.01 x 10^7	4.75 x 10^8 ± 1.76 x 10^7	2.56 x 10^7 ± 5.17 x 10^6	7.04 x 10^7 ± 5.19 x 10^6	3.23 x 10^8 ± 7.37 x 10^6
28	1.65 x 10^7 ± 3.20 x 10^6	**1.03 x 10^8 ± 9.74 x 10^6**	1.13 x 10^8 ± 1.37 x 10^7	9.69 x 10^6 ± 1.88 x 10^6	8.80 x 10^7 ± 8.41 x 10^6	3.97 x 10^8 ± 1.66 x 10^7	2.28 x 10^7 ± 4.66 x 10^6	5.36 x 10^7 ± 4.51 x 10^6	2.94 x 10^8 ± 6.83 x 10^6
30	1.51 x 10^7 ± 3.07 x 10^6	8.94 x 10^7 ± 7.81 x 10^6	7.93 x 10^7 ± 1.00 x 10^7	8.61 x 10^6 ± 1.78 x 10^6	7.58 x 10^7 ± 7.92 x 10^6	3.29 x 10^8 ± 1.58 x 10^7	2.17 x 10^7 ± 4.18 x 10^6	4.57 x 10^7 ± 2.22 x 10^6	2.66 x 10^8 ± 6.42 x 10^6
32	1.38 x 10^7 ± 2.91 x 10^6	7.51 x 10^7 ± 7.22 x 10^6	6.01 x 10^7 ± 8.72 x 10^6	7.65 x 10^6 ± 1.66 x 10^6	6.37 x 10^7 ± 7.51 x 10^6	2.71 x 10^8 ± 1.48 x 10^7	1.93 x 10^7 ± 3.78 x 10^6	3.97 x 10^7 ± 1.49 x 10^6	2.38 x 10^8 ± 6.32 x 10^6
34	1.27 x 10^7 ± 2.80 x 10^6	6.26 x 10^7 ± 6.60 x 10^6	4.74 x 10^7 ± 6.70 x 10^6	6.81 x 10^6 ± 1.59 x 10^6	5.39 x 10^7 ± 6.36 x 10^6	2.23 x 10^8 ± 1.59 x 10^7	1.72 x 10^7 ± 3.34 x 10^6	3.32 x 10^7 ± 2.04 x 10^6	2.12 x 10^8 ± 5.97 x 10^6
36	1.18 x 10^7 ± 2.73 x 10^6	5.31 x 10^7 ± 5.75 x 10^6	3.64 x 10^7 ± 5.27 x 10^6	6.00 x 10^6 ± 1.48 x 10^6	4.91 x 10^7 ± 5.48 x 10^6	1.80 x 10^8 ± 1.64 x 10^7	1.54 x 10^7 ± 3.24 x 10^6	2.66 x 10^7 ± 1.69 x 10^6	1.87 x 10^8 ± 5.78 x 10^6
38	1.11 x 10^7 ± 2.67 x 10^6	4.79 x 10^7 ± 4.57 x 10^6	3.23 x 10^7 ± 5.03 x 10^6	5.34 x 10^6 ± 1.38 x 10^6	4.55 x 10^7 ± 4.94 x 10^6	1.46 x 10^8 ± 1.66 x 10^7	1.40 x 10^7 ± 3.66 x 10^6	2.12 x 10^7 ± 1.38 x 10^6	1.64 x 10^8 ± 5.67 x 10^6
40	**1.04 x 10^7 ± 2.62 x 10^6**	4.27 x 10^7 ± 4.04 x 10^6	2.67 x 10^7 ± 4.43 x 10^6	4.69 x 10^6 ± 1.25 x 10^6	3.86 x 10^7 ± 4.39 x 10^6	1.23 x 10^8 ± 1.32 x 10^7	1.32 x 10^7 ± 3.41 x 10^6	1.68 x 10^7 ± 1.19 x 10^6	1.41 x 10^8 ± 5.71 x 10^6
42	9.86 x 10^6 ± 2.54 x 10^6	3.74 x 10^7 ± 3.61 x 10^6	2.12 x 10^7 ± 3.67 x 10^6	4.08 x 10^6 ± 1.15 x 10^6	3.21 x 10^7 ± 3.75 x 10^6	1.01 x 10^8 ± 1.24 x 10^7	1.28 x 10^7 ± 3.16 x 10^6	1.31 x 10^7 ± 1.08 x 10^6	1.18 x 10^8 ± 5.50 x 10^6
44	9.40 x 10^6 ± 2.48 x 10^6	3.17 x 10^7 ± 3.10 x 10^6	1.67 x 10^7 ± 2.99 x 10^6	3.53 x 10^6 ± 1.04 x 10^6	2.80 x 10^7 ± 3.62 x 10^6	8.52 x 10^7 ± 1.03 x 10^7	1.15 x 10^7 ± 3.02 x 10^6	1.01 x 10^7 ± 9.63 x 10^5	9.53 x 10^7 ± 5.18 x 10^6
46	9.01 x 10^6 ± 2.45 x 10^6	2.79 x 10^7 ± 2.98 x 10^6	1.33 x 10^7 ± 2.43 x 10^6	3.05 x 10^6 ± 9.44 x 10^5	2.47 x 10^7 ± 3.80 x 10^6	6.95 x 10^7 ± 9.11 x 10^6	**1.03 x 10^7 ± 2.81 x 10^6**	7.80 x 10^6 ± 8.79 x 10^5	7.44 x 10^7 ± 3.95 x 10^6
48	8.60 x 10^6 ± 2.39 x 10^6	2.47 x 10^7 ± 3.21 x 10^6	1.03 x 10^7 ± 1.97 x 10^6	2.54 x 10^6 ± 8.48 x 10^5	2.08 x 10^7 ± 3.44 x 10^6	5.55 x 10^7 ± 7.79 x 10^6	9.27 x 10^6 ± 2.63 x 10^6	5.98 x 10^6 ± 7.65 x 10^5	5.44 x 10^7 ± 2.69 x 10^6
50	8.25 x 10^6 ± 2.36 x 10^6	2.13 x 10^7 ± 2.95 x 10^6	8.18 x 10^6 ± 1.65 x 10^6	2.15 x 10^6 ± 7.91 x 10^5	1.74 x 10^7 ± 3.05 x 10^6	4.72 x 10^7 ± 6.65 x 10^6	8.37 x 10^6 ± 2.38 x 10^6	4.66 x 10^6 ± 6.92 x 10^5	4.53 x 10^7 ± 2.19 x 10^6

Chapter 6. Economic Viability of the Implementation of Microbubble Technology at the Full Scale

The overall aim of this research was to understand the potential benefit of switching from a conventional bubble delivery system for ozone treatment to one using a microbubble generator. Throughout the thesis, it has been evidenced that smaller bubbles enhance performance, predominantly through a function of a significantly greater surface area to volume ratio which provides a greater extent of ozone delivery for a given ozone input. Specific findings from the research are:

1. The performance enhancement observed when comparing microbubble systems to conventional bubble systems, both within this work and elsewhere, is due to the increased specific surface area delivered by the smaller bubbles. This enables faster mass transfer and therefore higher dissolved ozone concentrations when using a fixed input dose.
2. No difference in performance is observed between microbubble systems and conventional bubble systems when normalised for effective ozone dose.
3. Microbubbles do not produce proportionally more hydroxyl radicals than conventional bubble systems beyond those produced as a result of the higher dissolved ozone concentration when comparing fixed input doses.
4. The regenerative turbine microbubble generator produced both microbubble and nanobubbles, whose size distributions were between 1 and 2 orders of magnitude apart.
5. The nanobubble fraction remains stable in the water but does not provide a significant contribution towards treatment.

The following is a discussion on the appropriateness of the application of microbubbles to ozonation for drinking water treatment.

6.1. What is the Economic Basis for Using Microbubble Systems Over Conventional Bubble Systems?

6.1.1 Introduction

Gas-liquid contacting processes are some of the most expensive and energy intensive operations in water treatment and account for a significant proportion of the total operating cost of a water treatment works (Pabi et al., 2013). In an ozone (O_3) based WTWs, around 15 % of the total non-pumping energy requirement can be attributed to the generation of ozone (Santana et al., 2014). The instability of ozone gas means that it cannot be stored and must be generated on-site which makes the operational cost of the ozonation process significant as the generation of ozone gas is an intensive process with an energy demand of ~ 3.3 – 16 kWh kg^{-1} O_3 (Jodzis and Zięba, 2018; Magara et al., 1995). In addition to the cost associated with the generation of ozone, the dissolution of ozone into the aqueous phase is particularly problematic due to its low solubility, low rate of mass transfer (Quan et al., 2017) and the output gas from oxygen-fed ozone generators rarely exceeds 10 % ozone (Li et al., 2019; Vezzù et al., 2019; Kotlarz et al., 2018). Ozone is typically delivered into the liquid through fine pore diffuser plates which produce conventional bubbles with a diameter in the range of 2 – 6 mm (Terashima et al., 2016; Baquero-Rodríguez et al., 2018; Behnisch et al., 2018; Garrido-Baserba et al., 2018). Bubbles of this size rise very quickly through the liquid and burst at the surface so industrial ozone contactors require liquid depths of 4 – 7 m to increase the residence time of the bubbles in the water so as much of the gaseous ozone is dissolved as possible to minimise losses through off-gas (Supplementary Information [SI] Table 6 – S1).

The research findings within this thesis have demonstrated that microbubbles deliver an enhancement in mass transfer compared with conventional bubble systems through an increase in specific surface area. This enables near complete transfer of ozone delivered to the tank and hence has the potential to reduce the operational costs associated with ozone delivery. Further, microbubbles have the potential to reduce operational costs by reducing the need for off-gas destruction (Chu et al., 2008) by increasing gas utilisation efficiency (Zhang et al., 2018) which may also facilitate significant reductions in contact tank height. Finally, the improved mass transfer offers the potential for process intensification through the easy delivery of higher dissolved ozone doses; although these

would exhibit the same risks concerning bromate formation that a traditional system would experience (Chapter 4).

To explore the potential economic benefits, a series of business case scenarios assessing the viability of microbubble generation is explored for the case of a 1 megalitre per day (MLD) WTWs that contains 10 μg L^{-1} mecoprop as the target pollutant. The economic assessment is based on the operating costs and the purchase price for the microbubble generator and excludes all infrastructure costs and difference in cost if a new ozone plant was required. In all cases, ozone is assumed to be supplied from a pre-existing ozone generator using pure oxygen supplied in bulk. Pure oxygen was selected as the feed gas due to the shift in preference from air-fed systems to oxygen-fed systems (Loeb, 2018).

Scenario A is the benchmark case of a conventional bubble contactor system using a diffuser plate that generates bubbles with diameters between 2 – 6 mm. *Scenario A* comprises of a water inlet leading to 2 dosing chambers in which ozone gas is injected. Following this, the ozonated water flows through 6 reaction chambers in which the dissolved ozone reacts with contaminants and self-decomposes simultaneously. The reaction chambers are sized such that the ozone reacts and decomposes to a concentration of 0.1 mg L^{-1} or less. *Scenario B* utilises a microbubble generator that generates bubbles in the 1 – 100 μm range, as a direct retrofit into the existing tank. *Scenario B* uses the same design as *Scenario A*, however the microbubble generator is fit in-line with the water flow. The ozone gas is injected directly into the microbubble generator to facilitate gas-liquid mixing. In this case, all of the chambers are used as reaction chambers as there is no need for separate dosing chambers. *Scenario C* considers that ozone is pre-dissolved into a shallow depth side stream reactor and then mixed into the main reactor. The differences between *Scenarios B and C* are the water depth the generator has to pump against and the flow through the microbubble generator. In the case of *Scenario C*, advantage is taken of the very high transfer efficiency observed for microbubbles, enabling complete ozone transfer in a shallow depth and only processing 15 % of the flow. Whereas in *Scenario B*, the pump works against the deeper water depth and processes 100 % of the flow. As with *Scenario B*, all 8 chambers are used as reaction chambers as the ozone is dosed directly into the microbubble generator which feeds the side stream. In chamber 1, the main flow and the side stream flow are combined and the

high ozone dose is distributed throughout the bulk liquid. The water flows through the reaction chambers in which the ozone reacts with contaminants and self-decomposes such that the concentration at the outlet is less than 0.1 mg L^{-1}.

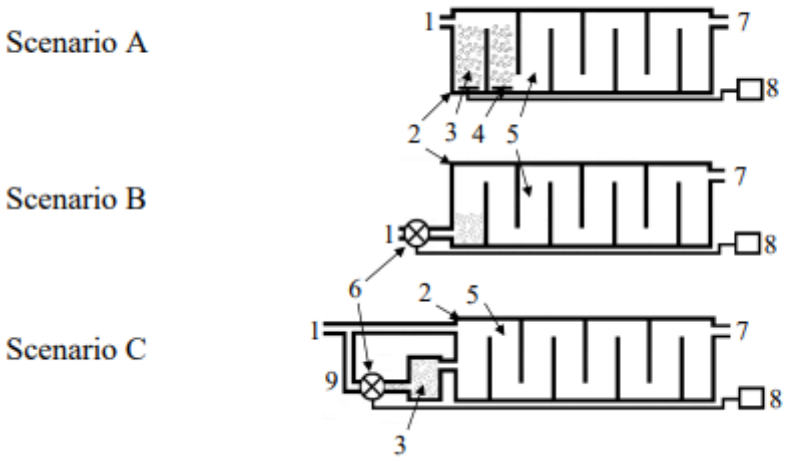

Figure 6 – 1. Business case scenarios with conventional bubble contactor (Scenario A, top), microbubble retrofit (Scenario B, middle) and microbubble side stream (Scenario C, bottom). Where (1) inlet, (2) contactor, (3) dosing chamber, (4) fine pore diffuser, (5) reaction chamber, (6) microbubble generator, (7) outlet, (8) ozone generator, (9) diverted flow.

6.1.2. Design Parameters

The main design philosophy is to simultaneously meet several requirements:

- The ozone exposure across the contactors must be sufficient to facilitate compliance to UK regulations for pesticides in drinking water, which is set at 0.1 μg L^{-1} and hence requires a removal efficiency of 99 %.
- The hydraulic retention time must be long enough to ensure < 0.1 mg L^{-1} ozone residual at the outlet of the contactor.

In addition to these requirements, when ozone is delivered into the aqueous phase, reactions with contaminants can proceed through both a direct reaction with molecular O_3 and indirect reactions with hydroxyl radicals produced from ozone self-

decomposition. The rate constant for ozone self-decomposition was taken from the experimental data obtained in Chapter 4 based on an incoming water pH of 8, with a value of 0.015 min^{-1}.

The ozone dose applied is made up of that required to treat mecroprop and that associated with the other background contaminants in the water. The ozone demand exerted by the non-target contaminants is often referred to as the instantaneous ozone demand and is assigned a value of 1 mg L^{-1} based on previous studies (Jeon et al., 2011; Tang et al., 2005; Roustan et al., 1998). The instantaneous ozone demand is assumed to occur in different parts of the reactor for the different scenarios due to the point at which the ozone is dissolved:

In *scenario A* (conventional bubble system), it is assumed that instantaneous ozone demand occurs within dosing chambers 1 and 2 (marked as 3 on Figure 6 – 1) and the ozone residual at the outlet of dosing chamber 2 is equal to Equation 6 – 1 as the system is assumed to be operating at a steady state. In addition, it is assumed that ozone exposure begins at the inlet of reaction chamber 1 (marked as 8 on Figure 6 – 1) and the system has a gas utilisation efficiency of 50 %.

In *scenario B* (retrofit), the instantaneous ozone demand occurs at the point of gas-liquid mixing in the microbubble generator and is assumed to operate at a steady state such that the ozone residual at the outlet of the microbubble generator is equal to Equation 6 – 1. It is also assumed that ozone exposure begins at this point and the gas utilisation efficiency of the system is 99 %.

In *scenario C* (side stream), 15 % of the total flow is diverted through a side stream reactor vessel to take advantage of the efficient transfer afforded by microbubbles. As such, 15 % of the flow is dosed with a high level of ozone which is sufficient to treat the full flow after mixing with the bulk flow and is assumed to operate at a steady state. 15 % of the instantaneous ozone demand occurs within the side stream reactor as it processes 15 % of the flow. The remaining 85 % of the instantaneous ozone demand occurs upon the mixture of the ozonated water with the bulk flow. All of the required ozone is delivered into the side stream reactor vessel and the ozone exposure across the contactor is sufficient for the required level of treatment. The gas utilisation efficiency of the ozone delivery into the side stream reactor vessel is assumed to be 99 %.

$$ID_{O_3} = C_{eff} - C$$ Equation 6 – 1

Where ID_{O_3} is the instantaneous ozone demand (mg L^{-1}), C_{eff} is the effective ozone dose (mg L^{-1}) and C is dissolved ozone concentration (mg L^{-1}).

6.1.2.1. Conventional Bubble Contactor (*Scenario A*)

The conventional bubble contactor is based on a typical ozone contactor using fine pore diffusers that generate bubbles with a diameter of 2 – 6 mm. The conventional bubble contactor was designed with two dosing chambers and six reaction chambers. The ozone dosing and contactor dimensions were calculated from an instantaneous ozone demand of 1 mg L^{-1}, a required ozone exposure of 6.4 mg L^{-1} min for 99 % mecoprop removal and an incoming flow rate of 694 L min^{-1}. The required ozone exposure was based on lab scale mecoprop removal experiments (Chapter 4).

The contactor dimensions were based on an assumed contactor depth of 7 m and a length to width ratio of 4:1 based on previous studies ([SI] Table 6 – S1). The required contactor volume was calculated based on the liquid flow rate and hydraulic retention time:

$$V_C = \tau . Q_L$$ Equation 6 – 2

Where V_C is total contactor volume (m^3), τ is the hydraulic retention time (min^{-1}) and Q_L is liquid flow rate (m^3 min^{-1}). The required hydraulic retention time was based on the time required for the dissolved ozone to self-decompose to <0.1 mg L^{-1}. This was found through the following:

$$\ln[C]_t = \ln [C]_0 - k_D . \tau$$ Equation 6 – 3

Where $[C]_0$ is the initial dissolved ozone concentration (mg L^{-1}), $[C]_t$ is the dissolved ozone concentration at time t (mg L^{-1}) and k_D is the rate constant for ozone self-decomposition (min^{-1}). Using these equations, the initial dissolved ozone concentration was varied until the ozone exposure requirement and outlet residual requirement were

met (Figure 6 – 2) (Table 6 – 2). The ozone generation requirement was based on the effective ozone dose required to meet the instantaneous ozone demand and required ozone exposure after accounting for gas utilisation efficiency:

$$C_{in} = \frac{C_{eff}}{\varphi} \qquad \text{Equation 6 – 4}$$

Where C_{in} is input ozone concentration (mg L^{-1}), C_{eff} is effective ozone dose (mg L^{-1}) and φ is the fractional gas utilisation efficiency. The ozone generation requirement was calculated by:

$$O_3\ generation\ requirement\ = C_{in}Q_L \qquad \text{Equation 6 – 5}$$

Table 6 – 1. Design parameters for the conventional bubble contactor.

Parameter	Value	Unit	Notes
Inflow	694	L min^{-1}	Assumed
Contactor volume	47.25	m^3	Calculated
Contactor height	7.0	m	Assumed
Contactor hydraulic retention time	56	min	Calculated
Gas utilisation efficiency	50	%	Assumed
Input ozone dose required	2.4	mg L^{-1}	Calculated
Ozone gas production	100	g h^{-1}	Calculated
Effective ozone dose	1.2	mg L^{-1}	Calculated
Instantaneous ozone residual	0.2	mg L^{-1}	Assumed
Actual ozone exposure	7.2	mg L^{-1} min	Calculated

6.1.2.2. Retrofit Microbubble Contactor (*Scenario B*)

The microbubble retrofit contactor is designed as a replacement for an existing conventional bubble contactor using a microbubble generator in place of fine pore diffusers. The selected microbubble generator is based on the regenerative turbine-type generator used in the work within this thesis. These types of microbubble generator deliver the gas directly into the liquid flow so the ozone is incorporated directly into the liquid without the need for dosing chambers. Since this is designed as a direct

replacement, the microbubble generator was sized to accommodate the full liquid flow and the contactor acts as eight reaction chambers rather than requiring dosing chambers. Due to the increased gas utilisation efficiency, the required ozone generation is significantly reduced from 100 g h^{-1} with the conventional bubble system to 50 g h^{-1} with the microbubble retrofit system (Figure 6 – 2) (Table 6 – 2).

Table 6 – 2. Design parameters for retrofit microbubble contactor.

Parameter	Value	Unit	Notes
Inflow	694	L min^{-1}	Assumed
Contactor volume	47.25	m^3	Calculated
Contactor height	7.0	m	Assumed
Contactor hydraulic retention time	56	min	Calculated
Gas utilisation efficiency	99	%	Assumed
Input ozone dose required	1.2	mg L^{-1}	Calculated
Ozone gas production	50	g h^{-1}	Calculated
Effective ozone dose	1.2	mg L^{-1}	Calculated
Instantaneous ozone residual	0.2	mg L^{-1}	Assumed
Actual ozone exposure	7.3	mg L^{-1} min	Calculated

6.1.2.3. Side Stream Microbubble Contactor (*Scenario C)*

The microbubble side stream contactor is designed as a potential retrofit option or as a new build option. For the microbubble side stream contactor, 15 % of the total liquid flow is diverted to a secondary reactor in which it is dosed with a high concentration of ozone and blended with the bulk liquid. The purpose of this design is to take advantage of the high gas utilisation efficiency offered by microbubbles. It also serves to reduce the required size of the microbubble generator as regenerative turbine pumps have a high power requirement and hence reducing the size of the microbubble generator is desirable to reduce power consumption. Assuming 99 % gas utilisation efficiency, ozone can be generated at a rate of 50 g h^{-1} to provide an ozone exposure of 7.3 mg L^{-1} min across the contactor over a period of 56 minutes which is sufficient to facilitate 99 % removal of the target compound. The microbubble side stream option still requires a similar HRT to the conventional bubble contactor since, despite efficient application of ozone, the ozone

must self-decompose to a residual of less than 0.1 mg L^{-1} at the outlet of the contactor (Figure 6 – 2) (Table 6 – 3).

Table 6 – 3. Design parameters for side stream microbubble contactor.

Parameter	**Value**	**Unit**	**Notes**
Inflow	694	L min^{-1}	Assumed
Contactor volume	47.25	m^3	Calculated
Contactor height	7	m	Calculated
Contactor width	1.5	m	Calculated
Contactor hydraulic retention time	56	min	Calculated
Gas utilisation efficiency	99	%	Assumed
Input ozone dose required	4.5	mg L^{-1}	Calculated
Ozone gas production	45	g h^{-1}	Calculated
Effective ozone dose	4.5	mg L^{-1}	Calculated
Instantaneous ozone residual	3.5	mg L^{-1}	Assumed
Actual ozone exposure	7.3	mg L^{-1} min	Calculated

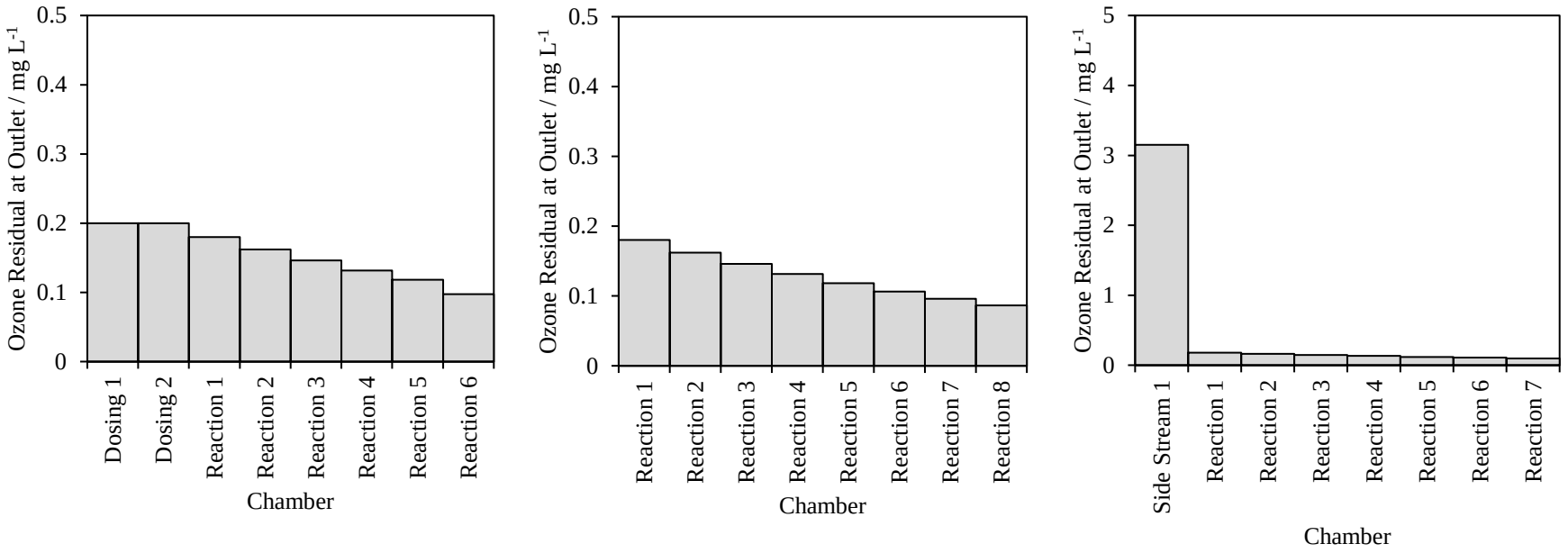

Figure 6 – 2. Ozone residual profile at the outlet of each chamber for the conventional bubble contactor (left), microbubble retrofit contactor (middle) and microbubble side stream contactor (right).

6.1.3. Operational Cost Estimate

The largest cost associated with the conventional bubble contactor is the cost of oxygen. In order to achieve the 100 g h^{-1} ozone production, an oxygen flow rate of 18 L min^{-1} is required from a 1.6 kW ozone generator with an ozone output concentration of ~ 6 % for a yearly oxygen requirement of 9,600 m^3 yr^{-1}. This equates to a cost of £28,000 yr^{-1}. Due to the significantly higher gas utilisation efficiency of the microbubble generators, the ozone production requirements of 50 and 45 g h^{-1} for the retrofit and side stream contactors, respectively, can be met with much lower oxygen flow rates. In addition, ozone generators produce a more concentrated ozone output at lower flow rates so ozone output concentrations of ~ 9 and ~ 10 % are possible from a 1.6 kW ozone generator for the retrofit and side stream contactors, respectively. The 50 g h^{-1} ozone demand of the retrofit contactor can be met with an oxygen flow rate of 8 L min^{-1} for a yearly oxygen requirement of 3,300 m^3 yr^{-1}. The 45 g h^{-1} ozone production requirement of the side stream contactor can be met with an oxygen flow rate of 6 L min^{-1} for a yearly oxygen requirement of 2,600 m^3 yr^{-1}. Based on the bulk price of oxygen of £2.91 m^{-3} (Table 6 – 4), these equate to yearly costs of £9,600 yr^{-1} and £7,400 yr^{-1} respectively which represents an oxygen cost reduction of 65 % for the microbubble retrofit contactor and an oxygen cost reduction of 74 % for the microbubble side stream contactor when compared to the cost for the conventional bubble system of £28,000.

Table 6 – 4. Major operational costs associated with ozone contactors.

Parameter	Value	Unit	Notes	Reference
Electricity	0.172	£ kWh^{-1}	Average weekly wholesale cost 2022	Wholesale market indicators (2022)
Oxygen	2.91	£ m^{-3}	Bulk purchase price	BOC limited (2022)

For the microbubble systems, electricity contributes significantly more to the total operational cost than for the conventional bubble contactors (Figure 6 – 3). For the conventional system, the only major contributor to electricity cost is the ozone generator with a power consumption of 1.6 kW which runs 24 hours per day to generate a yearly total of 14,016 kWh. At the current wholesale cost of £0.172 kWh^{-1} (Table 6 – 4), this

represents a yearly electricity cost of £2,400 yr^{-1}. The power consumption of the microbubble generator increases as their capacity increases. To illustrate, the microbubble generator for the side stream contactor is rated at 5.5 kW which a liquid flow capacity of 133 L min^{-1}. In contrast, the microbubble generator for the retrofit contactor is rated at 22 kW for a liquid flow capacity of 700 L min^{-1}. Continuous operation of these microbubble generators equates to a yearly power consumption of 48,000 kWh yr^{-1} for the side stream contactor and 193,000 kWh yr^{-1} for the retrofit contactor. The electricity cost associated with microbubble generators is therefore £8,300 yr^{-1} for the side stream generator and £33,000 yr^{-1} for the retrofit generator. Including the cost of ozone generation, the total electricity cost is £10,700 yr^{-1} for the side stream contactor and £35,400 yr^{-1} for the retrofit contactor and this compares to £2,400 yr^{-1} for the conventional system. Overall, the total operating costs of the three scenarios is £30,400 for the conventional system (Scenario A), £45,000 for the direct retrofit system (Scenario B) and £18,100 for the side stream system (Scenario C). This means that the utilisation of a side stream setup has the potential to reduce operating costs by £12,300 per year.

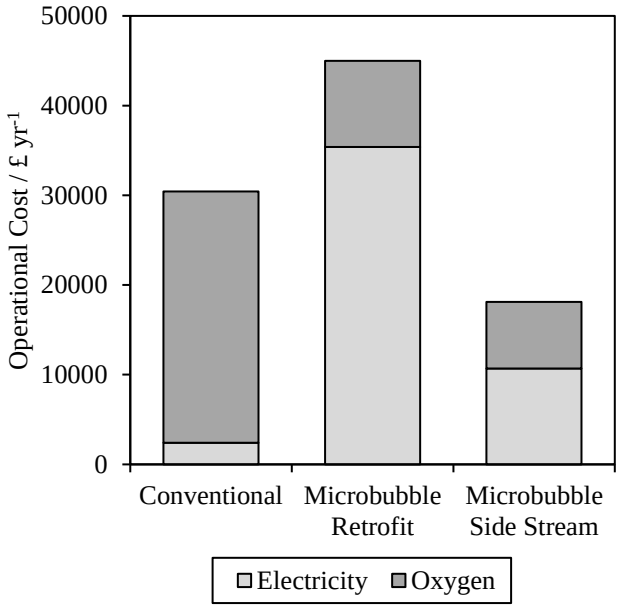

Figure 6 – 3. Contribution of the cost of electricity and oxygen to the operational cost for the conventional bubble contactor, microbubble retrofit contactor and microbubble side stream contactor.

6.1.4. Sensitivity Analysis

One of the major uncertainties in the viability of microbubble generators in the current climate is the wholesale cost of electricity which rose to unprecedented levels in December 2021 with a forward delivery cost of £262.52 MWh^{-1}. This represented a 6.5-fold increase from £39.94 MWh^{-1} since December 2020 and the future cost of wholesale electricity remains uncertain (Figure 6 – 4). To understand the significance of wholesale electricity cost on the overall operational cost of microbubble generation, a sensitivity analysis was conducted with respect to wholesale electricity cost on overall operational cost (Figure 6 – 5). The electricity costs required for the conventional system to be more economically viable than the microbubble retrofit contactor was £0.12 kWh^{-1} and for the side stream option £0.52 kWh^{-1}, which is two times higher than the all-time high seen in December 2021.

The other main component, pure oxygen, is also subject to price change with an increase improving the economic comparison of microbubble systems compared to conventional systems. The data associated with the changing cost of bulk oxygen supply is less clear. Available data on the US producer price index suggests that its cost has doubled over the last 20 years (US Producer Price Index: Industrial Gas Manufacturing: Oxygen, 2022). Assuming the electricity price stayed constant, the retrofit option (*Scenario B*) would be cost equivalent to the conventional approach (*Scenario A*) if the pure oxygen price became 180 % of its current value. Ultimately, the balance is based on the relative change in the price of the two commodities as to the relative attractiveness of using a microbubble generator system. The overall balance is also impacted by local generation of either electricity through renewables or oxygen as a by-product from hydrogen production using electrolysis. However, the side stream microbubble configuration appears economically robust to such issues and will offer potential saving over current approaches.

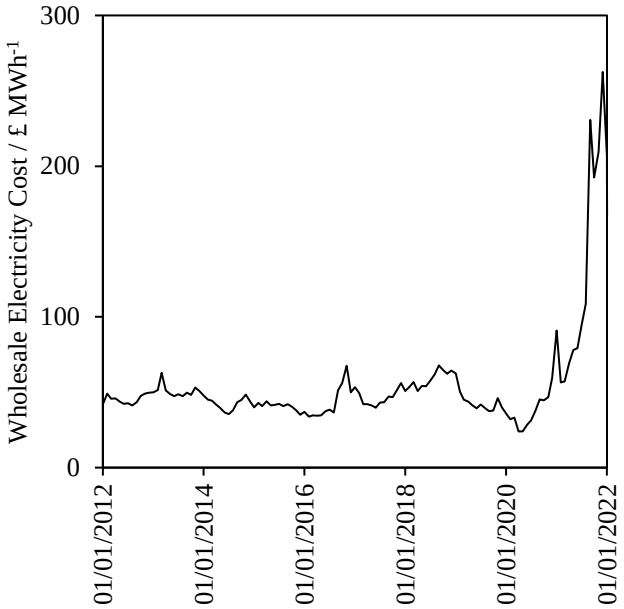

Figure 6 – 4. Historical wholesale cost of electricity for the past ten years (Data retrieved from https://www.ofgem.gov.uk/energy-data-and-research/data-portal/wholesale-market-indicators).

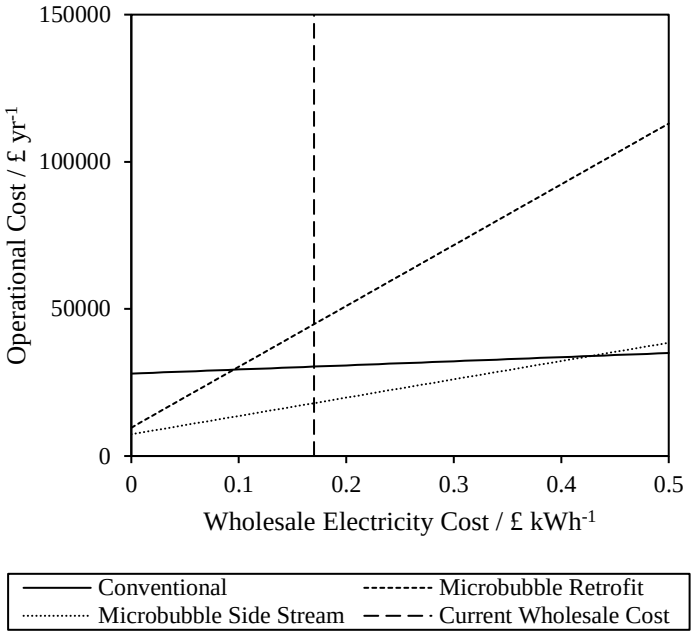

Figure 6 – 5. Operational cost (£ yr^{-1}) against wholesale electricity cost (£ kWh^{-1}) for the conventional bubble contactor, microbubble retrofit and microbubble side stream options.

6.1.5 Capital Cost and Payback Period Estimate

One of the main uncertainties around the implementation of microbubble generators to ozonation is their capital cost as there is currently a limited industrial supply chain. A preliminary quote for the supply of the required microbubble generators was obtained (Rotary Trading Company B.V., 2022) but should be viewed as an approximate value with a high degree of uncertainty. The quoted capital cost for the retrofit option (*Scenario B*) was £16,744 for the retrofit option of which £14,821 was for the generator and £1,923 for the associated baseplate. In the case of the side stream option (*Scenario* C), the cost was £6,200, which was £5,840 for the generator and £360 for the associated baseplate. Based on the operational saving, the investment in the generator would have a payback period of 6 months for *Scenario C* (Table 6 – 5). *Scenario B* would not pay back as the operational cost is greater for the microbubble system compared to the conventional. This system would only become economically beneficial if the electricity demand could be met internally through renewable generation. In such cases, there is a £18,400 yr^{-1} saving in oxygen supply by using the retrofit option which extends to £20,600 for the side stream

option which required additional infrastructure and hence becomes less attractive relative to the retrofit when electricity costs are not included.

Further savings are potentially possible in relation to cases where a new build is being constructed or the ozone plant is being replaced. In both cases the inclusion of a microbubble systems would reduce the scale of the ozone generation plant required. In addition, in the case of the side stream system (*Scenario C*), the ozone is pre-dissolved in the side stream reactor and then mixed with the rest of the flow. This removes the limitations of gas bubble-liquid reactor designs and enables more efficient reactor systems to be considered. Whilst the current work has not considered this it is suggested as an area for further consideration that could lead to even lower costs for new builds.

Table 6 – 5. Estimated payback period for microbubble generators.

Scenario	**Microbubble Generator Cost / £**	**Annual Operational Saving / £**	**Payback Period / months**
Microbubble side stream contactor	6,200	12,000	6
Microbubble retrofit contactor	16,744	- 12,200	n/a

6.2 What is the Optimum Bubble Size?

The work has shown that the use of smaller bubbles enables faster transfer such that near complete transfer occurs within short distances. This obviates the current need for deep tanks but also indicates that there is an optimum bubble size for any water depth which can be defined as delivering near 100 OTE. The theoretical time taken for a single bubble to dissolve can be estimated by (Xia and Hu, 2019; Shedd, 2005):

$$t_d = \frac{{R_0}^2}{2D_L k_H BT} \qquad \text{Equation 6 – 6}$$

Where R_0 is the initial radius of the bubble (m), D_L is the diffusion coefficient ($m^2\ s^{-1}$), k_H Henry's law constant (mol m^{-3} Pa^{-1}), B is the universal gas constant (J mol^{-1} K^{-1}) and

T is temperature (K). Measurement of microbubble size distributions throughout this experimental work (Chapters 3, 4, 5) found a Sauter mean diameters of 37 µm. The bubbles identified in this work, according to equation 6 – 6, would require ~ 232 seconds to deplete. Therefore, the water height required for 100 % bubble depletion can be calculated by:

$$h_L = t_d U_{\infty(S)} \qquad \text{Equation 6 – 7}$$

Where h_L is the liquid height (m), t_d is bubble depletion time (s) and $U_{\infty(S)}$ is the Stokes' terminal rise velocity of the bubble (m s^{-1}). Provided that the depletion time of the bubble is known, the optimal bubble size for a given reactor tank depth can be estimated and, if the depletion time is shorter than the residence time of the bubble in the contact tank, 100 % gas utilisation efficiency is theoretically achievable for any reactor since the contents of the bubble will be fully depleted before reaching the liquid surface. For all liquid depths up to 10 m, a relatively narrow range of bubble sizes are required for 100 % depletion. To illustrate, a reactor depth of 1 m requires a maximum bubble diameter of 56 µm whilst a 10 m depth requires a maximum bubble diameter of 99 µm (Figure 6 – 6). The conventional bubble sizes of 2 – 6 mm commonly found in fine-pore diffusers in conventional contactors are too large for optimal bubble depletion hence losses occur through off-gas. The challenges associated with optimising bubble size are that methods of bubble production, such as that used in this thesis, do not produce mono-sized uniform dispersions of bubbles. In addition, the flow arrangement and contactor depth will affect the optimum bubble size. For example, a counter-current contactor would be expected to be more efficient than a co-current contactor. Hence further work is required to understand how to achieve fine control of bubble diameter to produce monodispersed specific bubble sizes.

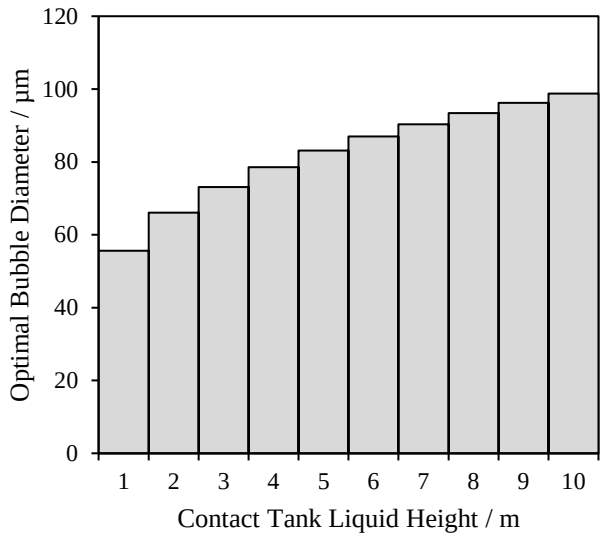

Figure 6 – 6. Optimal bubble diameters for 100 % depletion at liquid heights of 1 – 10 m.

The implications of this are that devices that can generate relatively narrow distributions around a mean bubble size of 30 – 40 µm range will generate the majority of the potential benefits (Table 6 – 6). It is likely that energy associated with generation will increase as bubble size decreases but will deliver no appreciable additional benefit. For instance, it may be difficult to downsize reaction chambers since after the ozone is delivered, it must have a high enough hydraulic retention time to self-decompose to a level of < 0.1 mg L^{-1} (Jeon et al., 2011), a factor which is heavily dependent on the incoming water characteristics.

Table 6 – 6. Potential scenarios in favour of the use of microbubble generators for ozonation.

Scenario	Benefit of Microbubbles
Source water has a high instantaneous O_3 demand	Microbubble generation can provide a significantly enhanced O_3 delivery for a given O_3 input dose.
Faster treatment required	The enhanced rate of mass transfer that microbubbles can achieve allows for a faster attainment of the required O_3 residual. The microbubble system can provide a higher effective O_3 dose for a given input O_3 dose compared with conventional bubble contactors.
Height limitations	Microbubbles can achieve 99 % gas utilisation with a limited water depth and have the potential for large reductions in required contactor depth.
Equivalent treatment to conventional bubble contactors	The use of microbubbles for ozonation allows for large reductions in oxygen requirement to achieve an equivalent level of treatment as a conventional bubble contactor.

6.3. References

Azuma, T., Otomo, K., Kunitou, M., Shimizu, M., Hosomaru, K., Mikata, S., Mino, Y. and Hayashi, T., 2019. Removal of pharmaceuticals in water by introduction of ozonated microbubbles. *Separation and Purification Technology*, 212, pp.483-489.

Baquero-Rodríguez, G., Lara-Borrero, J., Nolasco, D. and Rosso, D., 2018. A critical review of the factors affecting modeling oxygen transfer by fine-pore diffusers in activated sludge. *Water Environment Research*, 90(5), pp.431-441.

Behnisch, J., Ganzauge, A., Sander, S., Herrling, M. and Wagner, M., 2018. Improving aeration systems in saline water: measurement of local bubble size and volumetric mass transfer coefficient of conventional membrane diffusers. *Water Science and Technology*, 78(4), pp.860-867.

Boconline.co.uk. 2022. [online] Available at: <https://www.boconline.co.uk/en/images/Oxygen-factsheet_tcm410-54571.pdf> [Accessed 27 April 2022].

Broséus, R., Barbeau, B. and Bouchard, C., 2008. Verification of full-scale ozone contactor inactivation performance using biodosimetry. *Journal of Environmental Engineering*, 134(4), pp.304-315.

Chu, L., Yan, S., Xing, X., Yu, A., Sun, X., and Jurcik, B., 2008. Enhanced sludge solubilization by microbubble ozonation. *Chemosphere*, 72(2), pp.205-212.

Garrido-Baserba, M., Asvapathanagul, P., Park, H., Kim, T., Baquero-Rodriguez, G., Olson, B., and Rosso, D., 2018. Impact of fouling on the decline of aeration efficiency under different operational conditions at WRRFs. *Science of The Total Environment*, 639, pp.248-257.

International Organization for Standardization, 2017. *ISO/TC 281 - Fine bubble technology*. ISO. Retrieved 24 April 2022, from https://www.iso.org/committee/4856666.html.

Jeon, J., Jo, C., Kwon, S., Lee, K., Hwang, T. and Chung, Y., 2011. A case study on the automatic ozone dose control system based on the ozone decay rate in a full-scale advanced water treatment plant. *Desalination and Water Treatment*, 33(1-3), pp.337-350.

John, A., Brookes, A., Carra, I., Jefferson, B. and Jarvis, P., 2022. Microbubbles and their application to ozonation in water treatment: A critical review exploring their benefit and future application. *Critical Reviews in Environmental Science and Technology*, 52(9), pp.1561-1603.

Kim, D. and Cho, J., 2014. Obtaining real-time kinetic parameters on ozone decay from a full-scale ozone contactor using the axial dispersion reactor model. *Ozone: Science and Engineering*, 36(1), pp.100-109.

Kim, D., Lee, K., Lee, H., Kim, Y. and Hyun, I., 2015. The hydrodynamics of an ozone contactor with horizontal meandering flow to enhance disinfection efficiency. *Desalination and Water Treatment*, 54(4-5), pp.1150-1157.

Levitsky, I., Tavor, D. and Gitis, V., 2022. Micro and nanobubbles in water and wastewater treatment: A state-of-the-art review. *Journal of Water Process Engineering*, 47, p.102688.

Li, K., Xu, L., Zhang, Y., Cao, A., Wang, Y., Huang, H. and Wang, J., 2019. A novel electro-catalytic membrane contactor for improving the efficiency of ozone on wastewater treatment. *Applied Catalysis B: Environmental*, 249, pp.316-321.

Loeb, B., 2018. Forty years of advances in ozone technology. A review of Ozone: Science and Engineering. *Ozone: Science and Engineering*, 40(1), pp.3-20.

Loh, H.P et al. (2002), "Process equipment cost estimation final report". Available at: http://www.osti.gov/scitech/servlets/purl/797810/.

Jodzis, S. and Zięba, M., 2018. Energy efficiency of an ozone generation process in oxygen. Analysis of a pulsed DBD system. *Vacuum*, 155, pp.29-37.

Kotlarz, N., Rockey, N., Olson, T., Haig, S., Sanford, L., LiPuma, J. and Raskin, L., 2018. Biofilms in full-scale drinking water ozone contactors contribute viable bacteria to ozonated water. *Environmental Science and Technology*, 52(5), pp.2618-2628.

Magara, Y., Itoh, M. and Morioka, T., 1995. Application of ozone to water treatment and power consumption of ozone generating systems. *Progress in Nuclear Energy*, 29, pp.175-182.

Ofgem. 2022. *Wholesale market indicators*. [online] Available at: <https://www.ofgem.gov.uk/energy-data-and-research/data-portal/wholesale-market-indicators> [Accessed 27 April 2022].

Pabi, S., Amarnath, A., Goldstein, R., Reekie, L., 2013. Electricity use and management in the municipal water supply and wastewater industries. *Electric Power Research Institute*, 194, pp. 1-194.

Parmar, R., and Majumder, S., 2013. Microbubble generation and microbubble-aided transport process intensification—A state-of-the-art report. *Chemical Engineering and Processing: Process Intensification*, 64, pp.79-97.

Quan, X., Luo, D., Wu, J., Li, R., Cheng, W. and Ge, S., 2017. Ozonation of acid red 18 wastewater using O3/Ca(OH)2 system in a micro bubble gas-liquid reactor. *Journal of Environmental Chemical Engineering*, 5(1), pp.283-291.

Roustan, M., Debellefontaine, H., Do-Quang, Z. and Duguet, J., 1998. Development of a method for the determination of ozone demand of a water. *Ozone: Science and Engineering*, 20(6), pp.513-520.

Shedd, T., 2005. General model for estimating bubble dissolution and droplet evaporation times. *Journal of Micro/Nanolithography, MEMS, and MOEMS*, 4(3), p.033004.

Singh, B., Shukla, N., Cho, C., Kim, B., Park, M. and Kim, K., 2021. Effect and application of micro- and nanobubbles in water purification. *Toxicology and Environmental Health Sciences*, 13(1), pp.9-16.

Suwartha, N., Syamzida, D., Priadi, C., Moersidik, S. and Ali, F., 2020. Effect of size variation on microbubble mass transfer coefficient in flotation and aeration processes. *Heliyon*, 6(4), p.e03748.

Tang, G., Adu-Sarkodie, K., Kim, D., Kim, J., Teefy, S., Shukairy, H., and Mariñas, B., 2005. Modeling Cryptosporidium parvum oocyst Inactivation and bromate formation in a full-scale ozone contactor. *Environmental Science and Technology*, 39(23), pp.9343-9350.

Terashima, M., So, M., Goel, R., and Yasui, H., 2016. Determination of diffuser bubble size in computational fluid dynamics models to predict oxygen transfer in spiral roll aeration tanks. *Journal of Water Process Engineering*, 12, pp.120-126.

Vezzù, G., Lopez, J., Freilich, A. and Becker, K., 2009. Optimization of large-scale ozone generators. *IEEE Transactions on Plasma Science*, 37(6), pp.890-896.

Xia, Z. and Hu, L., 2019. Theoretical model for micro-nano-bubbles mass transfer during contaminant treatment. *Journal of Environmental Engineering and Science*, 14(3), pp.157-167.

Ycharts.com. 2022. *US Producer Price Index: Industrial Gas Manufacturing: Oxygen*. [online] Available at: <https://ycharts.com/indicators/us_producer_price_index_industrial_gas_manufacturing_oxygen_yearly> [Accessed 28 April 2022].

Zhang, J., Huang, G., Liu, C., Zhang, R., Chen, X., and Zhang, L., 2018. Synergistic effect of microbubbles and activated carbon on the ozonation treatment of synthetic dyeing wastewater. *Separation and Purification Technology*, 201, pp.10-18.

Zhang, J., Huck, P., Stubley, G. and Anderson, W., 2011. A comparison of the Eulerian and particle tracking approaches for prediction of ozone contactor performance. *Journal of Water Supply: Research and Technology-Aqua*, 60(4), pp.197-209.

Zhang, J., Tejada-Martinez, A., Lei, H. and Zhang, Q., 2016. Indicators for technological, environmental and economic sustainability of ozone contactors. *Water Research*, 101, pp.606-616.

Zhang, J., Tejada-Martínez, A., Zhang, Q. and Lei, H., 2014. Evaluating hydraulic and disinfection efficiencies of a full-scale ozone contactor using a RANS-based modeling framework. *Water Research*, 52, pp.155-167.

6.4. Supplementary Information

[SI] Table 6 – S1. Full scale ozone contactor dimensions.

Flow Rate / $m^3\ d^{-1}$	Dosing Chambers / #	Reaction Chambers / #	Contactor Length / m	Contactor Width / m	Contactor Height / m	Number of Contactors	Footprint / m^2	Volume / m^3	Reference
209,000	2	6	51.7	12.2	7.32	1	631	4617	Zhang et al. (2016)
210,000	1	7	17.8	16.8	6.0	1	299	1794	Kim et al. (2015)
209,000	2	6	51.7	12.2	7.32	1	631	4617	Zhang et al. (2014)
350,000	1	7	17.8	17.6	6.0	1	313	1880	Kim and Cho (2014)
1,200,000	1	1	23.8	5.5	7.16	6	785	5623	Zhang et al. (2011)
350,000	1	6	18.2	18.0	6.0	2	655	3931	Jeon et al. (2011)
1,136	1	1	20.2	5.5	6.5	6	667	4332	Broséus et al. (2008)
31,000	2	3	15.25	4.5	6.77	1	68	464	Tang et al. (2005)

Chapter 7. Implications for the Application of Microbubbles to Ozonation for Drinking Water Treatment

The aim of this research was to understand the mechanism by which microbubbles enhance the performance of ozonation and to assess the viability of the application of microbubbles to ozonation for drinking water treatment. The key observations from this research were:

- The use of microbubble systems for ozonation have been demonstrated to enhance several parameters relating to ozonation performance compared with conventional bubble ozonation. This includes an increase in the rate of mass transfer and an increase in the observed steady state concentration (Chapters 2 and 4).
- The enhanced ozone delivery afforded by microbubbles has been shown to increase the speed and extent of removal of a variety of different pollutants present in untreated water. This includes pesticides, herbicides, pharmaceuticals, dyestuff and a wide range of other micropollutants (Chapters 2 and 4).
- The mechanism by which microbubbles enhance ozonation performance has been shown to be unrelated to an increase in hydroxyl radical production. The production of hydroxyl radicals from the self-decomposition of ozone is an important component in the removal of contaminants as hydroxyl radicals are generated as part of the self-decomposition reaction chain. However, no evidence was found to suggest that microbubbles produce proportionally more hydroxyl radicals than conventional bubbles under typical operational pH's (Chapters 2, 3 and 4).
- Microbubble performance enhancement is predominantly driven by an enhancement in the volumetric mass transfer coefficient caused by a reduction in the mass transfer coefficient and an increase in the specific interfacial surface area compared with conventional bubbles (Chapter 4).
- Comparisons between microbubble and conventional bubble performance are typically performed in short columns at lab scale. The use of short columns and

shallow water depths may positively bias results in favour of the microbubble system, especially when experiments are normalised against ozone input dose (Chapters 2, 3 and 4).

- Direct-comparison experiments using part-treated pre-ozone water demonstrated that the extent of bromate formation resulting from microbubble ozonation was found to be equivalent to that of conventional bubble ozonation when the comparison was normalised for effective ozone dose (Chapter 4).
- Experimental work revealed that the presence of nanobubbles resulting from microbubble generation is unlikely to represent a significant contributor to the efficiency and effectiveness of ozonation. It was concluded that the majority of the ozonation performance is delivered through the microbubble fraction. The stability and longevity of the nanobubble fraction was demonstrated, however it was found that the volume of gas entrained within the nanobubble fraction was insignificant such that any risk associated with sending residual downstream is negligible (Chapter 5).
- Based on operational cost estimates, the use of microbubbles generators at full scale has potential economic viability. Due to the high electricity requirement of microbubble-based ozone contactors compared with conventional contactors, it was determined that a side-stream design was most appropriate to take advantage of the high gas utilisation efficiency of microbubbles at shallow water depths. This allowed for equivalent treatment with a smaller microbubble generator due to less oxygen being lost as off-gas. In this scenario, a sensitivity analysis revealed that a side-stream microbubble generator system can allow for a lower operational cost compared with conventional contactors provided that the wholesale electricity cost is lower than 0.44 £ kWh^{-1} (Chapter 6).

Chapter 8. Conclusions and Future Work

8.1. Conclusions

This research has demonstrated the performance enhancement that microbubbles can provide when applied to ozonation in comparison to conventional bubbles and demonstrates the viability microbubbles in drinking water treatment. The following conclusions in relation to the original objectives are:

Objective 1. To produce a state-of-the-art critical review assessing the current state of microbubble technology for application in ozonation.

- Using microbubbles as a delivery system for use with ozone has been demonstrated to enhance both the mass transfer rate and the steady state concentration that can be achieved (Chapter 1 and 4).
- The use of microbubbles has been demonstrated to significantly enhance target compound degradation with both faster and more extensive removal of a variety of contaminants including pesticides, herbicides, dyes and pharmaceuticals (Chapters 1 and 4).

Objective 2. To understand the controlling mechanisms by which microbubbles enhance the performance of ozonation.

- Evidence has been presented to suggest that the amount of hydroxyl radicals produced through microbubble and conventional bubble ozonation are the same for equivalent O_3-exposures and no evidence has been found to support the view that microbubble ozonation produces proportionally more hydroxyl radicals for a given effective O_3 dose at typical operational pH's (6 – 8). (Chapter 3).
- Experimental findings have been found to suggest that the method of O_3 delivery does not impact the rate at which O_3 self-decomposes. It was found that O_3 self-decomposition proceeds at the same rate irrespective of delivery method. The

biggest overall contributor is the concentration of hydroxide ions in the aqueous phase which is predominantly governed by pH (Chapter 4).

- The overall enhancement that microbubbles provide is predominantly driven by an increase in the volumetric mass transfer coefficient which is made up of a function of two components: a decrease in the mass transfer coefficient and an increase in the specific interfacial area such that the increase in specific interfacial area outweighs the decrease in mass transfer coefficient (Chapter 4).

Objective 3. To identify and quantify the risks associated with the application of microbubbles to ozonation for drinking water treatment.

- From comparison of microbubble and conventional bubble ozonation in real waters, no additional bromate formation was detected from microbubble ozonation when the systems were normalised for effective ozone dose (Chapter 4).

Objective 4. To quantify residual nanobubbles formed during microbubble generation and determine their significance for treatment during ozonation.

- The formation of nanobubbles from microbubble generation represented a small proportion of the overall bubble distribution. As such, the impact of the nanobubble fraction is unlikely to be a significant contributor towards performance enhancement as the majority of the process performance was attributed to the microbubble fraction (Chapter 5).

Objective 5. To determine the economic viability of the application of microbubbles to ozonation for drinking water treatment.

- A preliminary assessment of the economic viability of the application of microbubbles to ozonation at full scale suggests that side-stream microbubble contactors could provide an operational saving of approximately £12,000

compared with a conventional bubble contactor for a 1 megalitre per day drinking water treatment works. The payback period for the purchase of an appropriately sized microbubble generator is approximately six months. (Chapter 6).

8.2. Future Work

Throughout this work, a number of areas for future research have been identified as follows:

1. Hydroxyl radical production from microbubbles is still not yet fully understood outside of normal operational conditions. There is some evidence to suggest that under strongly acidic conditions, microbubbles may produce additional hydroxyl radicals through collapsing as some function of a changing zeta potential. To the best of our knowledge, no extensive probing tests with direct comparison with conventional bubbles, normalised for effective ozone dose, have been performed under these conditions.

2. The impact of column height is reasonably well understood theoretically however practical investigations into optimal column heights for particular microbubble sizes has not been performed; particularly for ozonation. This would provide a basis for the impact of reducing bubble size on the enhancement of mass transfer and degradation kinetics to enable better translation into real systems.

3. The high surface area to volume ratio demonstrates significant mass transfer advantages for microbubbles, however it may also result in disadvantages when considering the impact of bubble coating. Microbubble systems will be potentially more impacted by surface accumulation compared with conventional bubbles. Since most microbubble ozonation research has been focussed on pure systems, this is an important aspect to consider for real water applications. Surface accumulation at the gas-liquid interface can increase surface rigidity, decrease buoyancy and adds resistance to mass transfer. The importance of surface coating on microbubble ozonation therefore needs to be established to ensure that the

improvements seen in pure water laboratory tests translates across to more complex water matrices containing background organic matter.

4. More work is required to fully understand the route to implementation for microbubble generation at full scale. As the vast majority of microbubble research has been conducted at lab scale, a series of pilot scale studies are required to assess whether the performance enhancement observed at the lab scale can translate into pilot scale and full scale benefits. In addition, this thesis has explored only one type of microbubble generator and flow arrangement. Therefore, further research into different types of microbubble generator and flow arrangement is required.